

**Bangor University**

## **DOCTOR OF PHILOSOPHY**

**A novel microwave transmission Line with Impedance matching structures for Haemostasis of upper Gastrointestinal bleeding.**

Preston, Shaun

*Award date:*  
2018

*Awarding institution:*  
Bangor University

[Link to publication](#)

### **General rights**

Copyright and moral rights for the publications made accessible in the public portal are retained by the authors and/or other copyright owners and it is a condition of accessing publications that users recognise and abide by the legal requirements associated with these rights.

- Users may download and print one copy of any publication from the public portal for the purpose of private study or research.
- You may not further distribute the material or use it for any profit-making activity or commercial gain
- You may freely distribute the URL identifying the publication in the public portal ?

### **Take down policy**

If you believe that this document breaches copyright please contact us providing details, and we will remove access to the work immediately and investigate your claim.



---

---

A Novel Microwave Transmission Line with  
Impedance Matching Structures for Haemostasis  
of Upper Gastrointestinal Bleeding

---

---

WRITTEN BY

SHAUN CHRISTOPHER PRESTON BENG (HONS)  
*School of Electronic Engineering  
and Computer Science*



PRIFYSGOL  
**BANGOR**  
UNIVERSITY

2017/18

A THESIS SUBMITTED FOR THE DEGREE OF  
DOCTOR OF PHILOSOPHY



---

## *Acknowledgements*

---

My initial thanks must go to Professor Christopher P. Hancock; my supervisor, colleague and friend. Not only for his tireless efforts in the supervision of this project and many others but for his constant enthusiasm and positive attitude even when things seemed slightly more dire. I will also always be grateful for the excellent platform, or I suppose, springboard he has given me and set me up for what will hopefully be a very successful career.

I must also extend my thanks to my colleagues at Creo Medical Ltd for all their support. Special thanks must go to Malcolm White for providing me with many hours of support and mentoring in the general area of microwave engineering and especially the use of CST Microwave Studio. In a similar vein Sandra, Louis and Morgan all deserve acknowledgement for their assistance with the transition from design to actual device manufacture even at their busiest.

Paul Sibbons and Tahera Ansari, at Northwick Park Institute for Medical Research, also deserve special thanks for their support in the preclinical work discussed herein and also for their helping of an engineer to understand some of the intricacies of histopathology and biology.

My fourth round of thanks must go to some of my closest friends at Bangor University: William, James and Jake; for it would be remiss to call them just colleagues. Thanks for the sleepless nights, junk food marathons and for tolerating me throughout this program of research. They truly reminded me that although sometimes the work is difficult and arduous, there will always be time for socialising and enjoying

what I do.

My final thanks goes to my family; specifically my mother Julie, my father Denis and my brother Jay. Not only have they provided me with, what I consider, the best upbringing I could have had but they have also been tolerant and understanding of my workload and have shown nothing but support for everything I want in life.

Further thanks goes to the funding for this research from the Knowledge Economy Skills Scholarships (KESS 2) which is a pan-Wales higher level skills initiative led by Bangor University on behalf of the HE sector in Wales. It is part funded by the Welsh Government's European Social Fund (ESF) convergence programme for West Wales and the Valleys.



## Statement of Originality

The work presented in this thesis is entirely from the studies of the individual student, except where otherwise stated. Where derivations are presented and the origin of the work is either wholly or in part from other sources, then full reference is given to the original author. This work has not been presented previously for any degree, nor is it at present under consideration by any other degree awarding body.

Signed: 

Shaun C. Preston

## Statement of Availability

I hereby acknowledge the availability of any part of this thesis for viewing, photocopying or incorporation into future studies, providing that full reference is given to the origins of any information contained herein. I further give permission for a copy of this work to be deposited with the Bangor University Institutional Digital Repository, the British Library ETHOS system, and/or in any other repository authorised for use by Bangor University when the approved bar on access has been lifted. I acknowledge that Bangor University may make the title and a summary of this thesis/dissertation freely available.

Signed: 

Shaun C. Preston

# Declaration and Consent

## Details of the Work

I hereby agree to deposit the following item in the digital repository maintained by Bangor University and/or in any other repository authorized for use by Bangor University.

**Author Name:** Shaun Christopher Preston .....

**Title:** A Novel Transmission Line with Impedance Matching Structures for Haemostasis of Upper Gastrointestinal Bleeding .....

**Supervisor/Department:** Professor Christopher P. Hancock, School of Electronic Engineering .....

**Funding body (if any):** KESS .....

**Qualification/Degree obtained:** PhD Electronic Engineering .....

This item is a product of my own research endeavours and is covered by the agreement below in which the item is referred to as “the Work”. It is identical in content to that deposited in the Library, subject to point 4 below.

## Non-exclusive Rights

Rights granted to the digital repository through this agreement are entirely non-exclusive. I am free to publish the Work in its present version or future versions elsewhere.

I agree that Bangor University may electronically store, copy or translate the Work to any approved medium or format for the purpose of future preservation and accessibility. Bangor University is not under any obligation to reproduce or display the Work in the same formats or resolutions in which it was originally deposited.

## Bangor University Digital Repository


I understand that work deposited in the digital repository will be accessible to a wide variety of people and institutions, including automated agents and search engines via the World Wide Web.

I understand that once the Work is deposited, the item and its metadata may be incorporated into public access catalogues or services, national databases of electronic theses and dissertations such as the British Library’s EThOS or any service provided by the National Library of Wales.

I understand that the Work may be made available via the National Library of Wales Online Electronic Theses Service under the declared terms and conditions of use (<http://www.llgc.org.uk/index.php?id=4676>). I agree that as part of this service the National Library of Wales may electronically store, copy or convert the Work to any approved medium or format for the purpose of future preservation and accessibility. The National Library of Wales is not under any obligation to reproduce or display the Work in the same formats or resolutions in which it was originally deposited.

**Statement 1:**


This work has not previously been accepted in substance for any degree and is not being concurrently submitted in candidature for any degree unless as agreed by the University for approved dual awards.

Signed  (candidate)  
Date ..... 21/05/2018 .....

**Statement 2:**

This thesis is the result of my own investigations, except where otherwise stated. Where correction services have been used, the extent and nature of the correction is clearly marked in a footnote(s).

All other sources are acknowledged by footnotes and/or a bibliography.

Signed  (candidate)  
Date ..... 21/05/2018 .....

**Statement 3:**


I hereby give consent for my thesis, if accepted, to be available for photocopying, for inter-library loan and for electronic storage (subject to any constraints as defined in statement 4), and for the title and summary to be made available to outside organisations.

Signed ..... (candidate)  
Date .....

**NB:** Candidates on whose behalf a bar on access has been approved by the Academic Registry should use the following version of **Statement 3:**

**Statement 3 (bar):**

I hereby give consent for my thesis, if accepted, to be available for photocopying, for inter-library loans and for electronic storage (subject to any constraints as defined in statement 4), after expiry of a bar on access.

Signed  (candidate)  
Date ..... 21/05/2018 .....

**Statement 4:**

Choose **one** of the following options

a)	I agree to deposit an electronic copy of my thesis (the Work) in the Bangor University (BU) Institutional Digital Repository, the British Library ETHOS system, and/or in any other repository authorized for use by Bangor University and where necessary have gained the required permissions for the use of third party material.	
b)	I agree to deposit an electronic copy of my thesis (the Work) in the Bangor University (BU) Institutional Digital Repository, the British Library ETHOS system, and/or in any other repository authorized for use by Bangor University when the approved <b>bar on access</b> has been lifted.	✓
c)	I agree to submit my thesis (the Work) electronically via Bangor University's e-submission system, however I <b>opt-out</b> of the electronic deposit to the Bangor University (BU) Institutional Digital Repository, the British Library ETHOS system, and/or in any other repository authorized for use by Bangor University, due to lack of permissions for use of third party material.	

*Options B should only be used if a bar on access has been approved by the University.*

**In addition to the above I also agree to the following:**

1. That I am the author or have the authority of the author(s) to make this agreement and do hereby give Bangor University the right to make available the Work in the way described above.
2. That the electronic copy of the Work deposited in the digital repository and covered by this agreement, is identical in content to the paper copy of the Work deposited in the Bangor University Library, subject to point 4 below.
3. That I have exercised reasonable care to ensure that the Work is original and, to the best of my knowledge, does not breach any laws – including those relating to defamation, libel and copyright.
4. That I have, in instances where the intellectual property of other authors or copyright holders is included in the Work, and where appropriate, gained explicit permission for the inclusion of that material in the Work, and in the electronic form of the Work as accessed through the open access digital repository, *or* that I have identified and removed that material for which adequate and appropriate permission has not been obtained and which will be inaccessible via the digital repository.
5. That Bangor University does not hold any obligation to take legal action on behalf of the Depositor, or other rights holders, in the event of a breach of intellectual property rights, or any other right, in the material deposited.
6. That I will indemnify and keep indemnified Bangor University and the National Library of Wales from and against any loss, liability, claim or damage, including without limitation any related legal fees and court costs (on a full indemnity bases), related to any breach by myself of any term of this agreement.

Signature: .....  ..... Date : ..... 21/05/2018 .....

---

## ***Published Work***

---

### **Journal**

S.C. Preston, M. White, B. Saunders, Z. Tsiamoulos and C.P. Hancock, "A new hemostatic device utilizing a novel transmission structure for delivery of adrenaline and microwave energy at 5.8GHz", *International Journal of Microwave and Wireless Technologies*, vol. 9, no. 8 pp. 1575-1582, 2017.

### **Conference**

S.C. Preston, M. White, B. Saunders, Z. Tsiamoulos and C.P. Hancock, "A new haemostatic device utilising a novel transmission structure for delivery of adrenaline and microwave energy at 5.8 GHz," *2016 46th European Microwave Conference (EuMC)*, London, 2016, pp. 910-913.

S.C. Preston, W. Taplin, M. White and C.P. Hancock, "An impedance matching transformer structure with consideration of 3D printed electromagnetic shielding," *2017 IEEE MTT-S International Microwave Workshop Series on Advanced Materials and Processes for RF and THz Applications (IMWS-AMP)*, Pavia, 2017, pp. 1-3.

S.C. Preston, P.D. Sibbons, M. White, C.P. Hancock, "Preclinical Efficacy of a Microwave and Adrenaline based Haemostat Utilising a Novel Coaxial Cable Structure", *2018 IEEE-MTT-S International Microwave Symposium*, Philadelphia , PA, 2018.

S.C. Preston, W. Taplin, A.W. Jones, C.P. Hancock, "A Microwave Ablation System for the Visualisation and Treatment of Pulmonary Nodules and Tumours", *2018 IEEE MTT-S International Microwave Bio Conference (IMBIOC)*, Philadelphia, PA, 2018.

S.C. Preston, M. White, C.P. Hancock, "Methods of Coupling 400KHz and 5.8GHz

Energy into a Hollow Non-50ΩCo-axial Transmission Line Structure", *2018 48th European Microwave Conference (EuMC)*, Madrid, 2018.

## Patents

'Electrosurgical energy conveying structure and electrosurgical device incorporating the same', GB1705167.3, Lodged: 30/03/2017, Status: Pending

'Microwave energy transfer component for electrosurgical apparatus', GB1702305.2, Lodged: 13/02/2017, Status: Pending

'Electrosurgical Instrument having a coaxial line with a fluid channel', GB1521522.1, Lodged: 07/12/2015, Published: 14/06/2017, Status: Awaiting First Examination

'Electrosurgical instrument with selectable surface coagulation and deeper coagulation modes of operation' GB1603744.2, Lodged: 04/03/2016, Status: Awaiting First Examination

'An RF and/or microwave energy conveying structure, and an invasive electrosurgical scoping device incorporating the same', GB1518330.4, Lodged: 16/10/15, Published: 18/05/2016, Status: Granted



## **Abstract**

This research shows the development of a complete novel medical device capable of achieving haemostasis of upper gastrointestinal bleeding. A novel transmission structure has been designed and tested which includes a hollow central channel running through the inner conductor allowing for the delivery of fluid or introduction of clinical tools such as forceps, biopsy graspers or needles alongside the delivery of microwave energy. To facilitate the initial testing and subsequent clinical usage of the cable; multiple transformer structures were considered and developed both for the delivery of microwave and radio frequency energy. These allowed for the testing and characterisation of multiple cable prototypes developed throughout this research. In order to achieve the required clinical effect, namely coagulation of bleeding vessels, a solution which allowed optimal delivery of energy from the cable structure into the tissue at the treatment site was developed. Radiative tip prototypes were simulated, manufactured and tested to show matching between the lower impedance cable and the higher impedance tissue. Finally a number of complete devices were assembled and tested using microwave test equipment, on bench tissue testing using porcine liver and also during a pre-clinical investigation held at Northwick Park Institute for Medical Research, one of the UK's leading charity-based independent Medical Research Institutes. Clinician feedback and histological analysis is presented within and show successful coagulation of multiple simulated oesophageal bleeds.

---

# *Contents*

---

<b>1</b>	<b>Introduction</b>	<b>1</b>
<b>2</b>	<b>Background and Literature Review</b>	<b>5</b>
2.1	Microwave Engineering . . . . .	5
2.1.1	A Brief History . . . . .	5
2.1.2	Co-axial Cable . . . . .	7
2.1.3	Skin Depth . . . . .	8
2.1.4	Characteristic Impedance . . . . .	9
2.1.5	Quarter Wave Transformation . . . . .	14
2.1.6	Attenuation . . . . .	16
2.1.7	Microwave Test Measurements . . . . .	18
2.1.8	Microwave Simulation . . . . .	22
2.1.9	Biological Effects of Microwaves . . . . .	23
2.2	Upper Gastrointestinal Bleeding . . . . .	25
2.2.1	Oesophageal Anatomy . . . . .	26
2.2.2	Oesophageal Bleeding . . . . .	27
2.2.3	Gastric and Duodenal Bleeding . . . . .	27
2.3	Haemostasis . . . . .	28
2.3.1	Background . . . . .	28
2.3.2	The Biological Basics . . . . .	28
2.3.3	Thermal Haemostasis . . . . .	31
2.4	Current Methods of achieving haemostasis . . . . .	31
2.4.1	Mechanical Modalities . . . . .	32
2.4.2	Injection Modalities . . . . .	34

2.4.3	Energy Based Thermal Modalities . . . . .	36
<b>3</b>	<b>Device Introduction and Specification</b>	<b>44</b>
3.1	Clinical Need . . . . .	44
3.2	Physical Device Requirements . . . . .	45
3.2.1	Requirement for Maximum Outer Diameter (2.5mm) . . . . .	45
3.2.2	Requirement for Hollow Channel . . . . .	46
3.2.3	Requirement for Impedance Transformation . . . . .	46
<b>4</b>	<b>Impedance Transformation</b>	<b>48</b>
4.1	Transformer Structure Considerations . . . . .	49
4.2	Use of Microwave and RF Energy . . . . .	49
4.2.1	Co-axial Capacitive Coupling . . . . .	50
4.2.2	Double Choke structure for Microwave and RF . . . . .	57
4.2.3	Change from Microwave/RF to Microwave only delivery . . . . .	63
4.2.4	Co-axial Transformer . . . . .	63
4.2.5	Microstrip Line Based Transformer . . . . .	69
<b>5</b>	<b>A Novel Transmission Line...</b>	<b>90</b>
5.1	Design and Development . . . . .	90
5.1.1	Dimension Considerations . . . . .	90
5.1.2	Material Considerations . . . . .	91
5.1.3	Prototype Rigid Design . . . . .	92
5.2	Flexible Cable Design and Manufacture . . . . .	97
5.2.1	Prototype 1 - Company A . . . . .	100
5.2.2	Prototype 2 - Company A . . . . .	100
5.2.3	Prototype 3 - Company B . . . . .	101
5.3	Theoretical Cable comparison . . . . .	102
5.4	Cable Testing . . . . .	105

5.4.1	Co-axial Transformer . . . . .	106
5.4.2	Microstrip Transformer . . . . .	106
5.4.3	Estimation of Dielectric Constant . . . . .	109
<b>6</b>	<b>Radiative Tip Design</b>	<b>111</b>
6.1	Requirements . . . . .	111
6.1.1	Physical Constraints . . . . .	111
6.1.2	Clinical Requirement . . . . .	113
6.2	Simple Macor Collar . . . . .	116
6.3	Final Tip Design . . . . .	119
6.3.1	Variation in length . . . . .	130
<b>7</b>	<b>Microwave and Adrenaline Haemostat - Full Device</b>	<b>134</b>
7.1	Development and Design . . . . .	134
7.1.1	Overview . . . . .	134
7.1.2	Transformer and Connectors . . . . .	134
7.1.3	Consideration of handpiece shielding . . . . .	138
7.1.4	Radiative Tip . . . . .	143
7.1.5	Final Manufacture . . . . .	144
7.2	Bench Results . . . . .	146
7.2.1	VNA testing of completed devices . . . . .	146
7.2.2	Ex-vivo Tissue Testing . . . . .	149
7.3	Pre-Clinical Tests inc. Histology . . . . .	155
<b>8</b>	<b>Discussion and Conclusion</b>	<b>168</b>
8.1	Discussion . . . . .	168
8.2	Conclusion . . . . .	174
8.3	Further Work . . . . .	175
8.3.1	Microstrip Transformer Improvements . . . . .	176

8.3.2	Radiative Tip Improvements . . . . .	176
8.3.3	Novel Cable Improvements . . . . .	177
8.3.4	Thorough Device Comparison and Validation . . . . .	177
<b>Appendices</b>		<b>179</b>
<b>A Final Device - Bill of Materials</b>		<b>180</b>
<b>B Pre-clinical Documents</b>		<b>181</b>
B.1	Protocol . . . . .	181
B.2	Anaesthesia and notes documents . . . . .	186
<b>C Simulations: Preliminary investigation of varied materials on microstrip transformer shielding and radiation</b>		<b>189</b>

---

## *List of Figures*

---

1.1	Diagram showing rapid rise of endoscopy and paradigm shift in health care and surgical procedures. Image from Creo Medical Ltd . . . . .	2
1.2	Block diagram showing the structure of the device developed in this research . . . . .	3
2.1	Mobile early warning radar, similar to that used during Pearl Harbour	6
2.2	Co-axial cable simulation showing E and H Field with TEM propogation	7
2.3	Frequency dependence of skin depth in a silver conductor . . . . .	8
2.4	Graph showing variation in power transmission with change in cable impedance when connected to 50 $\Omega$ generator . . . . .	13
2.5	Graph showing maximum power handling and minimum attenuation as a function of impedance . . . . .	14
2.6	Diagram showing the operation of a quarter wave transformer . . . . .	15
2.7	Diagram showing the equal reflection coefficients at both ends of the transformer . . . . .	17
2.8	S Parameter Diagram . . . . .	18
2.9	Wiltron model vector network analyser . . . . .	20
2.10	Example output of magnitude S1,1 measurements . . . . .	20
2.11	Example output of time domain S1,1 measurements . . . . .	21
2.12	Dipole reorientation of water in response to an alternating electric field	24
2.13	Simple structure of the gastrointestinal tract . . . . .	25
2.14	Gastrosopic images of oesophageal varices . . . . .	26
2.15	Detailed pathway showing the natural response of the body to blood loss.	29
2.16	Examples of endoscopic clips used for haemostasis . . . . .	32

2.17	Examples of endoscopic band ligators used for haemostasis . . . . .	34
2.18	Needlemaster Single-Use Injection Needle from Olympus. . . . .	35
2.19	Diagram showing operation of monopolar RF electrosurgery. . . . .	37
2.20	ESP1 standard Bovie Pencil from Bovie Medical Corporation . . . . .	38
2.21	Diagram showing operation of bipolar RF electrosurgery . . . . .	39
2.22	Covidien Valleylab Bipolar Forceps from Medtronic . . . . .	39
2.23	Examples of bipolar haemostasis probes . . . . .	40
2.24	Diagram showing functionality of APC . . . . .	41
2.25	Various Microwave Generators . . . . .	43
3.1	Diagram showing the variation in coaxial outer conductor and corresponding impedance. . . . .	47
3.2	Graph showing the variation in impedance with varying inner diameter of outer conductor . . . . .	47
4.1	Side view diagram of the capacitive coupling structure . . . . .	51
4.2	Variation in reactance of a 3pF capacitor with frequency . . . . .	52
4.3	Equivalent circuit for the capacitive coupling structure . . . . .	53
4.4	S Parameters for the equivalent circuit capacitive coupling structure . .	54
4.5	S Parameters for the 3D EM simulation of the capacitive coupling structure . . . . .	54
4.6	Power Flow through the rigid prototype at 400KHz . . . . .	55
4.7	Power Flow through the rigid prototype at 5.8GHz . . . . .	56
4.8	Power Flow through capacitive coupling device at 400KHz . . . . .	56
4.9	Power Flow through capacitive coupling device at 5.8GHz . . . . .	57
4.10	Simulation model for double choke structure . . . . .	58
4.11	Simulated S Parameters for double choke structure . . . . .	58
4.12	Choke structure parts . . . . .	60
4.13	Fully assembled choke structure . . . . .	60

4.14 Time domain measurement of the double choke structure and open ended cable . . . . .	61
4.15 Measurement and testing of the double choke structure . . . . .	62
4.16 Variation in co-axial cable impedance with increasing inner diameter of outer conductor . . . . .	64
4.17 Dimensioned drawing of the co-axial transformer. . . . .	65
4.18 Model designed for the co-axial transformer simulation . . . . .	65
4.19 Simulated results for the co-axial transformer structure with tube extended and occluded . . . . .	66
4.20 Simulated results for the co-axial transformer structure . . . . .	67
4.21 Photograph of the various parts which make up the co-axial transformer. . . . .	68
4.22 Multiple photographs showing initial steps for the construction of the co-axial transformer. . . . .	68
4.23 Multiple photographs showing subsequent steps for the construction of the co-axial transformer. . . . .	69
4.24 Example of a microstrip structure . . . . .	70
4.25 Microstrip simulation showing E and H Field . . . . .	71
4.26 Characteristic Impedance and Effective Dielectric Constant variation with trace width for structure where $H = 1.575\text{mm}$ . . . . .	72
4.27 Side and Perspective 3D render sketches of the theoretical design of the transformer structure . . . . .	73
4.28 Initial Simulation model for the microstrip transformer . . . . .	74
4.29 Initial Simulation S Parameters for the microstrip transformer . . . . .	75
4.30 Equivalent circuit for a step discontinuity in microstrip . . . . .	76
4.31 Initial Simulation S Parameters for the microstrip transformer with parameter sweep . . . . .	76
4.32 Models to assess connection methods for microstrip . . . . .	77
4.33 Simulated S Parameters for tape microstrip attachment . . . . .	78



4.34 Simulated S Parameters for block microstrip attachment . . . . .	78
4.35 Excerpt of test report for IPC-4101D for material EM-827 . . . . .	80
4.36 Model used to simulate microstrip with varying dielectric constant and dissipation factor . . . . .	80
4.37 Simulation of microstrip with varying dielectric constant and dissipa- tion factor . . . . .	81
4.38 Photograph of assembled microstrip transformer with copper tape outer conductor connection . . . . .	82
4.39 Time domain plot of 4.66m cable connected to microstrip with copper tape outer conductor connection . . . . .	83
4.40 Illustration of the ground tray structure . . . . .	84
4.41 Perspective view of the final simulation model . . . . .	85
4.42 Simulated S Parameters for ground tray transformer structure . . . . .	85
4.43 Photograph showing the microstrip transformer and ground tray structure	86
4.44 Simulation Model used to assess the microstrip transformer with filled hollow channel . . . . .	86
4.45 Simulated S Parameters for microstrip transformer with filled hollow channel . . . . .	87
4.46 Simulated Power Loss Density for microstrip transformer with filled hollow channel . . . . .	88
5.1 Model showing the individual layers which comprise the rigid prototype structure . . . . .	92
5.2 Graph showing theoretical comparison between the use of brass vs silver conductors for the rigid prototype geometry at 5.8GHz. . . . .	93
5.3 Initial prototype design of the rigid novel microwave cable idea . . . . .	93
5.4 Simulated Model for Rigid Prototype design . . . . .	94
5.5 Simulated S <sub>1,1</sub> for Rigid Prototype design . . . . .	95

5.6	Assembly procedure for attaching the impedance transformer section to the rigid prototype. . . . .	96
5.7	Model showing the individual layers which comprise the novel microwave cable structure . . . . .	98
5.8	Diagram showing the size of each layer for the novel microwave cable structure . . . . .	98
5.9	Render of the Prototype 1 Cable . . . . .	100
5.10	Render of the Prototype 2 Cable . . . . .	101
5.11	Excerpt from the H&S Sucoform 47 datasheet [1] . . . . .	102
5.12	S <sub>1,1</sub> of transformer for various cable impedances . . . . .	105
5.13	Time domain plot of each prototype cable test using co-axial transformer	107
5.14	Time domain plot of each prototype cable test using microstrip transformer . . . . .	108
5.15	Testing of back to back microstrip transformers . . . . .	108
5.16	S <sub>2,1</sub> of back to back microstrip transformers . . . . .	109
5.17	Graph showing comparison of cable loss measurements with both transformers . . . . .	109
6.1	Diagram showing proximal end angle of insertion in endoscopic working channel . . . . .	112
6.2	Initial simple cylindrical radiative tip . . . . .	117
6.3	Simulated S Parameters for radiative tip 1 . . . . .	117
6.4	Simulated S Parameters for radiative tip 1 with variation in cable length	118
6.5	Simulated Power Loss Density for radiative tip 1 . . . . .	119
6.6	Simulated Power Loss Density for radiative tip 1 in perspective view .	119
6.7	Rendered image of the final tip design . . . . .	120
6.8	Simulation Model for the final tip design with Macor . . . . .	121
6.9	Simulated results for the final tip design with Macor . . . . .	122

6.10	Simulated power loss density plot for the final tip design with Macor .	123
6.11	Simulated power loss density plot for the final tip design with Macor in perspective view . . . . .	123
6.12	Simulated farfield monitor for final tip design with Macor . . . . .	124
6.13	Simulation Model for the final tip design with PEEK . . . . .	124
6.14	Simulated results for the final tip design with PEEK . . . . .	125
6.15	Simulated power loss density plot for the final tip design with PEEK .	125
6.16	Simulated power loss density plot for the final tip design with PEEK from perspective view . . . . .	126
6.17	Simulated farfield monitor for final tip design with PEEK . . . . .	126
6.18	Radiative tip variations . . . . .	127
6.19	Simulation Model for the final sloped tip design with PEEK . . . . .	127
6.20	Simulated results for the final sloped tip design with PEEK . . . . .	128
6.21	Simulated power loss density plot for the final sloped tip design with PEEK . . . . .	128
6.22	Simulated farfield monitor for final sloped tip design with PEEK . . . .	129
6.23	Simulated power loss density plot for final sloped tip design with PEEK inside oesophageal lumen . . . . .	129
6.24	Simulation model for second experimental simulation considering lack of step discontinuity . . . . .	131
6.25	Simulation model for third experimental simulation considering lack of fringing capacitance . . . . .	132
6.26	Simulated E field showing fringing fields at open circuit liver boundary	133
7.1	Photograph of the final connection used to access the hollow channel .	136
7.2	Designing of the handpiece in Autodesk Inventor Professional . . . . .	138
7.3	Slicing the handpiece model in Ultimaker Cura . . . . .	138
7.4	Ultimaker 2+ 3D Printer during printing of the initial handpiece design	139

7.5	CST Studio model used to simulate the effect of microstrip radiation .	139
7.6	Specific absorption rate illustrating the energy absorbed into the hand-piece and surrounding skin phantom with cutting planes through (top) x-axis and through (bottom) y-axis . . . . .	140
7.7	CST Studio model showing metallic shielding above microstrip . . . . .	142
7.8	Specific Absorption Rate plot from X cutting plane (top) and Y cutting plane (bottom) showing absorption of energy into the handpiece and surrounding skin phantom with shielded transformer . . . . .	143
7.9	Photograph showing connection of the cable to the microstrip transformer	144
7.10	Individual (left) and assembled (right) parts for final sloped tip design	145
7.11	Photograph of the final manufacture (left) and device ready for preclinical testing (right) . . . . .	145
7.12	Time Domain plot of the final MAH1 device . . . . .	147
7.13	Time Domain plot of the final MAH2 device . . . . .	147
7.14	Time Domain plot of the final MAH4S device . . . . .	148
7.15	Time Domain plot of the final MAH5S device . . . . .	148
7.16	Bench test results for initial prototype at various times . . . . .	149
7.17	Application of the haemostat to the tissue sample . . . . .	151
7.18	Simulation showing power loss density and approximate area of tissue effect . . . . .	151
7.19	Side application of haemostat probe . . . . .	152
7.20	Exposing of inner surface of oesophageal lumen . . . . .	153
7.21	Ex vivo oesophageal testing . . . . .	153
7.22	Initial results from comparison testing with Boston Scientific Gold Probe	154
7.23	Pre-Clinical setup at NPIMR . . . . .	156
7.24	Endoscopic stack setup at NPIMR . . . . .	156
7.25	Endoscopic graspers used to remove upper layers of oesophagus . . . .	158
7.26	Initial bleed and subsequent coagulation of lesion 1 . . . . .	158

7.27 Initial bleed and subsequent coagulation of lesion 2 . . . . .	158
7.28 Initial bleed and subsequent coagulation of lesion 3 . . . . .	159
7.29 Initial bleed and subsequent coagulation of lesion 4 . . . . .	160
7.30 Initial bleed and subsequent coagulation of lesion 5 . . . . .	160
7.31 Initial bleed and subsequent coagulation of lesion 6 . . . . .	160
7.32 Flow chart showing the various steps involved in the histology process	161
7.33 Flow chart showing the various steps involved in the staining process	162
7.34 Normal oesophageal structure under H & E staining . . . . .	163
7.35 Normal oesophageal structure under PicMill staining . . . . .	164
7.36 Lesion 1 under H & E and Picmill staining . . . . .	165
7.37 Lesion 2 under H & E and Picmill staining . . . . .	165
7.38 Lesion 3 under H & E and Picmill staining . . . . .	166
7.39 Lesion 4 under H & E and Picmill staining . . . . .	166
7.40 Lesion 5 under H & E and Picmill staining . . . . .	167
7.41 Lesion 6 under H & E and Picmill staining . . . . .	167
8.1 Final manufactured transformers . . . . .	170
8.2 Final Simulated and Manufactured Radiative Tip . . . . .	171
8.3 Overall Final Device . . . . .	172
8.4 Creation and Treatment of Oesophageal Bleed Lesion 5 . . . . .	173
8.5 Histological Slide of Lesion 5 . . . . .	174
A.1 Bill of Materials for the final device . . . . .	180
C.1 Simulation model for assessing the effect of various materials on shield- ing of the microstrip transformer . . . . .	189
C.2 Material parameters used to assess the effect of various materials on shielding of the microstrip transformer . . . . .	190

C.3 Simulated S Parameters showing the effect of various materials on shielding of the microstrip transformer . . . . .	190
C.4 Simulated power loss density used to assess the effect of various materials on shielding of the microstrip transformer . . . . .	191

---

## *List of Tables*

---

2.1	Table showing difference in Power Handling and Attenuation at $14\Omega$ and $50\Omega$ . . . . .	13
4.1	Table showing parameters for equivalent capacitive coupling circuit . .	52
4.2	Table showing variation in S Parameters at 5.8GHz for the co-axial transformer with and without extended hollow channel . . . . .	66
4.3	Excerpt of calculated values for the microstrip transformer. . . . .	73
4.4	Theoretical Calculation of temperature increase due to power delivery into saline . . . . .	89
5.1	Calculated power from simulated rigid prototype results . . . . .	95
5.2	Table showing the Sucoform 47 parameters used in theoretical comparison	103
5.3	Table showing the new cable parameters used in theoretical comparison	103
5.4	Table showing calculated values for sucoform 47 used in theoretical comparison . . . . .	104
5.5	Table showing calculated values for new cable used in theoretical comparison . . . . .	104
5.6	Specific Return Loss for each prototype . . . . .	106
5.7	Measured losses from open ended prototype cable testing using co-axial transformer . . . . .	107
5.8	Measured losses from open ended prototype cable testing using co-axial transformer . . . . .	107
5.9	Calculation of $\epsilon_r$ for each prototype cable . . . . .	110

6.1	Table showing the calculated values for wave impedance of various tissues at 5.8GHz . . . . .	115
6.2	Table showing dielectric properties and calculated quarter wavelength for each tip material . . . . .	121
6.3	Table showing variation in length with increasing tip length of PEEK tip	130
6.4	Table showing variation in length with increasing tip length of PEEK tip without step discontinuity . . . . .	132
6.5	Table showing variation in length with increasing tip length of PEEK tip without fringing end effects . . . . .	133
7.1	Results from time domain measurements for each device . . . . .	146
7.2	Table showing measurements of application sites during bench porcine liver testing . . . . .	150
7.3	Loss calculations for bench testing . . . . .	150
C.1	Simulation values for farfield monitors of each material . . . . .	191



---

## ***List of Abbreviations***

---

**AC** - Alternating Current

**APC** - Argon Plasma Coagulation

**CO<sub>2</sub>** - Carbon Dioxide

**CST** - CST Microwave Studio

**dB** - Decibels

**dB/m** - Decibels per meter

**dBm** - Decibels with respect to 1mW

**DC** - Direct Current

**E Field** - Electric Field

**GI** - Gastrointestinal

**H Field** - Magnetic Field

**H&S** - Haematoxylin and Eosin

**ICNIRP** - International Commission on Non-ionizing Radiation Protection

**IEEE** - Institute of Electrical and Electronics Engineers

**IFAC** - Istituto di Fisica Applicata "Nello Carrara" (Institute for Applied Physics)

**MAH** - Microwave and Adrenaline Haemostat

**MTT-S** - Microwave Theory and Techniques Society

**NPIMR** - Northwick Park Institute for Medical Research

**PEEK** - Polyether Ether Ketone

**PicMill** - Picrosirius Red and Miller's Elastin

**ppm** - Parts per Million

**PTFE** - Polytetrafluoroethylene

**RF** - Radio Frequency

**RMS** - Root Mean Squared

**SAR** - Specific Absorption Rate

**SHF** - Super High Frequency

**SMA** - Sub Miniature A

**UGIB** - Upper Gastrointestinal Bleeding

**VNA** - Vector Network Analyser

# ***Chapter. 1***

---

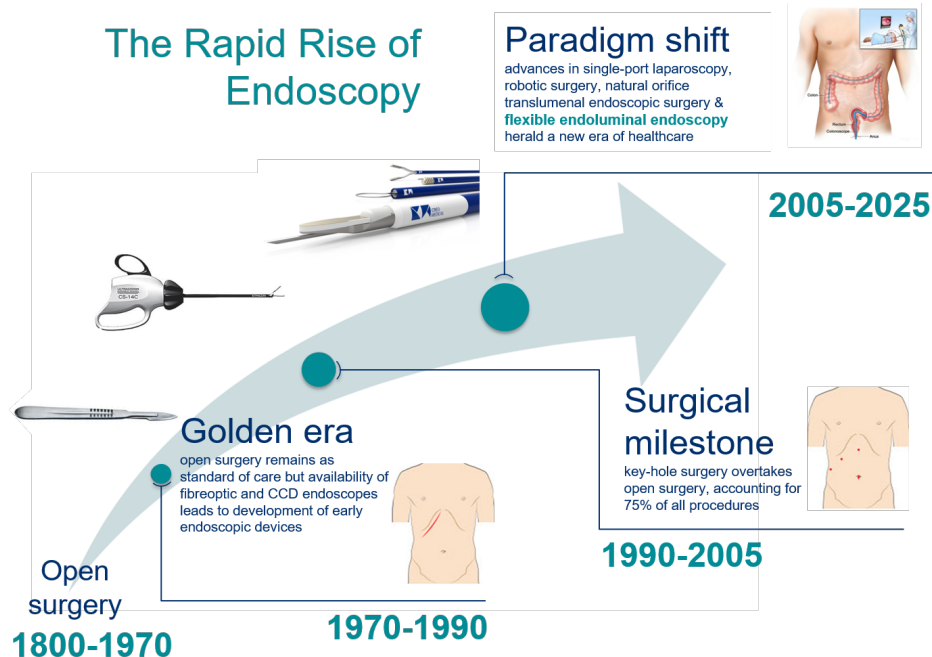
## ***Introduction***

---

Upper Gastrointestinal Bleeding (UGIB) is the cause of, in excess of, 300,000 hospital admissions and 52,000 deaths per annum in the US [2] and in the UK is one of the most common gastrointestinal (GI) emergencies leading to 4,000 deaths and up to 70,000 hospital admissions each year. [3] This leads to a definitive requirement for clinicians, especially endoscopists, to have the correct tools at their disposal to stop bleeding both rapidly and effectively. As a general aside, minimally or non invasive treatments have been shown to have a higher number of benefits when compared with open surgery including faster healing, less risk of infection due to less time spent in hospital, less pain and even minimisation of the bodies reaction to surgical stress [4]. As such less invasive procedures are becoming more and more popular and will evidently be the most common option for many surgical procedures in the future as can be seen in figure 1.1.

Endoscopic intervention in UGIB has generally been shown to not only address the current situation and achieve immediate control of the bleed but also to prevent recurrent episodes. This not only stabilises and prevents the patient from possibly dying but it also minimises strain on hospital resources from readmission, minimises further cost and lowers mortality rates. [5] This increase in technological ability alongside the added benefits of minimally invasive and non-invasive procedures has led to a paradigm shift in which procedures such as natural orifice endoscopy, robotic surgery and flexible endoluminal endoscopy are becoming the new healthcare standard as shown in figure 1.1.

A new modality of thermal haemostasis was therefore envisioned which can be



1

Figure 1.1: Diagram showing rapid rise of endoscopy and paradigm shift in health care and surgical procedures. Image from Creo Medical Ltd

achieved through delivery of a long, flexible and narrow instrument into the gastrointestinal tract to the treatment site via an endoscope or gastroscope. This thesis describes the design and development of a novel microwave structure capable of delivering microwave energy at 5.8GHz to controllably coagulate bleeding vessels whilst utilising a hollow channel running through the center of the structure which can be used for the delivery of adrenaline to promote vasoconstriction at the local site enabling instant control of the bleed and allowing subsequent usage of microwave energy to generate a permanent 'plug' for on going control of the bleed. The hollow channel can also be used to deliver liquids or even for the introduction of other tools such as vision sensors, biopsy graspers or simply as a method of irrigation and aspiration. The generation of the 'plug' is a thermally induced alternative to the natural response of the body to bleeding which comprises the interaction of a number of proteins, clotting factors and platelets which all bind together to create a physical barrier to prevent further loss of blood, promote healing and reduce the

need for re-admission into hospital.

Dual modality haemostasis such as the the delivery of fluid coupled with thermal energy, as in this device, has been shown to be provide a superior outcome over a single modality treatment process [6]. Palmer et. al states that one method of achieving this dual modality effect is through the use of adrenaline injection and mechanical clip. Clips however, whilst having a high success rate, tend to require accurate placement and a high level of technical proficiency to utilise correctly [7]. They also introduce a physical structure into the GI tract which could malfunction or come away due to movement or disturbance leading to re-bleed and other complications.

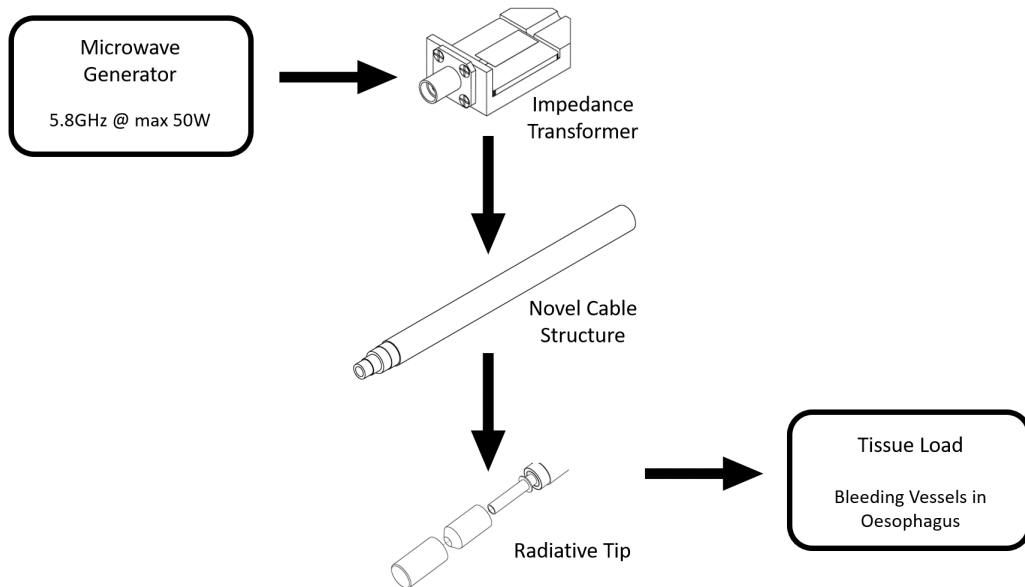


Figure 1.2: Block diagram showing the structure of the device developed in this research

This thesis focuses on a number of key areas related to this research and subsequent development of the overall device as shown in figure 1.2.

- **Chapter 2** considers background information on the clinical need and also provides a review of current techniques used to achieve haemostasis.
- **Chapter 3** highlights the physical and clinical requirements for the overall project and provide a setting for the other chapters.

- **Chapters 4, 5 and 6** focus on the design, development, manufacture and testing of the new device, comprising: a novel transmission line structure, bespoke impedance transformers and a complex radiative tip structure.
- **Chapter 7** describes the combination of the previous works chapters and the manufacture of the final device in its entirety along with results from an in-vivo pre-clinical study carried out during the research programme as well as ex-vivo bench testing.
- Finally the project is summarised and evaluated for its strengths, weaknesses and future work is discussed in **Chapter 8**.

## ***Chapter. 2***

---

### ***Background and Literature Review***

---

Study the past if you would define  
the future.

---

*Confucius*

*551 BC - 479 BC*

## **2.1. Microwave Engineering**

### **2.1.1 A Brief History**

Microwaves have been used in many applications for a long time, since their prediction by James Clerk Maxwell in 1864 and subsequent demonstration by Heinrich Hertz through his spark gap experiments. In fact, in 1897 Jagadis Chandra Bose described his research into microwave propagation including the use of horn antennas, waveguides and dielectric lenses at frequencies of up to 60GHz. [8] The majority of applications for microwaves began as point to point communication networks; with the most historically significant use being that of microwaves as radar. During the Pearl Harbour attacks an SCR-270 radar installation, similar to the one shown in figure 2.1 <sup>1</sup>, atop Kahuku point detected enemy planes whilst they were approximately 132 miles out, but the readings were initially ignored due to the relatively new technology being used [9]. Over time this technology has been refined and improved and is now one of the main engineering staples used throughout both military and civilian aviation.

---

<sup>1</sup>Credit: <http://www.monmouth.army.mil/historian/photolist.php?fname=Radio%2FSCR+270+and+271>

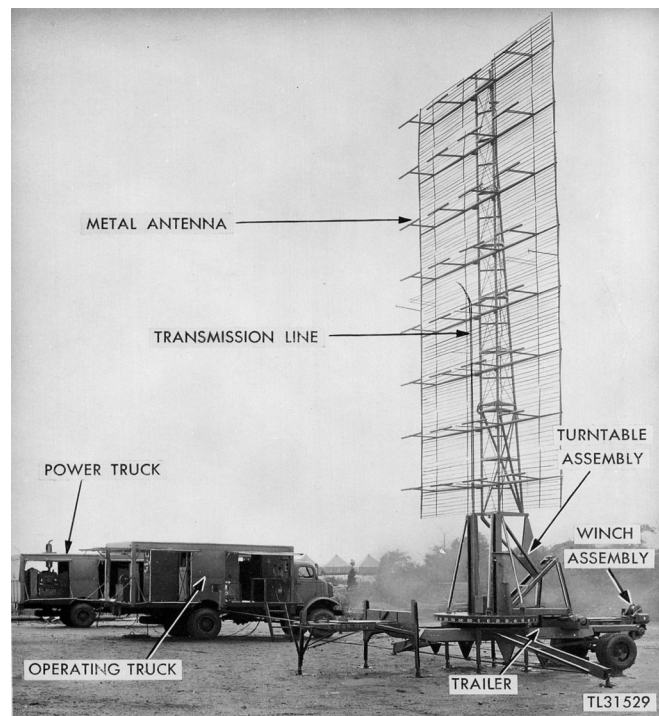


Figure 2.1: Mobile early warning radar, similar to that used during Pearl Harbour

When it comes to using microwaves to achieve thermal effects, the story goes that an electronics expert and war hero, Percy L. Spencer, was wandering around one of the Raytheon laboratories when he noticed that a chocolate bar in his pocket had begun to melt whilst he stood in front of a large magnetron [10]. He later went on to create the first batch of microwave popcorn and the first exploding egg. Whilst this initial story seems quite far fetched, the microwave oven has become a staple in most modern homes. With advances in military and telecommunication technology, this has created a drive for miniaturisation and optimisation of microwave generation technology from cavity magnetron to semiconductor technologies. This has allowed for the development of smaller and more efficient generators which subsequently allow for the creation of improved devices including many designed for a myriad of microwave applications throughout the medical sector.



### 2.1.2 Co-axial Cable

A co-axial line is an axial transmission line in which both the electric (E) field and the magnetic (H) field are enclosed by two conductors; an inner and an outer. The principle propagation mode for a co-axial cable is TEM, or transverse electromagnetic, and is where both the E field and the H field are transverse to the direction of propagation and perpendicular to each other. Consideration of this mode is only applicable when the frequency of propagation is lower than the cut-off frequency for a cylindrical waveguide, for frequencies above this multiple modes will propagate. The E field and H field for this TEM mode can be seen in fig 2.2

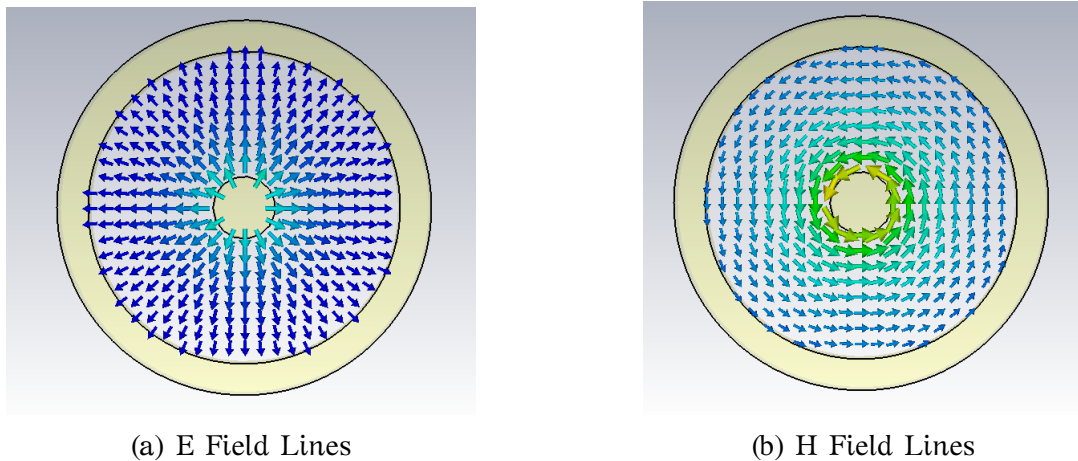


Figure 2.2: Co-axial cable simulation showing E and H Field with TEM propagation

The metal conductors are separated by a dielectric material which impacts the intrinsic properties of the cable such as characteristic impedance, power loss and velocity of propagation. An air filled co-axial line, whilst having minimal losses, would not be practical in any sort of application which requires flexion or bending of the cable. Two vital parts of co-axial cable design are choices of material, both for the conductor and dielectric structures, and also their geometry.

### 2.1.3 Skin Depth

The skin depth, in considering electrical conductors, concerns the distance into the conductor which the electric field penetrates into the conductor. It is defined as the level at which the field decreases to  $1/e$  or approximately 37%. More accurately it is defined as:

$$\delta_s = \sqrt{\frac{2\rho}{2\pi f \mu_0 \mu_R}}. \quad (2.1)$$

Where  $\delta_s$  (m) is the skin depth,  $\rho$  (ohm m) is the resistivity of the conductor,  $f$  (Hz) is the frequency and  $\mu_0$  (H/m) and  $\mu_R$  (H/m) are the permeability of free space and relative permeability of the conductor respectively.  $\mu_0$  is equal to  $4\pi \times 10^{-7}$  H/m. Variation in the skin depth of silver at various frequencies can be seen in fig 2.3

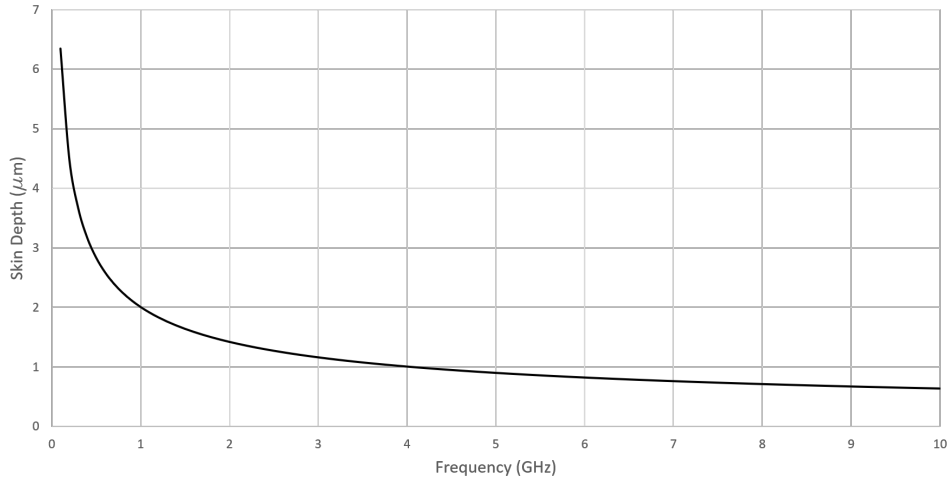


Figure 2.3: Frequency dependence of skin depth in a silver conductor

At the frequency of operation for this device at 5.8GHz and with silver having a resistivity of  $1.59 \times 10^{-8} \Omega\text{m}$ ; the skin depth of a silver conductor becomes much smaller than that at lower frequencies with a value of  $0.83\mu\text{m}$ .

It is this principle which ultimately allows for the creation of a cable with a hollow inner conductor as discussed herein. As the electric current tends to flow between the inner surface of the outer conductor and the outer surface of the inner conductor

it means that the inside of the inner conductor can be hollow. The understanding of these principles is not a new topic and has allowed for high power transmission lines to minimise losses whilst still retaining a strong and solid central core, however the application of this principle to co-axial cable for this application is a novel approach and allows the achievement of the required dual modality haemostasis device.

## 2.1.4 Characteristic Impedance

Characteristic Impedance is defined as the ratio of the E field or voltage and H field or current amplitudes for a single wave inside a transmission line. It is a function of the cable geometry and material choices. For the purposes of this document the characteristic impedance of a co-axial line can be calculated through knowledge of its capacitance and inductance per unit length as shown in eqs 2.2 and 2.3 , or through the use of an equation for known geometry given in eq. 2.4

$$L' = \frac{\mu_0 \mu_r}{2\pi} \ln \frac{b}{a} \text{ H/m} \quad (2.2)$$

$$C' = \frac{2\pi\epsilon_0\epsilon_r}{\ln (b/a)} \text{ F/m} \quad (2.3)$$

$$Z_0 = \sqrt{\frac{L'}{C'}} \quad \Omega \quad \text{or} \quad Z_0 = 60 \sqrt{\frac{\mu_r}{\epsilon_r}} \ln \frac{b}{a} \quad \Omega \quad (2.4)$$

This impedance can also be stated as the ratio of voltage to current for the travelling waves or:

$$Z_0 = \frac{V^+}{I^+} = \frac{V^-}{I^-} \quad (2.5)$$

Where  $V$  is the voltage and  $I$  is the current and the superscript + and - indicate the forward and reverse waves respectively.  $V$  and  $I$  can be described in phasor form

as follows:

$$\begin{aligned} \mathbf{V}^+ &= \mathbf{V}_0^+ e^{-\gamma z} \quad \text{and} \quad \mathbf{I}^+ = \mathbf{I}_0^+ e^{-\gamma z} \\ \mathbf{V}^- &= \mathbf{V}_0^- e^{+\gamma z} \quad \text{and} \quad \mathbf{I}^- = \mathbf{I}_0^- e^{+\gamma z} \end{aligned} \quad (2.6)$$

where  $\gamma$  is the complex propagation constant ( $\gamma = \alpha + j\beta$ ) and  $z$  is the position along the transmission line.

This impedance is intrinsic to the structure and is defined by the geometry and the chosen materials.

### Reflection Coefficient

Reflection coefficient measures how much an electromagnetic wave is reflected by some form of discontinuity such as the variation in impedance between source and cable. The reflection coefficient is the ratio of reflected voltage amplitude to that of the forward voltage amplitude and can be expressed in terms of impedance by the following. If we consider a transmission line of characteristic impedance,  $Z_0$ , terminated with a load impedance of  $Z_L$ , we know that the overall voltage at the terminals must be:

$$\frac{\mathbf{V}}{\mathbf{I}} = Z_L \quad (2.7)$$

Substituting the expressions for voltage and current of both the forward and reverse waves as given in equation 2.6 and as  $z$  is fixed:

$$\frac{\mathbf{V}^+ + \mathbf{V}^-}{\mathbf{I}^+ - \mathbf{I}^-} = \frac{\mathbf{V}^+ + \mathbf{V}^-}{\mathbf{I}^+ - \mathbf{I}^-} Z_0 = Z_L \quad (2.8)$$

The ratio of the voltage amplitudes of the reflected to the forward wave is the voltage reflection coefficient and can be solved as so:

$$\Gamma = \frac{V^-}{V^+} = \frac{Z_c - Z_g}{Z_c + Z_g} \quad (2.9)$$

Where  $Z_s$  is the impedance of the cable and  $Z_c$  is the impedance of the generator.

Given that we assume the generator to have a  $50\Omega$  output and the cable to have an impedance of approximately  $14\Omega$  we can estimate the reflection coefficient for the impedance discontinuity between the two objects.

$$\Gamma = \frac{14 - 50}{14 + 50} = -0.5625$$

### **Voltage Standing Wave Ratio**

With variation in the reflection coefficient, maximum and minimums of voltage can be plotted along the transmission line which repeat a full cycle every half wavelength. For the lossless transmission line these amplitudes are constant. The ratio of this maximum voltage to the minimum voltage is known as the VSWR and is equal to:

$$\text{VSWR} = \frac{V_{\max}}{V_{\min}} = \frac{V^+ + V^-}{V^+ - V^-} \quad (2.10)$$

Rearranging and dividing by  $V^+$  can also relate the VSWR to the reflection coefficient as follows:

$$\text{VSWR} = \frac{1 + |\Gamma|}{1 - |\Gamma|} \quad (2.11)$$

A VSWR of  $\infty$  implies that all of the wave is reflected back and is seen when the line is terminated in an open or short circuit. Alternatively a VSWR of 1 implies that there is no reflection and all the wave is absorbed by the load, when  $Z_0 = Z_L$ .

## Return Loss

For a mismatched termination, i.e.  $Z_0 \neq Z_L$ , part of the power incident at the load is delivered into the load whilst the rest is reflected back along the line. Return loss is defined as the ratio of this incident wave power to the power of the reflected wave. More generally:

$$RL = \frac{P_{in}}{P_{ref}} = \frac{P^+}{P^-} = \left( \frac{|V_{in}|}{|V_{ref}|} \right)^2 = \frac{1}{|\Gamma|^2} \quad (2.12)$$

Represented in terms of decibels:

$$RL = 10 \times \log_{10} \frac{1}{|\Gamma|^2} \quad (2.13)$$

## Transmission Coefficient

Using a further calculation, for the transmission coefficient, a graph can be constructed showing the variation in power transmission with varying cable impedance. Once again assuming a  $50\Omega$  generator output each impedance mismatch from  $0-100\Omega$  was calculated and converted to a power transmission percentage using the following equation.

$$\text{Power Transmission (\%)} = 100 \times (1 - \Gamma^2) \quad (2.14)$$

It is clear to see from fig 2.4 that variation in cable impedance, when connected to a  $50\Omega$  generator, affects power delivery especially as impedance deviates from that of the generator. A peak can be seen where the cable is optimally matched at  $50\Omega$  and any variation either side of this will lead to mismatch losses. The approximate decrease in power delivery if the cable was to be connected directly to a  $50\Omega$  microwave output can be seen at approximately  $14\Omega$  with a power transmission value of 68.4%. If a 100W input is assumed then a loss of 31.6W due to this

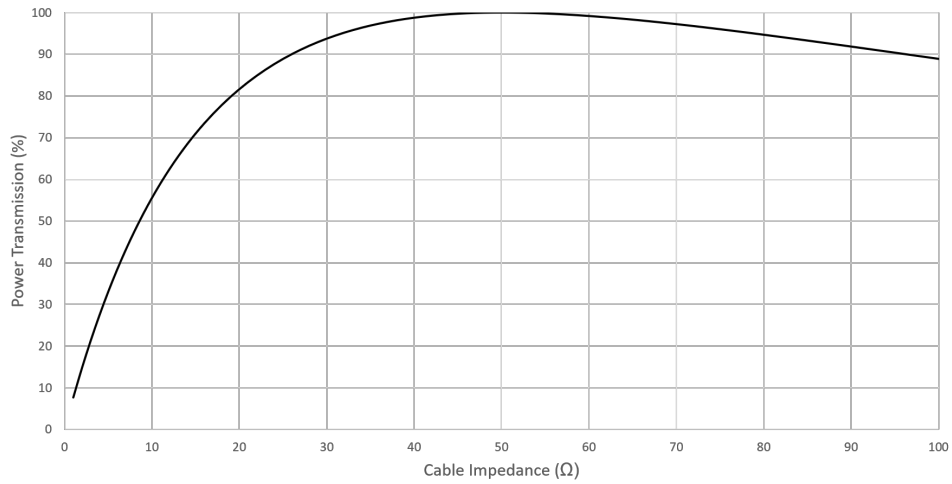


Figure 2.4: Graph showing variation in power transmission with change in cable impedance when connected to 50Ω generator

mismatch will manifest as heat and lead to the possibility of burns or of incorrect operation of the device.

This 50Ω impedance is also chosen as a balance between minimal attenuation and optimal power handling. Calculations and analysis have been conducted to show the effect of impedance on these parameters. Minimal attenuation occurs at approximately 77Ω whereas maximum power handling peaks at approximately 20Ω. A characteristic impedance of 50Ω is a reasonable compromise between the two and as such has become one of the industry standards. This analysis can also be used to justify the compromise in having a lower impedance for the cable created herein.

Table 2.1: Table showing difference in Power Handling and Attenuation at 14Ω and 50Ω

Impedance (Ω)	Minimal Attenuation (dB/m)	Maximum Power Handling (W)
14	0.26	519.35
50	0.11	325.69

It can be seen from figure 2.5 that optimum power handling and minimal attenuation occur at different impedances. Table 2.1 shows the difference between the expected cable impedance and 50Ω. Whilst there is slightly more attenuation due to impedance at 14Ω there is a distinct advantage when it comes to power handling

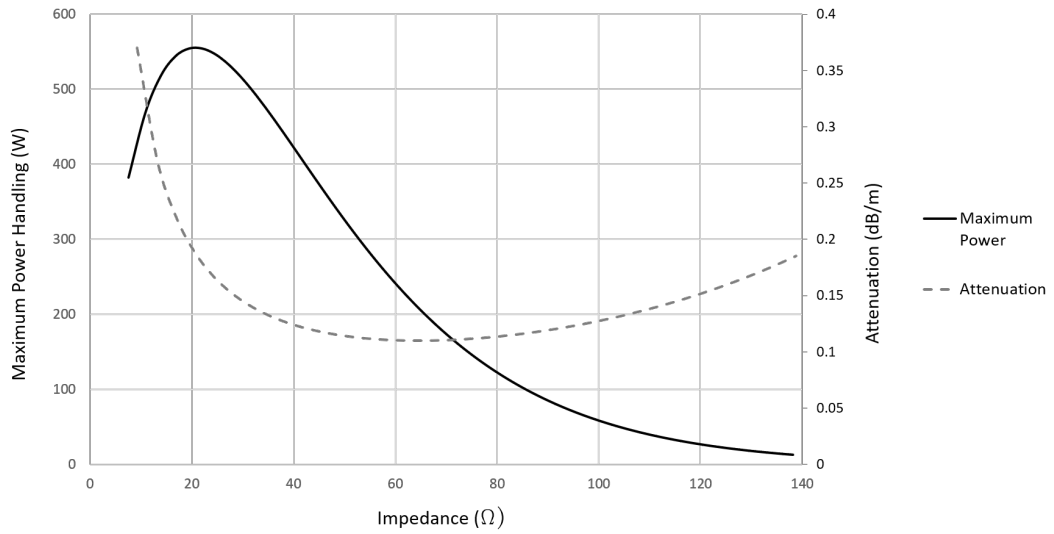


Figure 2.5: Graph showing maximum power handling and minimum attenuation as a function of impedance

most likely as a product of the varying geometry of the structure.

Figure 2.5 may seem to indicate that a cable with either lower or higher impedance than the standard would be of limited use. However this is not the case; the attenuation is more intrinsically linked to material selection than solely to the impedance. For example a cable made with a high dielectric strength solid PTFE will most likely handle much more power than would be calculated should only line impedance be considered.

## 2.1.5 Quarter Wave Transformation

One way to match structures with differing impedance is to use a quarter wave impedance transformer. For this research project the cable will have a lower impedance, as discussed later on, and will only be operated at a single frequency, 5.8GHz, so this becomes relatively straightforward. These transformer devices can be realised in a number of forms but at their core rely on the creation of a standing wave as a result of both creative and destructive interference of both voltage and current travelling waves along the line.



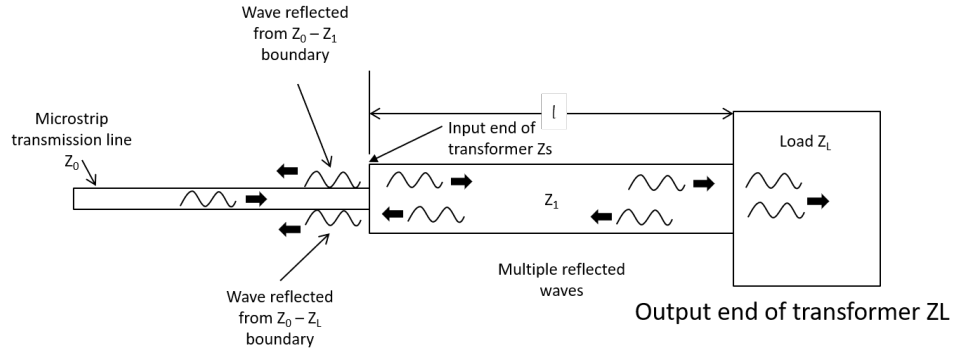


Figure 2.6: Diagram showing the operation of a quarter wave transformer

When the section is exactly a quarter wavelength or at least an odd multiple of quarter wavelength the waves reflected from the load destructively interfere with the wave reflected from the mismatch boundary and cancel each other out. This is possible because the reflection coefficients at the input and load have the same magnitude with opposite signs. The second requirement is that the impedance of the transformer be the geometric mean of the impedances that need matching. That is:

$$Z_{\text{trans}} = \sqrt{Z_1 \times Z_2} \quad (2.15)$$

Where  $Z_{\text{trans}}$  is the transformer impedance and  $Z_1$  and  $Z_2$  are the two impedances to be matched.

This stems from the impedance transformation equation as follows, assuming a lossless line, the propagation constant  $\gamma$  resolves to its imaginary phase constant of  $j\beta$ :

$$Z_{\text{in}} = Z_0 \frac{Z_L + jZ_0 \tan(\beta L)}{Z_0 + jZ_L \tan(\beta L)} \quad (2.16)$$

Where  $Z_{\text{in}}$  is the impedance at the specific point along the length  $L$ ,  $Z_L$  is the load impedance and  $Z_0$  is the characteristic impedance. For a quarter wavelength line the following is true:

$$L = \frac{\lambda}{4} \text{ and } \beta = \frac{2\pi}{\lambda} \rightarrow \beta L = \frac{\pi}{2} \quad (2.17)$$

and the impedance becomes, taking the limit as the tangent function argument approaches infinity.

$$Z_{in} = \lim_{\beta L \rightarrow \frac{\pi}{2}} Z_0 \frac{Z_L + jZ_0 \tan(\beta L)}{Z_0 + jZ_L \tan(\beta L)} \quad (2.18)$$

$$Z_{in} = Z_0 \frac{jZ_0}{jZ_L} = \frac{Z_0^2}{Z_L} \quad (2.19)$$

For example to match a  $50\Omega$  generator with a cable of  $14\Omega$  a transformer with an approximate impedance of  $26.46\Omega$  would be needed. The diagram shown in figure 2.7 shows the calculations of the reflection coefficients and impedances required.

$$50 = \frac{Z_0^2}{14} \rightarrow Z_0 = \sqrt{50 \times 14} = 26.46\Omega \quad (2.20)$$

As previously discussed this solution only works for a single frequency, although in practice even this approach will have a small bandwidth and could operate well either side of the match frequency and the structure must also have low loss such as for a short length of line. If a wider range of frequencies need to be used, a tapered transformer or multiple sections would allow a more broadband match could be achieved. [11, p. 84-87]

### 2.1.6 Attenuation

Attenuation is one of the most important characteristics of a co-axial line. Generating microwave power can be both complex and costly, to have that power just 'disappear' along the length of a line may be catastrophic. Consider a 6dB/m cable, by the time the power arrives at the distal end of a 1m cable you have lost almost 75% of the power which when coupled with any inefficiencies in the system could mean that

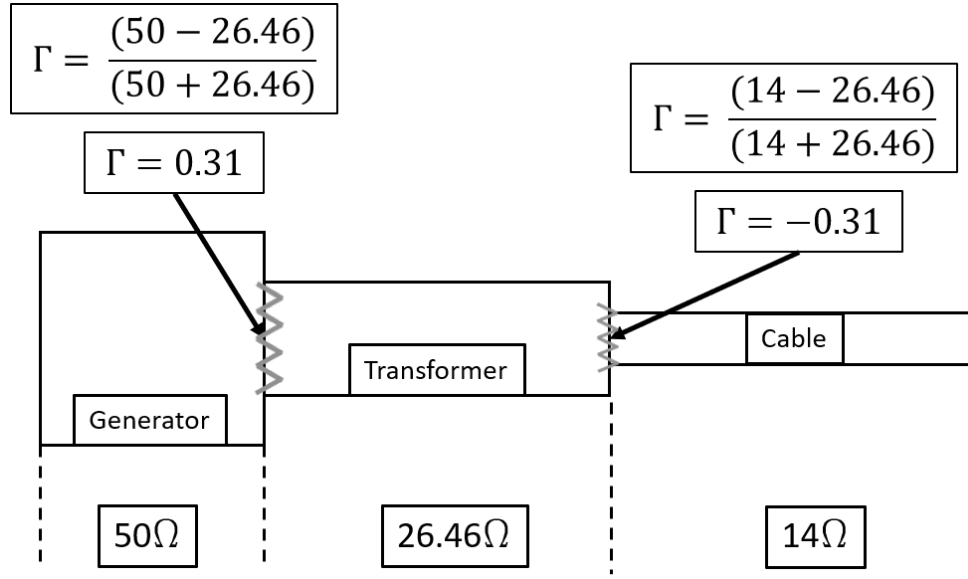


Figure 2.7: Diagram showing the equal reflection coefficients at both ends of the transformer

although the generator is capable of producing 100W, less than 25W of that power can be delivered into the tissue load, which also does not take into account the efficiency of the applicator or other losses introduced into the system.

Losses in co-axial cables can be split into two predominant categories; losses due to the conductive material associated with the inner and outer conductors and losses due to the dielectric material. Firstly let us consider the conductor losses.

$$\alpha_C = 13.6 \frac{\delta_s \sqrt{\epsilon_r} \left[1 + \frac{b}{a}\right]}{\lambda_0 \frac{b}{2} \ln \frac{b}{a}} \text{ dB/m} \quad (2.21)$$

where  $\delta_s$  is the skin depth of the conductive material as shown in eq 2.1,  $\epsilon_r$  is the relative permittivity of the dielectric material,  $b$  is the outer diameter of the inner conductor,  $a$  is the outer diameter of the inner conductor and  $\lambda_0$  is the wavelength in free space for the frequency of operation.

This equation will give an idea of the conductor losses but makes a few key assumptions. It assumes that the two conductors are of the same materials with the same conductivities; therefore having equal skin depth values. More complex forms of the equation can be found along with further information in [12]. What can be

seen from this equation is that the loss in a co-axial cable is directly related to the resistance through the conductive materials and that it also varies with frequency.

A similar equation can be given for losses due to the presence of the dielectric material:

$$\alpha_c = 27.3 \frac{\sqrt{\epsilon_r} \tan \delta}{\lambda_0} \text{ dB/m} \quad (2.22)$$

where  $\epsilon_r$  is once again the relative permittivity and  $\tan \delta$  is the dissipation factor of the dielectric material.  $\lambda_0$  is the same as in eq 2.21.

Both of these equations have been used extensively along with their more complex counterparts to ensure optimal material and geometry choices for the cable as discussed further on.

## 2.1.7 Microwave Test Measurements

### S Parameters

S, or scattering, Parameters describe the response of a system or network to a signal incident to any of its ports. Usually given in the form  $S_{i,j}$  where  $i$  is the responding and  $j$  is the incident port. A diagram showing the set-up of a standard device under test and associated S parameters can be seen in figure 2.8

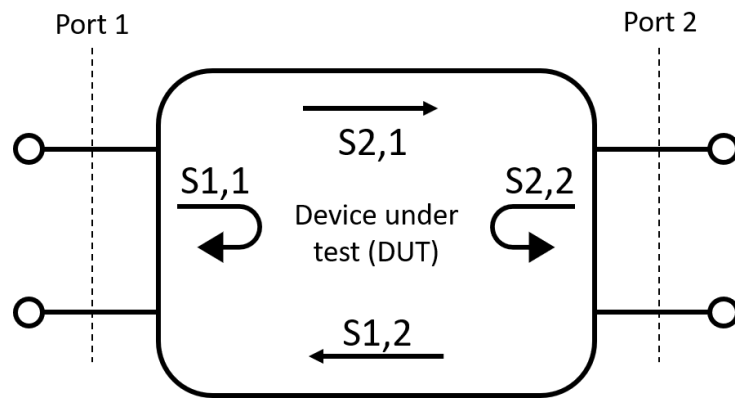


Figure 2.8: S Parameter Diagram

For a two port network, four S Parameters can be given:

- $S_{1,1}$  - Input Reflection Coefficient
- $S_{2,2}$  - Output Reflection Coefficient
- $S_{2,1}$  - Forward Transmission Coefficient
- $S_{1,2}$  - Reverse Transmission Coefficient

All these parameters are complex numbers, and whilst not always necessary, can be presented as both magnitude (dB) and phase (degrees). For magnitude, as the measurements are complex voltage ratios, it is calculated as:

$$S_{i,j}(\text{dB}) = 20 \times \log[S_{i,j}(\text{magnitude})] \quad (2.23)$$

Most of the time the S Parameters we talk about are the small signal S Parameters as measured by a Vector Network Analyser (VNA).

## VNA

The Vector Network Analyser is a device which measures the S Parameters of a system as discussed above. Usually consisting of a device with two ports, modern analysers can measure networks with an arbitrary number of ports. The VNA, a Wiltron 360b, used throughout this research can be seen in figure 2.9 <sup>2</sup>.

The most common measurement output is in the frequency domain. This means that for a specified range of frequencies a sinusoidal test signal is applied to the device under test (DUT) and the output measured. This can then be output as a magnitude plot as shown in figure 2.10.

As can be seen from the above figure, the x axis gives the frequency whilst the y axis gives either the phase or magnitude. As this is a  $S_{1,1}$  measurement the dip at XX GHz shows a good match or minimal reflection at that frequency.

---

<sup>2</sup>Credit: <https://www.anritsu.com/en-us/test-measurement/products/360>



Figure 2.9: Wiltron model vector network analyser

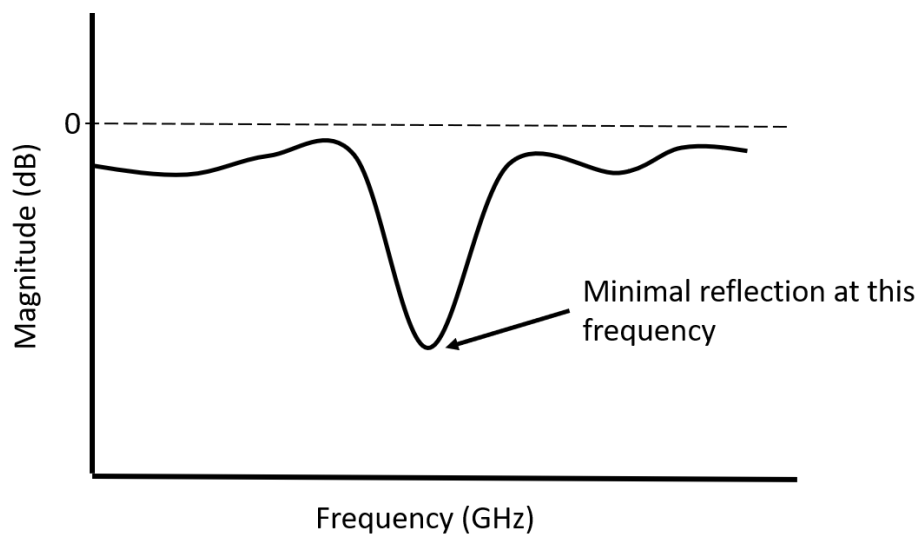


Figure 2.10: Example output of magnitude  $S_{1,1}$  measurements

An optional feature of the Wiltron 360b VNA is the ability to convert into the time domain. Use of the fourier transform allows for the frequency information to be converted into the time domain which allows for the locating of impedance discontinuities or the inspection of various parts of a structure. Time domain measurements have been used extensively throughout this research. An example plot can be seen in

figure 2.11

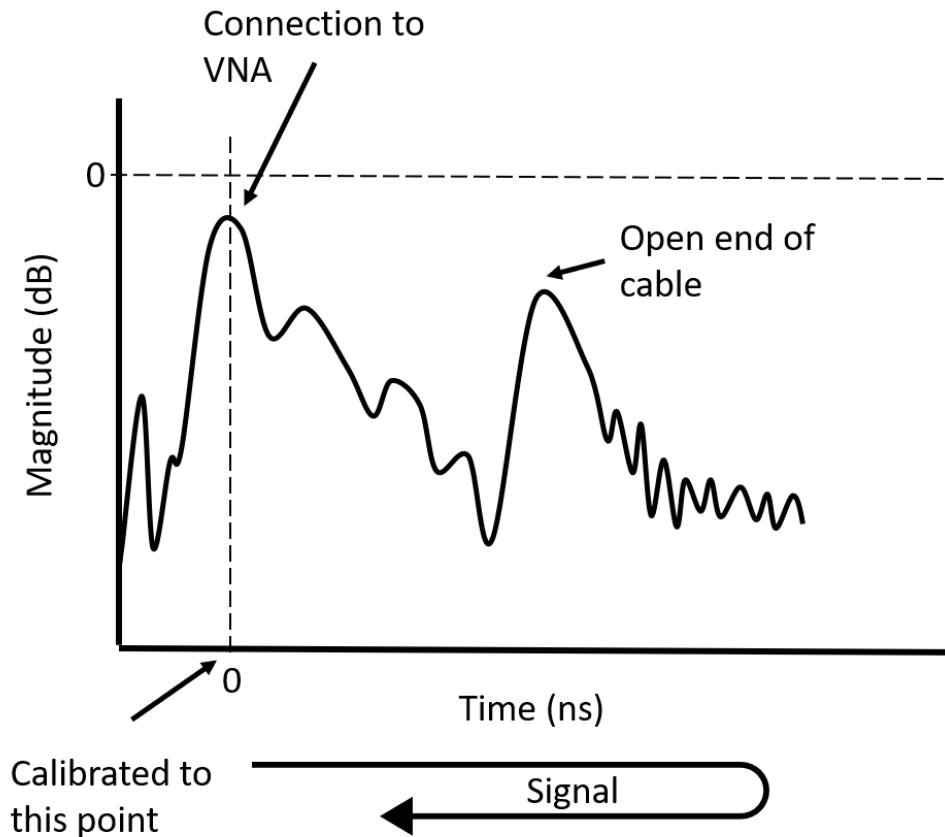


Figure 2.11: Example output of time domain S1,1 measurements

For these plots a frequency range of 5.6 - 6 GHz was used to ensure that the device was operating correctly at the intended frequency. A smaller frequency bandwidth is used to increase the distance measurement capability, as required for the cable measurements discussed later. Should a smaller distance and therefore higher resolution be needed a wider bandwidth should be used. The measurements herein are set up to be a balance between these two requirements.

The two humps shown in figure 2.11 show the connector end and the open end of the cable. Analysis of the magnitude of both of these humps is used further on to measure the cable attenuation and connector suitability. The signal, as a reflection measurement, takes into account the two way signal path and allows for the attenuation between the two points to be calculated.

## **2.1.8 Microwave Simulation**

Although a theoretical first approach has been used throughout this research, due to some of the more complicated structures further computer simulation was required. The majority of this electromagnetic simulation was carried out using CST Microwave Studio which is a tool for the 3D electromagnetic simulation of high frequency components.

### **CST Basics**

The simulations shown in this research were all carried out using the Time Domain Transient solver module in CST which allows the simulation of broadband frequency results such as S Parameters. This transient solver is based on the Finite Integration Technique and has high efficiency for most high frequency applications including connectors, transmission lines and antennas.

All the structures are modelled in 3D and simulation settings are then used to approximate the expected usage of the device. Predominantly this consisted of running a frequency sweep from 0GHz - 10GHz to give an idea of the device operation especially at the required frequency of 5.8GHz.

### **Results**

The reader will see a number of outputs from the CST simulations including 2D results such as S Parameters shown as magnitude vs frequency graphs and 3D results which include Power Loss Density or E/H Field results.

One of the most useful outputs is the Power Loss Density plot which shows the sum of electric or magnetic power dissipated inside of the calculation domain. The standard visualisation of this monitor shows a colour map which corresponds to the amount of dissipated power. These results are ideal for assessing energy delivery zones or finding possible power flow issues within structures.



This power loss density can be linked to temperature, as per equation 2.24, if one considers the thermal properties of the materials. The  $Q$  term directly relates to the power loss density. Suffice to say the areas which have a higher power loss density tend to indicate those areas which would increase in temperature. It is for this reason that these plots are used to estimate ablation zones and shapes. Assessment of temperature and power flow is shown later in section 4.2.5.

$$\rho C_p \frac{\delta T}{\delta t} = \nabla \cdot (k \nabla T) + Q - Q_p + Q_m \quad (2.24)$$

Where  $\rho$  is the mass density,  $c$  is the specific heat capacity,  $k$  is the thermal conductivity,  $T$  is temperature,  $Q$  is the absorbed electromagnetic energy,  $Q_p$  is the heat loss due to microvascular blood perfusion and  $Q_m$  is the metabolic heat generation. Further discussion on this is provided in [13].

Farfield monitors are also used to show the field behaviour far away from the corresponding source of the EM waves. These are portrayed in this research as absolute plots which is derived from the two tangential and radial components. The main reason for inclusion of these plots is to add confidence to the  $S$  parameters to ensure that the energy was being delivered into the tissue and not being radiated into the space around the device. Whilst the plots contain the original structure it is important to note that this visualisation is in the farfield and does not indicate exact positioning of radiation.

### 2.1.9 Biological Effects of Microwaves

For consideration of the use of microwaves within the medical industry, it is important to make two main distinctions; Diagnostic and Therapeutic. Diagnostic technology usually involves imaging of tissues and differentiate of their structures based upon their dielectric properties. Therapeutic technology usually employs microwaves to heat up structures to achieve various treatment effects; whether this be

to coagulate a bleeding vessel as in the device presented herein or the ablation of tumours.

### Dielectric Heating

The application of microwave energy to human tissue results in dielectric heating. The application of an alternating electric field causes the molecules to shift and rotate as the electrons constantly try to orient themselves in the field creating resistance due to the intermolecular forces holding the structure together. When considering application to human tissue, the majority of tissues within the body contain a substantial amount of water which, having a polar structure, continually reorientates itself within the electric field and when out of phase with this field results in heating due to energy loss [14].

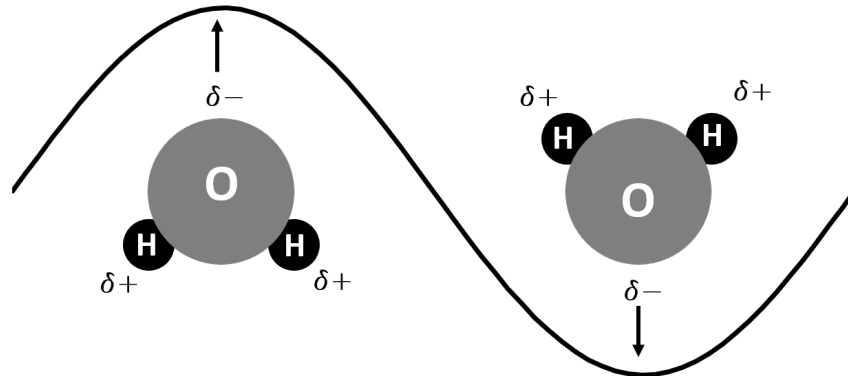


Figure 2.12: Dipole reorientation of water in response to an alternating electric field

### ICNIRP and Safety

The International Commission on Non Ionising Radiation Protection (ICNIRP) is a group formed to examine the problems arising in the field of protection against the various types of non ionising radiation. Their guideline on limiting exposure

to time-varying electric, magnetic, and electromagnetic fields (up to 300GHz) gives the recommended exposure limits to people who are in the vicinity of these kind of fields. Reference to this document and commission is given later on when discussing handpiece shielding.

## 2.2. Upper Gastrointestinal Bleeding

UGIB is defined as any bleeding proximal to the ligament of Treitz, a thin suspensory muscle found at the duodenojejunal flexure as seen in figure 2.13<sup>3</sup>. This is the standard used in clinical practice to separate the upper and lower parts of the gastrointestinal tract. UGIB can be diagnosed through a number of methods but will usually present as overt symptoms such as haematemesis (vomiting of blood, sometimes described as coffee grounds), melana (tarry black stool) or haematochezia (red blood per rectum). UGIB can also be diagnosed through secondary symptoms such as those related to anaemia or blood loss; including dizziness, fatigue or syncope.

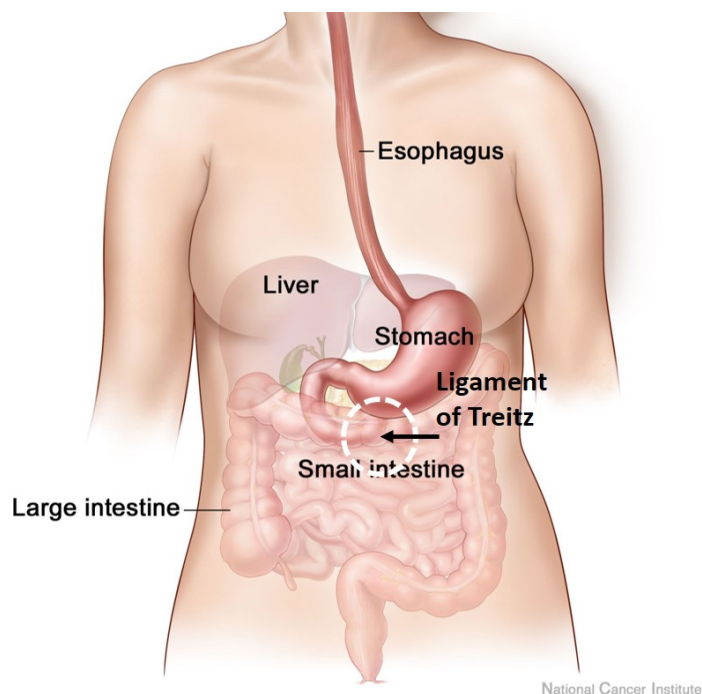


Figure 2.13: Simple structure of the gastrointestinal tract

<sup>3</sup>Credit: <https://www.ncbi.nlm.nih.gov/pubmedhealth/PMHT0022855/>

As such there are a number of conditions and a number of locations where UGIB can occur and this bleeding, therefore, can be classified in a number of ways. Initially bleeding can be classified as variceal or non variceal. The former concerns vessels which have become dilated and enlarged due to portal hypertension, an increase in blood pressure through the portal vein. This pressure can occur due to a number of reasons including blood clots or increased resistance in the liver due to cirrhosis. Examples of this can be seen in fig 2.14 <sup>4</sup> . When this pressure gets too high, these vessels can become damaged and potentially burst leading to UGIB.

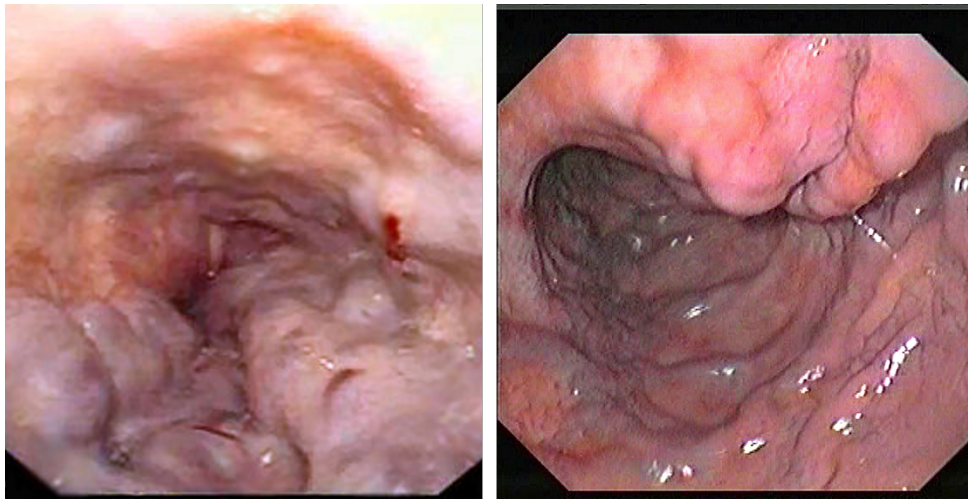


Figure 2.14: Gastroscopic images of oesophageal varices

UGIB can be further classified based upon anatomical location and can usually be separated into three categories; for this research and clinical application oesophageal bleeding will be most important but the other two include gastric and duodenal.

### 2.2.1 Oesophageal Anatomy

The oesophagus is a tube which connects the pharynx, or the part of the throat just behind the mouth, to the stomach. It is approximately 25cm long and is approximately 20mm in diameter when distended. The wall of the oesophagus comprises numerous

---

<sup>4</sup>Credit: [https://commons.wikimedia.org/wiki/File:Esophageal\\_varices\\_-\\_wale.jpg](https://commons.wikimedia.org/wiki/File:Esophageal_varices_-_wale.jpg)

layers as discussed in the histological section of this work but is usually around no more than 5.5mm [15].

### **2.2.2 Oesophageal Bleeding**

Oesophageal varices account for approximately 5-30% of UGIB cases although this varies with population. Patients are likely to have a higher chance of rebleed and possible death than patients with other sources of UGIB [16]. Oesophageal ulcers are a much rarer cause of UGIB and are defined as a break in the esophageal mucosa with a clear circumscribed margin [17]. Mallory-Weiss tears are defined as tears in the oesophagogastric junction, first described in 1929, and are found in approximately 3-15% of all patients with acute UGIB [18].

### **2.2.3 Gastric and Duodenal Bleeding**

Bleeding can also be classified as UGIB if it occurs within the stomach or the duodenum. There are numerous conditions including ulcers, tumours, varices and lesions which can occur in both of these places and have just as much an impact on the human body as those conditions found in the oesophagus. A relatively uncommon condition, Dieulafoy's lesions, usually occur at the gastro-oesophageal junction and are caused by a large vessel running close to the submucosa which becomes exposed through mucosal and/or arterial erosion [19]. More common is the incidence of bleeding due to peptic ulcers. A large proportion of UGIB is thought to be caused by these lesions [20], with duodenal ulcers being more common in the United States [21].

## 2.3. Haemostasis

### 2.3.1 Background

Haemostasis, from the Greek; *aima* (blood) and *stasis* (halt). Quite literally the halting of blood was first documented as the use of vegetable and mineral styptics by the physician Machaon to heal Menelaus before the walls of Troy circa 1200BC [22]. Fast forward to approximately 500BC and it is found that procedures such as wrapping a wound with cold bandages and the application of fig tree juice were used to stop bleeding. [23] Throughout history thermal techniques such as cauterisation have been used to stop major bleeds; the procedure largely consisted of a metal object heated until glowing red and then applied directly to the bleeding site. It is now known, however, that a more accurate and controllable method of thermal energy delivery is required as historical cauterisation will likely have caused damage to large amounts of tissue both at the intended site and also collateral damage to surrounding tissue, whilst providing a breeding ground for bacteria and infection [24].

Some forms of haemostasis used today mirror those used in history including haemostatic powders and mechanical clips or ties. This thesis focuses on the use of energy to produce haemostasis in a more controlled manner and demonstrates how the microwave energy can be delivered not only locally but precisely into tissue using non-invasive endoscopic techniques.

### 2.3.2 The Biological Basics

The bodies natural response to injury, specifically in the case of bleeding, is effectively to limit blood loss. To do this a number of biological processes occur as shown in fig 2.15 <sup>5</sup>

Figure 2.15 shows a detailed pathway of the bodies natural response to blood

---

<sup>5</sup>Credit: Diagram by Joe D, distributed under a CC BY-SA 3.0 Licence

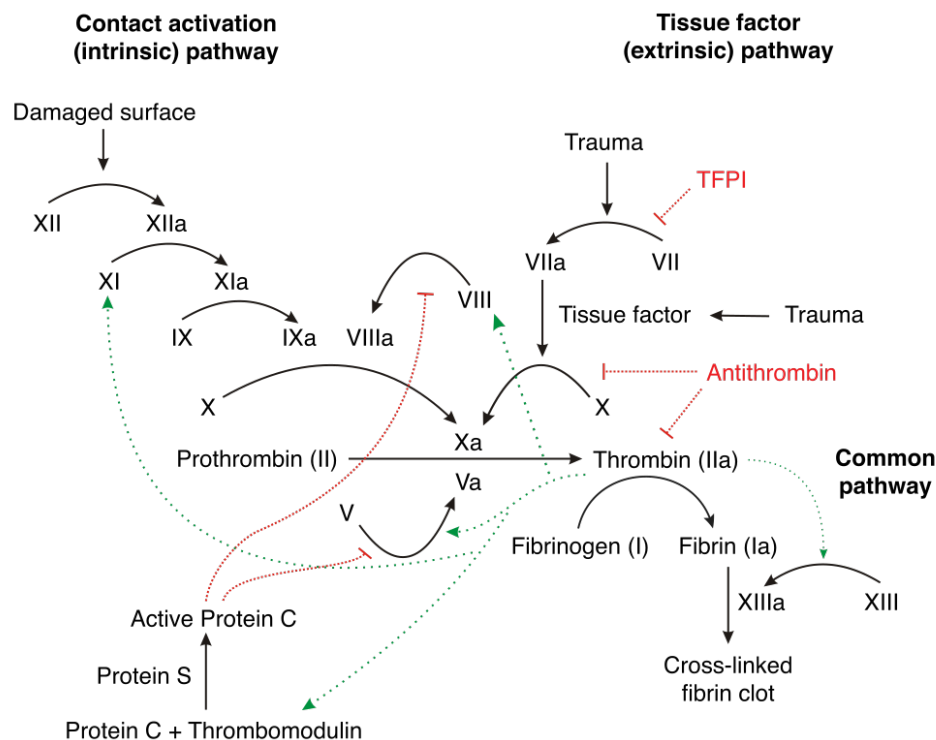


Figure 2.15: Detailed pathway showing the natural response of the body to blood loss.

loss. There are numerous enzymes and proteins which make up the pathway and the main 'spark' which sets off this cascade can be seen in the extrinsic pathway. Trauma causes the tissue factor, or factor III, to combine with factor VII and activate factor X which in turn catalyses the reaction of prothrombin into thrombin. This catalysation then causes the intrinsic pathway to begin with subsequent catalysation of each factor. This intrinsic pathway is also sometimes called the amplification pathway as this rapidly increases the amount of thrombin in the blood stream, in turn activating the common pathway as seen in the bottom right of figure 2.15. This common pathway concerns the conversion of fibrinogen to fibrin which subsequently cross links to harden into a 'plug' to stop the bleeding.

Whilst being quite a complex response, the coagulation pathway can be broadly defined under three main steps.

1. Vascular spasm or vasoconstriction acts to constrict the vessels surrounding

the site of injury both to limit blood flow and to expose collagen. Platelets then adhere to the surface of this exposed collagen and form an initially weak platelet plug.

2. Primary haemostasis then occurs with the release of numerous chemicals and proteins such as Von Willebrand factor, adenosine diphosphate and serotonin. [25]
3. Finally a number of clotting factors are activated following the coagulation cascade as shown, this step is effectively the platelet plug becoming harder as blood cells become trapped upon and within it and form a thrombus, or clot [26]. This is a major step in the healing of wounds but can have detrimental effects should the thrombus detach and migrate to any of the major organs leading to the possibility of ischaemic stroke.

Whilst being effective in healing everyday maladies and small bleeds associated with wear and tear, there needs to be effective techniques for the management of larger bleeds for which the natural response of the body is not sufficient or able to coagulate fast enough before too much blood is lost. These techniques can vary in application, efficacy and suitability and are later discussed in further detail. Some of the techniques enhance the bodies ability to undertake the coagulation cascade whilst some circumvent it entirely. In fact it is the bodies response to bleeding which, for the purposes of this research, allow us to define large and small bleeds. If the body can coagulate the bleed then we shall deem it small. If a further haemostatic intervention is required then it is classified as large.

Techniques such as the use of clips, ligation bands and suturing provide mechanical support to the wound edges to enable the coagulation cascade to take place and close the wound in order to limit patient blood loss. Energy based thermal techniques actually alter the structure of the wound and bypass most of the cascade entirely. This has certain advantages; such as much faster control of bleeding, and through



the use of novel device structures can be achieved endoscopically or in minimally invasive ways without the need to open up the patient and therefore less risk and cost, some disadvantages could include damage to surrounding tissue and infection risks but these can be mitigated with good design, technique and infection control policies. These considerations will be further assessed as specific modalities are discussed.

### **2.3.3 Thermal Haemostasis**

The application of heat to a bleed causes the breakdown of all cellular and extra cellular matrix membranes. Subsequently all of the released proteins are coagulated and aggregate into an amalgamation of tissue to produce a contiguous tissue mass which closes vasculature and joins tissue structures. Collagen is one of the most common structural proteins, especially in blood vessels and heat causes this to unravel, shrink in length and swell in diameter. As the temperature increases the collagen morphs into a glassy state and once completely denatured, it is reabsorbed and replaced by scar tissue [27].

This breakdown of cellular structures through the application of heat drives the development of devices which can initiate this process through the application of energy controllably into a specific area thus minimising the risk of damage to healthy surrounding tissue.

## **2.4. Current Methods of achieving haemostasis**

There are a number of methods commonly used throughout the world for the treatment of UGIB and various other causes of bleeding. These have been discussed below and form a reference with which to compare the complete device presented herein.

## 2.4.1 Mechanical Modalities

All mechanical methods of haemostasis work in a similar way biologically and emulate that of sutures or plasters as used for external skin wounds. They are there to provide structure and closure to the wound and allow the body to naturally activate the coagulation cascade to stop the bleed and allow the wound to heal. These devices take many forms and some are discussed below.

### Clips

Endoscopic clips can be used for a number of reasons within the gastrointestinal tract but mostly emulate the effect of sutures. They can be used for marking of treatment sites to allow for radiologically recognisable landmarks [28], treatment of polyps [29], and of course for haemostatic treatment.



(a) Instinct Hemoclip from Cook Medical.



(b) Resolution Clip from Boston Scientific.

Figure 2.16: Examples of endoscopic clips used for haemostasis

Clips have been shown to be successful in the treatment of many casuses of gastrointestinal (GI) bleeding [30] including ulcers, Mallory-Weiss tears and many other indications. Two examples of clips can be seen in fig 2.16 <sup>6, 7</sup> with many more

<sup>6</sup>Credit: <https://www.businesswire.com/news/home/20140423005134/en/Cook-Medical-Launches-Instinct%E2%84%A2-Endoscopic-Hemoclip>

<sup>7</sup>Credit: <http://www.bostonscientific.com/en-US/products/clips/resolution-clip.html>

currently on the market or in development. Some studies suggest that clips offer an advantage over other haemostatic modalities [31], but the general consensus appears to show no obvious and definite improvement in outcome over other methods [32]. Some literature has suggested that there may be difficulty in the accurate and correct placement of the clips [33] depending on the indication and technique required.

The duration of effective clipping has been shown to also vary from patient to patient; ranging from less than one week up to five weeks [34]. One case study suggests a clip was able to remain in place for at least 26 months [35]; this however may be much shorter should the bleed be superficial and the clip only attached to the outermost mucosal layers of the GI tract. Due to this introduction of a physical construct within the GI tract the risk of clips detaching from the treatment site and causing complications or post-operative bleeding is a genuine concern for the clinician for a number of reasons such as due to poor placement and adhesion to the mucosa or due to being knocked off by expansion and contraction as food passes through the GI tract.

### **Ligation Bands**

Ligation bands offer similar mechanical outcome as clips but are especially useful in cases where clipping would be difficult such as in retroflex, where the release mechanism is difficult to activate or where a bleed has a large fibrotic base and clip usage may lead to further trauma to the vessel and therefore actually increase bleeding [36]. Ligation banding has, however, been shown to be technically easier and more able to be used in larger perforations or at differing angles [37]. These devices are especially useful in the treatment of oesophageal varices.

Examples of the devices used in endoscopic band ligation can be seen in fig 2.17<sup>8</sup>,  
<sup>9</sup>. These devices fit over the top of the endoscope to allow for maximum visualisation

---

<sup>8</sup>Credit: [https://www.cookmedical.com/products/esc\\_mbl\\_webds/](https://www.cookmedical.com/products/esc_mbl_webds/)

<sup>9</sup>Credit: <http://www.bostonscientific.com/en-US/products/band-ligator/speedband-superview-super-7.html>



(a) 6 Shooter Universal Saeed Multi from Cook Medical.



(b) Speedband Superview Super 7 from Boston Scientific.

Figure 2.17: Examples of endoscopic band ligators used for haemostasis

of the bleed prior to placement and also allows for multiple bands to be placed without the need to remove the endoscope to reload the bands in between applications.

Literature suggests that the use of banding for acute variceal bleeding within the oesophagus is an effective therapy and has few adverse outcomes. For instance some patients report difficulty swallowing or experience mild chest discomfort for a few days following band ligation [38].

## 2.4.2 Injection Modalities

The most common modality for the treatment of upper GI bleeding is to use injection to stop bleeding either through physical blocking of vessels as in the use of surgical glues, or to achieve chemical constriction of the vessels as in the use of adrenaline. Injection provides high levels of successful haemostasis in gastrointestinal bleeding but usually requires the use of an additional modality such as mechanical clamping or thermal coagulation to minimise re-bleed rates. One device can be seen in figure 2.18 <sup>10</sup>

<sup>10</sup>Credit: <https://medical.olympusamerica.com/products/needle-master-injection-needles>



Figure 2.18: Needlemaster Single-Use Injection Needle from Olympus.

### **Adrenaline**

The use of adrenaline has been used to achieve haemostasis since 1970 [39] and is reported to have positive outcomes [40]. Standard clinical procedure is to inject small amounts of 1:10,000 concentration adrenaline into four quadrants around the bleed or lesion and finally inject into the center of the bleed.

This has a dual effect of combining both temporary local tamponade of the vessels with chemical vasoconstriction. Literature suggests that approximately 13ml of adrenaline is required for optimal haemostasis. [41]. As the haemostatic effect results from this temporary local tamponade and vasoconstrictive effect, adrenaline injection is usually followed by treatment of a longer lasting modality such as mechanical or thermal haemostasis.

### **Sclerosing Agents**

Sclerotherapy, along with band ligation, remain one of the most popular treatments and methods for control of oesophageal varices, or dilated and enlarged vessels within the oesophagus, with the most common chemicals being Ethanolamine Oleate, Polidocanol or Sodium Morrhuate as discussed in [42]. As a general overview the agent is injected into the lumen of the varix or vessel which causes thrombosis and inflammation of the surrounding tissues thus inducing haemostasis both via

temporary local tamponade, similar to the use of adrenaline, but also stimulating the bodies natural coagulation cascade.

### **Surgical Glues and Haemostatic Powders**

Other chemicals are used to achieve haemostasis within the upper GI tract and accomplish this in various ways. Tissue glues such as Histoacryl [43] and Glubran2 [44] have shown good efficacy in the treatment of various bleeds with polymerisation of the chemical occurring on contact with blood and sealing of the wound occurring quite rapidly.

Haemostatic powders, depending upon their functionality, achieve haemostasis in different ways. They can either form a seal around the vessel to physically occlude it or they can actually enhance the natural response of the body by initiating the coagulation cascade earlier than intended. Hemospray [45] showed optimal haemostasis when compared with the use of Histoacryl, or medical 'super glue', and Lipiodol. This works by forming a physical barrier over the bleeding site, increasing local concentration of clotting factor and activating the coagulation cascade [46].

### **2.4.3 Energy Based Thermal Modalities**

Thermal energy has been used for many years to achieve cauterisation of wounds and to treat disease. Initial concept cauteries have been known since the development of the first commercial electrosurgical equipment in 1920 which was then introduced to clinical practice by Harvey Cushing [47].

#### **Radio Frequency**

The use of radio frequency (RF) energy to cut, coagulate and remove tissue involves the introduction of alternating current (AC) energy at frequencies around the AM radio band eg; 540kHz to 1700kHz, but can be lower than this; such as the generator

used by Creo Medical which utilises an RF frequency of 400KHz. This energy is delivered into the tissue to achieve the desired treatment or clinical effect. RF modalities can be subdivided into two categories.

### Monopolar RF

Monopolar RF, as shown in figure 2.19, where the energy travels from the single pole treatment applicator through the body into a large ground return electrode applied elsewhere on the body.

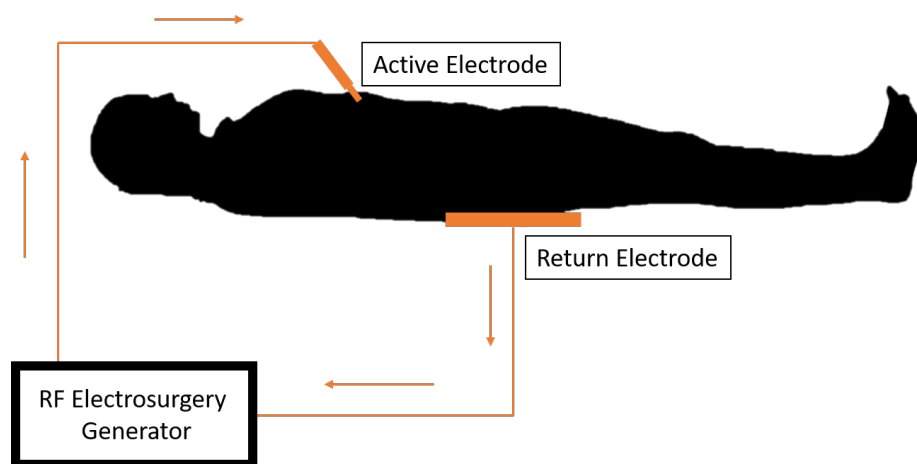


Figure 2.19: Diagram showing operation of monopolar RF electrosurgery.

These systems require the treatment applicator to have a very small area compared to the return plate; this difference in area means the current density at the applicator and therefore delivered into the tissue is very large compared to the current density at the return electrode. This energy focus at the treatment site is designed to limit the risk to the patient.

The standard surgical tool used in monopolar RF treatments is often referred to as a Bovie and an example of this can be seen in fig 2.20.

Multiple electrode tips can be attached to the device in fig 2.20 <sup>11</sup> to achieve various surgical effects. When coupled with a generator capable of controlling the

---

<sup>11</sup>Credit: <http://www.boviemedical.com/pencils/>



Figure 2.20: ESP1 standard Bovie Pencil from Bovie Medical Corporation

energy delivery waveforms and delivery power levels, it is clear to see why devices such as these are widely used in a variety of medical applications and treatments.

At its most basic monopolar RF treatment is based on the passing of electrical current completely through the patient where they can easily be burned through the incorrect use of grounding pads. Current can pass through the patient in unusual and unexpected paths which can cause internal burns, adhesions or even fistulas; which are unintended communication paths or channels between two surfaces. These can cause many problems and possibly introduce other comorbidities for the patient especially if they occur within vital organs such as the bladder or even the heart. Due to the high voltages associated with monopolar RF, it can also produce electromagnetic interference and have an effect on other devices including patient monitoring equipment [48].

### **Bipolar RF**

Bipolar devices, as seen in figure 2.21 have both poles on the applicator itself which allows the energy to travel between them and through the patient tissue allowing for a much more controlled and localised tissue effect without the risk of unintended burns as the energy travels away from the treatment site to the return electrode.

RF energy based modalities tend to require a much higher voltage. Monopolar RF treatments usually range between 1-5kV whilst bipolar treatments are around 200-600V. Conversely microwave treatments use much lower voltages usually in the range of 5-50V. These are all peak to peak voltages and as such it is obvious that



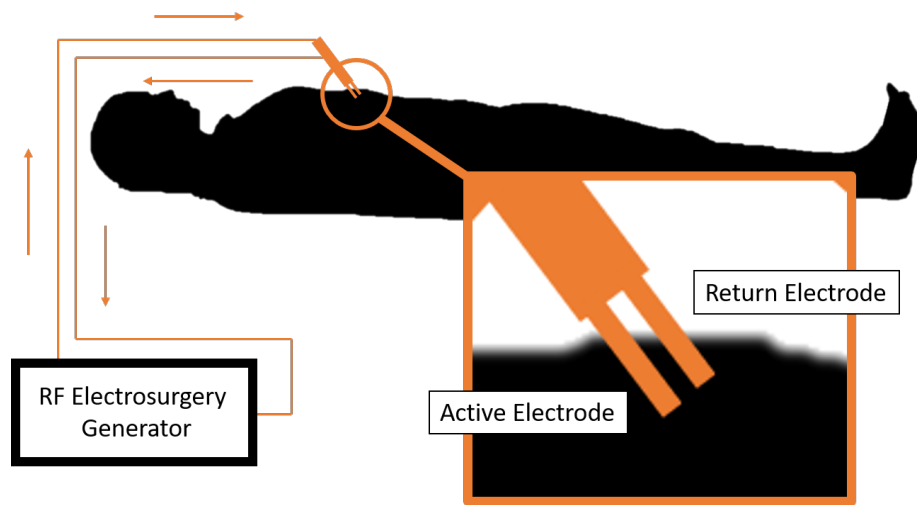


Figure 2.21: Diagram showing operation of bipolar RF electrosurgery

microwave applicators use a much lower and therefore safer voltage range.

One interesting development in RF electrosurgery is the use of precision bipolar forceps as seen in fig 2.22<sup>12</sup>. These combine the efficacy of bipolar RF energy delivery into a structure which can allow for much more diversity in treatment than having a single probe. They can be used to coagulate or dessicate tissue between them or each probe can be used individually.



Figure 2.22: Covidien Valleylab Bipolar Forceps from Medtronic

Bipolar devices allow for more precise control of the current delivered into the patient between the electrodes and a variety of different devices have been developed to suit a number of clinical needs.

Bipolar RF electrosurgery, overall, has less risk and therefore fewer adverse effects on the patient as the current passes from a first electrode locally through tissue and back to the second electrode. This creates a current path which is much shorter and

<sup>12</sup>Credit: [http://atriummeditech.com/product.php?cat\\_id=58&subcat\\_id=567](http://atriummeditech.com/product.php?cat_id=58&subcat_id=567)

contained; meaning the clinician can tailor the energy delivery to the exact location or structure where it is needed. Voltages are much lower as previously discussed as well meaning a much safer treatment option for the patient.

A number of devices have been specifically designed to use bipolar RF energy to achieve haemostasis. Two examples of these can be seen in fig 2.23<sup>13 14</sup>.



(a) Injection Gold Probe from Boston Scientific.



(b) BiCOAG Haemostasis Probe from Olympus.

Figure 2.23: Examples of bipolar haemostasis probes

The Gold Probe from Boston Scientific utilises two helical electrodes to deliver bipolar RF energy and is supplied in two different sizes. The smaller version is 7Fr (2.3mm) and the larger is 10Fr (3.3mm) both contain an extendable needle to achieve the delivery of liquids such as adrenaline for vasoconstriction. Studies have shown that the Gold Probe with integrated needle performs more optimally, is quicker and more convenient when compared to separate probe and needle devices [49, 50]. Due to the very similar nature, both in terms of clinical effect and physical size of the device, to the haemostat presented in this piece of research comparison bench tests have been carried out between the two devices; the results of which are given in section 7.2.2.

The BiCOAG Haemostasis probe, figure 2.23b, from Olympus is a single use probe which uses bipolar RF energy to achieve haemostasis at virtually any angle with ease of attachment to many bipolar generators. It is provided in two sizes; 10Fr and 7Fr

<sup>13</sup>Credit: <http://www.bostonscientific.com/en-US/products/probes/injection-gold-probe.html>

<sup>14</sup>Credit: [https://www.olympus.com.ru/medical/en/medical\\_systems/products\\_services/product\\_details/product\\_details\\_108994.jsp](https://www.olympus.com.ru/medical/en/medical_systems/products_services/product_details/product_details_108994.jsp)

or 3.3mm and 2.3mm with a working length of 3.5 meters.

### Argon Plasma Coagulation

Argon Plasma Coagulation (APC) is an alternative to the bipolar RF haemostasis probe and makes use of a stream of ionized argon gas to conduct the high frequency current to the site of application. Due to the use of this ionized gas it is termed as a non contact method of treatment. Due to the physical process of the APC the plasma creates uniformly deep zones of devitalisation, coagulation and desiccation [51]. The basic function of APC can be seen in fig 2.24 <sup>15</sup> as discussed in [52].

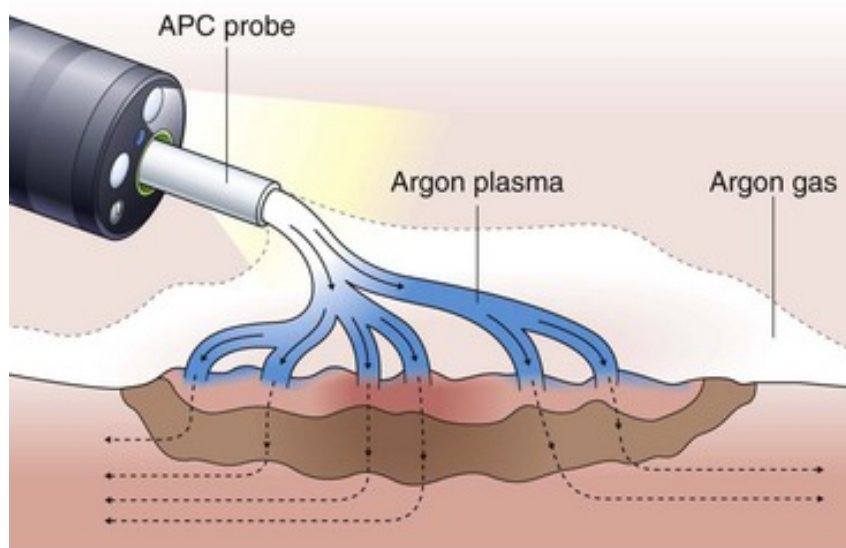


Figure 2.24: Diagram showing functionality of APC

As can be seen, the device emits a stream of argon gas which is then ionised by a high frequency voltage and becomes a plasma. The high frequency current then generates heat which causes the surface tissue to become devitalised, coagulated and shrunken [53]. Due to the change in electrical tissue properties once devitalised; namely a drop in electrical conductivity, [54] the current, and therefore heat, begins to flow through the next section of tissue allowing for a larger area to be treated.

<sup>15</sup>Credit: <https://clinicalgate.com/electrosurgery-in-therapeutic-endoscopy/>

For a surface bleed, the APC is used almost like a paint brush to apply the streams of ionized argon gas to the total surface area of the bleed.

One of the major advantages with the APC modality is that it can be used to stop bleeding over a much large surface area than other modalities in an efficient and controlled manner [55] Literature has also shown that deep tissue destruction which can lead to perforation is rare with endoscopic APC [56]. In one study, out of 640 lesions treated from the stomach, small intestine and colon; no perforations were created through the use of APC. [54]. The risk of perforation has been stated at approximately 0.5% [57].

## **Microwave**

Microwave coagulation and haemostasis has been achieved through a number of devices and is usually carried out either laparoscopically, through a small incision, or endoscopically. An experimental study carried out in China showed that percutaneous microwave coagulation therapy was effective in the cessation of active liver bleeding in rabbits using 2450 MHz [58]. Another laparoscopic application showed promise for the coagulation of solitary hepatocellular carcinoma once again using 2450 MHz. [59]. Endoscopically a number of positive outcomes have been presented [60], [61], [62], [63] and mostly utilise generators with an output frequency of 2450 MHz. Some generators used for Microwave coagulation and ablation include the Microtaze, Emblation Microwave MSYS245, Medwaves AVECURE and of course the Creo Medical CROMA Generator which is the main generator device used in the testing portion of this research. Examples of these can be seen in figure 2.25<sup>16 17</sup>.

The Creo Medical CROMA generator has both an RF (400KHz) and Microwave (5.8GHz) and is capable of delivering up to 60W. A thorough review of the devices and systems available for microwave therapy is presented in [64] and covers both RF

---

<sup>16</sup>Credit: [https://link.springer.com/referenceworkentry/10.1007%2F978-1-4419-0751-6\\_13](https://link.springer.com/referenceworkentry/10.1007%2F978-1-4419-0751-6_13)

<sup>17</sup>Credit: <http://investors.creomedical.com/what-we-do/our-products>



(a) Microtaze Generator



(b) Creo Medical Generator.

Figure 2.25: Various Microwave Generators

and Microwave applications throughout the clinical spectrum.

### Use of 5.8GHz

The device, as previously stated, made use of microwave energy in the Super High Frequency (SHF) band between 3GHz and 300GHz, specifically at a spot frequency of 5.8GHz. This is one of the highest microwave frequencies to be used within the gastrointestinal tract and there are a number of reasons for this choice.

Due to advances in the communication, military and commercial sectors the cost of microwave power generators at 5.8GHz has decreased and therefore there has been an increase in the availability of such devices. The use of 5.8GHz can be seen as a compromise between the ability to deliver energy into tissue as discussed in section 6.1.2 with an insertion loss which is not excessively high which is important due to the size constraints for the outer diameter of the device.

## ***Chapter. 3***

---

### ***Device Introduction and Specification***

---

#### **3.1. Clinical Need**

The requirement for rapid and effective haemostasis is one of great importance to surgeons throughout the medical field. This is especially needed in endoscopic procedures during which a serious bleed can be life threatening if not managed correctly. Upper Gastrointestinal Bleeding (UGIB) is one of the most common GI emergencies in the United Kingdom [65]. Further literature over the past ten years, along with that discussed in the introduction, has suggested that UGIB accounts for up to 20,000 deaths per annum and the incidence of acute UGIB is approximately 50-100 per 100,000 persons per year. [66]. Some studies show this to be much higher up to 160 cases per 100,000 and indicate that mortality as a result of UGIB generally ranges from 10 - 14 % [67]. An audit in 2007, in the UK, shows that UGIB still continues to have substantial mortality although it appears to be lower than found in 1993. [68]

Not only can patients present to the emergency room following incidence of upper GI bleeding but effective haemostasis is also required to treat any injury or insult to the upper GI tract caused during routine surgeries. A retrospective study of 409 patients showed that 27 events of significant postoperative gastrointestinal bleeding following the surgical management of obstructive jaundice [69]. A smaller percentage, although still significant (0.4%), of patients undergoing open heart surgery were shown to sustain postoperative UGIB necessitating endoscopic evaluation [70]

Haemostasis can currently be achieved in a number of ways as previously dis-

cussed in section 2.4 and it is clear that all of these modalities have both advantages and disadvantages when it comes to the management of upper gastrointestinal bleeding.

One consistent theme throughout literature indicates that a multi-modality approach to haemostasis is not only more effective at the time of treatment but also leads to lower rebleed rates [71, 72, 73] when compared with single modality haemostasis; most notably the sole use of injection modalities.

The need for a device capable of not only utilising injection or topical application of haemostatic chemicals alongside the ability to immediately apply thermal energy to achieve haemostasis is believed, by the authors and in consultation with clinical professionals, to be a device which would be highly sought after by endoscopists and surgeons during UGIB treatment or any procedure in which UGIB can occur.

## **3.2. Physical Device Requirements**

### **3.2.1 Requirement for Maximum Outer Diameter (2.5mm)**

There is a definite clinical trend, as discussed in the introduction of this research, for non invasive procedures to be carried out using smaller and more narrow devices. With this trend the maximum outer diameter of endoscopes, gastroscopes and even bronchoscopes are becoming much smaller. As such the devices needing to be inserted into them need to follow this trend also and become much smaller in diameter.

2.8mm is becoming one of the most common working channel diameters and it was therefore decided that the haemostatic device should be compatible with scopes having such a working channel. To ensure that the device would be compatible with such working channels and to ensure that the device could easily be inserted and removed, an outer diameter of 2.5mm was chosen. This tolerance was also to allow for any variation in the size of the scope working channel or any variation in

the outer diameter of the cable structure. This size constraint was also part of the requirements indicated by Creo Medical who have a lot of expertise in this area.

### **3.2.2 Requirement for Hollow Channel**

As previously discussed the device need not only deliver microwave energy into tissue to achieve haemostatic effect but also be capable of a secondary modality. This second modality is the introduction of adrenaline, other medicine or even other medical tools such as cameras or lasers. To be capable of this the device needed to have a hollow channel running through its length. To ensure that the hollow channel could be used with a number of other devices, it was decided that a diameter of 1mm would provide enough space. This would mean less pressure is required to inject liquid through the device and also allows for tools such as biopsy forceps and needles to be used in the hollow.

### **3.2.3 Requirement for Impedance Transformation**

Due to the requirements discussed above the way to achieve such a device geometry was to utilise a co-axial line with a hollow inner conductor. Maximising this hollow channel diameter whilst maintaining a minimal outer diameter will force the two conductors to be in close proximity to each other, which will impact the impedance of the cable. Figure 3.1 shows three different structures and there associated parameters.  $d$  is the outer diameter of the inner conductor,  $D$  is the inner diameter of the outer conductor and  $Z_0$  is the characteristic impedance. This was calculated using equation 2.4 and the full range is shown in figure 3.2.

As can be seen in figure 3.2 with a 1mm hollow channel and an outer diameter of 2.5mm it would be impossible, at least using polytetrafluoroethylene (PTFE) ( $\epsilon_r = 2.1$ ) as a dielectric, to achieve a  $50\Omega$  line. The maximum values in this graph are also assuming infinitely thin conductors and no protective layers such as a structural



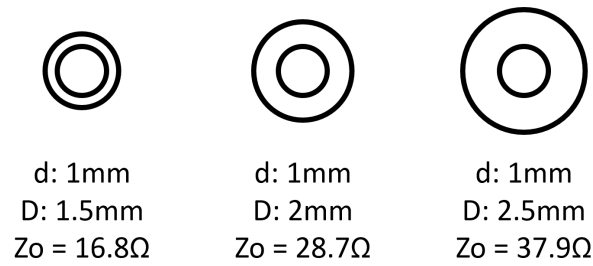


Figure 3.1: Diagram showing the variation in coaxial outer conductor and corresponding impedance.

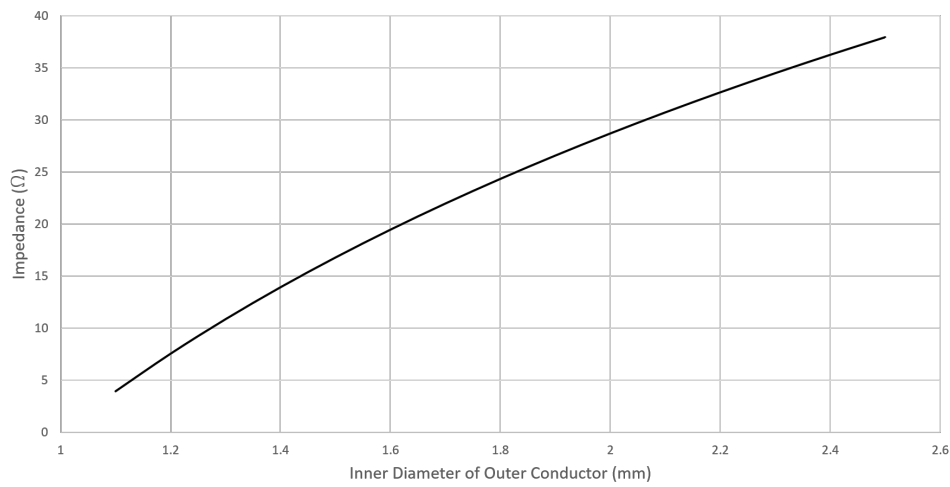


Figure 3.2: Graph showing the variation in impedance with varying inner diameter of outer conductor

insert for the hollow channel or outer protective jacket. If these are also considered then there will be even less space between conductors making the cable likely to be much lower than  $50\Omega$ . Further discussion regarding the impedance and structure of the cable is undertaken in chapter 5 and has been introduced here to provide a background for subsequent chapters.

## ***Chapter. 4***

---

### ***Impedance Transformation***

---

A large number of electrosurgical generators; particularly for microwave energy delivery, including those in use by Creo Medical Ltd have a standard output with an impedance of  $50\Omega$ . Traditional RF electrosurgical generators are either optimised to a particular impedance whilst still operating over a large range or are optimised for a single impedance output. For example the Gyrus PlasmaKinetic generator delivers energy at varying settings depending on expected tissue impedance and can have an output impedance as high as  $300\Omega$  [74]

Many microwave specific generators have a standard output of  $50\Omega$ , this is especially the case for a lot of test and measurement equipment such as vector network or spectrum analysers. The cable designed to be used in this piece of research, and discussed in further detail in chapter 5 has a much lower impedance than many co-axial cables. An analysis of the geometry, previously shown in section 3.2.3 required a minimal outer diameter to facilitate insertion into most endoscopes along with the need for a central hollow channel for the delivery of liquids, medicines or even tools and showed that the cable would definitely deviate from the standard  $50\Omega$  impedance.

In order to allow for both laboratory bench testing using a vector network analyser (VNA) and for eventual tissue testing of the final haemostat device using the Creo Medical generator an impedance transformer was required to match the cable. The need for this transformer can be expressed in terms of mismatch loss and reflection coefficient, as discussed earlier, which indicate how much power will be lost due to impedance difference at the generator-cable interface.

## **4.1. Transformer Structure Considerations**

Whilst the theory behind the quarter wave transformer may seem straightforward; a number of considerations needed to be addressed before an actual device could be realised. These are summarised in the following list:

1. Transition between distal end of the impedance transformer and the cable needs to be secure both electronically and mechanically
2. Proximal end of the impedance transformer needs to allow for ease of connection to multiple microwave delivery devices
3. Maintenance of access to the hollow channel

A standard microwave connector can be used to maintain connectivity with a number of microwave devices both during testing and operation fulfilling both the first and the second requirement. The first requirement was also considered when various attachment methods were used and further assessed in subsequent chapters.

The final consideration required more thought and two ways were considered to achieve this. Most existing structures provided good connectivity and were stable and secure, but they would have occluded the hollow channel which would reduce the cable to standard microwave functionality making such structures not suitable for the dual modality haemostasis probe delivered through this research.

## **4.2. Use of Microwave and RF Energy**

A section of preliminary work was carried out to assess the efficacy and ability to deliver both microwave and RF energy either in combination or succession to achieve haemostasis. The microwave energy was to be delivered at 5.8GHz as previously discussed and the RF energy was to be delivered at 400KHz as per the hardware constraints of the Creo Medical generator. In clinical usage the RF energy

could be applied then followed by the microwave energy or dual energy could be delivered at the same time. The rationale behind successive delivery was to initially deliver a large burst of energy through conduction to the bleeding vessel. As the tissue properties change and RF energy becomes more difficult to deliver, the microwave frequencies would be used to permit the delivery of even more energy through radiation. Combined delivery is believed to offer the advantages of both energy delivery modalities over a shorter time frame.

#### 4.2.1 Co-axial Capacitive Coupling

An initial structure was designed to allow delivery of microwave energy whilst also allowing RF to be delivered through the device. The basic aim of the device was to use capacitive coupling to provide an effective short circuit at the microwave frequency whilst acting as an open circuit at RF frequency.

The initial structure was designed as a rigid structure for a number of reasons, including maintenance of access to the hollow channel and ease of connection. Two cylindrical capacitors were developed; the first on the outer conductor and the second on the inner. The basic structure can be seen in fig 4.1 with the darker lines showing the location of the capacitors.

The capacitance was selected such that the impedance was high enough at RF frequency to prevent the structure from looking like a short circuit but low enough at microwave frequency to act as one.

Due to the described geometry of the device both capacitors are cylindrical and as such the capacitance can be calculated:

$$C = \frac{2\pi\epsilon_0\epsilon_r}{\ln(b/a)} L \quad (4.1)$$

Where  $\epsilon_0$  is the permittivity of free space,  $\epsilon_r$  is the dielectric constant of the dielectric material used to separate the two conductors,  $b$  is the inner diameter of

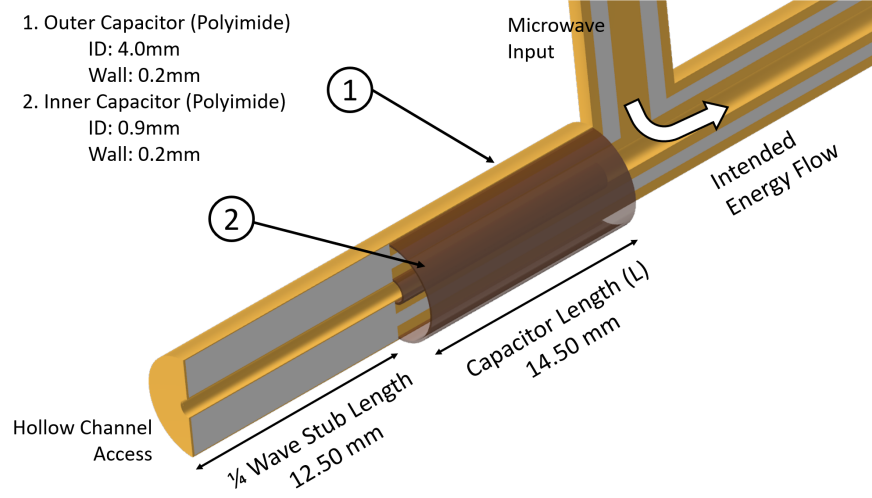


Figure 4.1: Side view diagram of the capacitive coupling structure

the outer conductor,  $a$  is the outer diameter of the inner conductor and  $L$  is the length of the capacitor.

Once this capacitance is known its reactance can be calculated at various frequencies to give the impedance of the structure.

$$\left[ Z = \sqrt{R^2 + X_C^2} \right]_{R \rightarrow 0}, \quad Z = \sqrt{0 + X_C^2} = X_C \quad (4.2)$$

$Z$  is the impedance of the structure,  $R$  is the resistance of the structure and  $X_C$  is the reactance. As the resistance of the structure decreases the reactance element of the impedance dominates until for a zero resistance the impedance is equal to the reactance. This assumption can be made due to both the use of low loss materials and also the relatively small length of the structure which should introduce minimal losses into the system. The reactance is then calculated:

$$X_C = \frac{1}{2\pi f C} \quad (4.3)$$

Where  $f$  is the frequency and  $C$  is the capacitance.

It can be seen that, if we consider the capacitance to be the same; i.e. the properties of the dielectric material are the same at RF and microwave frequencies, the reactance decreases as the frequency increases. It is this principle that enables a high reactance at RF frequencies and a low reactance at microwave frequencies. The reactance of a 3pF capacitor against frequency can be seen in fig 4.2. The diagonal line shows the log response of reactance against frequency, whilst the vertical lines show the specific frequencies of RF and microwave energy as used in this project.

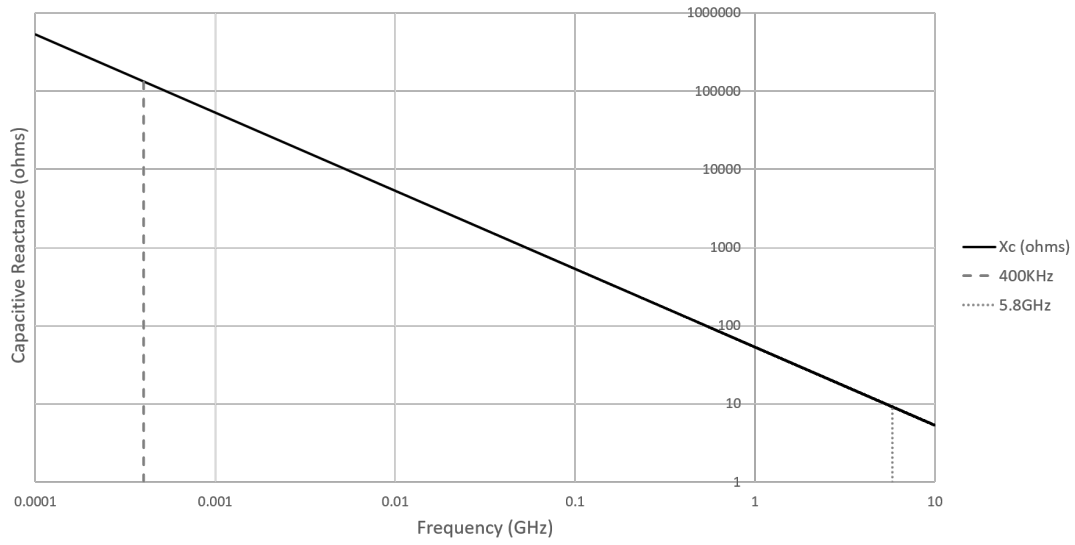


Figure 4.2: Variation in reactance of a 3pF capacitor with frequency

## Equivalent Circuit

An equivalent circuit was created in CST Microwave Studio to approximate the theoretical operation of the capacitive coupling structure.

Table 4.1: Table showing parameters for equivalent capacitive coupling circuit

Number	Length (mm)	D (mm)	d (mm)	Er
1	27	3.1	1.5	2.1
2	50	3.1	2	2.1
3	17	3.1	2	2.1
4	13	4.2	0.9	2.1

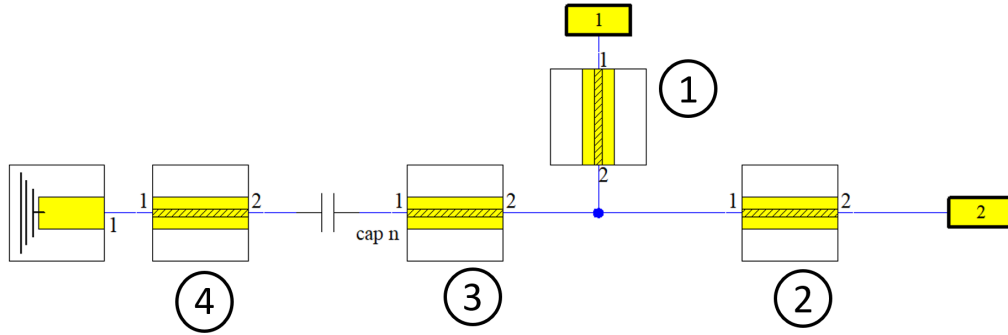


Figure 4.3: Equivalent circuit for the capacitive coupling structure

The structure is made up of four ideal co-axial sections with final geometry as given in table 4.1. The two co-axial lines to the left are separated by a capacitor and terminated in a short circuit as in the 3D model, figure 4.1. Parameter sweeps for the lengths of co-axial section 1,3 and 4 as well as the capacitor value were used to match the S Parameters to the 3D model.

The variation in lengths from the 3D model can be accounted for by extra capacitance and inductance introduced through the steps in conductor diameters and also the method of connection which the theoretical equivalent circuit does not take into account.

The S Parameters for the equivalent circuit can be seen in figure 4.4. These can then be compared to the 3D EM simulation results as shown in figure 4.5. It is clear to see that the operation around 5.8GHz is quite similar with both structures having  $S_{1,1}$  values of below -30dB.  $S_{2,1}$  values are equally good with both being better than -0.2dB.

### Material Selection

The material for the capacitor section needed to be chosen based on dissipation (loss), breakdown strength and dielectric constant. Not only did the capacitance need to be calculated correctly but due to the RF waveform and associated voltage used within the Creo Medical generators the material needed to have a high dielectric strength.

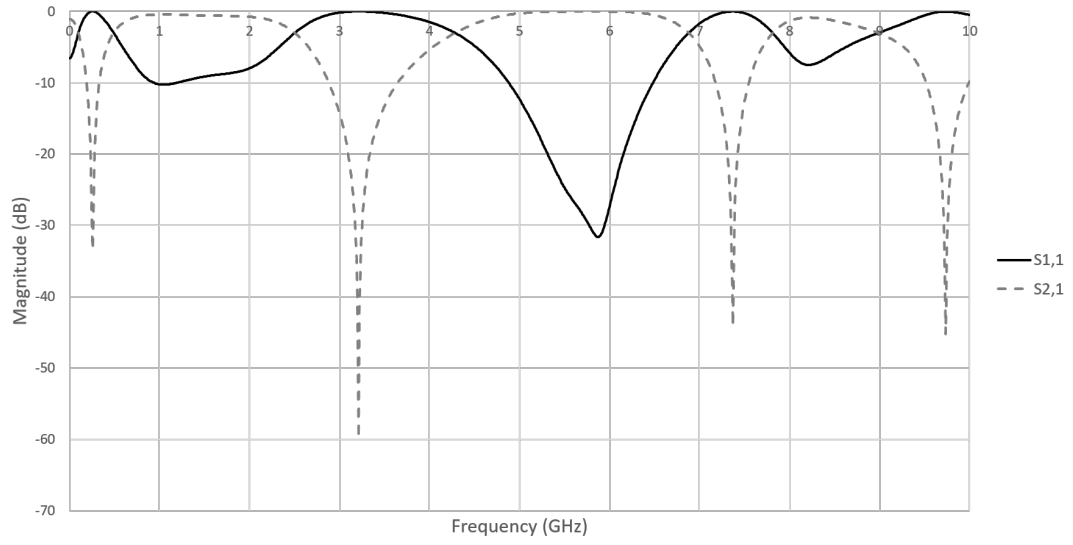


Figure 4.4: S Parameters for the equivalent circuit capacitive coupling structure

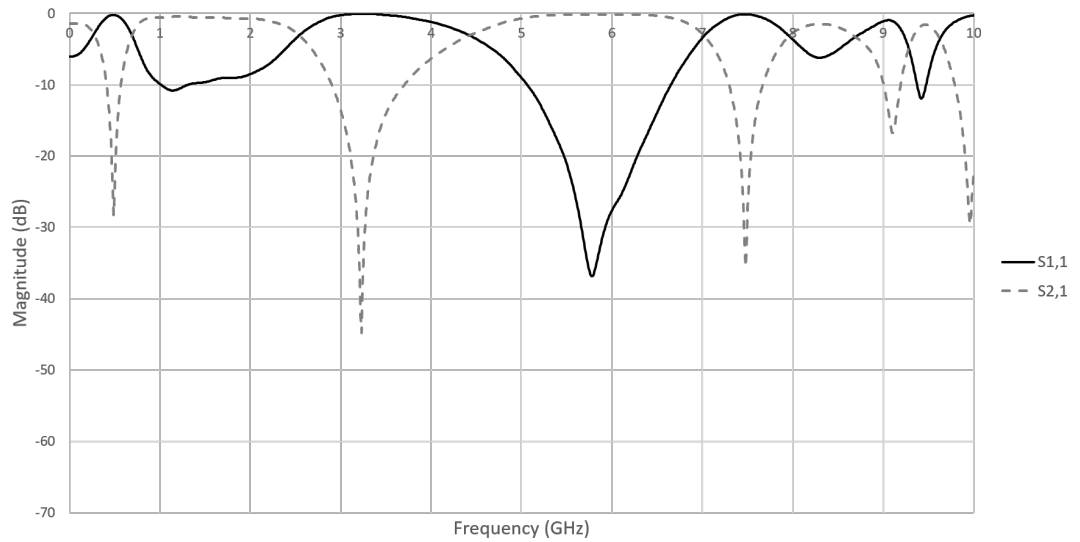


Figure 4.5: S Parameters for the 3D EM simulation of the capacitive coupling structure

The maximum RF voltage to be used is approximately  $400V_{pk}$  and a headroom factor of 2.5 is recommended; meaning the material will need to be able to withstand up to  $1kV_{pk}$ . The chosen polyimide film had a dielectric strength of  $339kV/mm$  [75]. This high value allows a much thinner film to be used, technically a layer of around  $3\mu m$ , to achieve the breakdown strength of  $1kV_{pk}$  required. This means that a wide range of dielectric thickness can be considered during the theoretical design of the



structure.

A sensitivity analysis was conducted to ascertain exactly which of the parameters would be most crucial in the design. These parameters included dielectric constant, capacitor length and capacitor dielectric thickness. As the geometry of this structure was based on a rigid co-axial design where similar conductors and dielectric layers were used. The inner and outer conductors were extended an odd multiple of quarter wavelength at the frequency of operation and shorted at the distal end. At the microwave frequency of interest this will cause a short circuit to be 'seen' at the proximal end of the stub. Due to the added capacitance and variation in structure it was expected that the actual length would vary from the theoretical length and therefore CST microwave studio was used to optimise the structure.

The initial rigid prototype structure for the new cable without the capacitive coupling structure is discussed in chapter 5 but a simulation of it can be seen at 400KHz and 5.8GHz in figures 4.6 and 4.7 respectively. The energy input port is at the top, the hollow channel access port is on the left and the output port is on the right. It is clear that although operating correctly at 5.8GHz, when the 400KHz RF signal is used the device does not deliver energy to the output port correctly and the RF signal propagates towards the hollow channel input port.

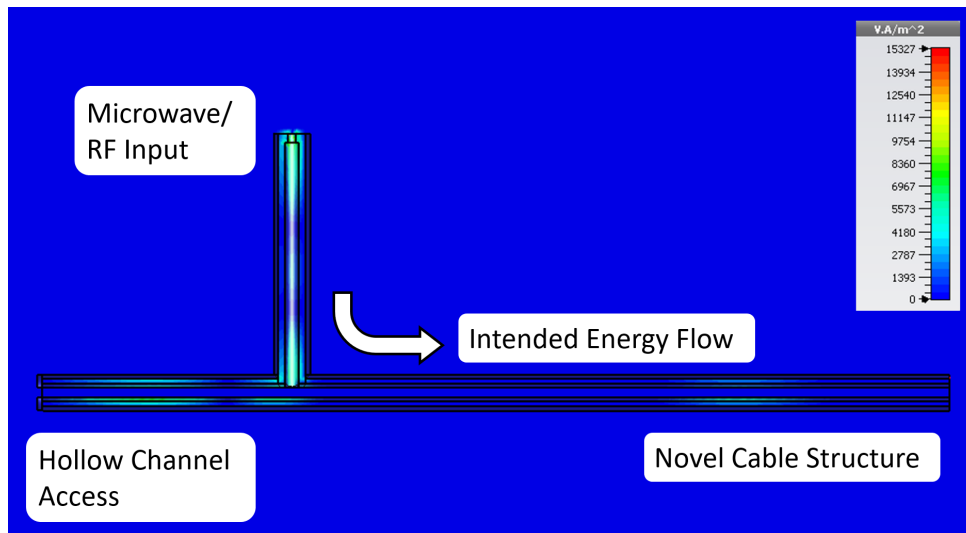


Figure 4.6: Power Flow through the rigid prototype at 400KHz

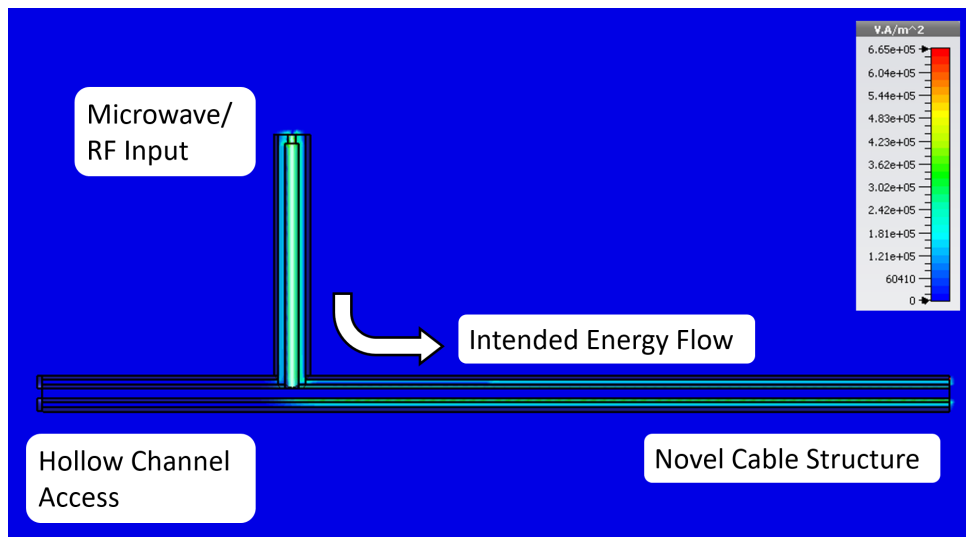


Figure 4.7: Power Flow through the rigid prototype at 5.8GHz

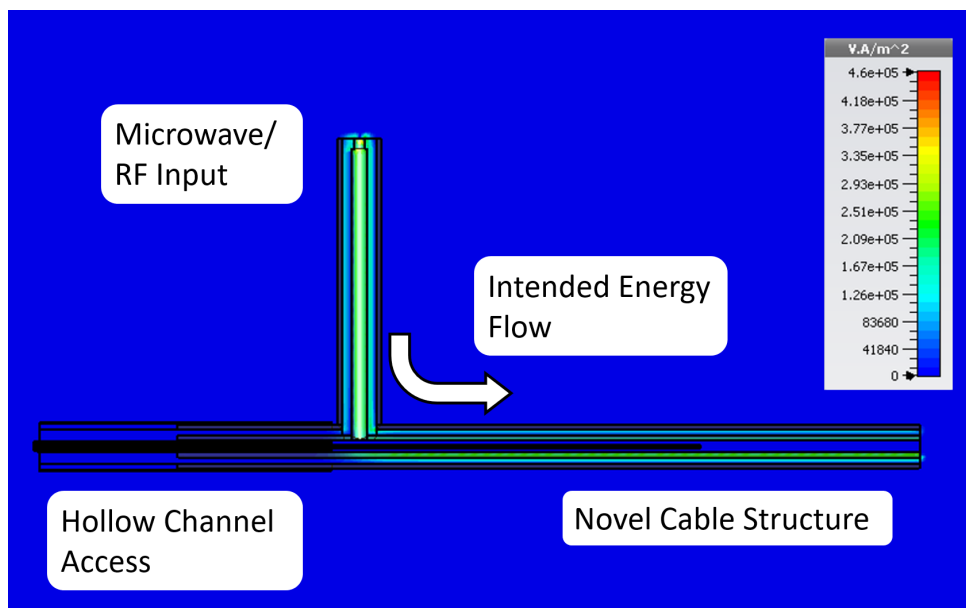


Figure 4.8: Power Flow through capacitive coupling device at 400KHz

Figures 4.8 and 4.9 show the capacitively coupled structure at both 400KHz and 5.8GHz. It can be seen that the structure is working well at both frequencies.

The advantage of this structure is that the proximal end of the structure is a short circuit to the microwave energy meaning no fringing fields can escape and there is no risk of the patient or clinician getting burned by making contact with the proximal end of the structure or through radiation burns. Although this is the case at the

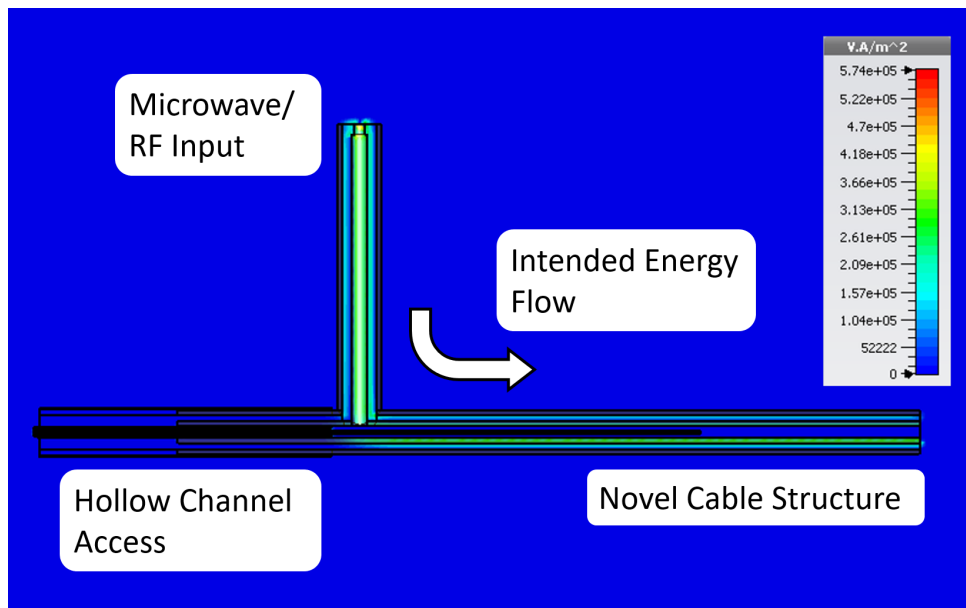


Figure 4.9: Power Flow through capacitive coupling device at 5.8GHz

hollow channel, RF energy can still be propagated through the structure effectively in the correct direction.

#### 4.2.2 Double Choke structure for Microwave and RF

A second method of allowing energy at both RF and microwave frequencies to be launched into the structure and propagated through the cable to the energy delivery antenna is to use a double choke structure as shown in fig 4.10.

The structure makes use of a quarter wave length T junction to initially match the novel microwave cable impedance with the  $50\Omega$  microwave/RF input. The thin hatched structures shown are radial air gaps of approximately quarter wavelength long which converts a short circuit to an open circuit. These act as chokes and are spaced at nominal half wavelengths from each other. The effect of this is that the entire structure to the right of the microwave input is seen as an open circuit regardless of what is attached to port 3. This is required if a conductive instrument was to be fed through the hollow channel, i.e. control rods, endoscopic tools or even saline.

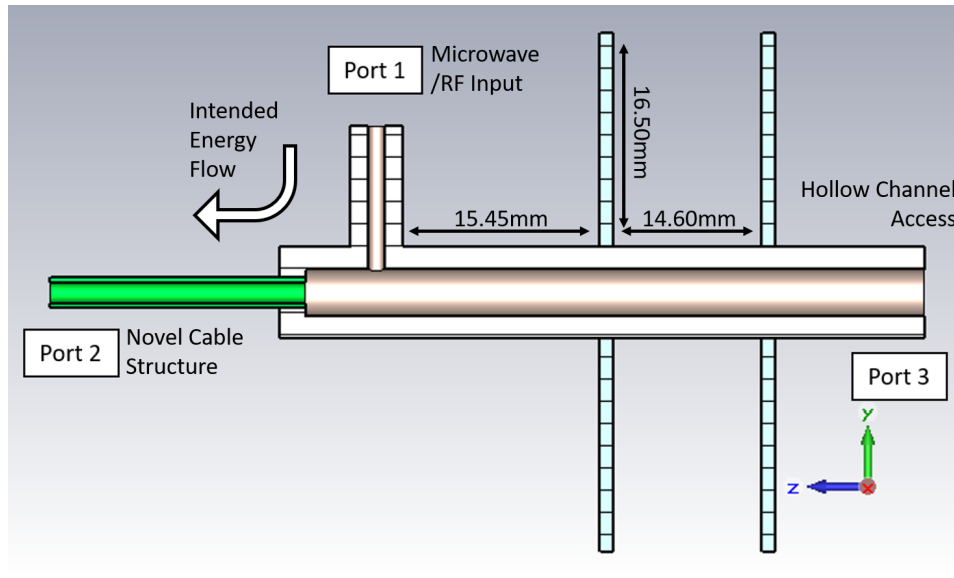


Figure 4.10: Simulation model for double choke structure

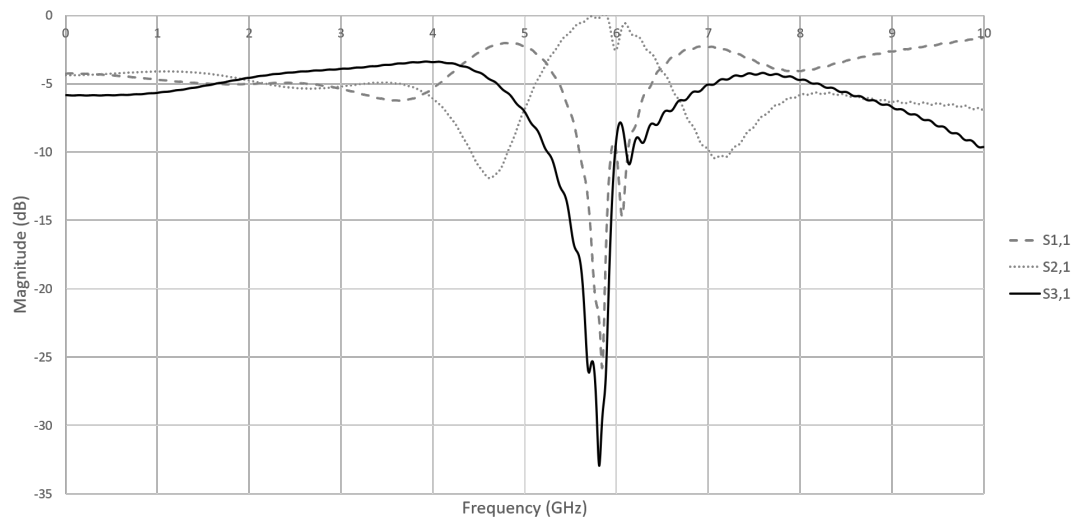


Figure 4.11: Simulated S Parameters for double choke structure

The simulation was set up as follows: the dielectric structures are modelled directly in their relevant materials and the overall simulation was given a conductive background with the same properties as brass. The outer geometry of the brass layer for the device does not affect the operation as long as there is at least several skin depths, approximately 5 micron, surrounding the dielectric structures of both the choke structure and the cable. This layer, albeit much thinner than would practically be used, allows for at least 99% of the E field to propagate within it. From a

manufacturing point of view this is ideal as it allows the outer conductive material to be shaped in such a way as to allow for ease of machining and connection to the cable. This could be achieved a number of ways from the milling of separate metal sections or even the milling of the dielectric material and then coating with a thin layer of conductive paint or through vapour or thermal deposition of metal.

As can be seen from figure 4.11 the structure shows expected performance at and around 5.8GHz.  $S_{2,1}$  gives a transmission from microwave input to the cable and is -0.22dB which is a transmission of approximately 95.06%.  $S_{11}$  (-21.74dB) gives the power reflected at the microwave input and cable junctions and is simulated as a reflection of 0.67%. The important measurement in terms of this structure is the isolation at port 3 which, according to these simulated results, is better than -32dB which is less than 0.06% meaning that almost no energy is reflected to port 3 or transmitted directly from port 1 to port 3.

## **Manufacture**

Due to the requirement of accurate air gaps for the radial chokes and PTFE inserts, the choke structure was manufactured in six parts as can be seen in figure 4.12. Variation in the sizes of these parts would deviate from the simulated structure and may even cause some of the integral parts of the structure such as the quarter wave length input port and the radial chokes to function incorrectly. The microwave input made use of a standard SMA connector cut down to the correct size. The three main body parts of the structure were milled and drilled to allow all three to be secured together to form the chokes and transformer structures. The inner rods were machined to form the main co-axial structure of the transformer.

The fully assembled double choke structure can be seen in figure 4.13.

It can be seen from the figures that this structure is quite large and would be cumbersome to include in its current form in a device for example in a small hand piece. There are a number of ways in which this structure could be altered to make

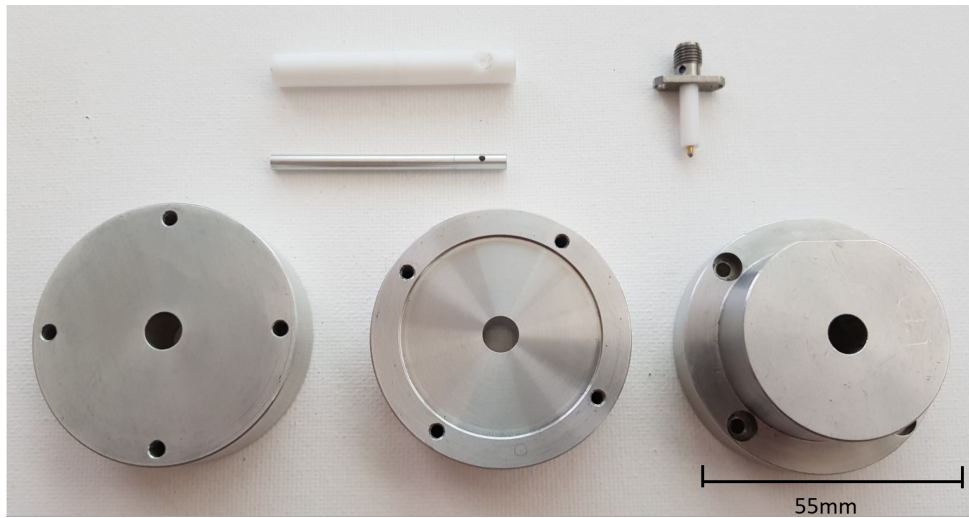


Figure 4.12: Choke structure parts

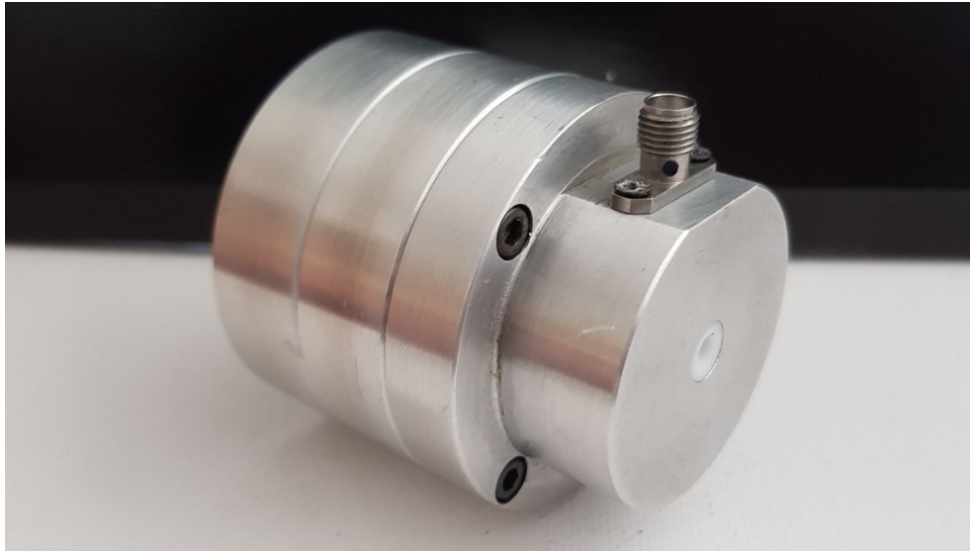


Figure 4.13: Fully assembled choke structure

a smaller form factor whilst maintaining the operation of the structure. One simple alteration would be to bend the air chokes at 90 degrees which would allow for a much thinner transformer structure but may become slightly longer.

This would make the structure much thinner and should still allow the required isolation at port 3. The structure could also be made from a lighter material and then coated with a conductive layer to provide a much lighter structure as currently used for many microwave structures such as horn antennas [76, 77].

## Testing

Testing for the choke structure was carried out in a similar way to that of the testing of the transformers discussed later in this chapter.

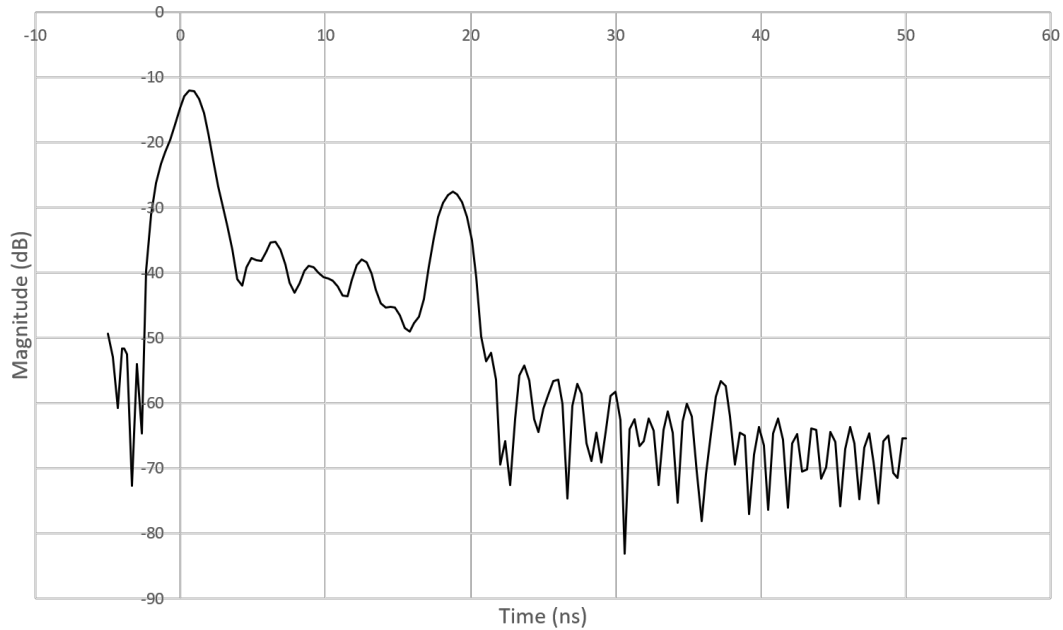
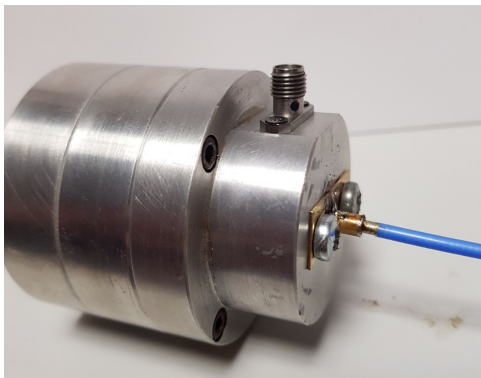


Figure 4.14: Time domain measurement of the double choke structure and open ended cable

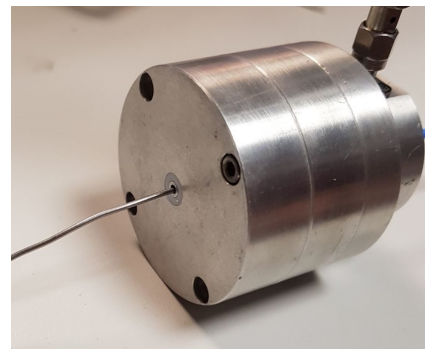
These measurements are presented in the time domain using a frequency range from 5.6GHz to 6GHz. The use of this frequency range gives an average reflection measurement at each point along the line and allows for the easy analysis of any discontinuities through the structure. This gives a much clearer picture of the device performance when compared with the frequency domain in which discontinuities along the structure can either add or subtract from each other and mask the true performance of the device.

Time domain measurements were taken of the transformer attached to a long length (4.61m) of the novel cable structure as shown in figure 4.15a. A long length of cable was used in order to compare these results to those of the cable measurements conducted in a later chapter. Use of the time domain allows the transformer to be

separated from the measurement of the cable. The structure can be seen to have a reflection of approximately -12.0dB or 6.25% at the initial peak which shows the connection of the double choke structure to the VNA. The other noticeable peak is the open end of the cable which shows a measurement of -27.58dB or 0.17%. We can then consider the length of the cable, multiplied by two to consider the forward and return path of the measurement, to estimate a value for the attenuation of the cable. The measurement shown in figure 4.14 gives a loss value of approximately 2.99dB/m. This value is calculated from the second peak which shows the open end of the cable structure. This peak measurement is then divided by the length of the cable to give a loss per meter estimation for the cable. It can be seen from subsequent chapters that this value is quite close to the measured loss of the cable and indicates that there is less than 1dB loss in the transformer structure itself. Full frequency domain S Parameters were unable to be measured due to the presence of only a single port.



(a) Connection method for attaching the cable to the double choke structure



(b) Insertion of a conductive rod into the hollow channel of the double choke structure

Figure 4.15: Measurement and testing of the double choke structure

These results show that the double choke structure is not only plausible in design and simulation but that the manufactured version of this structure propagates microwave energy as expected. This measurement was also stable even with the introduction of a conductive rod into the hollow channel, as in figure 4.15b showing that the isolation and choke structures are operating as expected and are stable even with use of the hollow channel.



### 4.2.3 Change from Microwave/RF to Microwave only delivery

Although the previous designs show the capability of the cable and its usage in a multitude of electrosurgical applications using microwave and RF energy the usage of RF energy was removed from the user and device requirements due to the specific clinical application in this research i.e. the coagulation of bleeding vessels in the upper GI tract. The use of microwave energy has been found to be sufficient to coagulate bleeding vessels and does not suffer from the drawbacks associated with RF energy delivery. This was especially evident when considering the requirement for a minimal depth of penetration and accurate control of the energy delivery.

The following structures act as quarter wave impedance transformers for microwave energy only at 5.8GHz.

### 4.2.4 Co-axial Transformer

The initial prototype for the microwave only transformer utilised a co-axial structure which was designed to give the correct impedance and length to provide an optimal impedance transformation being based on a quarter wavelength, or odd multiple thereof, structure as discussed in section 4.

Recalling the wavelength in a dielectric, it can be calculated:

$$\lambda_g = \frac{c}{f \times \sqrt{\epsilon_r}} \quad (4.4)$$

Where  $\lambda_g$  is the wavelength in the dielectric material being used in meters,  $c$  is the speed of light in m/s,  $f$  is the frequency in Hz and  $\epsilon_r$  is the dielectric constant of the medium in which the wave is propagating.

From eq. 4.4 using the values  $f = 5.8 \times 10^9$  and  $\epsilon_r = 1$ ; that of air, the length required for the transformer would be 8.92mm. Whilst possible in theory, from a manufacturing point of view this would be difficult to achieve and would most likely

provide little to no support for the cable and the associated transformer structure. For this reason the design made use of a  $\frac{3}{4}\lambda_g$  transformer to allow for a more robust design meaning a transformer section of approximately 26.76mm.

For the planned air filled co-axial line structure the dimensions shown in figure 4.17 were calculated to plot the variation in impedance as the inner diameter of the outer conductor increases.

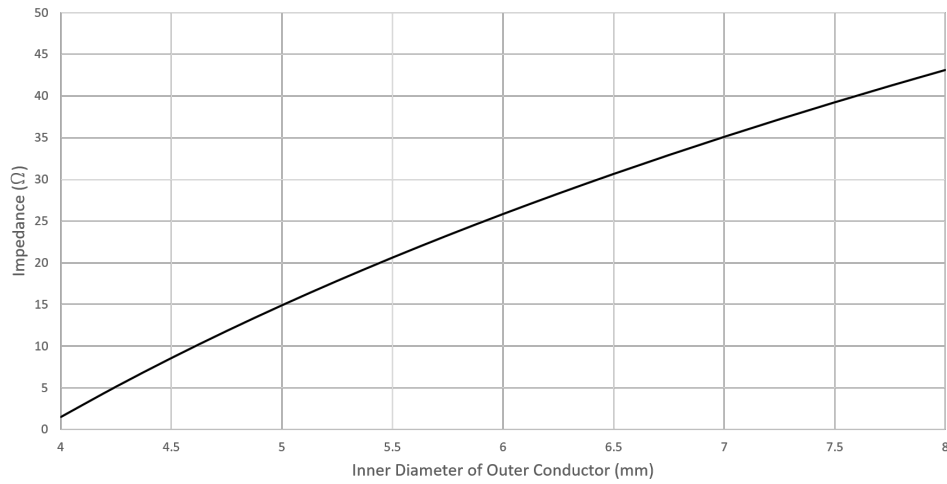


Figure 4.16: Variation in co-axial cable impedance with increasing inner diameter of outer conductor

Eq. 2.4 shows how the impedance of a section of co-axial line can be calculated. This was used to calculate the optimal diameters for both the inner and outer conductors for use in the co-axial transformer. An inner conductor of 3.9mm was used as this allowed for holes to be drilled into the metal to allow the placement of the other transformer parts and allow for ease of soldering to ensure a good electrical connection during assembly. This hole would not affect the microwave propagation as the thickness of the conductor, approximately 1mm, was much larger than the skin depth of  $1.66\mu\text{m}$ . Holes drilled into this inner conductor were also used to route the inner PTFE tube through in order to maintain access to the hollow channel. The dimensions shown in fig 4.17 were then chosen to provide the correct impedance and length whilst allowing for ease of manufacture. The previous outer diameter

constraints were not applicable to the transformer devices as they would be held within a handpiece and would not be required to be inserted into working channel of the endoscope.

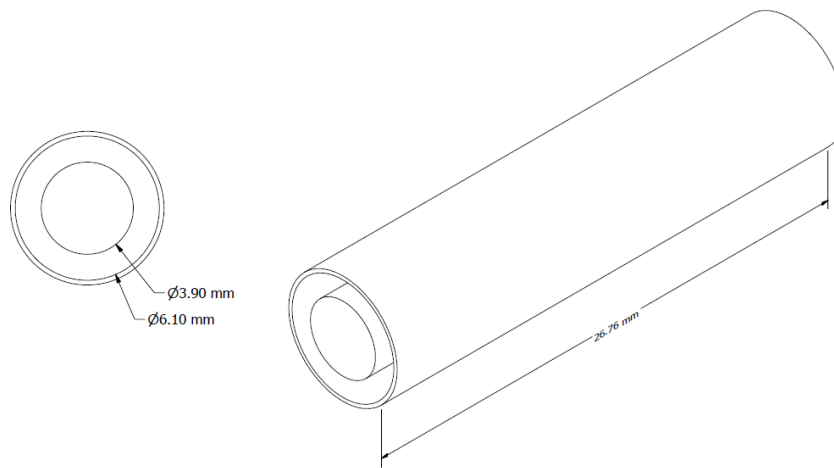


Figure 4.17: Dimensioned drawing of the co-axial transformer.

Once theoretical calculations gave an indication of suitable geometry and optimal structure these were validated and optimised using CST Microwave Studio to take into account non-ideal geometries, line steps, fringing fields etc. Each part, intended operation and structure is shown in figure 4.18.

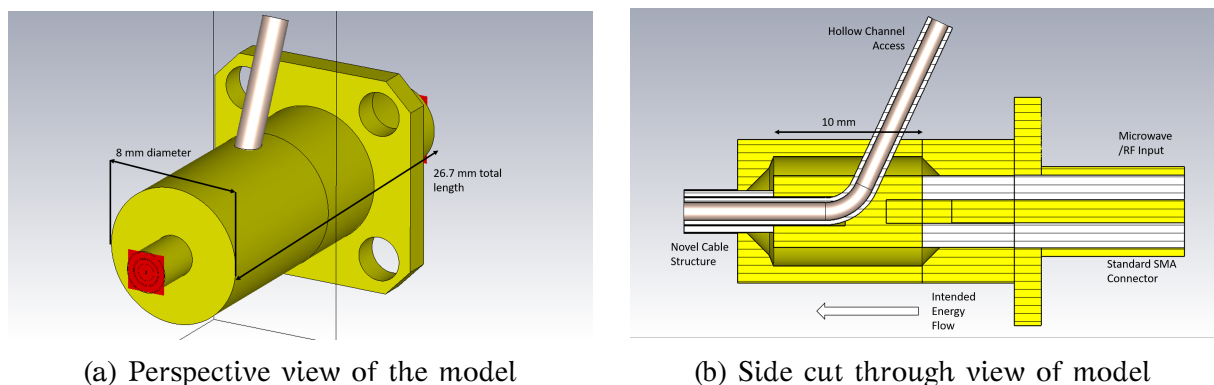


Figure 4.18: Model designed for the co-axial transformer simulation

CST Microwave Studio was also used to validate the entirety of the design of

the co-axial transformer including SMA connector and to assess the effects of the hollow channel. The most feasible way to allow access the hollow channel whilst maintaining the ability to connect to the microwave generator was to route the PTFE tube through both the inner and outer conductors of the transformer as shown in figure 4.18. Simulations showed good transmission and return characteristics both when the hollow channel was occluded and also when the channel was routed through the conductors. These characteristics can be seen in the S parameter plot given in figure 4.19.

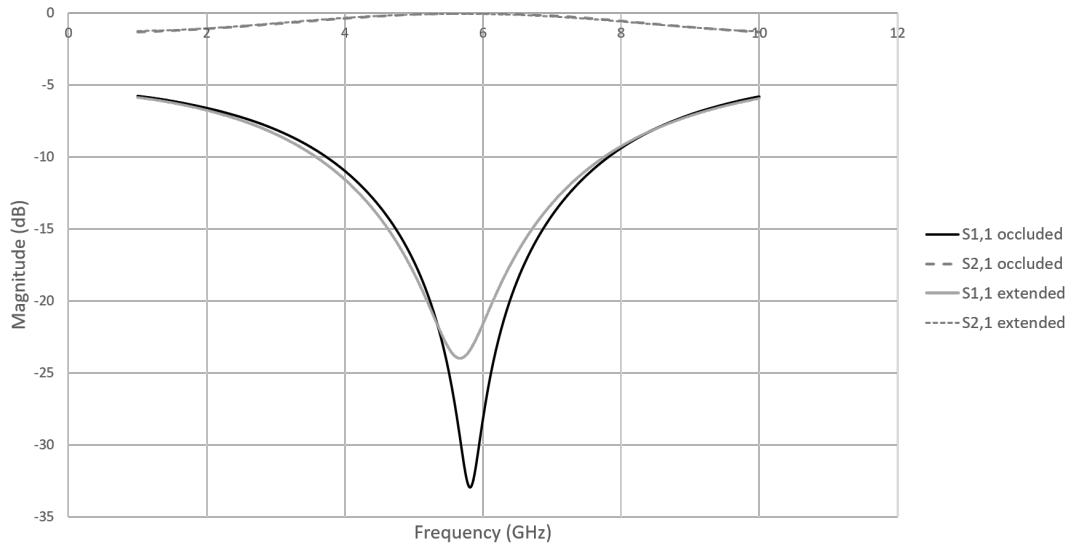


Figure 4.19: Simulated results for the co-axial transformer structure with tube extended and occluded

Although there is a small change in both the  $S_{1,1}$  and the  $S_{2,1}$  when the hollow channel is routed through the conductors the actual power difference is minimal and can be seen in table 4.2.

Table 4.2: Table showing variation in S Parameters at 5.8GHz for the co-axial transformer with and without extended hollow channel

Structure	$S_{1,1}$ (dB)	$S_{1,1}$ (%)	$S_{2,1}$ (dB)	$S_{2,1}$ (%)
Occluded	-32.92	0.05	-0.02	99.54
Extended	-23.50	0.45	-0.05	98.86

There is a slight increase in the return and transmission loss through the structure

but this is minimal and is a necessary compromise for access to the hollow channel.

Figure 4.20 show the parameter sweep simulation for the co-axial transformer. The length of the transformer was varied to find the most optimal solution. The lines with prominent dips between 5GHz and 7GHz show the  $S_{1,1}$  or reflection from the input port. A low value for the simulated  $S_{1,1}$  gives assurance that the energy is being propagated through the structure into the cable as expected. The dip at 5.8GHz shows a return loss of -26.2dB or approximately 0.24% reflection.

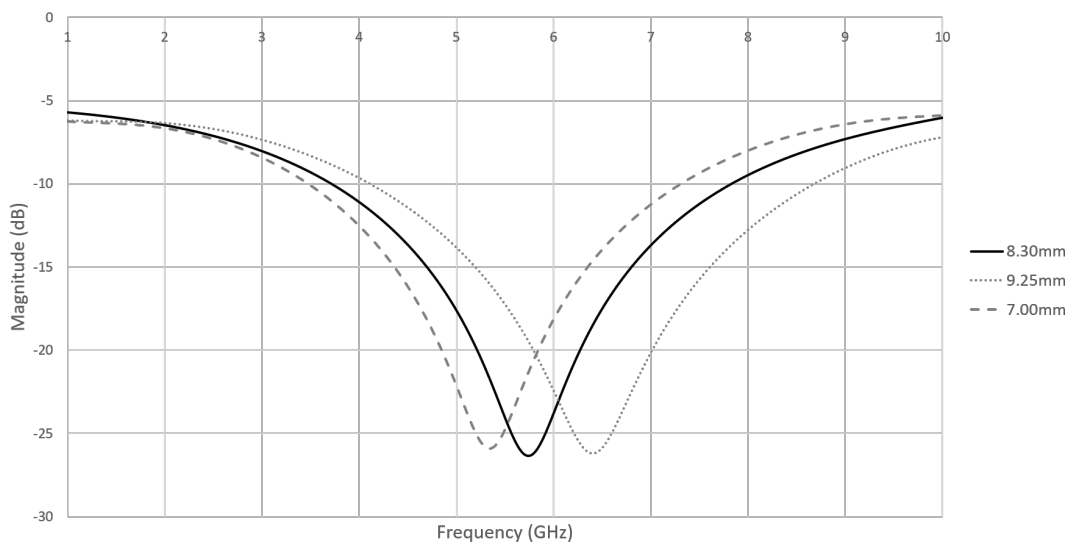


Figure 4.20: Simulated results for the co-axial transformer structure

The transformer used a standard SMA connector to provide the initial 50 $\Omega$  impedance environment and also to allow ease of connection initially to the microwave test equipment and later to the generator being used for testing. A larger air filled co-axial structure then provided the actual transformation environment.

Due to the requirements for hollow channel access whilst maintaining good electrical connections the transformer was manufactured in parts and fitted together in the final manufacture. The individual transformer parts, excluding the SMA connector, were all machined in house at Creo Medical Ltd.

The following procedure was followed to allow for adequate and repeatable connection to the new cable.

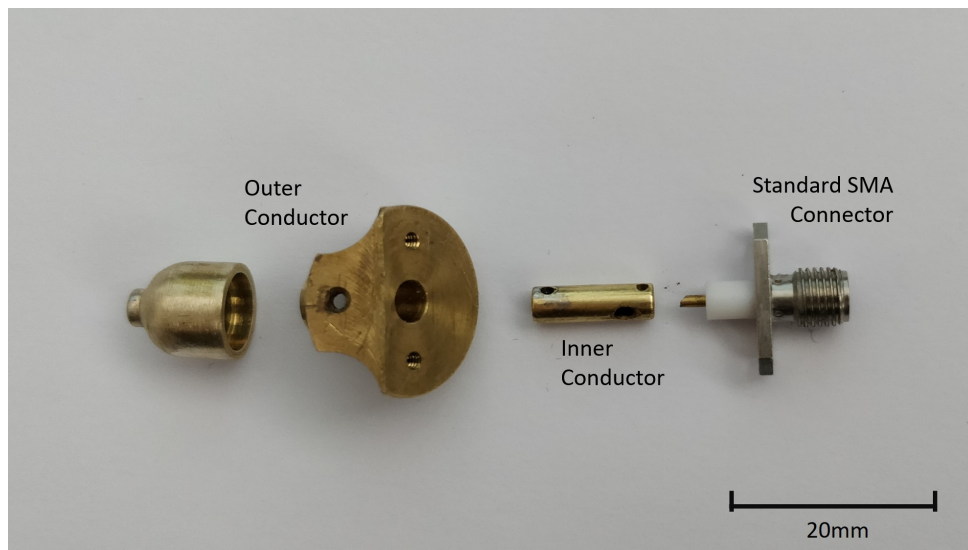


Figure 4.21: Photograph of the various parts which make up the co-axial transformer.

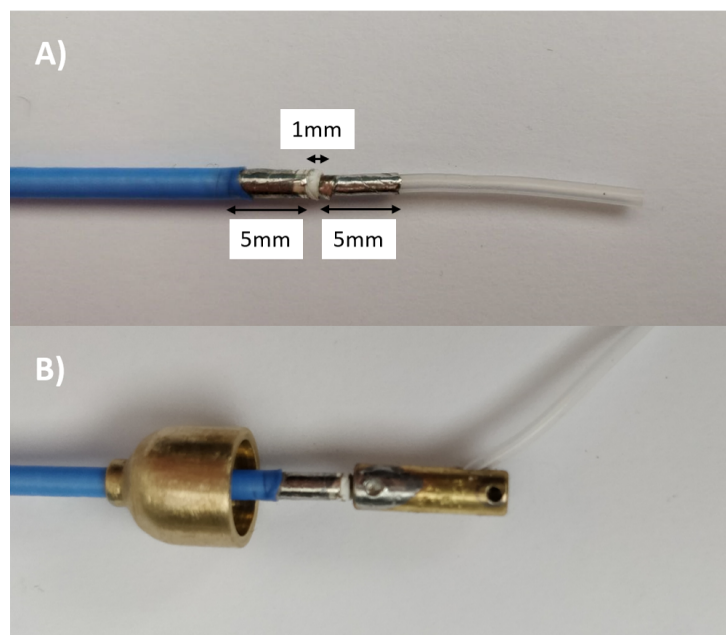


Figure 4.22: Multiple photographs showing initial steps for the construction of the co-axial transformer.

Initially, the novel microwave cable was prepared as shown in figure 4.23A. Each of the layers were removed ensuring that enough of the PTFE wrap remained to ensure isolation between the inner and outer conductor. The inner conductor was left extended up to 5mm, the PTFE extended to a length of 1mm and the outer jacket removed to a length of 5mm also.

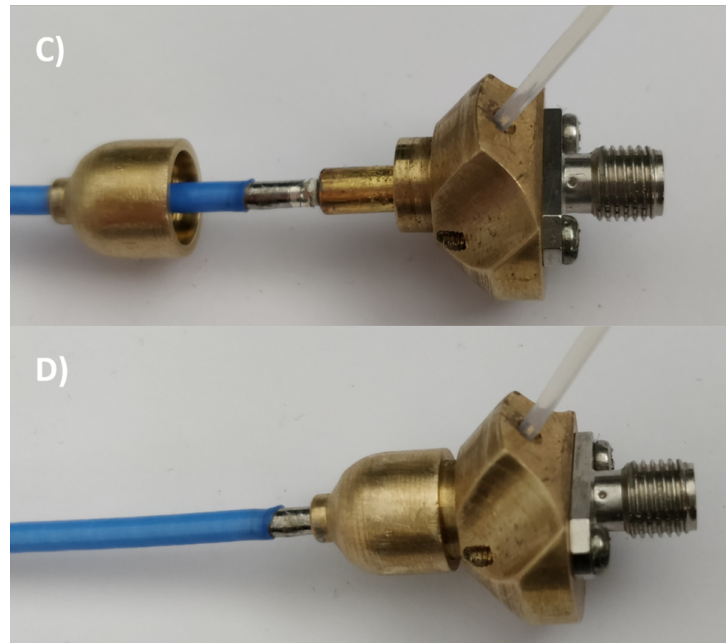


Figure 4.23: Multiple photographs showing subsequent steps for the construction of the co-axial transformer.

This ensured the required breakdown strength similar to the cable. The hollow channel was kept longer than required to ensure it could be routed through the transformer. Once the cable has been prepared, the inner conductor of the transformer was soldered to the inner conductor of the new cable as shown in figure 4.23B. Figure 4.23C and D show the final steps which include locating the SMA connector inner conductor into the inner conductor of the transformer and ensuring all pieces are fitted correctly. Finally screws were used to secure the SMA connector to the outer body of the transformer. Continuity testing was undertaken throughout the assembly process to ensure that good electrical connections were created and that no unwanted electrical shorts had been introduced into the structure.

#### 4.2.5 Microstrip Line Based Transformer

Whilst providing suitable impedance transformation, the co-axial structure was difficult and time consuming to machine and could introduce unacceptable mismatches due to the process required in attaching the conductors in the same way each time.

Specifically with regard to maintaining the length and geometry of the air filled transformer section. An alternative transformer was realised using a microstrip structure. This proved to be easier to manufacture and more repeatable than the individually machined co-axial structures.

These structures also made use of a single frequency quarter wave transformer section but comprised a microstrip line. A microstrip line is a planar electrical transmission line which usually comprises a conductive trace atop a dielectric substrate as shown in figure 4.24

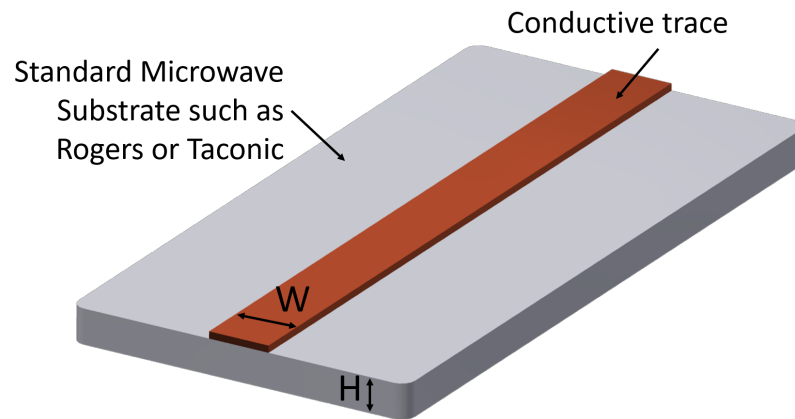


Figure 4.24: Example of a microstrip structure

A theoretical model was used to assess the required parameters for the design and highlighted a number of choices based on the operation of the transformer. Considerations were:

1. Substrate material, including effective dielectric constant and desired dissipation factor
2. Track width and therefore impedance of the line
3. Track length required to achieve quarter wave impedance matching taking into account the dielectric constant of the substrate and interaction and/or coupling with air.



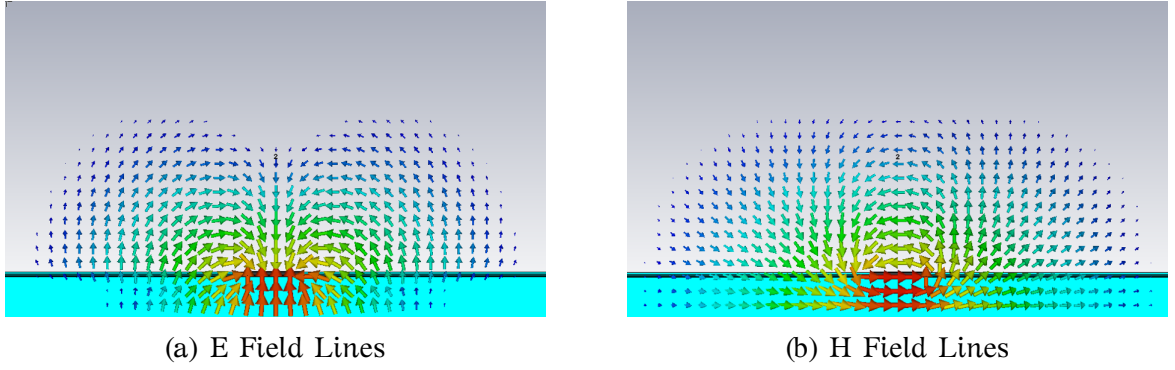


Figure 4.25: Microstrip simulation showing E and H Field

As can be seen in figure 4.25, for a microstrip line the electromagnetic field exists and propagates both through the substrate material and the surrounding air. This gives rise to a principle known as effective dielectric constant. This slightly alters the required geometry for a given microstrip line as would be calculated using the provided dielectric properties from substrate datasheets.

Effective dielectric constant and characteristic impedance have been considered in many publications and are discussed in detail in [78] where an homogeneous medium which takes the place of both the air and the substrate regions is presented. The effective dielectric constant is usually somewhere between the dielectric constants of air and that of the substrate material. These calculations slightly vary depending on the ratio of the line width and the substrate thickness.

$$\text{If } \left(\frac{W}{H}\right) < 1:$$

$$\epsilon_{\text{eff}} = \frac{\epsilon_r + 1}{2} + \frac{\epsilon_r - 1}{2} \left[ \frac{1}{\sqrt{1 + 12\left(\frac{H}{W}\right)}} + 0.04 \left(1 - \left(\frac{W}{H}\right)\right)^2 \right] \quad (4.5)$$

$$Z_0 = \frac{60}{\epsilon_{\text{eff}}} \ln \left( 8 \left(\frac{H}{W}\right) + 0.25 \left(\frac{W}{H}\right) \right) \quad (4.6)$$

$$\text{If } \left(\frac{W}{H}\right) > 1:$$

$$\epsilon_{\text{eff}} = \frac{\epsilon_r + 1}{2} + \left[ \frac{\epsilon_r - 1}{2\sqrt{1 + 12\left(\frac{H}{W}\right)}} \right] \quad (4.7)$$

$$Z_0 = \frac{120\pi}{\sqrt{\epsilon_{\text{eff}} \left[ \frac{W}{H} + 1.393 + \frac{2}{3} \ln \left( \frac{W}{H} + 1.444 \right) \right]}} \quad (4.8)$$

Where  $H$  and  $W$  are the height of the substrate and the width of the microstrip trace respectively,  $\epsilon_{\text{eff}}$  is the effective dielectric constant of the structure,  $\epsilon_r$  is the dielectric constant of the substrate material and  $Z_0$  is the impedance of the structure.

For example; a substrate such as RT 5880 from Rogers Corp [79] has a dielectric constant of 2.2. However, when this is used in a microstrip application with  $H = 1.575\text{mm}$  and  $W = 10\text{mm}$  this dielectric constant approaches a value more like 1.95 as calculated using eq. 4.7. As the dielectric material gets thinner and the line gets wider this effective dielectric constant approaches the original quoted constant for the substrate itself as more of the field is confined within the substrate structure and not the surrounding air. A graph showing this variation and impedance variation with line width can be seen in figure 4.26.

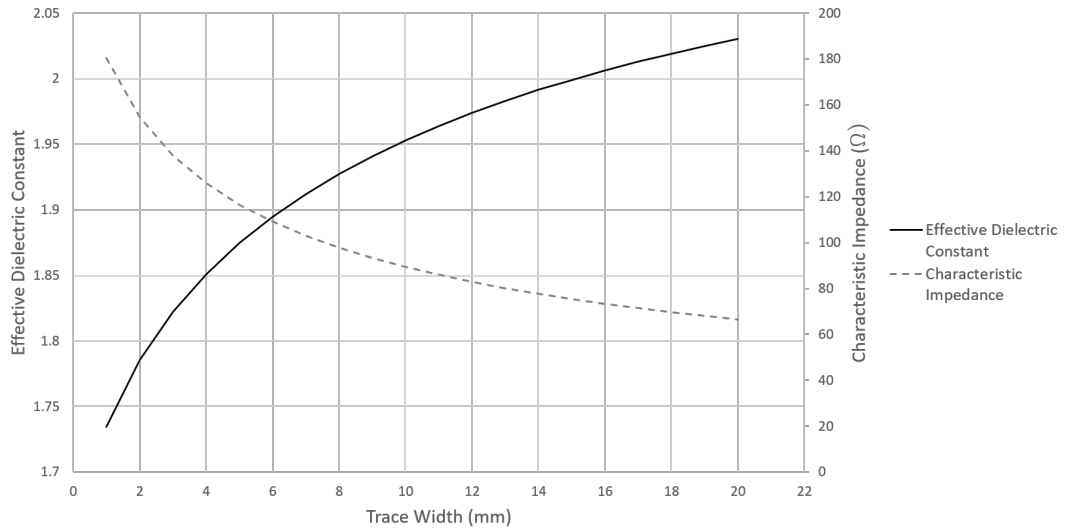


Figure 4.26: Characteristic Impedance and Effective Dielectric Constant variation with trace width for structure where  $H = 1.575\text{mm}$ .

Table 4.3: Excerpt of calculated values for the microstrip transformer.

H	W	$\epsilon_r$	$\epsilon_{eff}$	$Z_o$
1.524	4.5	9.2	6.922	26.87
1.524	4.6	9.2	6.938	26.46
1.524	4.7	9.2	6.954	26.07

### Initial Theoretical Design

Whilst theoretically possible to have a single microstrip line with the correct impedance to match the  $50\Omega$  input to the approximately  $14\Omega$  cable, it was decided for their to be an initial  $50\Omega$  microstrip section to allow for ease of connection to the SMA connector. For the initial theoretical design Rogers TMM10 material was used. This has a stated dielectric constant of 9.2 and the eqs. 4.5 to 4.8, given above, were used to determine the values required to match impedances given in table 4.3. A nominal length of 14.7mm was calculated with the new effective dielectric constant using eq. 4.4 and multiplying by three, for the same reasons as discussed when considering the co-axial transformer, to allow for ease of attachment to the new cable.

A render of the intended structure is given in figure 4.27. This helped to to assess connection strategies and to ensure the transformer would be small and lightweight enough to allow for inclusion in a handpiece and for intended use of the device as a whole.

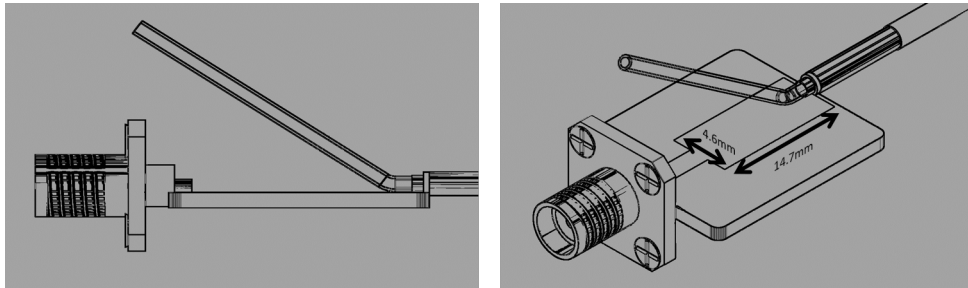


Figure 4.27: Side and Perspective 3D render sketches of the theoretical design of the transformer structure

This structure was then modelled in CST Microwave Studio to determine the

optimal geometry for the traces. Initially these simulations were conducted on the Rogers TMM10 material [80].

The library material for Rogers TMM10 from within CST was used to ensure that the properties would closely match those of the actual material. Both the ground and trace material are modelled as annealed copper with a thickness of 35 micron as given in the datasheet for TMM10. To excite the structure and to match the intended excitation in the manufactured transformer, two discrete edge ports were used between the input and output and the ground metallisation. The ports were set to  $50\Omega$  and  $14\Omega$  for the input and output respectively. Initial trace thickness and length were chosen based on the theoretical calculations discussed earlier.

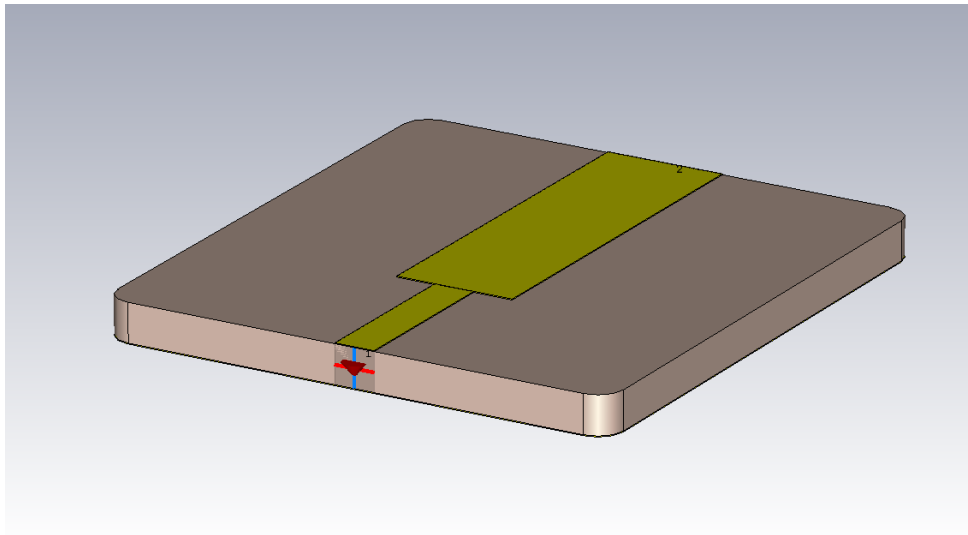


Figure 4.28: Initial Simulation model for the microstrip transformer

Due to the operating frequency and the high dielectric constant of the TMM10 material,  $\epsilon_r = 9.20$  it was decided to multiply the quarter wavelength transformer by three. This will still operate to alleviate the impedance mismatch but will be easier to manufacture. This increase in length will not introduce significant additional insertion loss and so this extra length is acceptable. Should the transformer, in the future, need to be smaller then more precise manufacturing processes can be considered to create a much smaller structure using a single quarter wave length.

The S Parameters for those initial values can be seen in figure 4.29

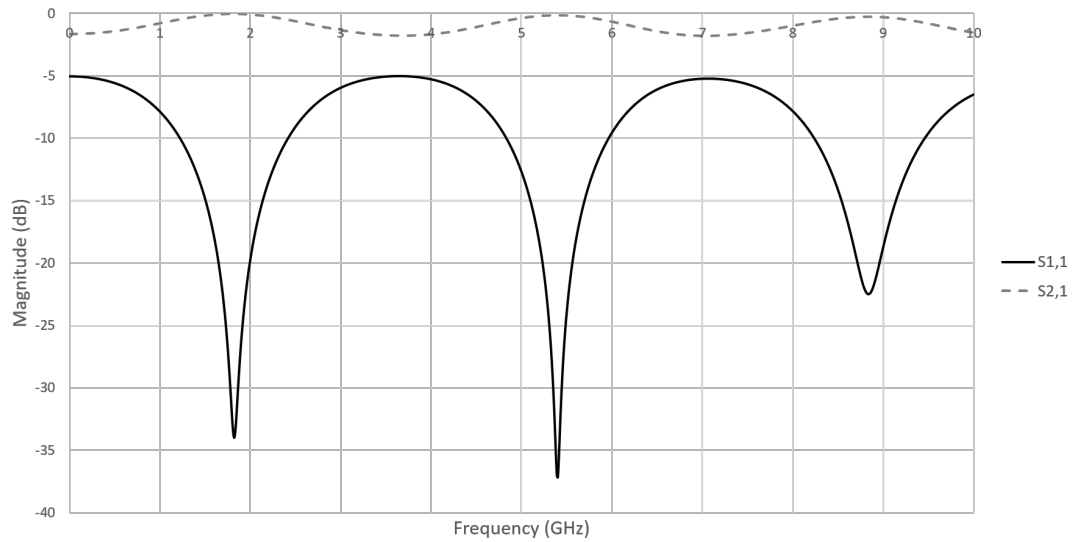


Figure 4.29: Initial Simulation S Parameters for the microstrip transformer

As can be seen from these initial values the transformer is not quite working at the intended frequency but is operating well at 5.4GHz. This could be due to a number of reasons and is one of the advantages of using simulation software is recommended when designing microwave components. Even when considering a simple microstrip trace with ideal stimulation ports there is still some deviation from the theoretical values.

One reason for this apparent change in length could be due to the T shape of the trace itself. This step in width will create a minor discontinuity and introduce both capacitance and inductance into the structure as can be seen in the equivalent circuit given in figure 4.30, for which further information and the original diagram can be found in [81]. This additional capacitance and inductance will alter the match frequency and will need alteration of the length to counteract this.

One way to mitigate the capacitive effect of the stepped microstrip trace would be to chamfer or taper the steps to provide a more smooth transition between impedances. Due to the issues discussed above concerning effective dielectric constant and the introduction of extra capacitance, CST Microwave Studio allowed parameter

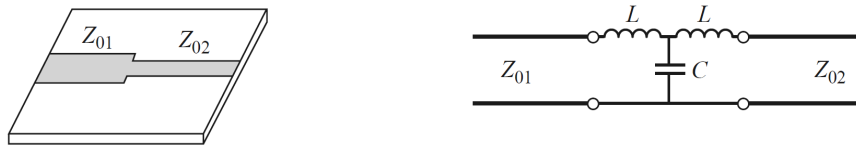


Figure 4.30: Equivalent circuit for a step discontinuity in microstrip

sweeps to be conducted to find the optimal geometry to ensure that the performance of the transformer was acceptable.

Due to the transformer operating optimally at a lower frequency than required it was expected that the transformer trace was slightly longer than a quarter wavelength at 5.8 GHz. The parameter sweep was conducted to see what this optimal length would be given the particular transformer geometry.

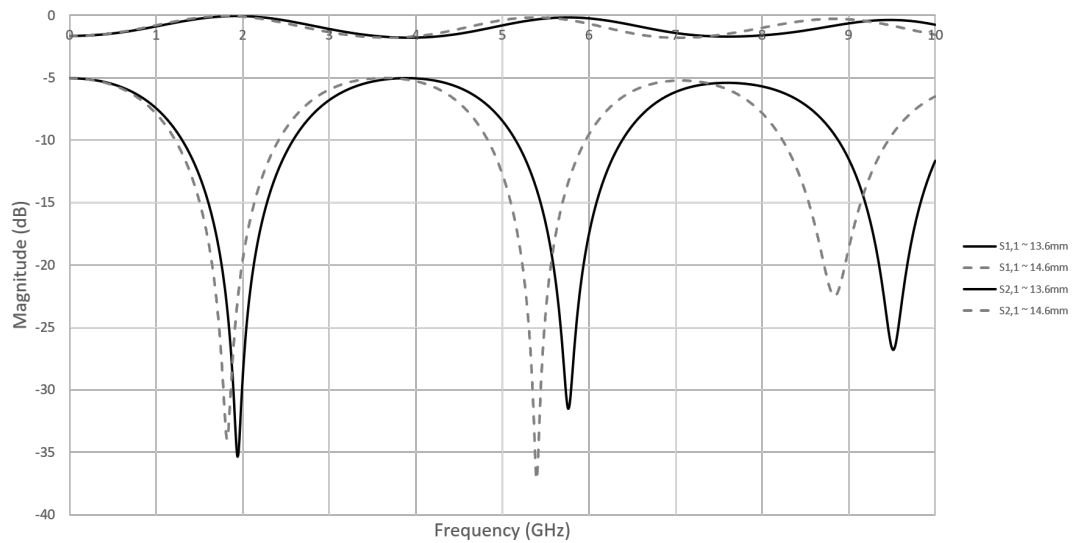


Figure 4.31: Initial Simulation S Parameters for the microstrip transformer with parameter sweep

As can be seen in figure 4.31 both the original theoretical parameters along with the parameters which create the most optimal transformer structure are shown giving an optimised length of 13.6mm.

## SMA and cable connections

The next consideration was how both the SMA and the cable would be connected to the transformer in practice. Not only was it important to ensure these connections operated well electrically but also that they were structurally stable enough to withstand breakage due to movement in the device or flexing of the cable. Not only this, it was clear that variation in connection and the introduction of any extra capacitance or inductance would alter the operating frequency of the transformer.

The initial connection method consisted of soldering the inner conductor of both the SMA and the cable to the trace directly which created problems, in terms of connecting the outer conductors to the ground plane of the transformer. This problem was simulated in CST with the optimal parameters as found previously.

The first solution to this problem considered was the use of conductive copper tape to bridge the gap between the outer conductor of the cable and the transformer. The second simulated solution used a specifically machined block of copper to provide good electrical connection to both the outer conductor of the cable and also the ground plane of the transformer. Both the models, figure 4.32, and the simulated S Parameters, figures 4.33 and 4.34, are shown below.

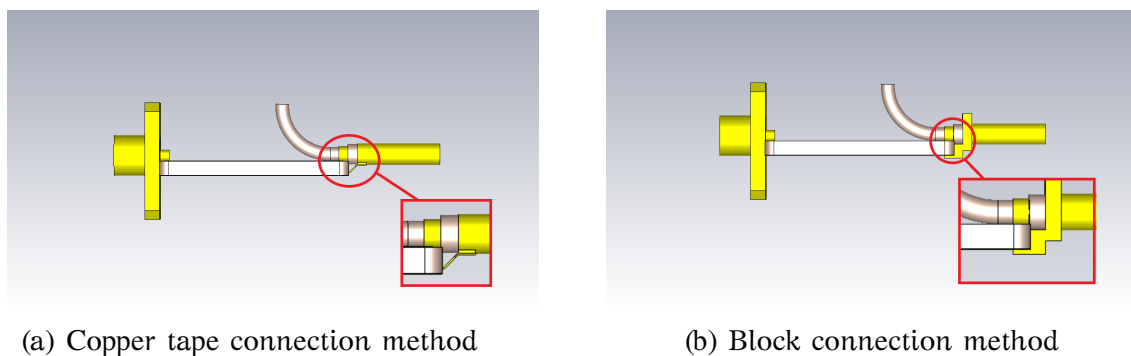


Figure 4.32: Models to assess connection methods for microstrip

It can be seen that the results indicate impedance transformation at the required frequency but the conductive copper tape had higher loss than the machined block and also a much higher reflection from the input port, as such both were unsuitable.

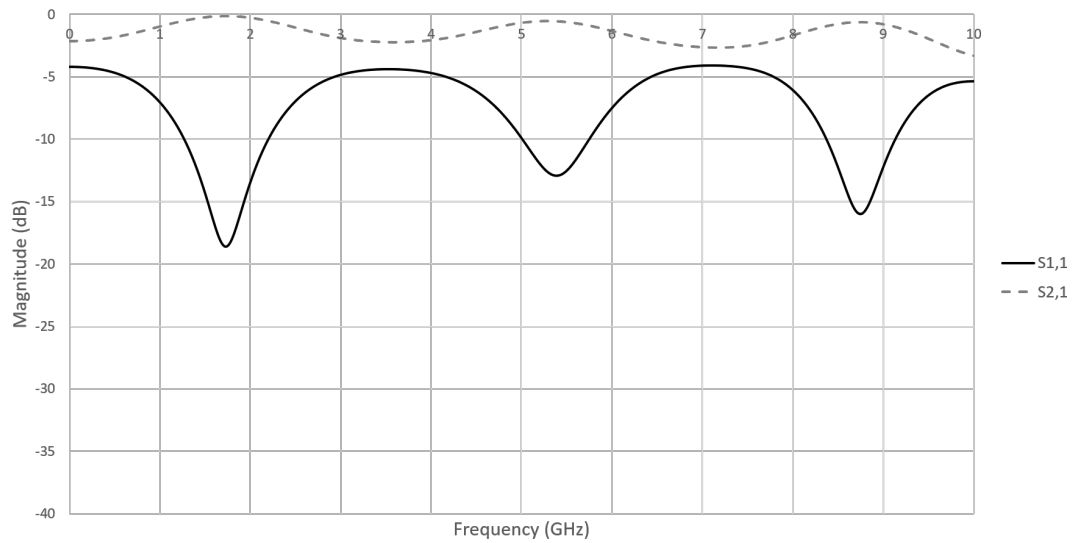


Figure 4.33: Simulated S Parameters for tape microstrip attachment

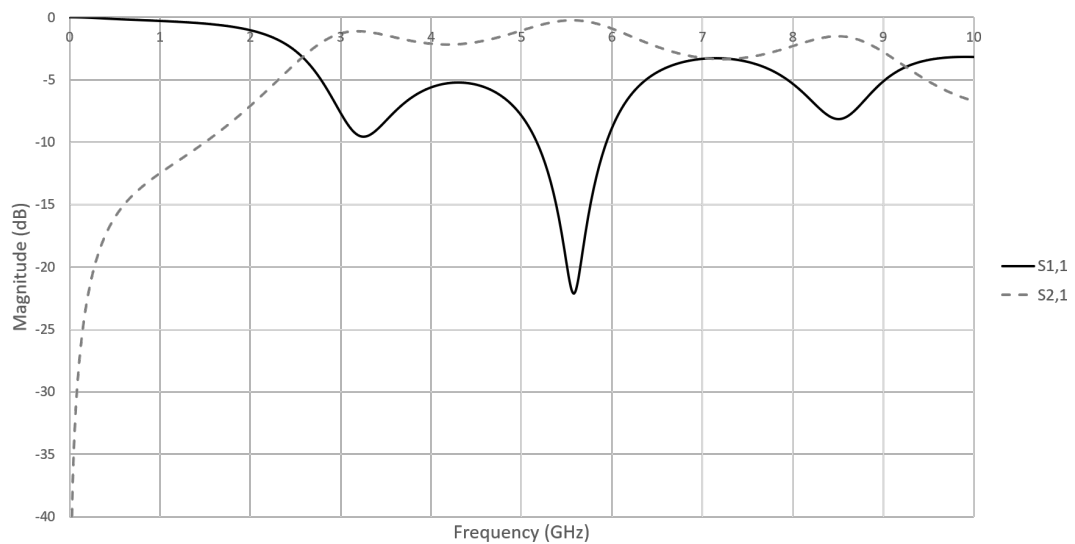


Figure 4.34: Simulated S Parameters for block microstrip attachment

The final transformer structure was prototyped on FR4 board. There were a number of issues with this but as these prototypes were intended to test the operation of the transformer and overall device it was deemed suitable for this task.

### Consideration of using FR4

Initial test transformer prototypes were created with Rogers TMM10 material. The copper layer was hand cut to form the two required traces. This was quite a difficult



process and whilst providing an approximate shape for the required traces, it was clear that the transformer boards would need to be manufactured professionally in order to obtain the desired performance which was done using FR4 board.

FR4 is an industry standard material used in electronic printed circuit boards. It is cheap and relatively easy to prototype with which makes it one of the most popular printed circuit board materials.

However it falls down slightly when it comes to the development of higher frequency microwave circuits. This is due to a number of reasons; initially the loss associated with the substrate can be quite high when compared to that of specific high frequency substrates such as those developed by Taconic and Rogers. This is especially problematic when high power is to be transmitted as the structure can heat up excessively. Power loss is equal to the dissipation factor  $\times$  power and as such a loss tangent of 0.1 and input power of 100W will lead to approximately 10W being lost, usually manifesting as heat. FR4 is not quite this bad, with a loss tangent of approximately 0.015, but this was still a concern. Secondly, the design of high frequency boards can be quite sensitive to both the dielectric constant and the loss tangent of materials. Due to the availability and relatively low cost of FR4 boards it is difficult to specify both of these quantities and tests have shown that both characteristics can vary even within the same batch.

As can be seen in figure 4.35 both the dielectric constant and the dissipation factor vary by a few percent and is even specified at a max of 5.2 and 0.035 which is a large variation, especially when designing devices which require known dielectric characteristics such as this microstrip transformer.

A mock simulation of a microstrip structure, model shown in figure 4.36 with varying dielectric constants and dissipation factors is shown which highlights the values in this report compared to the maximum values discussed here. For example wavelength varies by approximately 1.3mm with given dielectric constant values of 4.67 and 5.20.

## Permittivity & Dissipation factor

- (1) Test Specimen: 100 mm x 100 mm Etched CCL  
 (2) Test Condition: 1 GHz frequency  
 (3) Test Method: Shall confirm to IPC TM 650 2.5.5.9.



Dk spec : Max 5.2, Df spec : Max 0.035

No	1	2	3	4	5	Judge
Dk	4.68	4.69	4.62	4.7	4.67	OK
Df	0.016	0.015	0.014	0.015	0.013	OK

Figure 4.35: Excerpt of test report for IPC-4101D for material EM-827

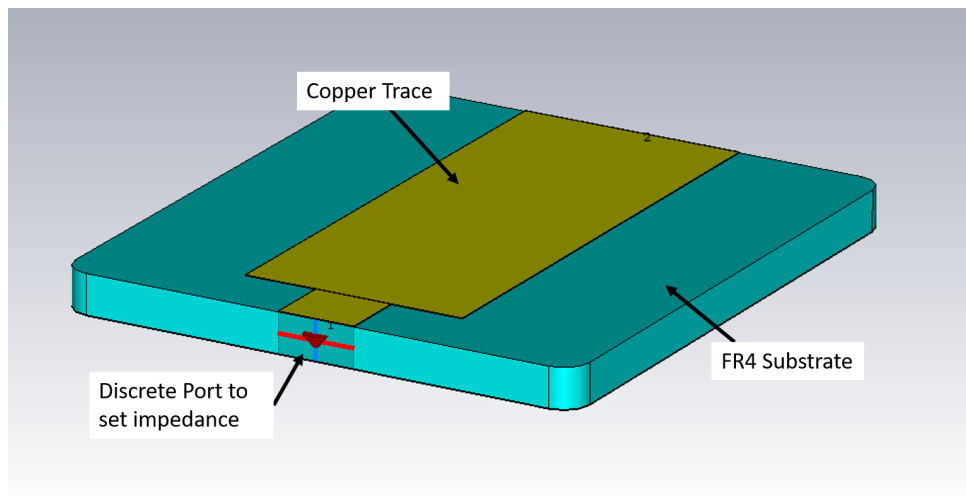


Figure 4.36: Model used to simulate microstrip with varying dielectric constant and dissipation factor

Whilst remaining relatively similar to the data provided from the test batch (grey lines), it could well be that the material supplied could be at the maximum values or even exceeding these (black lines). This can be seen in the highlighted line in figure 4.37 which represents the same design with maximum dielectric properties.

It can be seen from this that the variation in dielectric properties would not

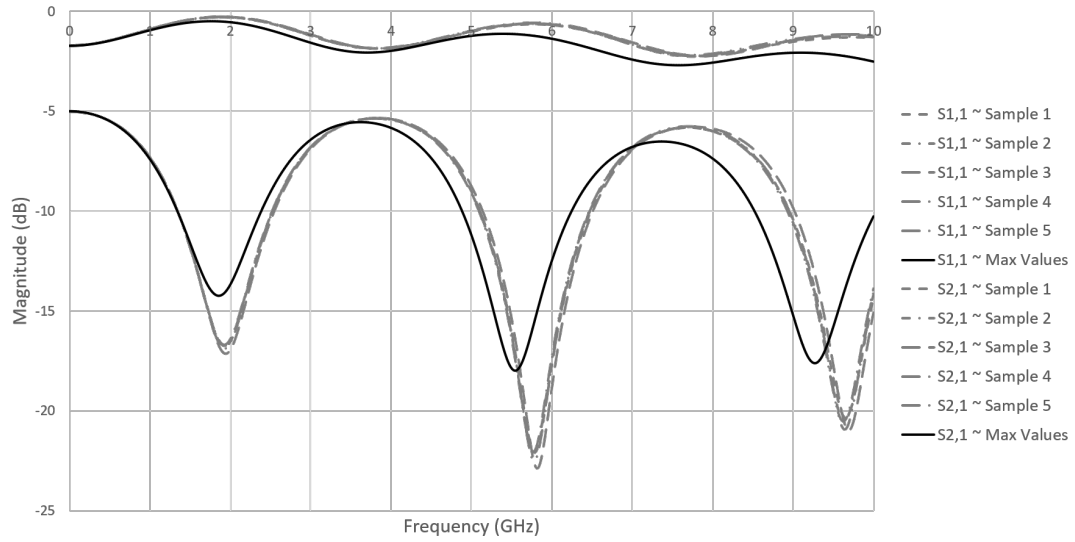


Figure 4.37: Simulation of microstrip with varying dielectric constant and dissipation factor

strongly affect the operation of the transformer. Due to the variability of the dielectric properties in FR4 it was decided to use averages for both the dielectric constant ( $\epsilon_r = 4.67$ ) and the dissipation factor ( $\tan\delta = 0.015$ ) as given in the test report shown in figure 4.35. It was also deemed that FR4 was sub-optimal but would still be suitable for the initial scope of this research.

### Manufacture of the microstrip transformer

Gerber files and images were created and sent off to printed circuit board manufacturer Cambridge Circuit to create a number of transformer of varying sizes. From the simulations previously carried out it was deemed that the most important dimension was the length of the transformer section. The boards were manufactured with the optimal length from the simulations and variant boards created at length  $\pm 1\text{mm}$ . A 1mm variation was chosen to account for any manufacturing tolerance issues which may cause the electrical length of the structure to be marginally different to the structure as simulated. 1mm equates to approximately 340MHz variation in matching frequency. Subsequent testing of the tables as discussed in section 5.14

showed that the tolerances and dimensions of the manufactured boards were correct and the simulated length of 3mm showed good operation of the transformer.

The boards were manufactured on 1.6mm FR4 board via etching and routing at Cambridge Circuits to ensure accurate dimensions and consistency between boards.

Once the board had been prototyped methods of connecting the SMA connector and the cable were considered. Failure to provide an adequate ground connection would lead to increased losses due to a portion of the wave being reflected and failure to provide an adequate signal connection would prevent the device from operating as expected due to mismatch and or complete device failure.

A number of coax to microstrip adapters have been developed and these suggest that co-axial cable to be soldered directly onto the microstrip trace [82]. Initial tests showed this would be possible and the transformer would operate, however, the connections were weak and there was a risk they would break with any movement of either the cable or the transformer itself.

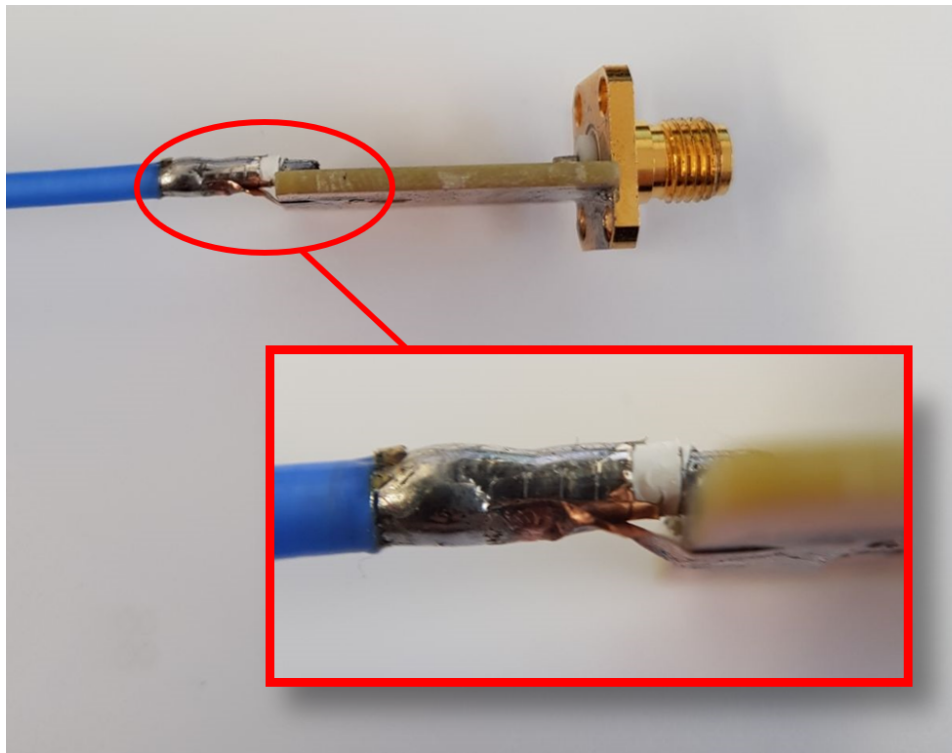


Figure 4.38: Photograph of assembled microstrip transformer with copper tape outer conductor connection

Another issue with this connection was the gap between transformer ground and cable outer conductor. Due to the substrate thickness, a small section of copper tape was used to bridge the gap between both the conductors. Whilst providing a good electrical connection, it was unclear as to how much affect this had at 5.8GHz with the resultant device having much higher attenuation as per previous simulated results. Once again this connection was weak and tended to come apart or malfunction with movement. Due to the small size of the cable connection and the difficulty in working with copper tape it would have also been difficult to achieve a consistent connection throughout multiple devices. Another concern with the use of copper tape was the presence of the adhesive backing. This effectively introduces a further dielectric layer altering the structure and the copper may not adhere fully to the substrate.

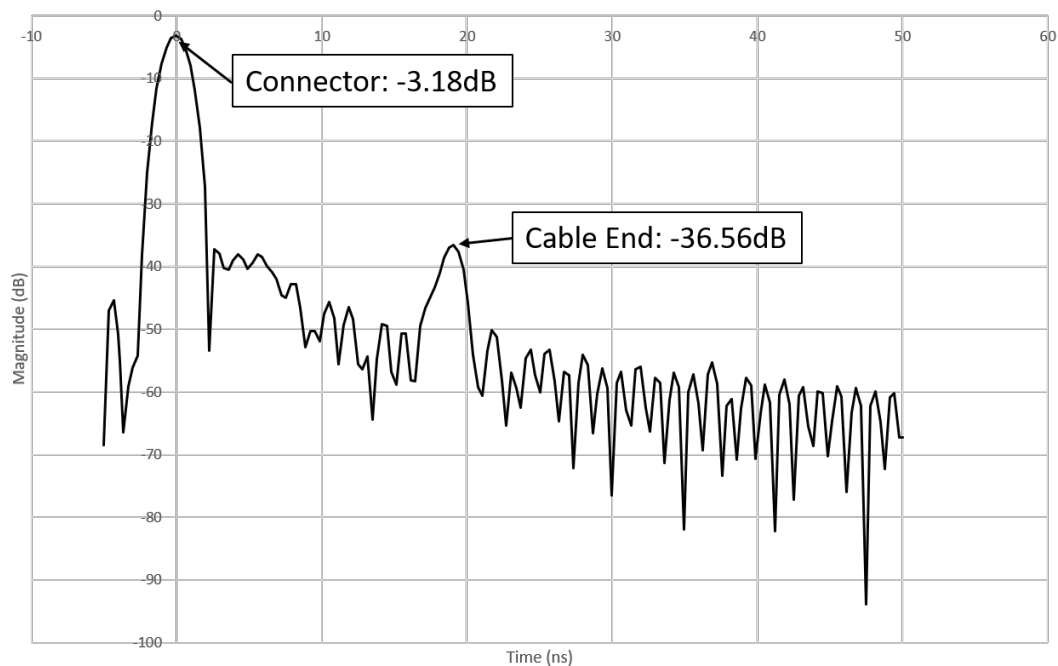


Figure 4.39: Time domain plot of 4.66m cable connected to microstrip with copper tape outer conductor connection

It can be seen from the time domain plot in figure 4.39 that the connection between the transformer and cable is pretty poor at -3.18dB which is unacceptable. This means that only 48.07% of the power would be launched into the cable. If we

consider other test results, which give a cable loss of approximately 2.9dB/m, then we can expect a peak in the time domain at the distal open end of -27.02dB for the 4.66m cable used here. Considering this value with the measured value in figure 4.39 it can be seen that the connection method used here may introduce up to 6dB of additional loss.

To solve the situation of unsuitable ground connections, extra attenuation and breakage due to movement, a ground tray structure was designed. This houses the transformer board, allows for good ground connections and also ensures a stronger connection to both SMA and novel microwave cable.

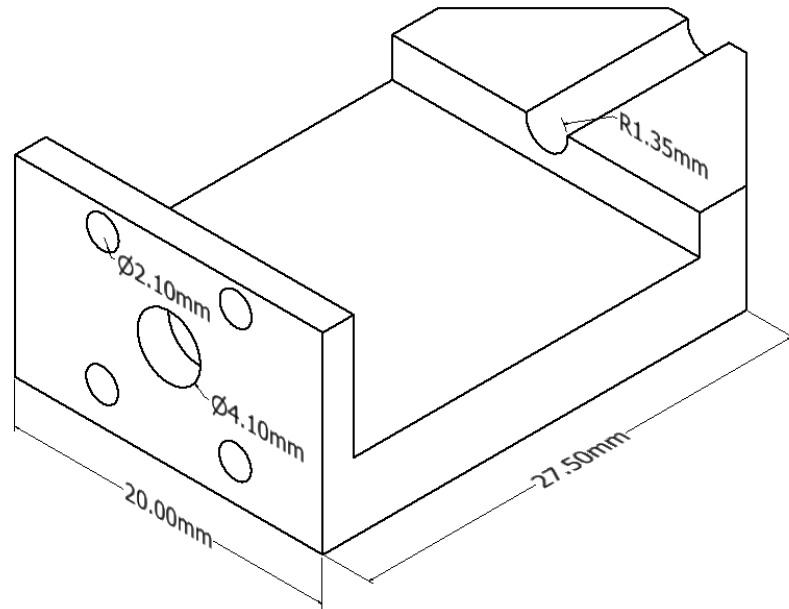


Figure 4.40: Illustration of the ground tray structure

Simulated S Parameters gave confidence to the design which is illustrated in figure 4.40 and show good matching between the generator and the cable impedances. Overall this indicates good operation of the transformer structure even when placed inside the ground tray.

An initial prototype was machined out of aluminium with the same geometry as shown in figure 4.40. Holes were drilled and tapped to allow the SMA connector to be

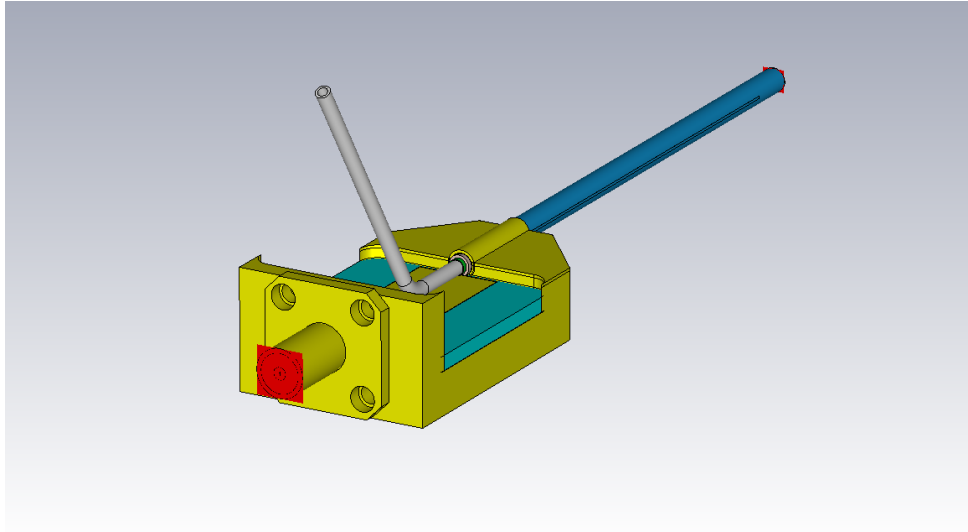


Figure 4.41: Perspective view of the final simulation model

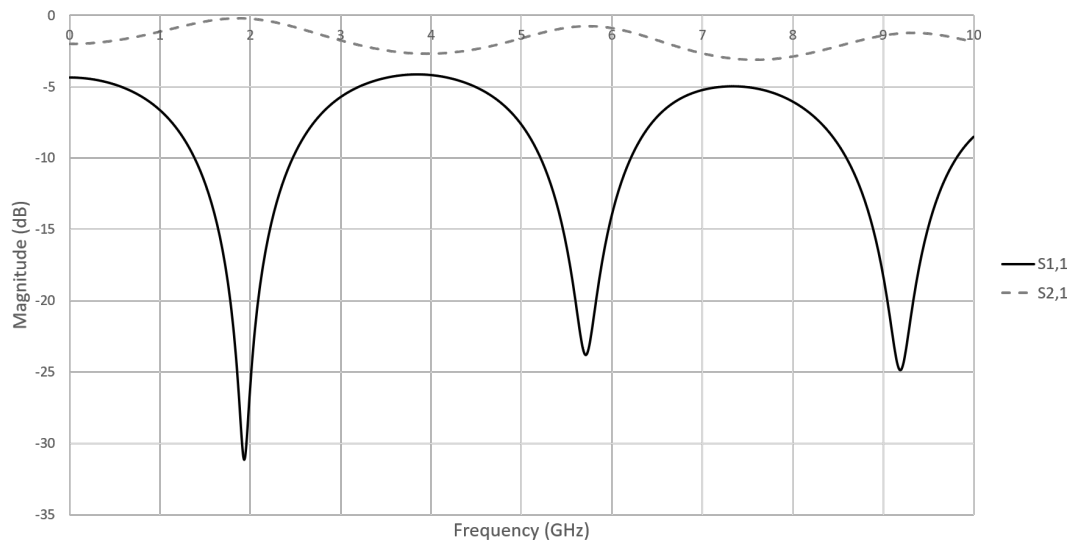


Figure 4.42: Simulated S Parameters for ground tray transformer structure

screwed directly into the ground tray structure for optimal connection and included a ridged section for the cable to fit into this providing structure and strength even when bending the cable. Due to difficulty in soldering to aluminium the cable was held in place and mechanically secured to the ground tray. This ensured good connection between the cable and tray.

The entire ground tray structure itself acts as a ground. The cable, SMA connector and the transformer board itself are all electrically connected to the structure in a

much more secure way than previous methods of attachment.

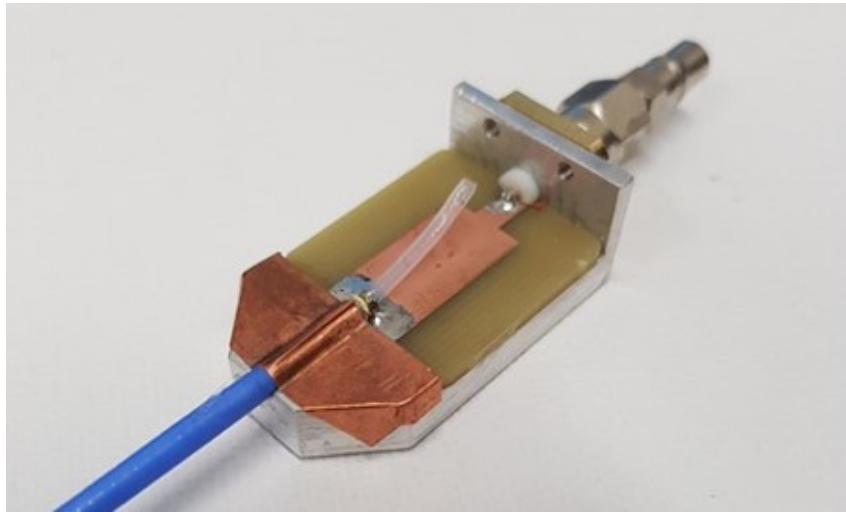


Figure 4.43: Photograph showing the microstrip transformer and ground tray structure

### Effect of microwave on saline during delivery

One concern with the use of a microstrip structure was whether the fields radiating from the trace would interfere with the hollow channel; if this was filled with saline for instance. One possible outcome was that this saline would absorb the electromagnetic energy and be heated to a dangerous level causing damage to the device or more importantly to the patient.

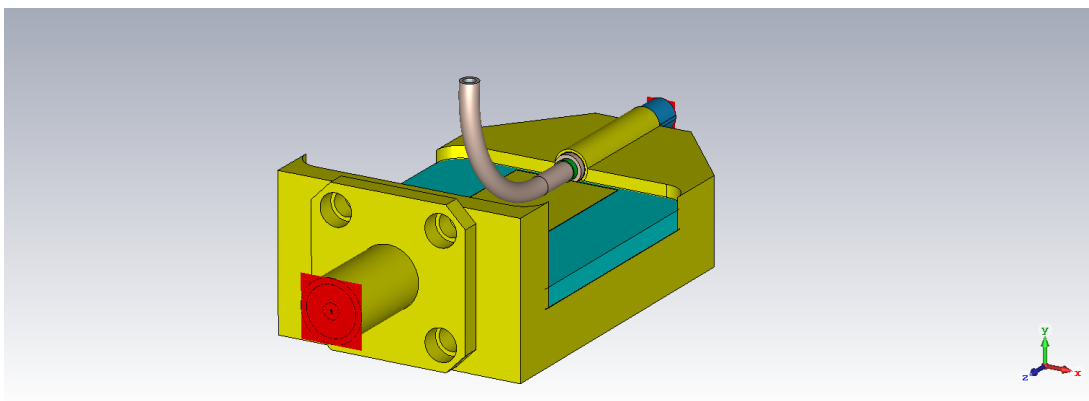


Figure 4.44: Simulation Model used to assess the microstrip transformer with filled hollow channel



The transformer structure was simulated with the hollow channel of the cable filled with sea water. This is to approximate saline which has comparable electrical properties due to salinity. Sea water has an average of 35,000 parts per million (ppm) whereas the sodium chloride solutions commonly used in medical procedures have around 9000 ppm. Sea water has been used here due to its presence in the CST Microwave Studio material library and as a worst-case scenario for a conductive liquid in the hollow channel.

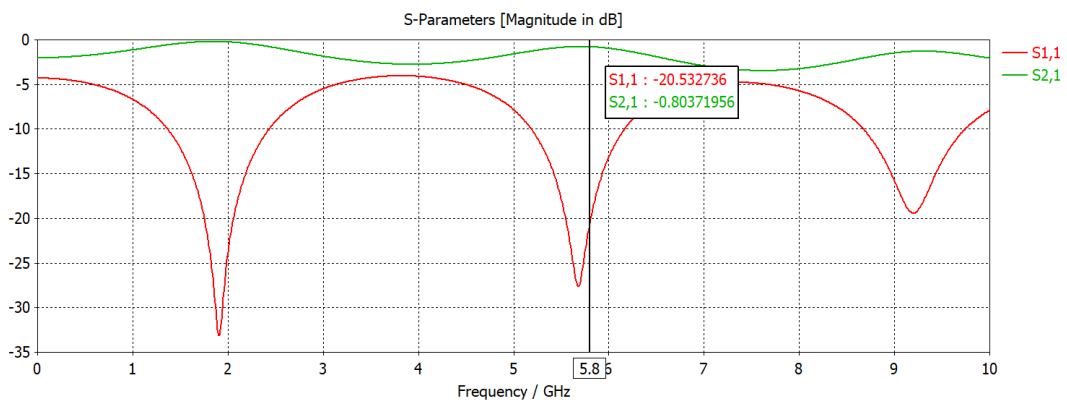


Figure 4.45: Simulated S Parameters for microstrip transformer with filled hollow channel

The S Parameters, as shown in figure 4.45 remain relatively unchanged, which is to be expected. The main reason for this simulation was to ensure that the fields generated in the air gap above the microstrip transformer board did not affect the contents of the hollow channel such as the heating of the solution being delivered to the patient.

It can be seen from figure 4.46 that there is some power delivery into the salt water within the hollow channel. The simulated volume loss within the entire cylinder of water is 0.000452W, however the power loss density plot shows that not all the fluid is being affected. If this value is taken as worst case and applied to a small length of the fluid cylinder, say 10mm, the theoretical temperature increase due to that power can be calculated. This volume loss is calculated with respect to a simulation input of 1W. A 50W input from the generator, once again worst case, was considered although

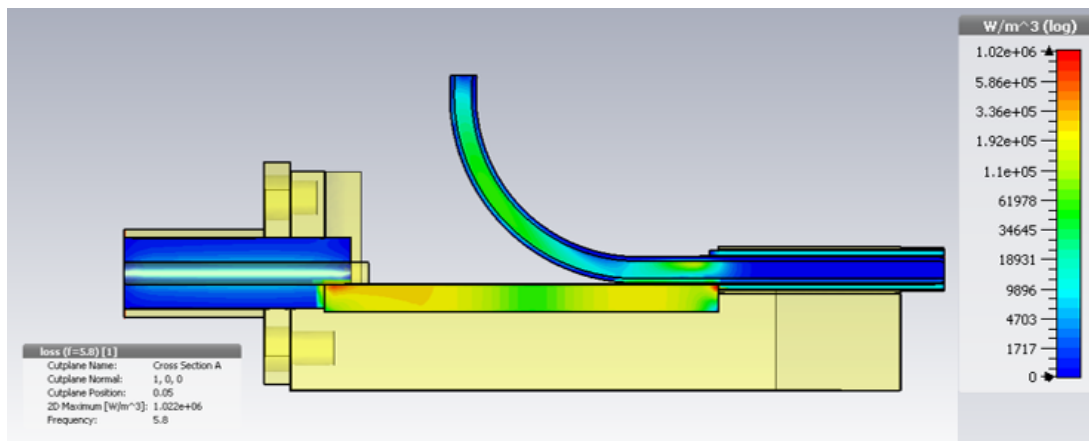


Figure 4.46: Simulated Power Loss Density for microstrip transformer with filled hollow channel

some energy will be lost through the cables and connectors before the transformer.

First multiplying this volume loss by 50W to match our generator input power the power loss in the whole body of fluid is 0.021W. This is then considered as a maximum loss in a 10mm cylinder. The following table 4.4 shows the calculations used to calculate the temperature increase.

The situation however is not as clear as this. Although the liquid may experience a 6.2 degree increase in temperature, it is likely that either the liquid will be used when microwave energy is not active, or alternatively will be used at the same time; in which case the liquid will be flowing through the channel and thus the energy delivery will be spread out, for instance the 10mm cylinder of liquid as described above may only pass through the fields for 1s or less which gives a temperature rise of 0.62 degrees.

Table 4.4: Theoretical Calculation of temperature increase due to power delivery into saline

Sea Water Density	1025	kg/m <sup>3</sup>
Sea Water Specific Heat Capacity	4.2	kJ/kg/C
Cylinder Radius	5.00E-04	m
Cylinder Length	1.00E-02	m
Cylinder Volume	7.85E-09	m <sup>3</sup>
Cylinder Weight	8.05E-06	kg
To heat volume by 1 degree	3.38E-05	kJ
	0.0338	J
Delivery Power	0.021	W
Delivery Time	10	s
Delivery Energy	0.21	J
Temperature Increase	6.21	Degrees

## ***Chapter. 5***

---

### ***A Novel Transmission Line...***

---

## **5.1. Design and Development**

### **5.1.1 Dimension Considerations**

With the advent and increase in popularity of minimally invasive surgical procedures carried out using flexible scoping devices, e.g. endoscopes and gastroscopes, rather than shorter more rigid devices as used in laparoscopic or key-hole surgery, medical devices are required to be much longer, more flexible and have smaller diameters than those previously used for more traditional laparoscopic procedures. [83] These requirements brought about a number of constraints for the development of the energy delivery cable. These include:

- Maximum attenuation of 3dB/m to minimise loss over the entire length of the device
- Maximum outer diameter of 2.5mm for all parts of the proximal end of the device (cable and radiative tip)
- Minimum diameter of hollow channel of 1mm

Following on from the previous sections, it is clear that these requirements make the design and development of the cable rather challenging. Maximising the available hollow channel and minimising the outer diameter, limits the amount of dielectric material between the two conductor and therefore increases attenuation. Not only does this affect the loss but it also means that the cable inevitably has to be a

non  $50\Omega$  line which gives a requirement for impedance matching or transforming sections between the  $50\Omega$  generator impedance and the new co-axial cable.

### 5.1.2 Material Considerations

A number of decisions had to be made with regard to material choices for both the conductors and the dielectric material. The main consideration was a balance between optimal performance and cost.

Conductor materials needed to be chosen to maximise conductivity and therefore minimises losses without being prohibitively expensive. Use of the skin depth concepts discussed above allow the coating of a base metal with a more conductive layer. As this can be very thin, a more expensive metal such as silver or gold can be used. As the E and H fields will be mainly focused within this layer the cable will have lower attenuation along with lower cost.

Dielectric material needed to be chosen both with respect to minimising loss but also to ensure that the cable can withstand the power required to achieve the desired tissue effects. The dielectric breakdown strength, in V/m, required for this application is minimal as the final device will only make use of microwave energy as discussed in section 2.4.3. Should the cable be used for higher voltage applications such as Radio Frequency ablation, dessication or resection then modification of the design may be required to ensure that the amount of dielectric material between the two conductors is sufficient to handle voltage levels associated with either monopolar or bipolar RF treatment.

PTFE, however, has a high voltage breakdown strength at approximately  $23.6\text{kV/mm}$  [84]. As the microwave cable contains a PTFE wrap with wall thickness of approximately  $0.28\text{mm}$  theoretically it should be able to withstand voltages of up to  $6.6\text{kV}$ . This indicates that the novel cable structure should be suitable for the propagation of RF energy but further testing should be carried out before being used for RF

electrosurgical applications.

### 5.1.3 Prototype Rigid Design

An initial prototype consisted of a rigid design to prove the concept of a hollow channel co-axial line concept. This comprised a PTFE tube as the dielectric and two brass tubes forming the inner and outer conductor. The inner conductor had an outer diameter of 2mm whilst the outer conductor had an outer diameter of 4mm. Both conductive tubes had a wall thickness of 0.45mm. The PTFE dielectric tube had a wall thickness of 0.55mm. This geometry can be seen in figure 5.1.

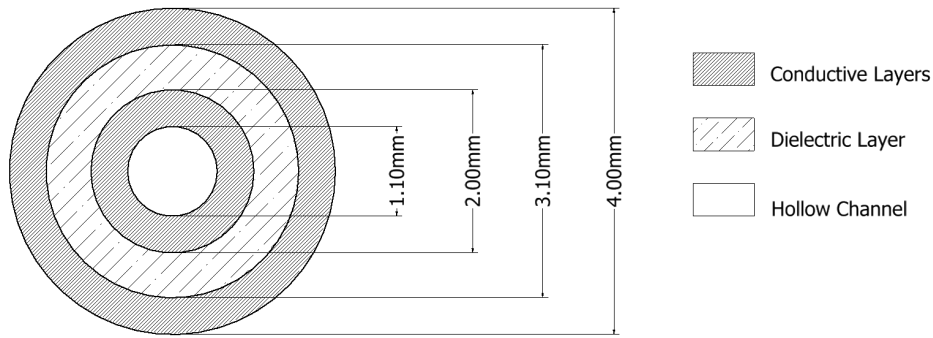


Figure 5.1: Model showing the individual layers which comprise the rigid prototype structure

Brass has relatively good conductivity and is much more practical compared to copper tubing. It has a conductivity of approximately  $15.9 \times 10^6$  S/m. Theoretical loss calculations show a slightly higher attenuation due to the use of brass when compared to silver. For this prototype however this was not a major concern. Figure 5.2 shows this comparison of loss.

An initial manufacturing attempt can be seen in fig 5.3. Whilst having an outer diameter of approximately 1.5 times larger (4mm) than the required diameter of the actual cable (2.5mm) and despite being inflexible this prototype served as a positive step in identifying issues and considerations ready for the actual design and

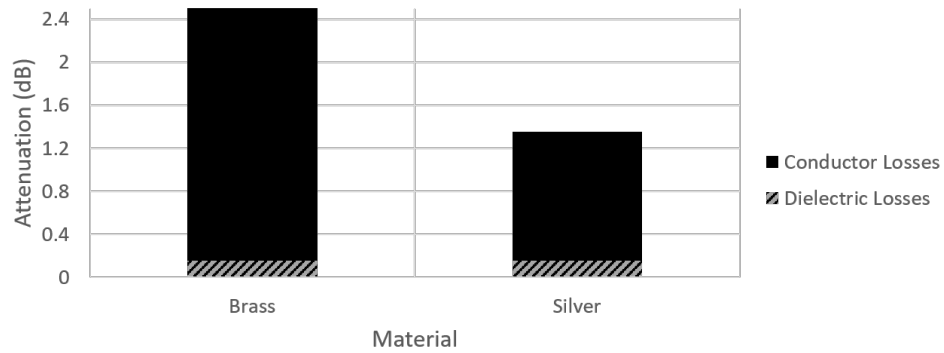


Figure 5.2: Graph showing theoretical comparison between the use of brass vs silver conductors for the rigid prototype geometry at 5.8GHz.

development of the flexible and much thinner cable.

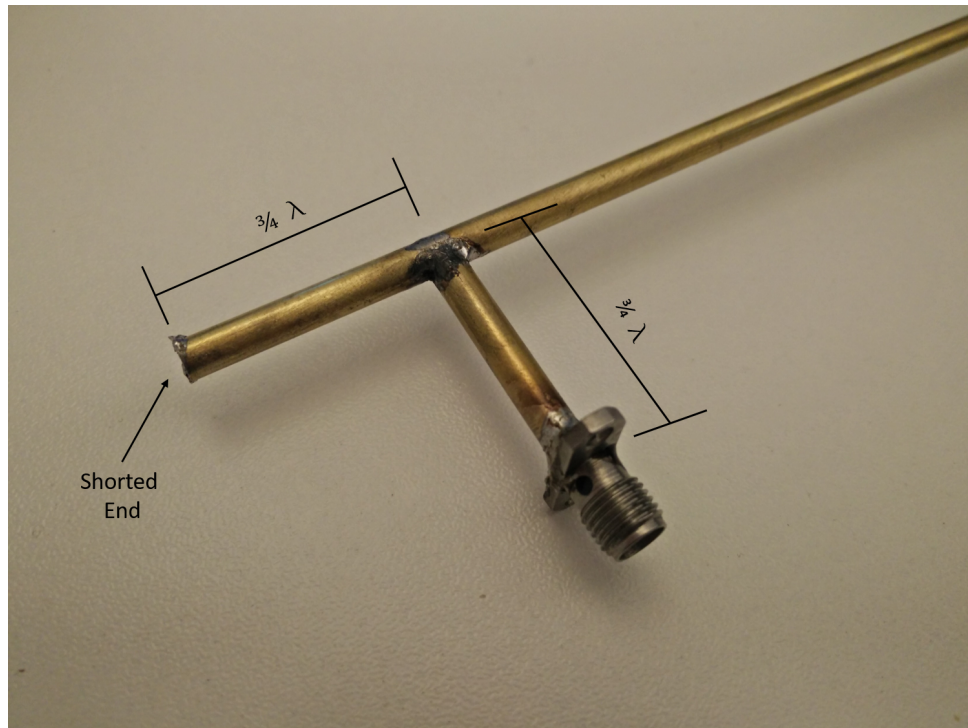


Figure 5.3: Initial prototype design of the rigid novel microwave cable idea

As can be seen, a standard 50Ω SMA connector is used to connect the structure to the VNA. Due to the deviation from 50Ω impedance as discussed in section 5.1, a quarter wave transformer section was required to minimise mismatch losses at both the input and output of the rigid prototype.

The quarter wave impedance transformer section comprises a length of transmis-

sion line that is equal to any odd multiple of quarter wavelength in the dielectric material used. The impedance of the section needs to be the geometric mean of the two impedances which are to be matched. This simple structure works through destructive interference where the reflected waves from the load interfere with the reflected waves of the mismatch boundary and are cancelled out. Further explanation of this principle is given in section 2.1.5.

CST Microwave Studio (CST) was used to simulate the structure to provide optimal geometry for both the quarter wavelength from the shorted end and also for the length of the impedance transformer and results indicated acceptable insertion loss and minimal reflections at the interfaces between the line and transformer section.

Theoretical calculations suggested that both transformer sections should be the same length. To correctly equate the simulation with the device design a 1mm section of co-axial line with an impedance of  $50\Omega$  was used along with a waveguide port to provide the correct impedance input to the cable. This extra section was required as the standard waveguide ports used within CST provide an input which matches the geometry they are applied to, i.e. matching the impedance of the quarter wavelength section rather than having the standard  $50\Omega$  input.

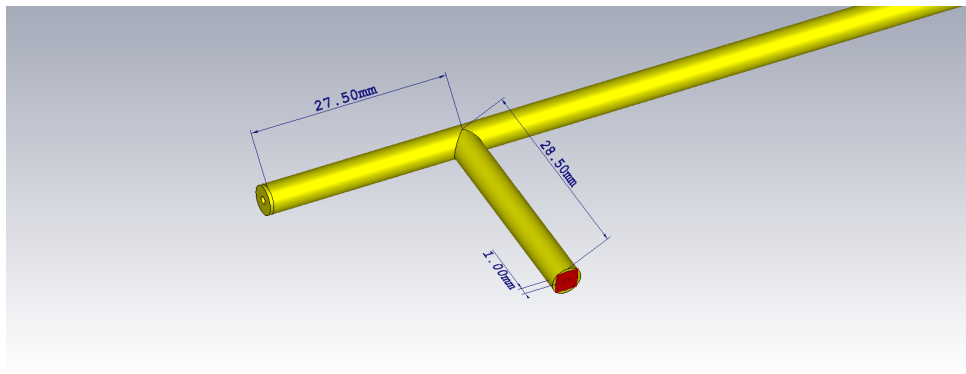


Figure 5.4: Simulated Model for Rigid Prototype design

Simulated S Parameters for the above structure can be seen in fig 5.5 and corresponding reflected and transmitted power for varying lengths can be seen in table 5.1. A parameter sweep was conducted to assess how sensitive the prototype was to



errors in the measurement and manufacture of the quarter wave transformer. As can be seen even with an offset error of 2mm, a mismatch loss of less than 2% will only be introduced. This is due to a shift in the matching frequency but due to the bandwidth of the match the transformer section remained usable.

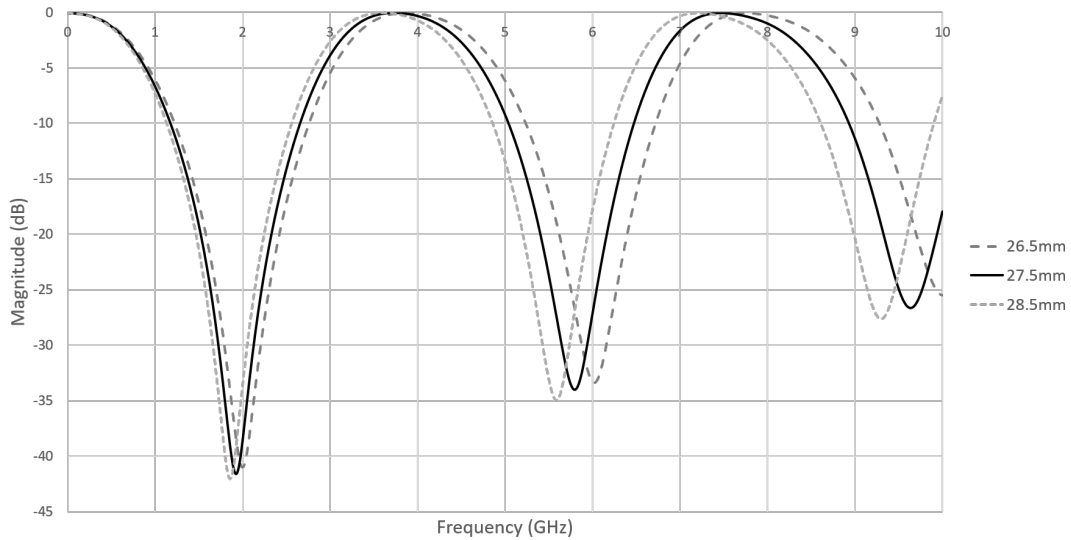


Figure 5.5: Simulated  $S_{1,1}$  for Rigid Prototype design

Table 5.1: Calculated power from simulated rigid prototype results

Length (mm)	$S_{1,1}$ (dB)	Reflected Power (%)	Transmitted Power (%)
25.5	-18.83	1.45	98.55
26.5	-26.87	0.21	99.79
27.5	-33.95	0.04	99.96
28.5	-26.73	0.21	99.79
29.5	-17.62	1.73	98.27

Unfortunately, during the testing phase of the rigid prototype it was clear that the method used for attaching the quarter wave transformer was not suitable and shorting occurred between the conductors.

Initially a 4mm hole was drilled into the outer conductor of the main structure. A smaller hole (1mm) was then drilled through the PTFE dielectric tube and partially into the inner conductor. Each component of the transformer section was then inserted into these holes. The transformer inner conductor was initially electrically

connected to the inner conductor of the main structure. The PTFE dielectric tube for the transformer was then inserted. Finally the transformer outer conductor was electrically connected to the outer conductor of the main structure. Figure 5.6 shows this process.

It was difficult to adequately connect the two inner conductors together due to the presence of the dielectric tube in the main structure. It is believed that the heat required for soldering the two connections damaged the dielectric material and allowed a short to form between the two conductors. The use of flux to allow for ease of soldering may have also left residue in between the structures and as it heated will have likely caused damage to the dielectric or created a short between the two conductors also.

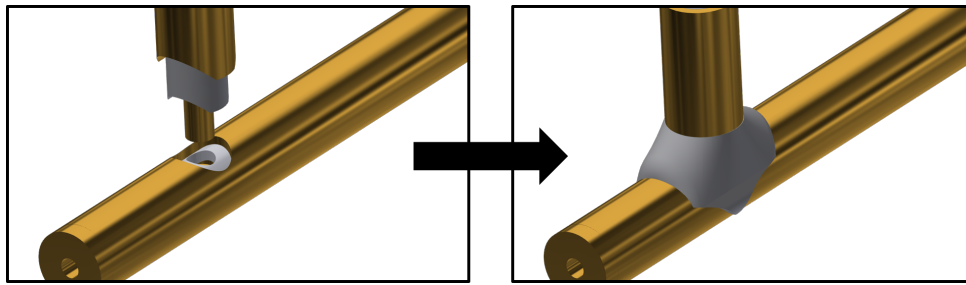


Figure 5.6: Assembly procedure for attaching the impedance transformer section to the rigid prototype.

Whilst it was clear that the hollow co-axial structure would function as expected, a new approach to manufacture the cable needed to be considered. Not only did this quarter wave connection method cause issues, but it was clear that the use of brass tubes would never fulfil the project requirements. The development of this prototype structure however, enabled a non 50 $\Omega$  co-axial line and a  $\lambda/4$  wavelength impedance transformer to be prototyped and measured. This was the first feasibility study for the hollow non 50 $\Omega$  co-axial line.

## 5.2. Flexible Cable Design and Manufacture

Three prototypes were developed during the work using a common style of manufacturing which will subsequently be discussed. Due to the requirement for the cable to be flexible in order to allow for endoscopic insertion to the treatment site, wrapped foil based conductors were considered to be the most suitable for this application. The basic structure of the cable can be seen in fig 5.7. Attempts at applying a thin layer of silver directly onto the PTFE tubing were discussed at the very beginning of this research project. The difficulty in this method is the presence of carbon-flourine bonds which are very strong and prevent other molecules from attaching via substitution reactions, the very small van der Waals forces associated with the molecules of the PTFE also give it the characteristic 'non-stick' surface. A number of possible solutions were investigated with the most promising being a technique which Zeus Inc. are currently developing which would include the pre-treatment of the PTFE tube and then the deposition of silver on both the internal and external surfaces. Unfortunately this technology is not readily available at this moment but will be considered in the future. The application of a thin layer directly onto the PTFE structure would not only allow for ease of manufacture but also allow for a much thinner conductor layer to be used, thus creating more space. This extra space can either be used to increase the diameter of the hollow channel, lessen the attenuation by having a thicker layer of dielectric material or minimise the total outer diameter of the cable for applications which are required for much smaller scopes such as treating deep into the bronchial tree.

The 3 main parts; inner conductor, outer conductor and the dielectric layer are all wrapped around a central inner tube made of solid but flexible PTFE. This provides structure for the cable and also forms the hollow channel to allow the passage of liquids, visualisation systems or other devices such as graspers or biopsy forceps. The whole cable is then encapsulated in an outer jacket extrusion.

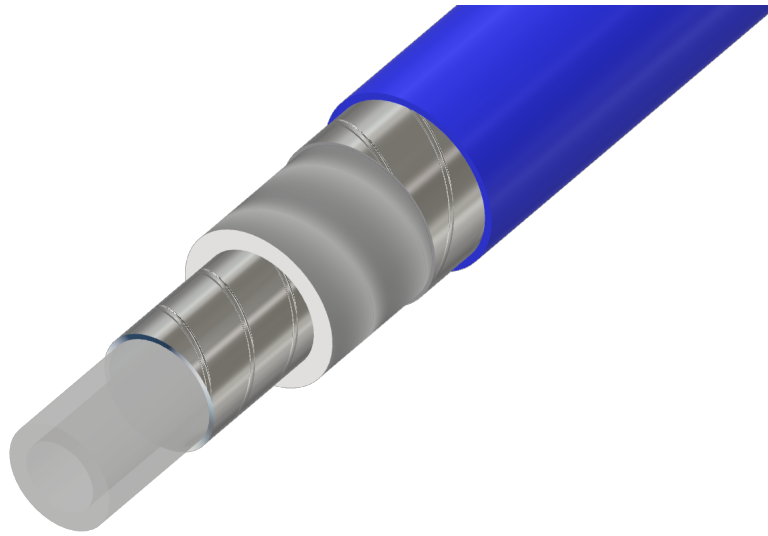


Figure 5.7: Model showing the individual layers which comprise the novel microwave cable structure

The geometry of the new cable can be seen in fig 5.8. As can be seen the cable has a maximum outer diameter of 2.5mm with a minimum hollow channel of 1mm.

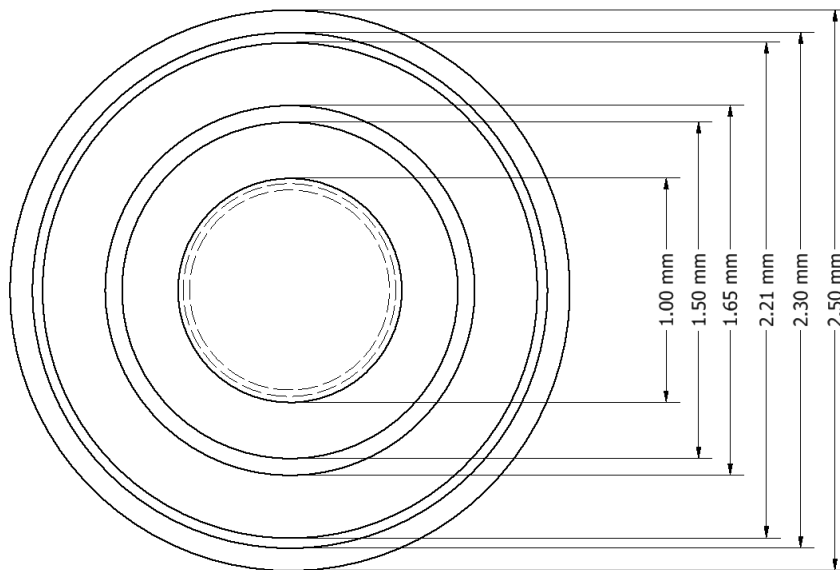


Figure 5.8: Diagram showing the size of each layer for the novel microwave cable structure

Each conductive layer consists of a wrap of silver coated copper tape. The copper provides a less expensive base structure for the more conductive silver layer to be

coated onto. Due to skin depth considerations only a thin layer of silver is required to be used meaning that there will be lower loss throughout the cable. Similarly the dielectric layer comprises a wrapped low density PTFE tape.

As previously mentioned, and as demonstrated in the design of the rigid prototype, the structure of the cable means that it must deviate from the industry standard of  $50\Omega$ . The expression to find this deviation in impedance is given in eq 2.4 and gives an impedance of approximately  $14\Omega$ . Whilst this is a deviation from the normal and seems to be contrary to the points discussed in section 2.1.2, this deviation was required in order to ensure that the specifications of loss, hollow channel size and maximum outer diameter were still maintained.

Whilst not of considerably affecting the performance of the cable, this deviation does require the use of an impedance transformer both for the testing and subsequent operation of the device. Further details regarding these transformer structure can be found in chapter 4.

One other advantage of this concentric structure is the ease of rotation for endoscopically inserted devices on the whole. Testing on non-concentric devices conducted at Creo Medical Ltd showed that a non concentric cable does not perform optimally when rotating, this is especially the case when the device is inserted into an endoscope in retroflex, where the tip of the device is fully inverted at its maximum bend radius, or when the device is navigated through the tortuous path of the gastrointestinal tract. Optimal performance in this case refers to the ability of a clinician to rotate the proximal end of the device and experience a 1:1 turn ratio with the distal tip. It is believed that the use of a concentric structure will equalise friction forces and lead to improved rotation.

### 5.2.1 Prototype 1 - Company A

The initial prototype developed by Company A comprised the novel microwave cable construction made up of multiple wrapped layers as discussed above. However the dielectric material used in this initial design was as expanded PTFE which had a dielectric constant of approximately 1.5 when wrapped. From eq. 2.4 the cable was designed with an impedance of approximately  $17.8\Omega$ .

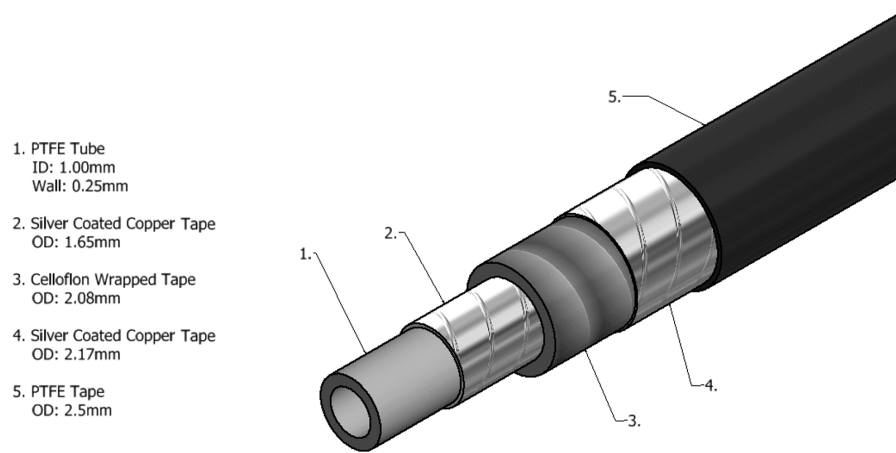


Figure 5.9: Render of the Prototype 1 Cable

### 5.2.2 Prototype 2 - Company A

Prototype 2 was developed based on the findings from prototype 1. Special focus was placed on the wrapped conductors as inspection of the first prototype indicated that the silver coated copper tape was not wrapped as tightly and evenly as required. Any variation in this; such as the wrap overlapping too much in certain parts or having gaps in the conductive layer would lead to multiple small reflections along the line and therefore higher attenuation whilst also making the cable more susceptible to faults when bending. For this reason a braided inner conductor was tested, once

again made of silver coated copper.

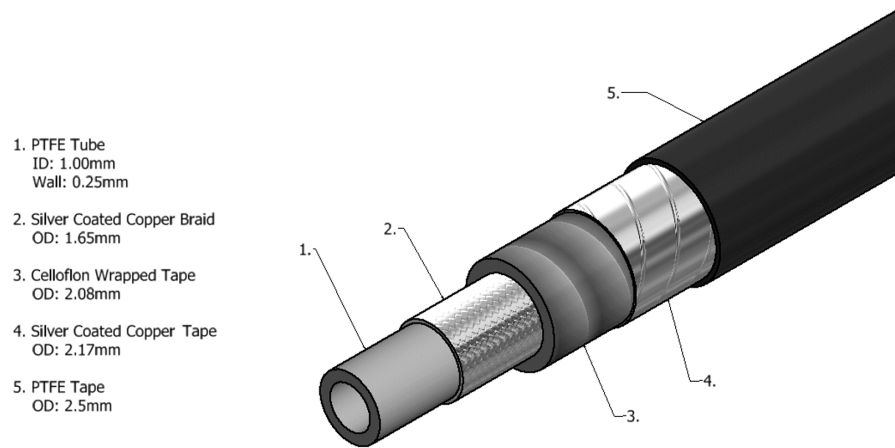


Figure 5.10: Render of the Prototype 2 Cable

One theoretical trade off for this prototype was the increased resistance, and therefore conductor losses, due to the braided metal. This effect arises due to the proximity effect where any current carrying metal in close proximity has its current charge confined to a smaller region. Eddy currents created by induced magnetic fields can also increase the AC resistance of the cable [85], even to such an extent where the AC resistance is much higher than its DC counterpart. [86].

### 5.2.3 Prototype 3 - Company B

Prototype 3 was a cable created with the same design as prototype 1 but using a different manufacturer. For this prototype it was stressed to the manufacturing company that all of the wrapped layers needed to be tightly wrapped and even throughout the cable. Visual inspection of this prototype showed a much greater attention to detail of the wrapped layers and also gave the cable an improved overall feeling both in regard to structure and flexural strength even when approaching maximum bend radius.

### 5.3. Theoretical Cable comparison

Before manufacture a theoretical comparison was carried out between a common co-axial cable such as the Huber & Suhner Sucoform 47 and the new cable developed as part of this research.

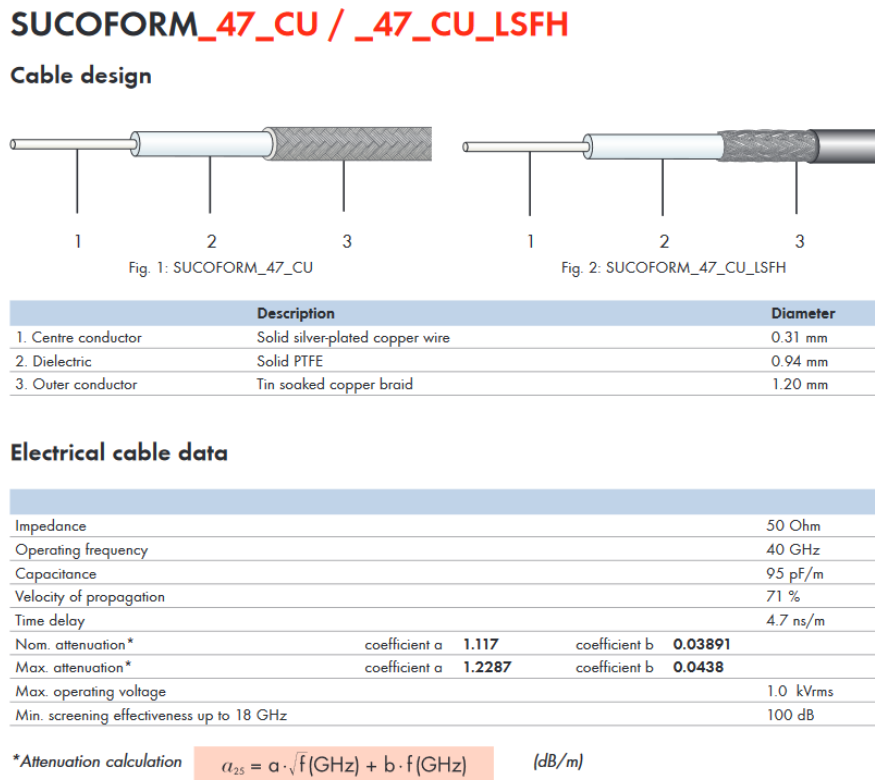


Figure 5.11: Excerpt from the H&S Sucoform 47 datasheet [1]

The sucoform 47 cable was chosen for its small diameter. When considering the intended clinical use of the device for this research project an alternative structure would be to have a 2.5mm catheter which contains a microwave delivery cable such as the sucoform 47 cable and have another lumen to act similarly to the hollow channel.

A number of assumptions were required to allow for a theoretical analysis of both cables. The datasheet only gives generic details for the material types so the resistivity of each conductor and also the properties of the dielectric material were



all estimated as shown in figure 5.11 <sup>1</sup>.

Table 5.2: Table showing the Sucoform 47 parameters used in theoretical comparison

	Inner Conductor	Outer Conductor
Material	Silver Plated Copper Wire	Tin Soaked Copper Braid
Resistivity (ohm.m)	1.59E-08	1.10E-07
Inner Diameter (mm)	0.00	0.94
Outer Diameter (mm)	0.31	1.20
Wall Thickness (mm)	0.155	0.13

Table 5.3: Table showing the new cable parameters used in theoretical comparison

	Inner Conductor	Outer Conductor
Material	Silver Plated Copper Foil	Silver Plated Copper Foil
Resistivity (ohm.m)	1.59E-08	1.59E-08
Inner Diameter (mm)	1.50	2.21
Outer Diameter (mm)	1.65	2.30
Wall Thickness (mm)	0.075	0.045

The skin depth for each conductor was calculated using eq. 2.1. This was then used to calculate the equivalent area of each conductor as shown in eq. 5.1.

$$\text{Equivalent Area} = 2\pi\delta_s r \quad (5.1)$$

Where  $\delta_s$  is the skin depth in the conductor and  $r$  is the radius.

$$\text{Loss/length} = 8.686 \times \frac{\text{Resistivity/Equivalent Area}}{2Z_0} \quad (5.2)$$

Once this equivalent area was known it was used to calculate the loss per length as in eq. 5.2. The constant 8.686 is used to convert the value from nepers to dB. The results of this gave the loss per length in dB for the cable as a result of the resistivity of the conductors.

The attenuation due to dielectric was shown in eq. 2.22 and has been used to estimate a value for each of the cables. Once again this calculation makes a few

<sup>1</sup>Credit: [http://www.nkt-rf.ru/upload/iblock/da4/F\\_cat\\_Sucoform.pdf](http://www.nkt-rf.ru/upload/iblock/da4/F_cat_Sucoform.pdf)

assumptions regarding the materials being used. The dielectric constant for PTFE has been shown to vary from between 1.4 to 2.1 depending upon its density, i.e. the amount of air contained within it. Dissipation factor can also vary but is usually stated at 0.0004. For these calculations  $\epsilon_r = 2.1$  and  $\tan\delta = 0.0004$  were used.

Table 5.4: Table showing calculated values for sucoform 47 used in theoretical comparison

	Inner Conductor	Outer Conductor
Skin Depth (m)	2.24E-06	8.33E-07
Equivalent Area (m)	6.62E-09	8.07E-10
Resistance/Length (ohm)	17.29	19.70
Conductor Loss/Length (dB)	1.50	1.71
Dielectric Loss/Length (dB)		0.31
Total Loss/Length (dB)		3.52

Table 5.5: Table showing calculated values for new cable used in theoretical comparison

	Inner Conductor	Outer Conductor
Skin Depth (m)	8.33E-07	8.33E-07
Equivalent Area (m)	5.79E-09	4.32E-10
Resistance/Length (ohm)	2.75	3.68
Conductor Loss/Length (dB)	0.81	1.08
Dielectric Loss/Length (dB)		0.31
Total Loss/Length (dB)		2.20

Tables 5.4 and 5.5 show that there is a clear difference between the theoretical loss for the sucoform 47 cable when compared with the new cable developed for this project. It is pertinent once again to mention that there were many assumptions made when carrying out these calculations so they may vary from measured results. One thing to consider though is the much lower resistance for both conductors within the new cable. This meant two things, less loss throughout the cable but also that, due to the increased surface area, any heating of the conductors is more dispersed and should lead to a much better average power handling for the cable.

## 5.4. Cable Testing

In order to accurately test all of the prototype cables, specifically in terms of attenuation, an impedance transformer was required due to the lower impedance of the cable and the  $50\Omega$  impedance of the test equipment. All three prototype cables were measured using both the co-axial and the microstrip transformer structures. One disadvantage of this was the varying impedance of the cables. Both transformers, as discussed in sections 4.2.4 and 4.2.5 were designed with an impedance of approximately  $26\Omega$  to match an impedance of  $50\Omega$  and  $14\Omega$ . This was based on previous calculations which have been shown to be marginally incorrect via the time domain measurements presented in this section. A preliminary analysis of the amount of loss this variation in match impedance would introduce was carried out and is shown here. This calculation considered various line impedances compared to the optimal impedance which would be matched by the transformer.

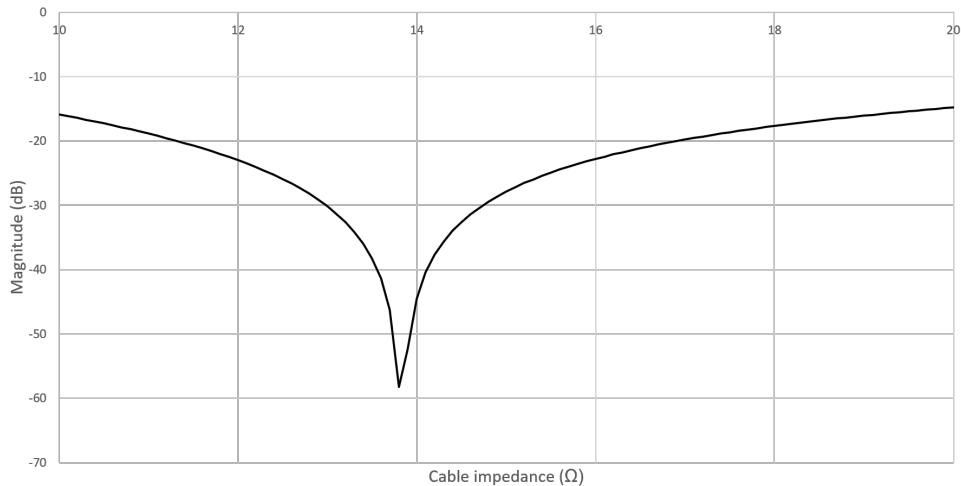


Figure 5.12:  $S_{1,1}$  of transformer for various cable impedances

It can be seen from figure 5.12 that the transformer is quite effective even over the variation in impedance of each prototype cable. Table 5.6 shows the exact calculated values for each prototype cable. Due to the minimal amount of power being reflected for each cable it was assumed that the transformers would work appropriately for

Table 5.6: Specific Return Loss for each prototype

Prototype	Line Impedance ( $\Omega$ )	Return Loss (dB)	Power Reflected (%)
1	18.43	-16.93	2.03
2	12.18	-23.97	0.40
3	18.43	-16.93	2.03

each of the prototype cables.

### 5.4.1 Co-axial Transformer

Initially the cables were tested using the co-axial transformer. The transformer was connected to a long length of cable, of 4.82m, as the attenuation due to the long length would be greater than any losses due to the transformer. Data from these tests for each prototype cable can be found in table 5.7. Due to the length of the transformer and the structure, especially due to the use of air as a dielectric, the losses in the co-axial transformer were considered to be negligible.

It can be seen from both table 5.7 and figure 5.13 that all three cables contain no large discontinuities along their length and the connector and open end of the cable can clearly be seen in the first and second peak respectively. There is a small shift in the data for prototype 2 and it is believed that this may be due to the manufacture of the cable. The second prototype uses a braid which might have affected how tightly the PTFE tape can be wrapped which would slightly alter the overall dielectric constant and therefore the velocity of propagation giving this slight shift in the time domain data. The magnitude shown at the open end of the cable is in effect the two way loss of the cable; i.e.  $\text{Loss per meter} = \text{Mag(dB)} / (\text{Length of cable} \times 2)$

### 5.4.2 Microstrip Transformer

The same testing was carried out with each prototype cable attached to the microstrip transformer. It was expected that this transformer would have higher loss than the

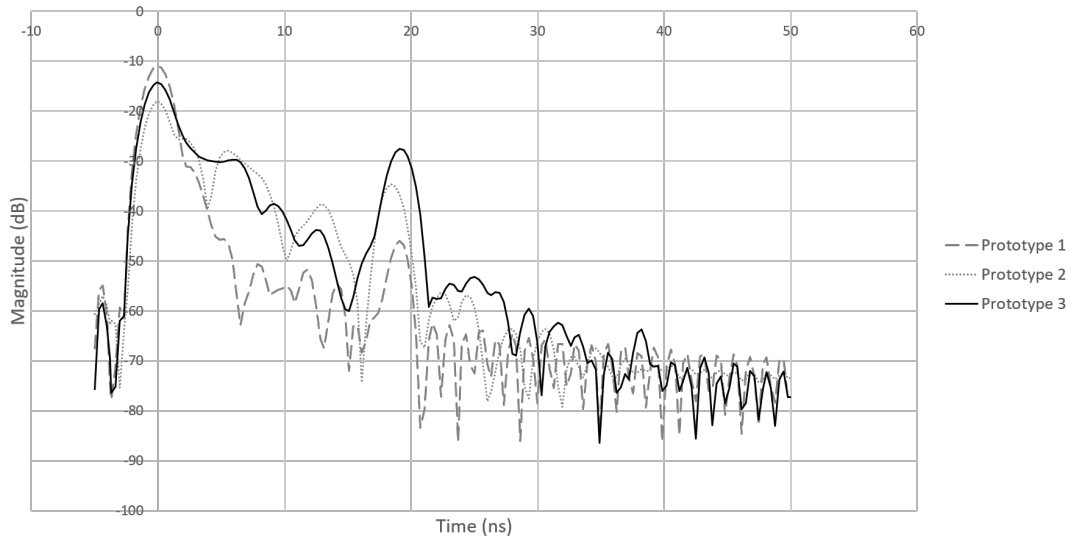


Figure 5.13: Time domain plot of each prototype cable test using co-axial transformer

Table 5.7: Measured losses from open ended prototype cable testing using co-axial transformer

Prototype	Open End time (ns)	Loss (dB)	Loss (dB/m)
1	19.09	-46.03	-4.77
2	18.43	-34.63	-3.59
3	19.09	-27.5	-2.85

co-axial transformer. The values obtained below and marked with an \* include consideration of this loss as discussed below.

Table 5.8: Measured losses from open ended prototype cable testing using co-axial transformer

Prototype	End time (ns)	Loss (dB)	Loss (dB/m)	Loss (dB) *	Loss (dB/m) *
1	19.09	-48.38	-5.06	-46.53	-4.87
2	18.43	-35.40	-3.70	-33.55	-3.51
3	19.09	-28.81	-3.01	-26.96	-2.82

## Back to Back Transformer Testing

To ascertain the amount of loss introduced to the device due to the microstrip transformer, two structures were tested back to back with a small length of cable between them. The loss measurement, at 5.8GHz, was then divided by two, disregarding the

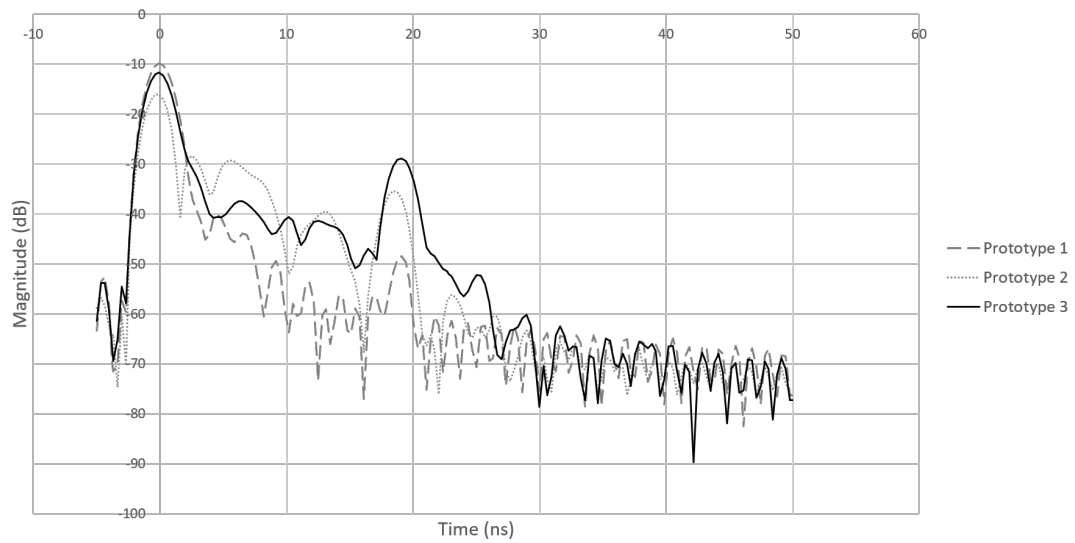


Figure 5.14: Time domain plot of each prototype cable test using microstrip transformer

small amount of loss due to the cable which was approximated to be around 0.07dB, to give an approximate value for the loss in each transformer.

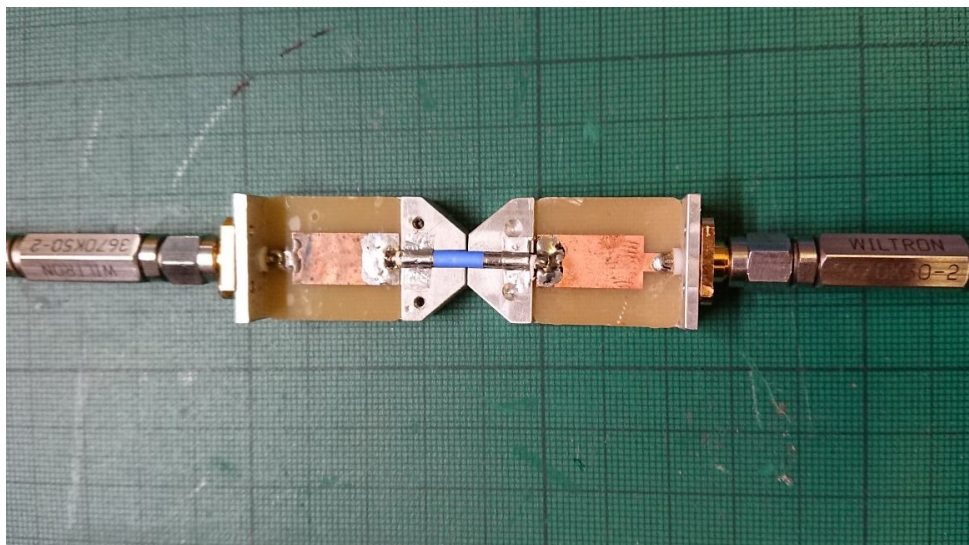


Figure 5.15: Testing of back to back microstrip transformers

As can be seen in figure 5.16 this value is approximately -3.69dB, giving an estimate of the attenuation in each transformer of around -1.85dB.

Figure 5.17 shows a graph of both tests with microstrip \* denoting the additional loss term due to the transformer attenuation being taken into account. It can be seen

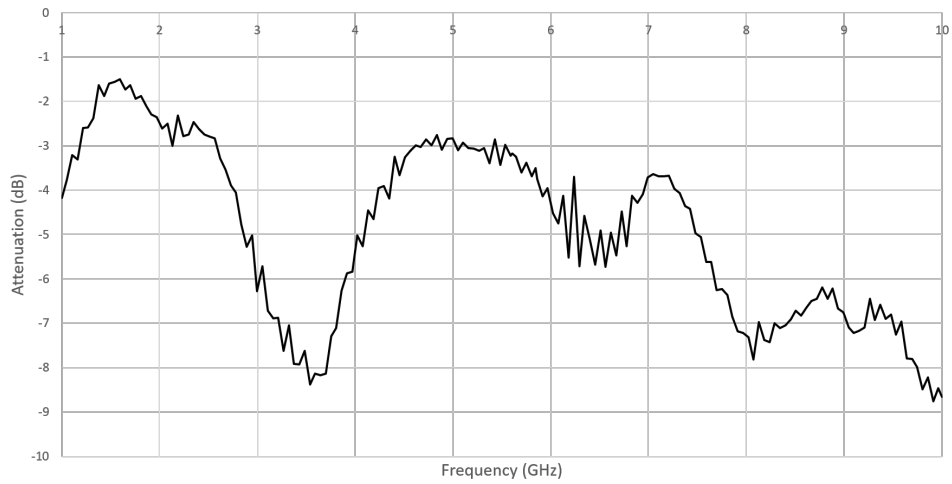


Figure 5.16: S<sub>2,1</sub> of back to back microstrip transformers

that the results correlate quite well with each other and give the novel cable structure an approximate attenuation of slightly above 2.8dB/m.

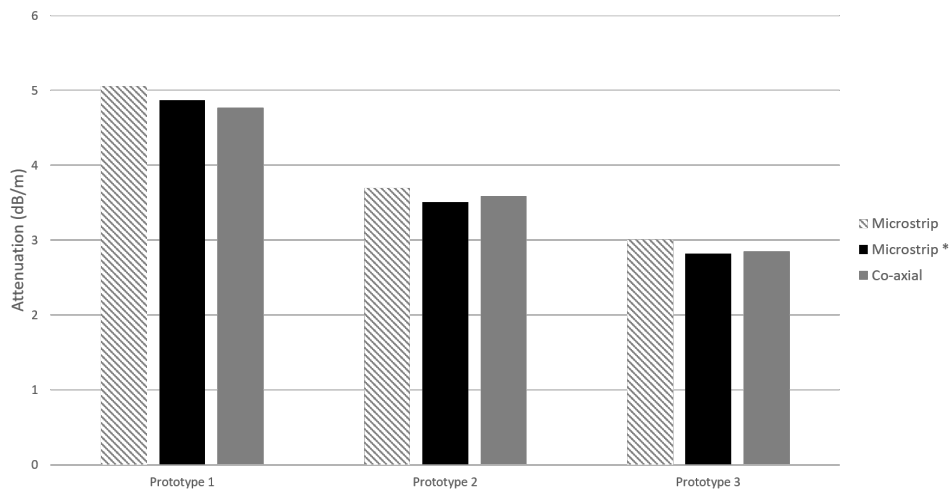


Figure 5.17: Graph showing comparison of cable loss measurements with both transformers

### 5.4.3 Estimation of Dielectric Constant

The time domain plots shown in figures 5.13 and 5.14 were also used to estimate the dielectric constant of the PTFE wraps used in each of the cables.

It can be seen that the end time values for prototype 1 and prototype 3 are the same at 19.09ns whereas prototype 2 has a lower value of 18.43ns. Calculating the

velocity factor of the cable and rearranging eq. 5.3 gave an estimation of the dielectric constant. The velocity factor is a measure of how fast a signal travels through the cable when compared with the transmission of light in air; 299,972,458m/s.

$$V_F = \frac{1}{\sqrt{\epsilon_r}} \rightarrow \epsilon_r = \frac{1}{V_F^2} \quad (5.3)$$

Table 5.9: Calculation of  $\epsilon_r$  for each prototype cable

Prototype	Time (ns)	Length (m)	Velocity (m/ns)	$V_F$	$\epsilon_r$
1	19.1	4.82	0.252	0.84	1.41
2	18.4	4.82	0.262	0.87	1.32
3	19.1	4.82	0.252	0.84	1.41

Of course this does not give a fully accurate answer as this calculation assumes that the transformer has very little effect on the propagation of the waves through the structure. The small variation with prototype 2 could be due to a number of factors including how tightly the PTFE has been wrapped or whether it is being compressed by the wrap of the outer conductor which would remove some of the air and therefore increase the density of the PTFE.



## **Chapter. 6**

---

### ***Radiative Tip Design***

---

#### **6.1. Requirements**

The overall device presented herein utilises the novel cable structure to deliver microwave energy at 5.8GHz to successfully coagulate bleeding vessels in a controlled and accurate manner. Whilst it was proven in chapter 5 that the cable was capable of carrying energy from the generator, this energy propagation is useless in this application without a suitable and efficient way to couple the energy into the treatment site. Not only did the design need to be considered from an energy delivery standpoint but the unique feature remains that this cable includes the presence of a hollow channel. Any tip design considered needed to still allow the delivery of fluids or other tools through this hollow channel. A number of other factors also needed to be taken into consideration both in terms of physical device constraints and also clinical effect requirements which are subsequently detailed.

##### **6.1.1 Physical Constraints**

These constraints included the physical structure of the tip and how this would interact with both the patient and the environment during the procedure.

##### **Size**

Figure 6.1 shows an example of the working channel insertion angle of most endoscopes and gastroscopes. Due to the angle of this channel any rigid part of the device, specifically the radiative tip, needed to be short enough to be able to be in-

serted not only through this angle but also through any tortuous path experienced whilst the endoscope is being navigated through the gastrointestinal tract especially during retroflex; where the tip of the scope is flexed back on itself.



Figure 6.1: Diagram showing proximal end angle of insertion in endoscopic working channel

The outer diameter of the tip needed to also be able to fit into the entirety of this working channel and as such the maximum allowable size for this diameter was set to 2.5mm; the same outer diameter as the cable itself. It must be noted that the inner liners of the working channels can vary between scopes. For example it would be absurd to consider using a 2.8mm device within a 2.8mm working channel as the device would likely not fit or would become stuck during operation. A similar statement can be made for using larger working channels. A buffer of 0.1mm around the outer circumference of a device is a safe margin to allow for free movement and rotation. This gives a maximum outer diameter for a 2.8mm working channel of 2.6mm. 2.5mm was subsequently chosen to allow for tolerances both in the manufacture of the cable and radiative tip but also during assembly.

### **Mechanical Connection**

This device will be introduced into the gastrointestinal tract and as such requires a certain level of mechanical stability. Not only did the tip need to be robust but

it also needed to be securely attached to the cable to prevent accidental detachment and risk leaving a foreign body inside the patient, especially during insertion and extraction into the digestive tract. It is also quite likely that, during haemostasis, the clinician will need to apply local tamponade, or pressure to a specific area on a vessel, to ensure that a good coagulum or 'plug' is produced. For this reason the radiative tip connection needs to withstand both push and pull forces. Whilst out of the initial scope of this research it is expected that further validation will subsequently be carried out should the device go further in the mechanical device design process. This includes the use of accurate force measurements, to ensure that the tip connection is capable of withstanding the various forces associated with expected clinical usage.

### **6.1.2 Clinical Requirement**

Generally the radiative tip needs to deliver microwave energy into vessels or tissue in order to coagulate and stop bleeding. However this needs to be considered in two ways.; firstly the device needs to be able to deliver the energy efficiently, in order to avoid energy wastage and unwanted heating of the device. Secondly the device needs to be able to deliver the energy into the required area accurately and controllably. For ease of use and to allow the clinician to be able to coagulate specific vessels it was decided that the radiator be end fired.

#### **Specific Oesophageal Anatomy and Penetration Depth at 5.8GHz**

The use of 5.8GHz initially comes from the fact that the generator used for this project is provided by Creo Medical Ltd and utilises that specific frequency. But there are a number of benefits achieved by using this frequency as previously discussed. One main consideration is the ability to deliver energy precisely into the tissue. The oesophageal wall, when dilated, is approximately 1.87 - 2.4mm and infor-

mation from the Institute of Applied Physics (IFAC) in Italy and presented in [87] gives a penetration depth in oesophageal tissue of approximately 6.41mm at 5.8GHz. This may seem to suggest that 5.8GHz is not suitable for use in the oesophagus without penetrating too deep and causing perforation but the situation is not quite as straightforward as it appears.

The penetration depth describes the point at which the field strength has dropped to  $1/e$  and therefore the power has dropped to  $1/e^2$  or approximately 13%. This means that at half the penetration depth i.e. 3.2mm the power level is approximately 36.8% of that delivered. We further minimise this depth as the provided values from IFAC are calculated considering the energy being propagated as a plane wave. This is not the case with most surgical instruments, especially as the radiative tip has a much smaller cross sectional area than the wavelength being used. This means that the power flowing through the tissue, the power density, decays according to the inverse square law; that is  $1/r^2$ . What actually happens is that there is an area of high intensity within the first millimetre which then lessens deeper into the tissue. This is especially noticeable when considering penetration depths at much lower frequencies. For example at RF (400KHz) the penetration depth in oesophagus is over 1 meter.

Whilst energy delivery into the tissue to seal a bleeding vessel is the main requirement of this device, it needs to be specific to the treatment area and not interfere or interact with surrounding tissue structures. As previously discussed the ability of this device to deliver energy in a controlled and accurate manner is one of the main advantages of using microwave haemostasis over other haemostatic modalities such as chemicals or powders which as previously discussed are likely to interfere with and cause damage to surrounding tissue and structures.

A clinical human use study carried out by Creo Medical was the first study of its kind and demonstrated the clinical efficacy of using 5.8GHz within the gastrointestinal tract [88]

## Impedance Transformation

The complex impedance of the oesophageal tissue, blood and also liver were calculated assuming a plane wave propagating through a lossy dielectric. Whilst not strictly accurate for consideration of penetration depth as discussed above it gives enough information to estimate the impedance of the tissue and therefore allows preliminary theoretical design of the radiative tip to be modelled and simulated to efficiently couple microwave energy into the tissue.

$$Z = \sqrt{\frac{j\omega\mu_0\mu_R}{\sigma + j\omega\epsilon_0\epsilon_r}} \quad (6.1)$$

Eq. 6.1 gives the wave impedance of an electromagnetic wave travelling through a medium. Where  $\omega$  is the angular frequency,  $\mu_0$  is the magnetic permeability of free space,  $\mu_R$  is the relative magnetic permeability of the material,  $\sigma$  is the conductivity of the material,  $\epsilon_0$  is the permittivity of free space and  $\epsilon_r$  is the relative permittivity of the material.

Table 6.1: Table showing the calculated values for wave impedance of various tissues at 5.8GHz

Tissue	Conductivity (S/m)	Relative Permittivity	Complex Impedance (ohm)	Impedance Magnitude (ohm)
Oesophagus	6.31	56.46	48.06 + 8.09j	48.74
Blood Vessel	4.35	38.23	58.32 + 9.98j	59.17
Liver	4.64	38.13	58.06 + 10.58	59.02

It can be seen that the values for blood vessels and liver are quite similar and due to the higher impedance, when compared with the cable, a specifically designed radiative tip was required at the distal end of the cable to allow for the efficient coupling not only from radiative tip into tissue but also from cable to radiative tip. The values for blood and liver were used as the radiative tip will be predominantly in contact with a mixture of oesophageal tissue and blood. Although there is a large

amount of blood expected to be present in the oesophagus tailoring the design of the structure to match blood would likely cause the majority of the energy to coagulate the blood. In order to achieve good haemostasis a plug needs to be created from the coagulation of the blood vessels and surrounding tissue rather than just blood itself. For this reason the impedance for blood vessels and liver were used. Liver has been used throughout the project in CST Microwave Studio as a homogeneous mass for ts

If we consider the expected impedance of the cable and the calculated values for the liver impedance from table 6.1. The impedance required to match cable to tissue can be calculated using eq. 2.15. This gives an impedance of approximately  $\sqrt{14 \times 59} = 28.7\Omega$  to provide the best match between tip and tissue.

A number of iterations were developed and the most viable designs are presented. Each tip was simulated connected to a short length of cable to allow for a return loss or  $S_{1,1}$  simulation to be conducted. To ensure that the simulations showed the effect due to the tip structure only, all were simulated using a waveguide port which ideally matches the simulated impedance of the attached co-axial structure which was modelled to emulate the new cable design.

## 6.2. Simple Macor Collar

One of the initial tip comprised a simple cylinder made from Macor, a machinable ceramic. This material was chosen for its ability to be machined whilst having a high dielectric constant allowing the electrical length of the tip to be shortened as a quarter wavelength in the material is much shorter. This is desirable for a device that is to be introduced into an endoscope due to the angles required to be navigated through at the proximal end of the scope.

The tip was simulated, as a nominal quarter wavelength to provide matching to the higher impedance tissue, using CST Microwave Studio as being partially inserted into a cylinder of liver to emulate the delivery of energy into vascular/bleeding tissue.

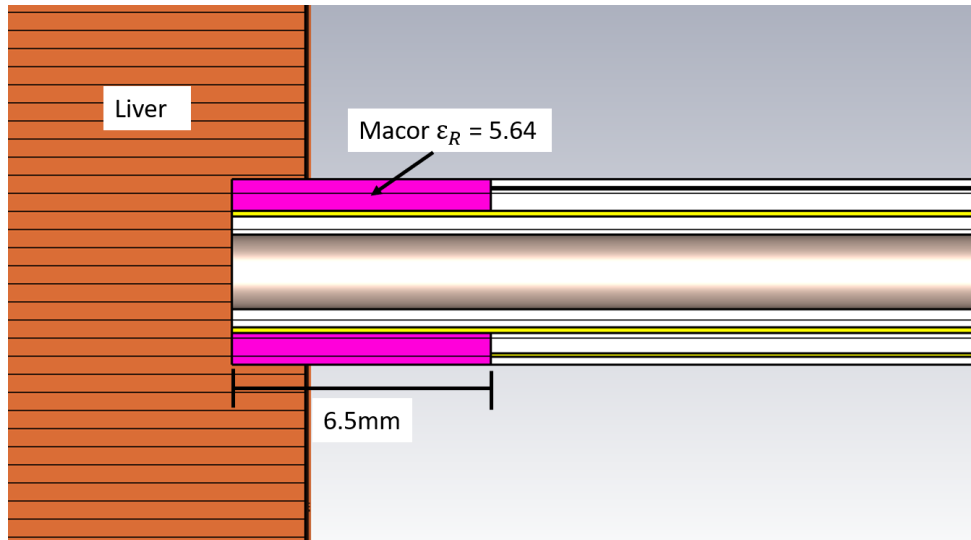


Figure 6.2: Initial simple cylindrical radiative tip

The S parameters and power loss distributions were then considered. These can be seen in figures 6.3 and 6.5 respectively. The novel microwave cable structure was modelled as per the geometry for prototype 3. The Macor can be seen inserted approximately 1mm into the tissue, this would be similar to the amount of tissue surrounding the tip once the clinician applies local tamponade.

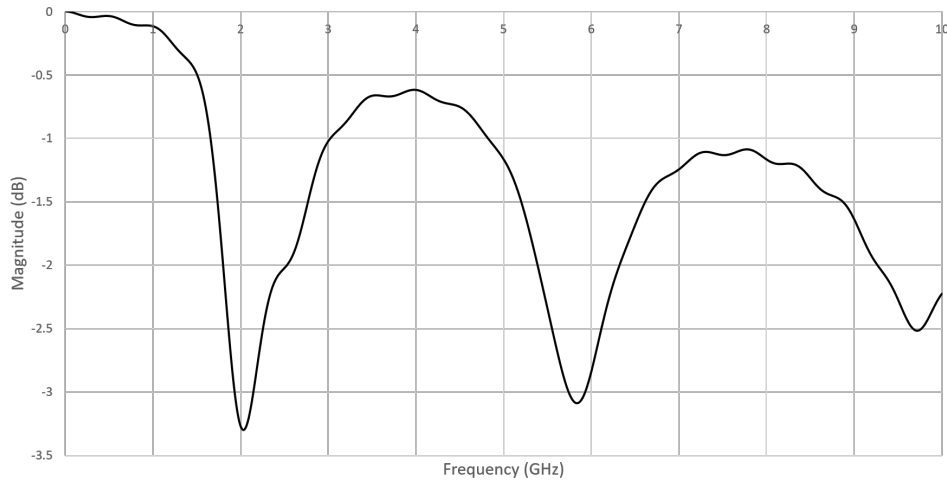


Figure 6.3: Simulated S Parameters for radiative tip 1

As can be seen in figure 6.3 as well as figures 6.5 and 6.6 minimal energy is being delivered into the tissue. It is quite likely however that these apparent S parameter values are due to the length of the overall structure including the small length of

cable rather than due to the functionality of the tip itself. The repeated 'dips' in the  $S_{1,1}$  result suggested that this was the case and variation in the length of the cable structure distal to the liver changed the S parameters significantly. This effect can be seen in the simulated return loss shown in figure 6.4 which shows the variation in match due to change in cable length whilst the tip geometry remains the same. This would suggest that the match into the tissue is not correct and would need alteration of the geometry to try and improve this. Due to the inner hollow and outer diameter constraints this was difficult to achieve with this simple structure.

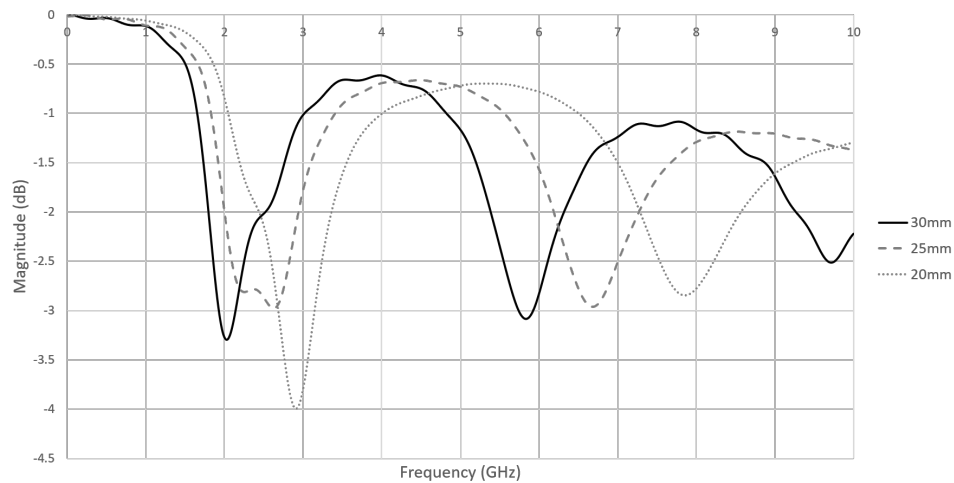


Figure 6.4: Simulated S Parameters for radiative tip 1 with variation in cable length

Even though energy delivery into the tissue is present it is still minimal and the  $S_{1,1}$  shows that there is only a -3.07dB reflection equating to approximately 49.32% of the power was being reflected into the input port.

It was clear from the simulated results that an alternative radiative tip structure was required. For the radiative tip to work correctly the return loss needed to stay constant with variation in cable length and to have at least 80% efficiency meaning that the majority of energy will be delivered into the treatment site.



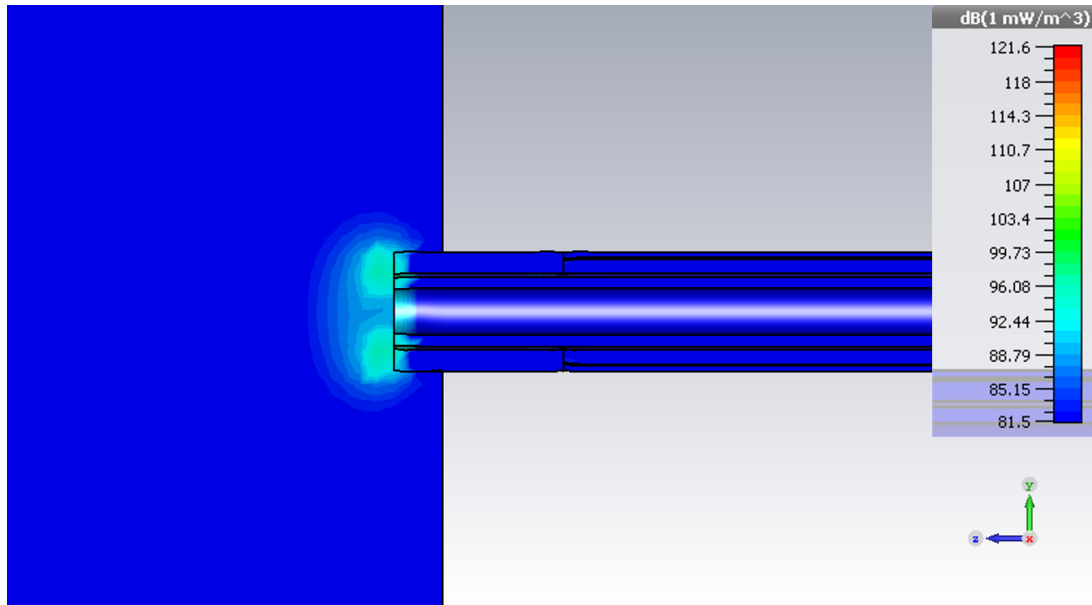


Figure 6.5: Simulated Power Loss Density for radiative tip 1

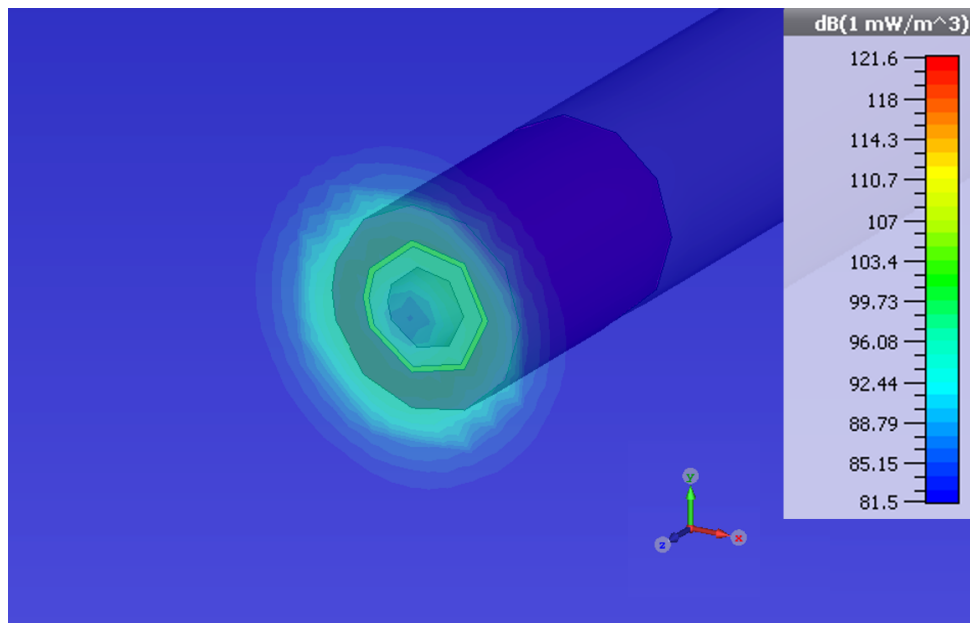


Figure 6.6: Simulated Power Loss Density for radiative tip 1 in perspective view

### 6.3. Final Tip Design

It was clear from previous consideration that the impedance of the tip structure would need to vary from that of the cable itself in order to provide a match into the higher impedance tissue as discussed in section 6.1.2. To do this whilst maintain-



Table 6.2: Table showing dielectric properties and calculated quarter wavelength for each tip material

Material	Dielectric Constant	Loss Tangent	1/4 Wave (mm)
Macor	5.64	0.0025	5.44
PEEK	3.20	0.0020	7.22

### Macor

Initially the structure was simulated using Macor. CST studio was used to find the optimal length of the structure having been initially set to a nominal quarter wavelength in the material i.e. approximately 5.4mm at 5.8GHz. This was then varied via parameter sweep to find the length which matched most optimally with the tissue. Explanation as to why this length might vary from theoretical calculation is discussed in section 6.3.1

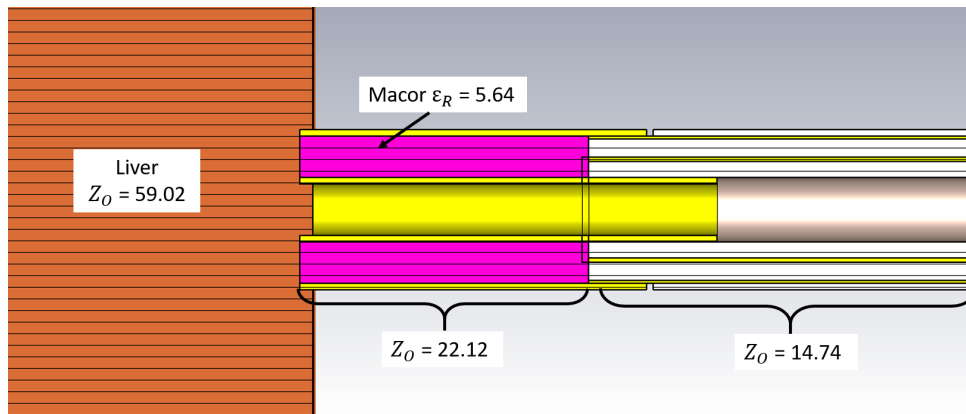


Figure 6.8: Simulation Model for the final tip design with Macor

The simulated return loss shown in figure 6.9 give the values at the theoretical calculation of quarter wavelength and also at the optimal length for matching of this structure to the tissue. A broadband dip around the operating frequency can be seen when the length is 4.5mm. The magnitude of this reflection however is only -5.3dB or 70% power delivery. Using eq. 2.4 the impedance of the tip can be calculated and as shown in figure 6.8 is approximately 22.12Ω. This is slightly lower than the match

impedance required,  $28.70\Omega$ , and by rearranging eq. 2.4 it can be calculated that the tip would need to be 3.1mm, at least, to approximate the required impedance. This was unsuitable for the application so indicated the need for an alternative material to provide a better match into the tissue.

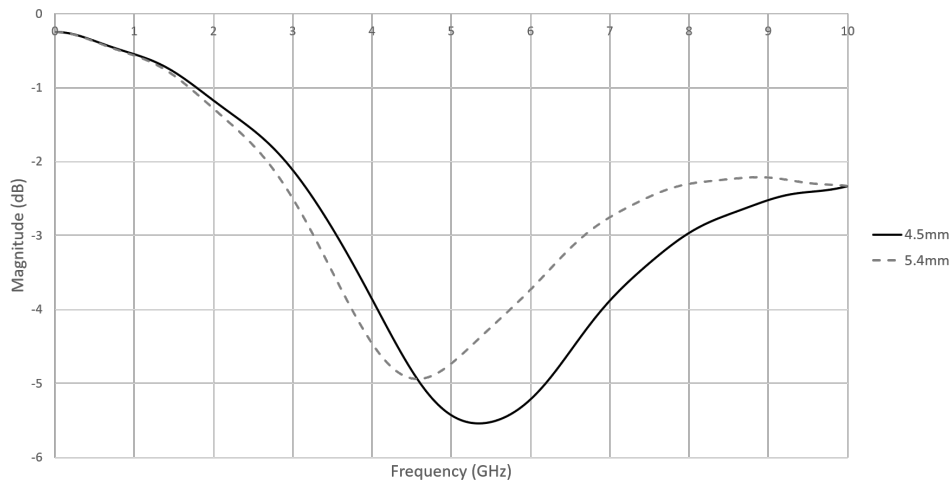


Figure 6.9: Simulated results for the final tip design with Macor

The power loss density plots, figures 6.10 and 6.11 give an indication of the energy delivery into the tissue. The energy delivery pattern comprises two 'hot' spots where the inner conductor makes contact with the tissue but extends around these spots and does not penetrate too deeply into the surface of the tissue. This is advantageous for surface coagulation and will limit the risk of damage to surround vessels or tissue.

A simulated farfield monitor, as shown in figure 6.12, was used to ensure that the return loss results were due to the energy being delivered into the tissue and not being radiated into the air surrounding the treatment site.

The farfield monitor Radiation efficiency is recorded at -15.86dB or 2.59%. This gives confidence that, at the operating frequency, the energy is being delivered into the tissue as expected. This test is required as the majority of the efficacy of the radiative tip is only being deduced from a single port return measurement. All that the return loss S parameters in figure 6.9 show is that there is an amount energy being returned back to that input port. If the radiative efficiency was much higher

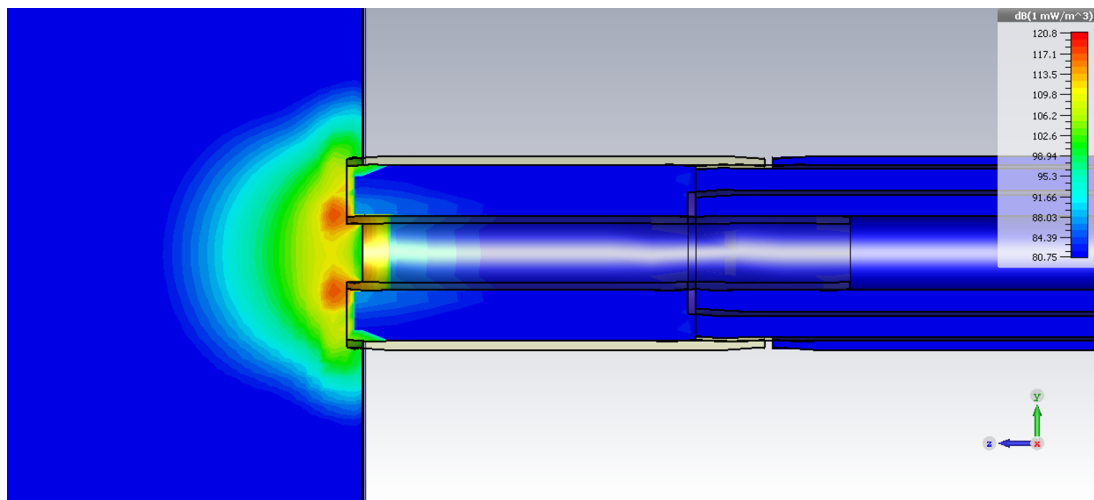


Figure 6.10: Simulated power loss density plot for the final tip design with Macor

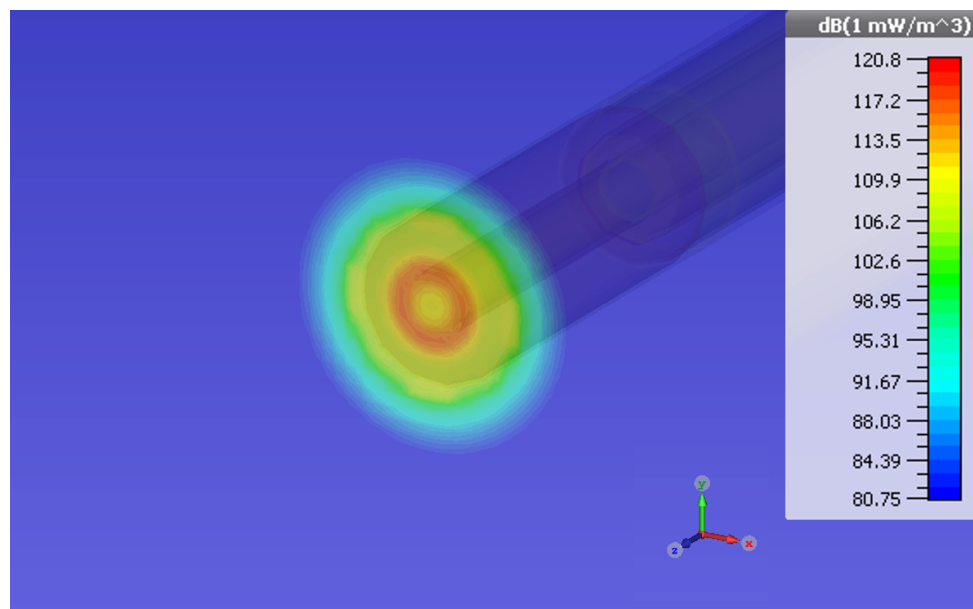


Figure 6.11: Simulated power loss density plot for the final tip design with Macor in perspective view

then although a small return loss would be measured the actual energy delivery into the treatment site might be minimal or even non existent. This may be fine when the device is outside of the body cavity but for a closed lumen, such as in the oesophagus, could affect or damage surrounding tissue.

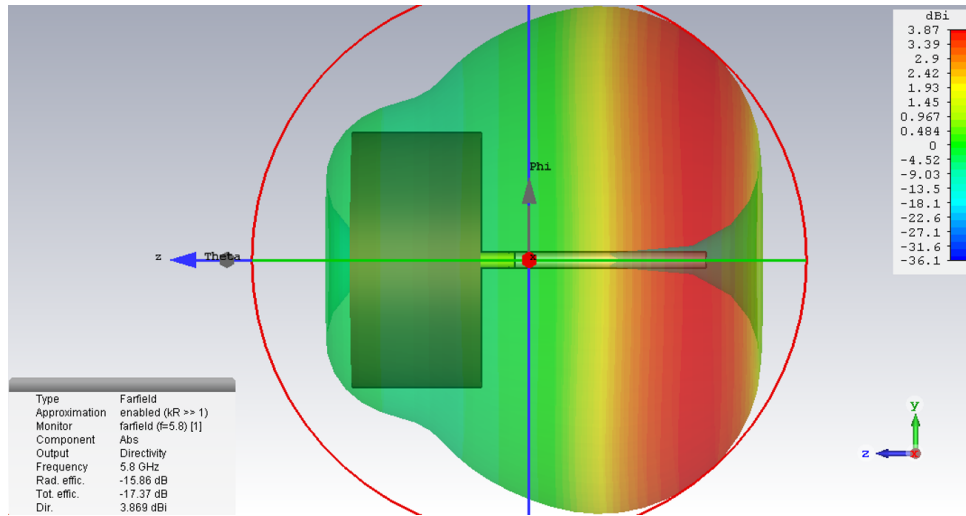


Figure 6.12: Simulated farfield monitor for final tip design with Macor

## PEEK

The second simulation for this tip structure replaced the Macor dielectric with PEEK. This has a slightly lower dielectric constant, which theoretically required the structure to be slightly longer but was able to maintain the required outer diameter whilst providing an impedance much closer to the required match impedance.

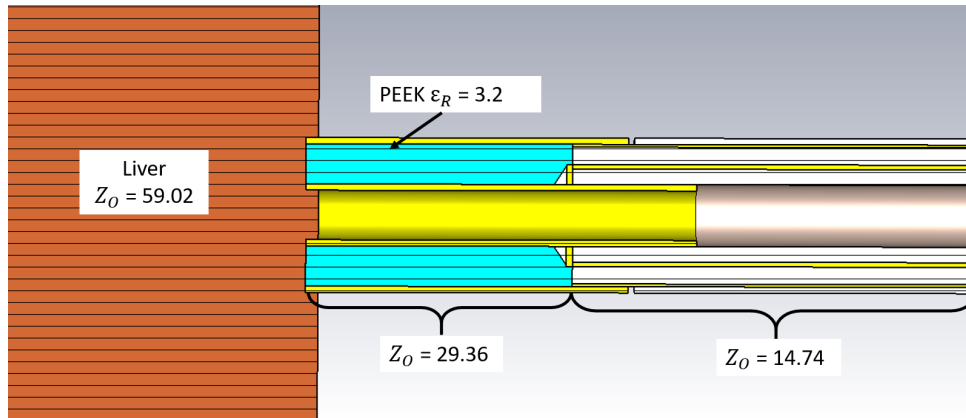


Figure 6.13: Simulation Model for the final tip design with PEEK

Figure 6.14 shows simulated return loss for both the theoretical quarter wave-length and the optimised length as per CST. Once again an explanation for this variation is considered later in this chapter. At a length of 4.2mm a return loss of approximately -8.6dB or 86.2% delivery is shown, a much better match due to the

higher  $29.36\Omega$  impedance providing better matching at the tip-tissue interface.

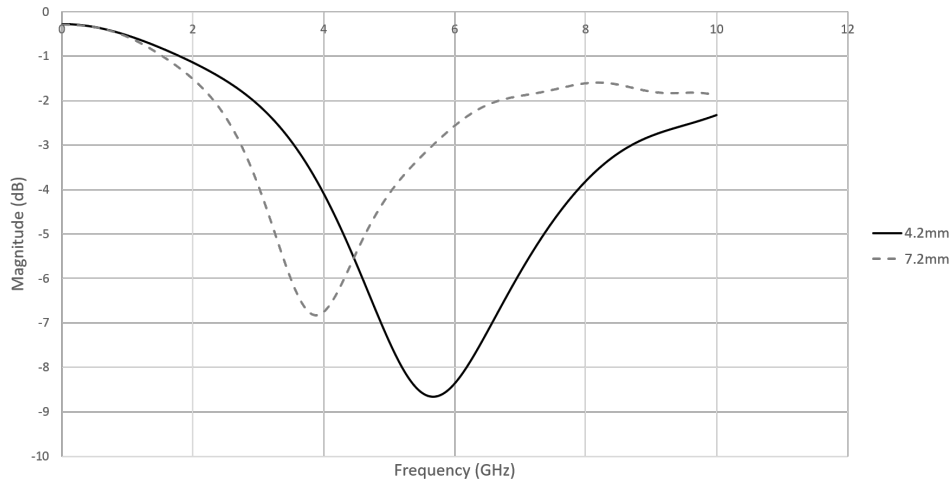


Figure 6.14: Simulated results for the final tip design with PEEK

The power loss density plots shown in figures 6.15 and 6.16 show very similar results to the Macor structure with the same focussed energy spots but at higher power due to the increased return loss; i.e. more energy is being delivered into the tissue but still shows a similar delivery pattern with the advantages previously discussed including depth of penetration and accurate application to a lesion/bleed.

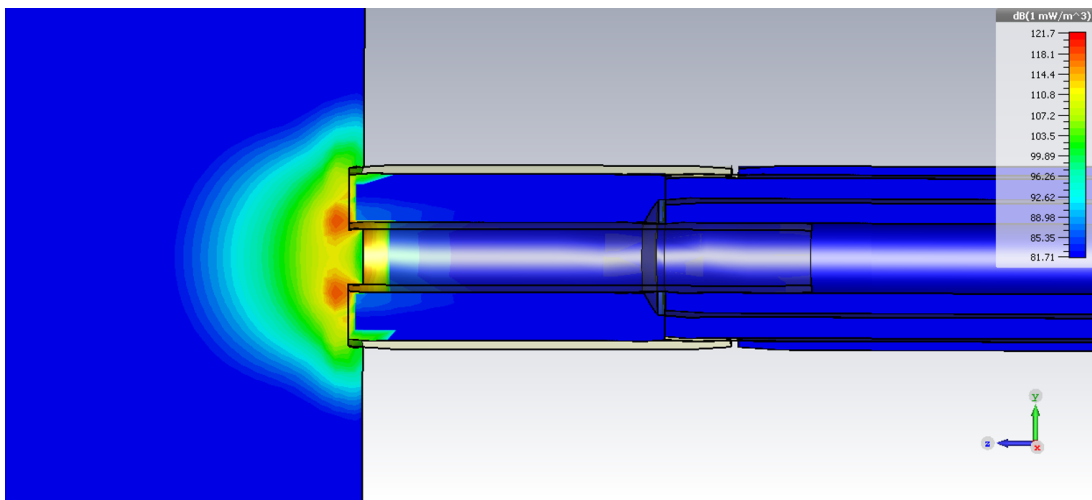


Figure 6.15: Simulated power loss density plot for the final tip design with PEEK

The farfield monitor, figure 6.17, was once again used to confirm that the low value for return loss is due to the delivery of energy into tissue and not due to

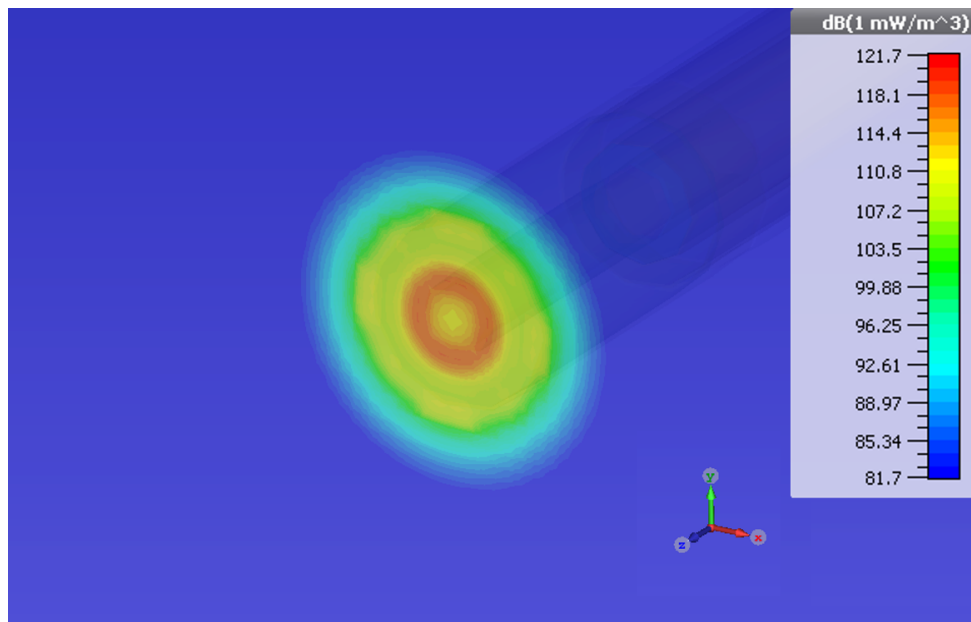


Figure 6.16: Simulated power loss density plot for the final tip design with PEEK from perspective view

radiation into surrounding air. The farfield monitor shows a radiative efficiency of -17.19dB which equates to 1.91% of the power being radiated.

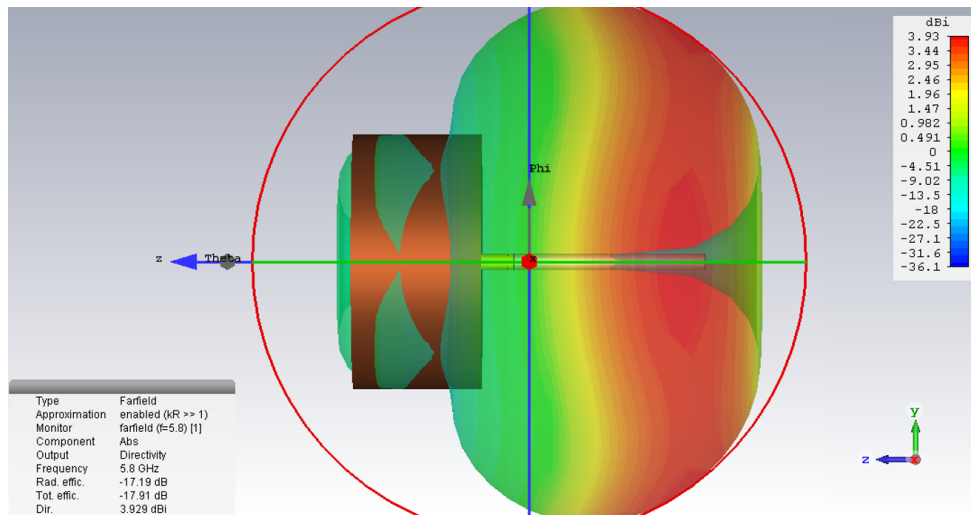


Figure 6.17: Simulated farfield monitor for final tip design with PEEK

### Flush or sloped tip

As the PEEK structure appeared to be optimal in its design and simulation, it was re-simulated both as a flush end and also as a sloped end structure, as seen in figure



6.18. Due to the size of the oesophageal lumen, which is not that much larger than the device especially when constricted, it would be difficult to fully apply the tip flush with the mucosal surface which was further validated during initial pre-clinical investigations at Northwick Park institute for Medical Research. It was also believed that if only one side of the tip is applied, then the energy would be focussed at a single spot, which would assist the surgeon in accurately coagulating a specific location without risk of damage to surrounding tissue structures or vessels. Figure 6.21 shows this spot of focus at the inner conductor.

Figures 6.19, 6.20 and 6.21 show similar experimental simulations as the previous sections concerning the dielectric tip material and show good matching between tip structure and liver at -11.21dB or 92.43%. This is much larger than the previous tip designs, however the farfield monitor results should be especially considered here as half of the structure is not actually in contact with the tissue.

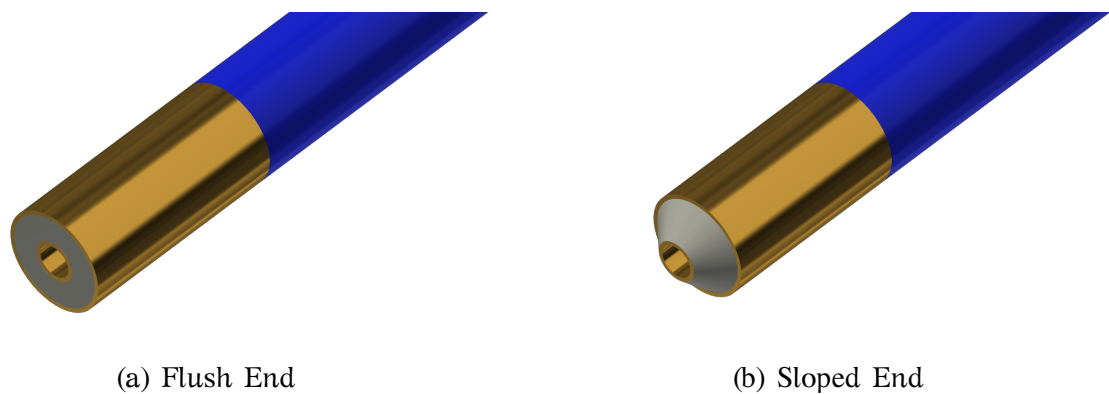


Figure 6.18: Radiative tip variations

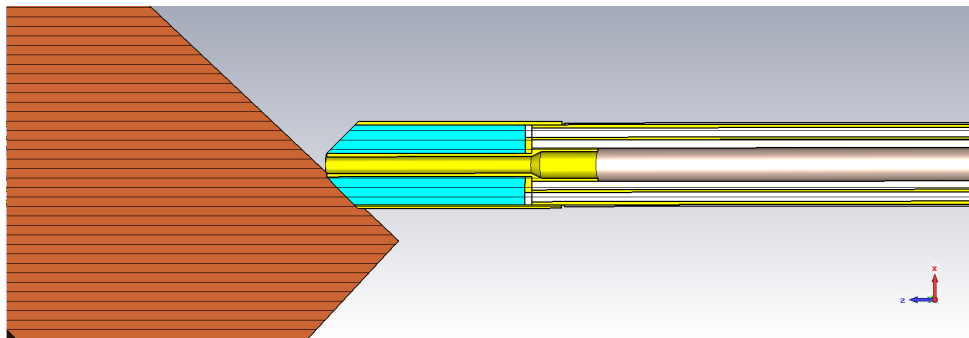


Figure 6.19: Simulation Model for the final sloped tip design with PEEK

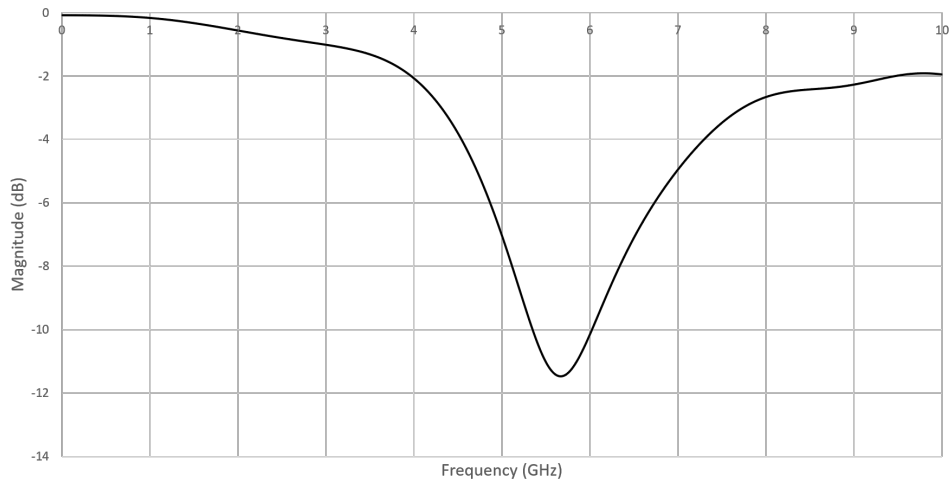


Figure 6.20: Simulated results for the final sloped tip design with PEEK

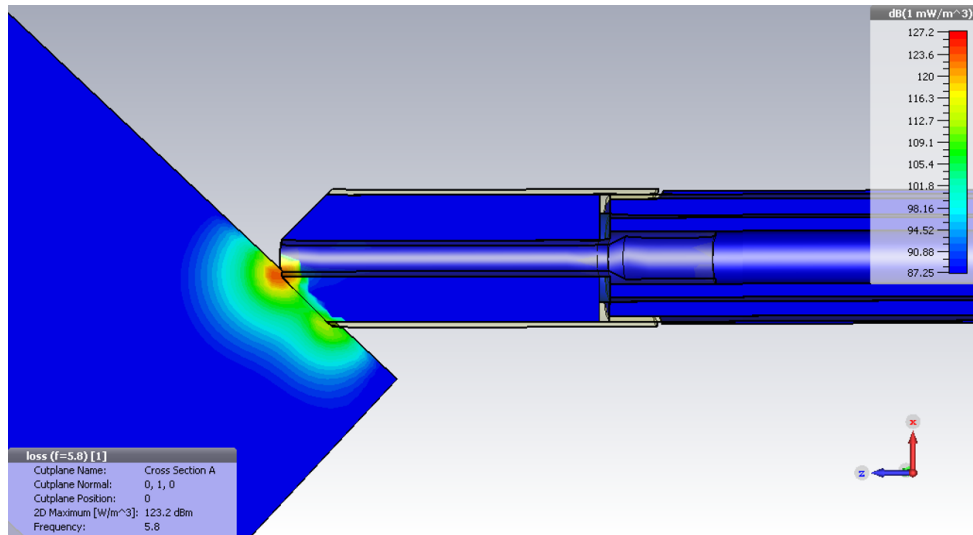


Figure 6.21: Simulated power loss density plot for the final sloped tip design with PEEK

Figures 6.12, 6.17 and 6.22 all show the simulated farfield monitors from CST. The initial two flat structures show that a minimal amount of energy is being radiated from the structure, approximately 1.6-1.8%. The sloped tip shows a much higher value as only half of the radiative tip is placed onto the tissue and half is exposed to the surrounding air. with this setup there is only a radiation of approximately -9.7dB or 10.6%. This energy will also fall off relatively quickly. Figure 6.23 shows the power delivery into a cylindrical tube of oesophageal material at 20mm in diameter which approximates the distended diameter of the human oesophagus [91]. It can be seen

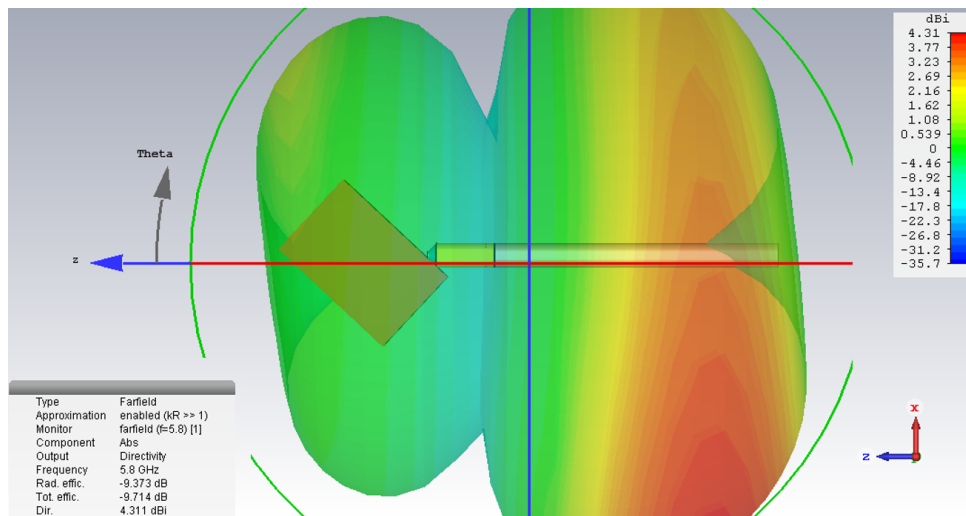


Figure 6.22: Simulated farfield monitor for final sloped tip design with PEEK

that the power is delivered into the tissue but has no noticeable effect on the opposite side of the lumen. The majority of the energy is still being delivered into the tissue at the intended treatment site and the energy falls off too rapidly to affect the opposite side of the oesophageal lumen. During clinical usage the clinician will be aware that the entire tip radiates energy and to be aware of any unwanted tissue effects.

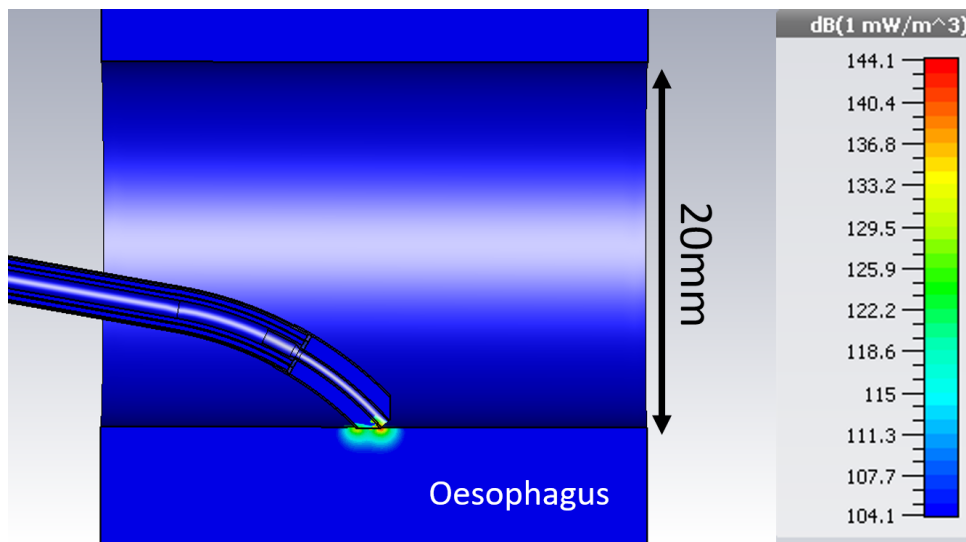


Figure 6.23: Simulated power loss density plot for final sloped tip design with PEEK inside oesophageal lumen

### 6.3.1 Variation in length

The simulated length, as discussed above, varies from the theoretical calculation for a quarter wave impedance transformer. Three experimental simulations were carried out to assess the reasoning for this. For the radiative tip to act as a quarter wave transformer it needs to approximate a quarter wavelength when considering the dielectric through which the wave is travelling. Considering the earlier eq. 4.4, the calculated value for the PEEK radiative tip was approximately 7.2mm whereas simulated results, shown above, give a much smaller tip length of 4mm at 5.8GHz.

#### Experiment 1

The initial experimental simulation was a re-run of the PEEK radiative tip model and used a parameter sweep to assess the variation in tip length between 3.9mm and 4.3mm. This gave resonance or matching at varying frequencies which corresponded to an electrical length which should then be equal to a quarter wavelength and can be seen in table 6.3. Eq. 4.4 was used to calculate the expected value for a quarter wavelength at the corresponding frequencies which allowed the difference between simulation and theoretical to be quantified.

Table 6.3: Table showing variation in length with increasing tip length of PEEK tip

Tip Length (mm)	Frequency (GHz)	1/4 Wave (mm)	Difference (mm)
3.90	6.08	6.89	2.99
4.00	5.98	7.01	3.01
4.10	5.89	7.11	3.01
4.20	5.79	7.24	3.04
4.30	5.70	7.35	3.05

This gave a base line showing the amount of length variation for the simulated structure along with relevant matching frequencies.

## Experiment 2

The second experimental simulation was intended to ascertain whether the step discontinuities present where the radiative tip attaches to the cable would affect the tip length due to change in capacitance and inductance variations. To do this a simulation was set up in which the radiative tip and cable had the same geometry in terms of inner and outer conductor. This can be seen in fig 6.24.

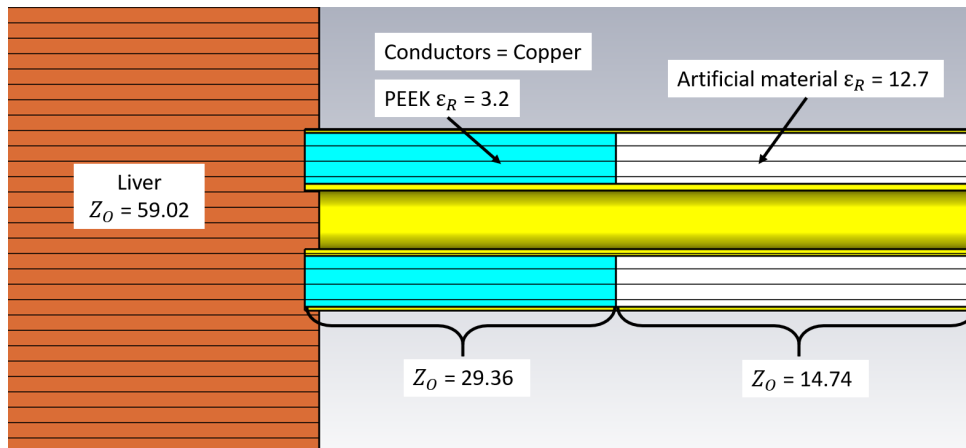


Figure 6.24: Simulation model for second experimental simulation considering lack of step discontinuity

An artificial material was created with a dielectric constant of 12.7 which provides a  $14.74\Omega$  input for the radiative tip to approximate the cable impedance without the need for a step in conductor diameter. The results of this experiment can be seen in table 6.4. It can be seen that there is a small difference of approximately 0.2mm when compared to the previous experiment. This means that there is a small length change required to compensate for additional capacitance introduced due to the stepped conductor but this does not account for the over 3mm difference.

## Experiment 3

The final experiment considered open circuit end effects introduced as the energy is propagated through the liver. The open structure gives rise to fringing fields and a fringing capacitance which can have a large impact on the effective electrical length

Table 6.4: Table showing variation in length with increasing tip length of PEEK tip without step discontinuity

Tip Length (mm)	Frequency (GHz)	1/4 Wave (mm)	Difference (mm)
3.70	6.06	6.91	3.21
3.80	5.95	7.04	3.24
3.90	5.85	7.16	3.26
4.00	5.75	7.29	3.29
4.10	5.67	7.39	3.29

of the structure. [92, 93]. To assess the effect of this a method similar to the previous experimental simulation was used. The model for which can be seen in figure 6.25.

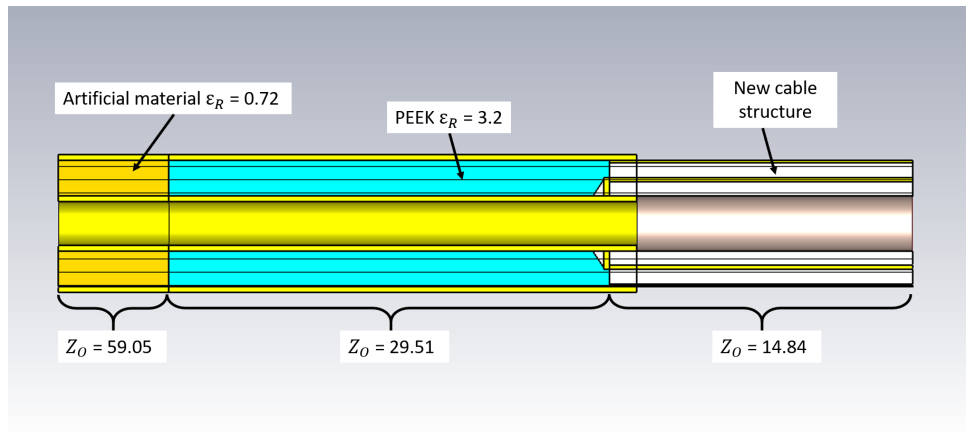


Figure 6.25: Simulation model for third experimental simulation considering lack of fringing capacitance

This co-axial load provided a similar impedance in magnitude to the liver whilst a waveguide port ensured that the open circuit end effects were removed. The results of this were assessed to locate resonant frequencies and the difference between theoretical quarter wave and simulated length was once again calculated as seen in table 6.5

It is clear from the three experimental simulations above that the largest component responsible for the variation in physical length from theoretical calculations is open ended structure within the liver load. The capacitance introduced due to the fringing fields at the open circuit causes the effective electrical length to be much longer than the physical tip length. The simulated E field shown in figure 6.26 shows

Table 6.5: Table showing variation in length with increasing tip length of PEEK tip without fringing end effects

Tip Length (mm)	Frequency (GHz)	1/4 Wave (mm)	Difference (mm)
6.80	6.04	6.94	0.14
6.90	5.95	7.04	0.14
7.00	5.86	7.15	0.15
7.10	5.77	7.26	0.16
7.20	5.69	7.36	0.16

these fringing fields. The discontinuity is frequently assumed to be capacitive [94] and is a combination of the fringing fields both within the tip dielectric and within the liver. When this is taken into consideration the small variation left can be explained in terms of extra capacitance within the stepped conductor method of attaching the radiative tip, as shown in experiment 2, and also in simulation errors and minor considerations which the theoretical calculations do not consider.

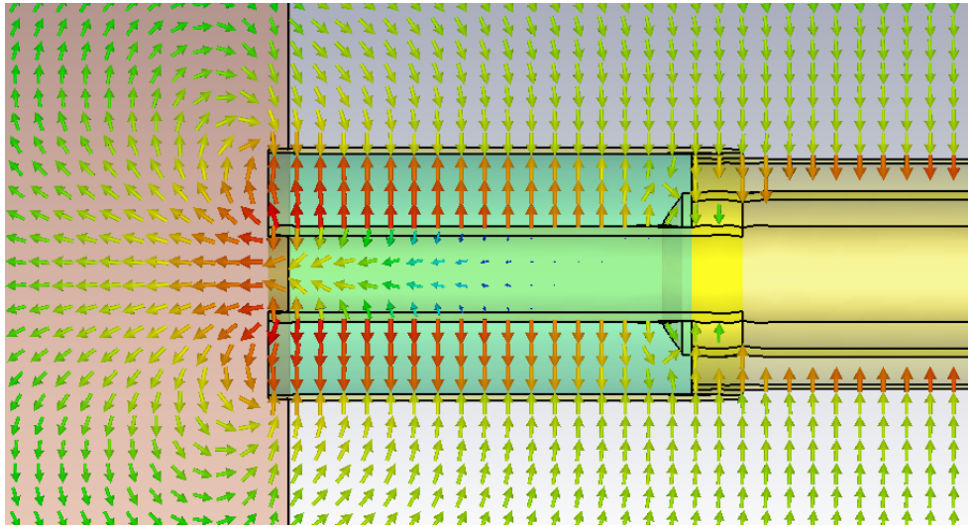


Figure 6.26: Simulated E field showing fringing fields at open circuit liver boundary

## **Chapter. 7**

---

### ***Microwave and Adrenaline Haemostat - Full Device***

---

#### **7.1. Development and Design**

##### **7.1.1 Overview**

The final devices consisted of the microstrip impedance transformer, a length of the novel cable structure along with the radiative tip coupled with a 3D printed handpiece. Due to the planned protocol during preclinical testing as shown in appendix B. As only the oesophagus is being used, a length of 1.7m of cable was decided upon. The device need not be too long as it will only be used to coagulate lesions in the upper GI tract however for other devices this could be changed.

Overall four devices were created, two with the flat ended radiative tip and two with the sloped radiative tip. It was unclear at the time of manufacture whether the clinician would find it easier to apply energy through the flat or sloped tip. As previously discussed the minimal diameter of the oesophageal lumen may make it difficult to apply the tip fully against the tissue which would make the use of the sloped tip much easier as the structure need only be applied at a 45° angle. Devices containing both tips were manufactured to allow for this to be tested.

##### **7.1.2 Transformer and Connectors**

As per the impedance transformer test results previously shown, for ease of manufacture and to allow the structure to be assembled in a repeatable way, it was decided to make use of the microstrip transformer with ground tray structure to ensure that both



a good electrical/microwave connection and also good structural connections were made. This was vital for the testing that was to be carried out, especially for use in the operating theatre in which the device will be subject to much more strenuous and harsh forces/usage than during initial bench testing.

### **Hollow Channel Connection**

For the full device to be able to support both intended modalities i.e. energy delivery alongside the introduction of other tools or fluids, a solution needed to be found on how to access the hollow channel. Leaving the PTFE tube exposed through the handpiece would create difficulty in insertion or injection. The chosen solution was to use a Luer lock connector which is an industry standard for many device which require the attachment of a syringe and allows for compatibility between different devices. A simple syringe could be connected to this luer lock attachment and allow for easy injection of either saline or adrenaline or even attachment to a syringe pump system could be connected for aspiration and irrigation.

The luer lock needle was wrapped in heatshrink to increase the outer diameter and inserted into the hollow channel to ensure a tight fit. A small brass collar was then placed over the connection and mechanically compressed into place. This ensured that the connection would be robust enough to handle the high pressure during injection and repeated connection and disconnection of syringes. This is vitally important as the pressure required to inject fluid could increase significantly if the hollow in the distal tip was to become partially occluded due to blockage by tissue or partially coagulated blood.

### **Handpiece and Transformer Enclosure**

Once the cable had been connected to the transformer and a strong mechanical connection achieved whilst allowing access to the hollow channel the next step was to enclose the device with a handpiece. This needed to not only provide protection

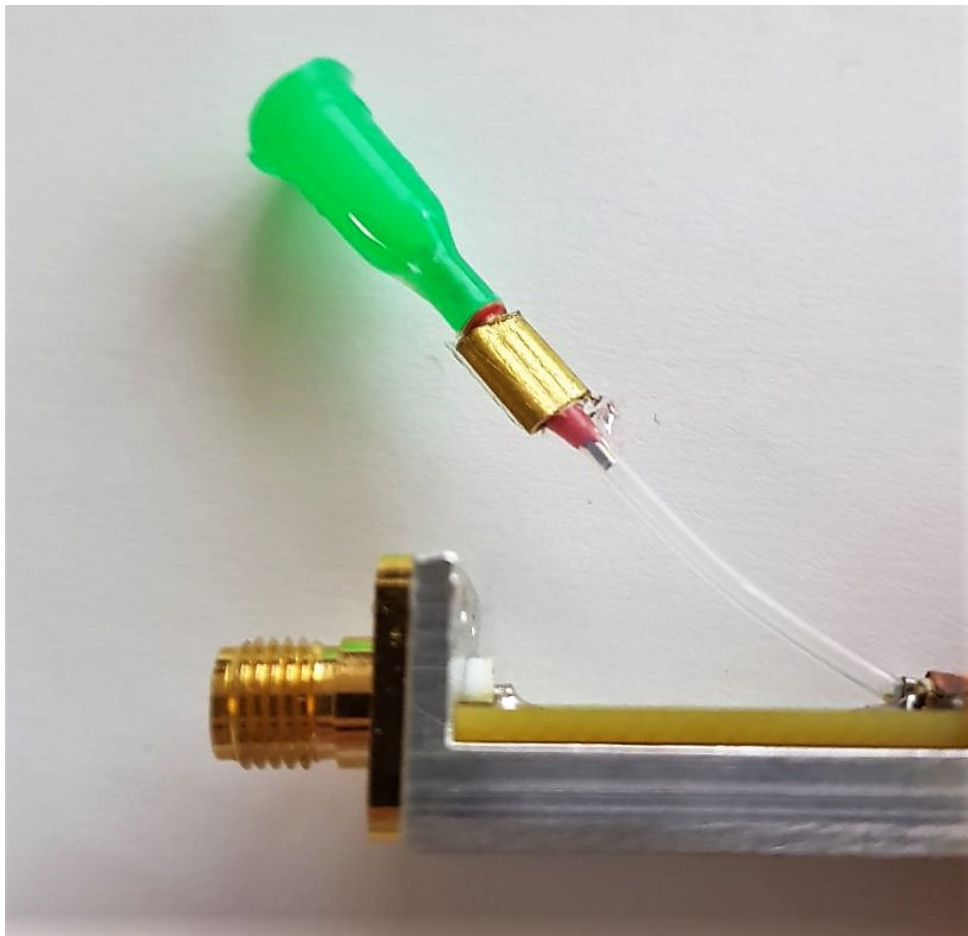


Figure 7.1: Photograph of the final connection used to access the hollow channel for the clinician from accessing parts of the transformer which could cause injury but to also allow for ease of use and comfort for them.

Due to the radiative nature of microstrip a section of work was carried out to consider the effect of radiation from the microstrip transformers. Work presented at the IEEE MTT-S International Microwave Workshop Series on Advanced Materials and Processes considered the difference between a milled aluminium enclosure and a 3D printed conductive filament enclosure [95]. The latter being much easier to prototype and iterate through various designs. It is thought that the handpiece used in the final design offers enough shielding due to its thickness to ensure that no electromagnetic interference is present during operation. All laboratory testing was undertaken using a Nard alert monitor to ensure that excess levels of radiation were

not present during operation.

### **Final Handpiece Design**

The final handpiece design was 3D printed using an Ultimaker 2+ Printer with standard Polylactic Acid (PLA) material.

The initial structure was designed in Autodesk Inventor Professional and had a number of constraints.

- Ensure enough room for the transformer structure with a small air gap above the microstrip so as not to affect the electromagnetic fields.
- Provide a secure structure for a small section of cable after the transformer to minimise breakage and stress on the transformer - cable connection.
- Contain openings for access to both the SMA connector and Luer lock hollow channel access.
- Be of suitable size to allow for ease of use and comfort in holding for the clinician.

Once the final design was finished, the model was split into two halves and imported into Ultimaker Cura to slice the model ready for loading onto the 3D printer. This converts the model into G code which the printer can then read layer by layer. This structure can be seen in figure 7.3

This g code was then loaded into the printer and allowed to print, once complete they were then removed from the printer and cleaned up. Due to the slight overhang at the cable end of the handpiece scaffold material was needed; this is a less dense structure of plastic which supports any overhanging edges to ensure that they don't droop and maintain their intended shape during the print process. This support is then removed once the print is completed and the part is finished.

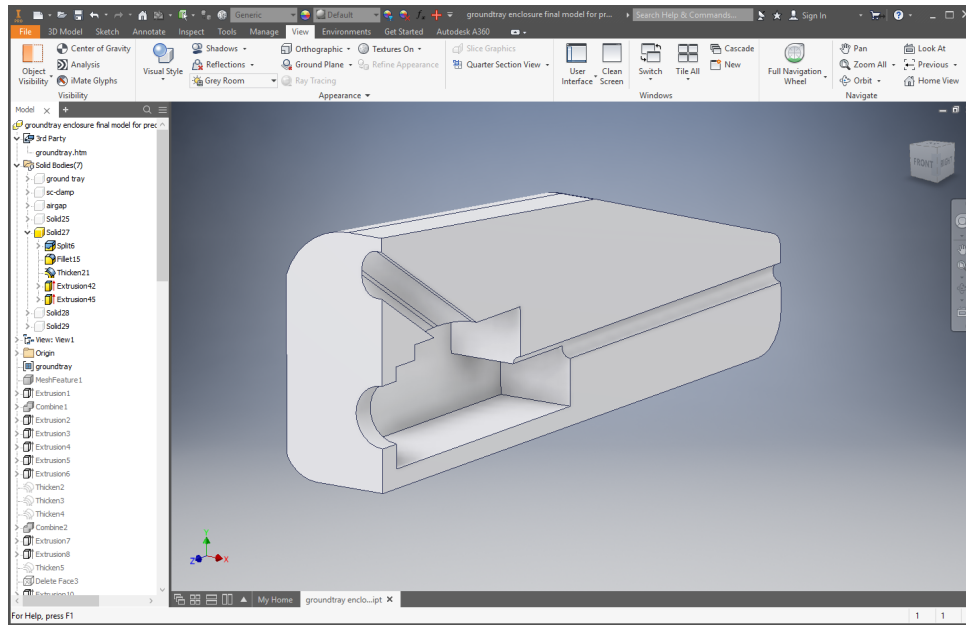


Figure 7.2: Designing of the handpiece in Autodesk Inventor Professional

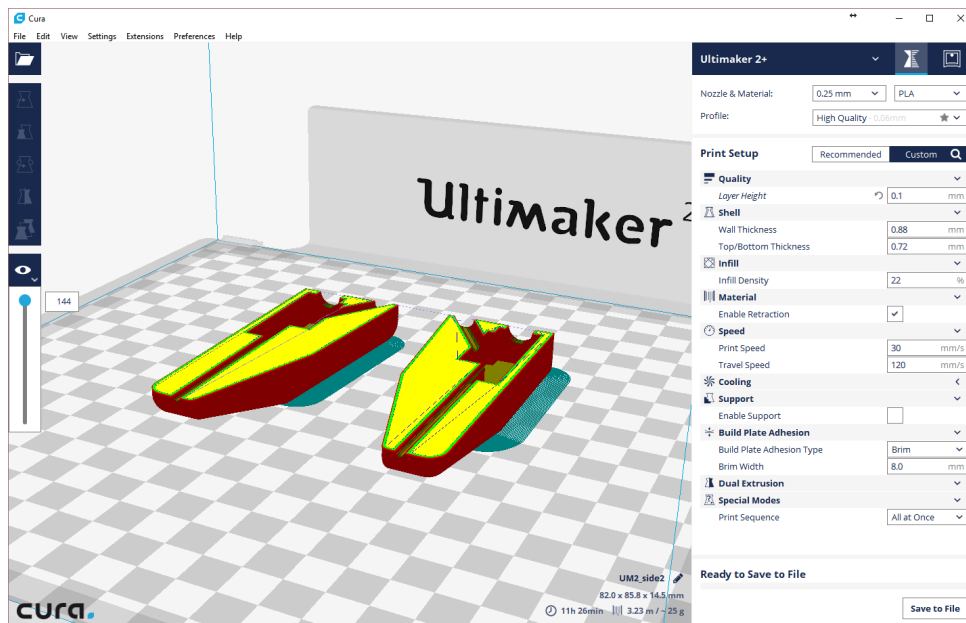


Figure 7.3: Slicing the handpiece model in Ultimaker Cura

### 7.1.3 Consideration of handpiece shielding

As PLA was used for the final handpiece design a section of work was carried out to ensure that the plastic enclosure would provide enough protection for the user from the radiation from the microstrip trace on the impedance transformer. Prelim-

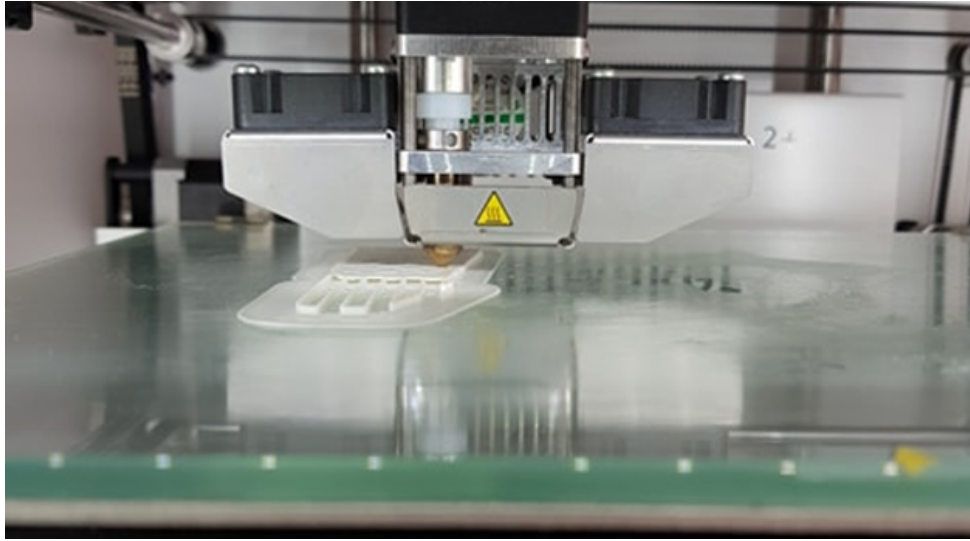


Figure 7.4: Ultimaker 2+ 3D Printer during printing of the initial handpiece design

inary simulations which consider both aluminium and conductive plastic shielding are shown in appendix C whilst this section considers the effect of the the PLA enclosure in terms of specific absorption rate (SAR). It was believed that the majority of this radiation would be minimised by the handpiece but CST Microwave studio was used to quantify this. The model designed and used for this is shown in fig. 7.5 and comprises the microstrip impedance transformer connected to a standard SMA connector and also to a length of cable. The handpiece then surrounds the transformer and a cylinder of skin is placed around this to emulate the handpiece being in contact with the hand of the clinician.

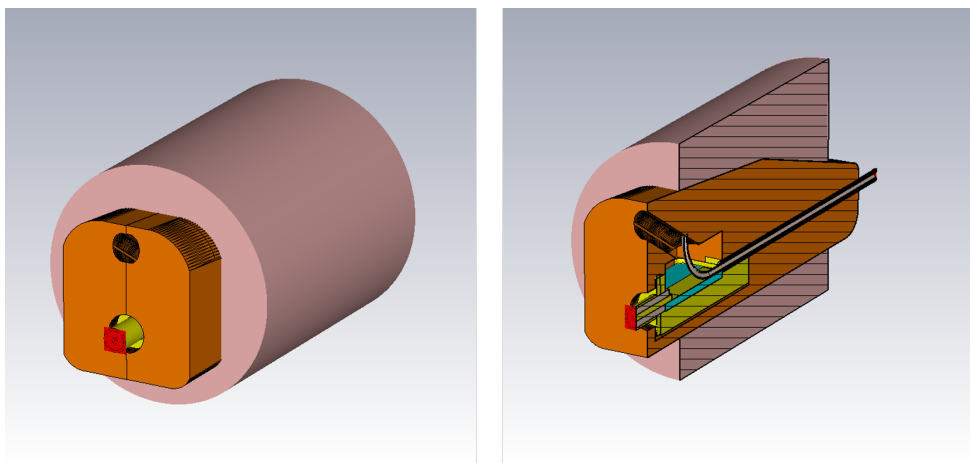


Figure 7.5: CST Studio model used to simulate the effect of microstrip radiation

Due to the expected penetration depth and the complexity of human tissue due to its inherent inhomogeneity only the CST model for skin was used. For further accuracy it would be necessary to model the entire structure of the hand including the various tissue structures within. For the purposes of this research it is believed that the method used will give a good indication of the outcome.

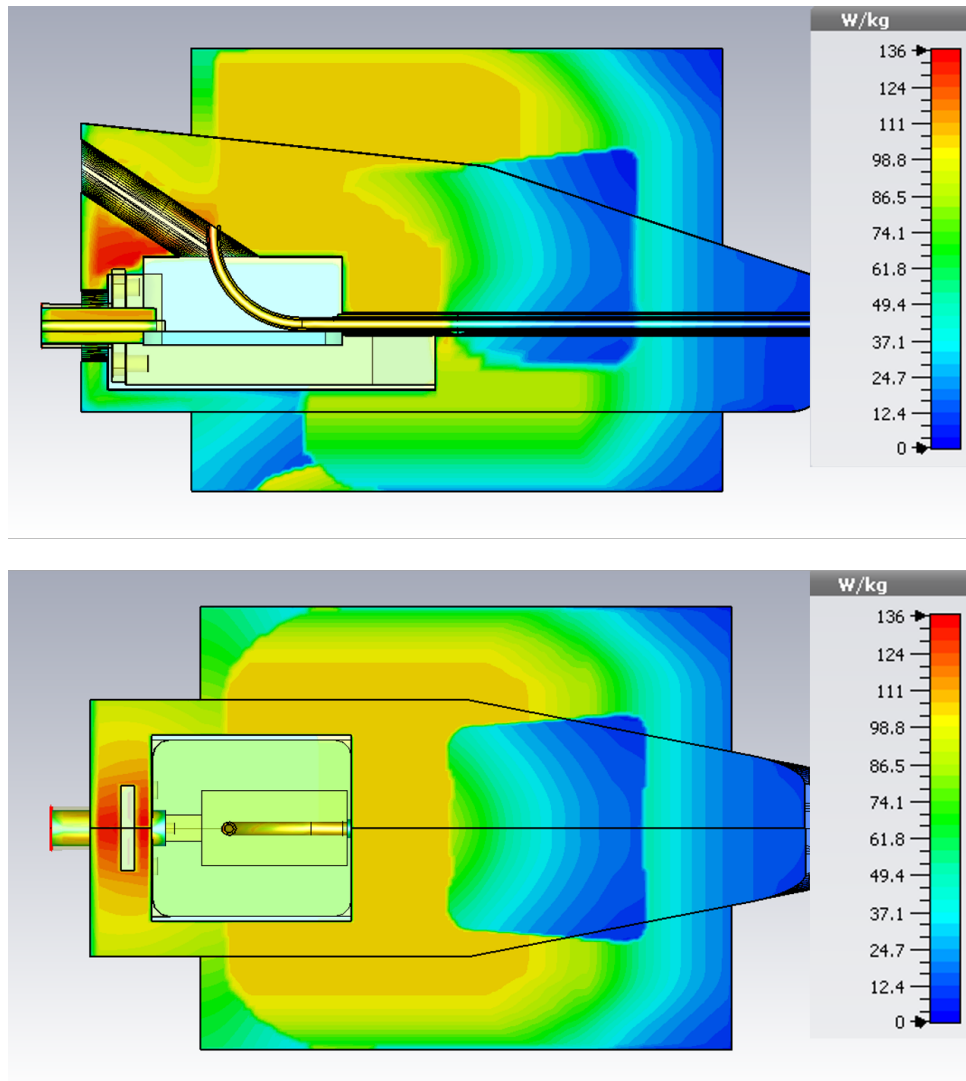


Figure 7.6: Specific absorption rate illustrating the energy absorbed into the handpiece and surrounding skin phantom with cutting planes through (top) x-axis and through (bottom) y-axis

Fig. 7.6 shows the SAR in the skin phantom structure at 5.8GHz. It can be seen that the energy is travelling through the handpiece and is being delivered into the

skin. Once scaled up to approximate the power input of the device this gives an SAR of the skin of 107 W/kg.

The SAR value is a measure of how much electromagnetic energy is absorbed by biological matter when exposed to radiation. This value can be given as total SAR, which takes into account the entire structure, or it can be averaged over a specific mass usually 1g or 10g. For these measurements an averaging mass of 10g was used within CST studio and applied to a power loss density simulation for the structure which had been scaled up to approximate the expected input power of 50W, i.e. the COAG9 setting on the Creo Medical generator.

The International Commission on Non Ionising Radiation Protection (ICNIRP) gives a safe occupational exposure limit of 20 W/kg localised SAR into limbs [96]. It can be seen that the 107 W/kg SAR shown in fig. 7.6 is approximately five times higher than the recommended exposure limit. One proviso made by ICNIRP, however, is that this maximum exposure should be averaged over any six minute period. For all bench testing carried out the device was held within a clamp and secured away from the operator. For the pre-clinical testing this six minute average needs to be taken into account.

Each lesion was created prior to haemostasis and as such the device was only active for approximately 30 seconds. To allow for a further safety margin in addition to those already implemented by ICNIRP it was assumed that the clinician would have the device active for 1 minute for every 6 minutes of procedure. This takes the exposure limit down to roughly 17.83 W/kg.

### **Metallic insert for handpiece shielding**

Although the previous section proves that the clinician was at minimal risk and was exposed to electromagnetic energy under the recommended exposure limits as stated by ICNIRP, it was deemed necessary to include some shielding within the handpiece to limit this exposure even further. This would become especially necessary should

the clinician need to keep the device active for a longer amount of time such as required for a larger bleed or for multiple bleeding lesions.

To achieve this a small layer of metallisation was applied to the inside of the handpiece above the microstrip transformer structure as can be seen in fig. 7.7

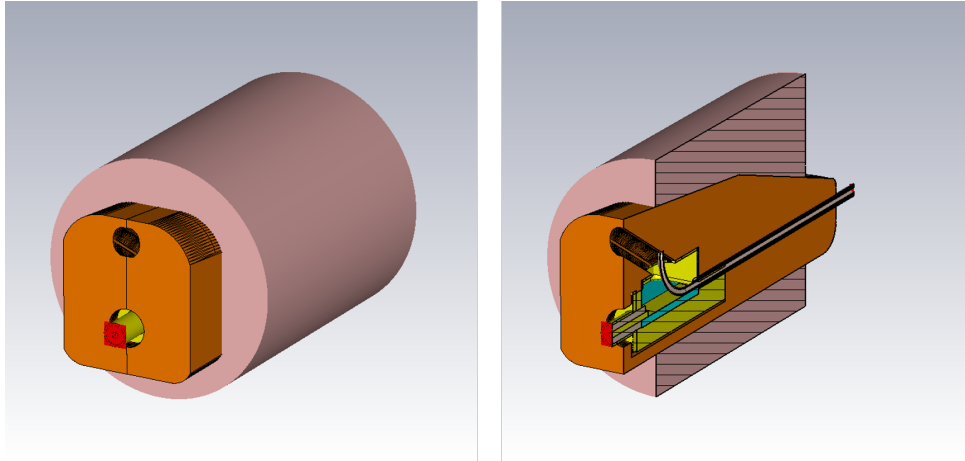


Figure 7.7: CST Studio model showing metallic shielding above microstrip

The structure was then re-simulated and the SAR re-calculated considering the effect of this shielding and the SAR plot is shown in figure 7.8. The highest recorded SAR value in the skin phantom is 0.096 W/kg which is well below the safe exposure limit as previously discussed.

This shielding can be achieved through the use of a metallisation layer such as through the use of conductive paint or simply by using conductive tape. Ongoing work could include the use of a machined enclosure or the use of the co-axial transformer which would prevent this radiation as the fields are confined between the two conductors. These simulations provided a safe alternative to the original structure which requires very little alteration to the current design and still allows for the manufacture of the handpiece using readily available 3d printing manufacturing techniques. Further shielding could be achieved through the use of EMC finger strips or gaskets along the joins of the device. Further work could be carried out in altering the transformer structure to ensure that the E field is at a minimum at any point where leakage could occur.



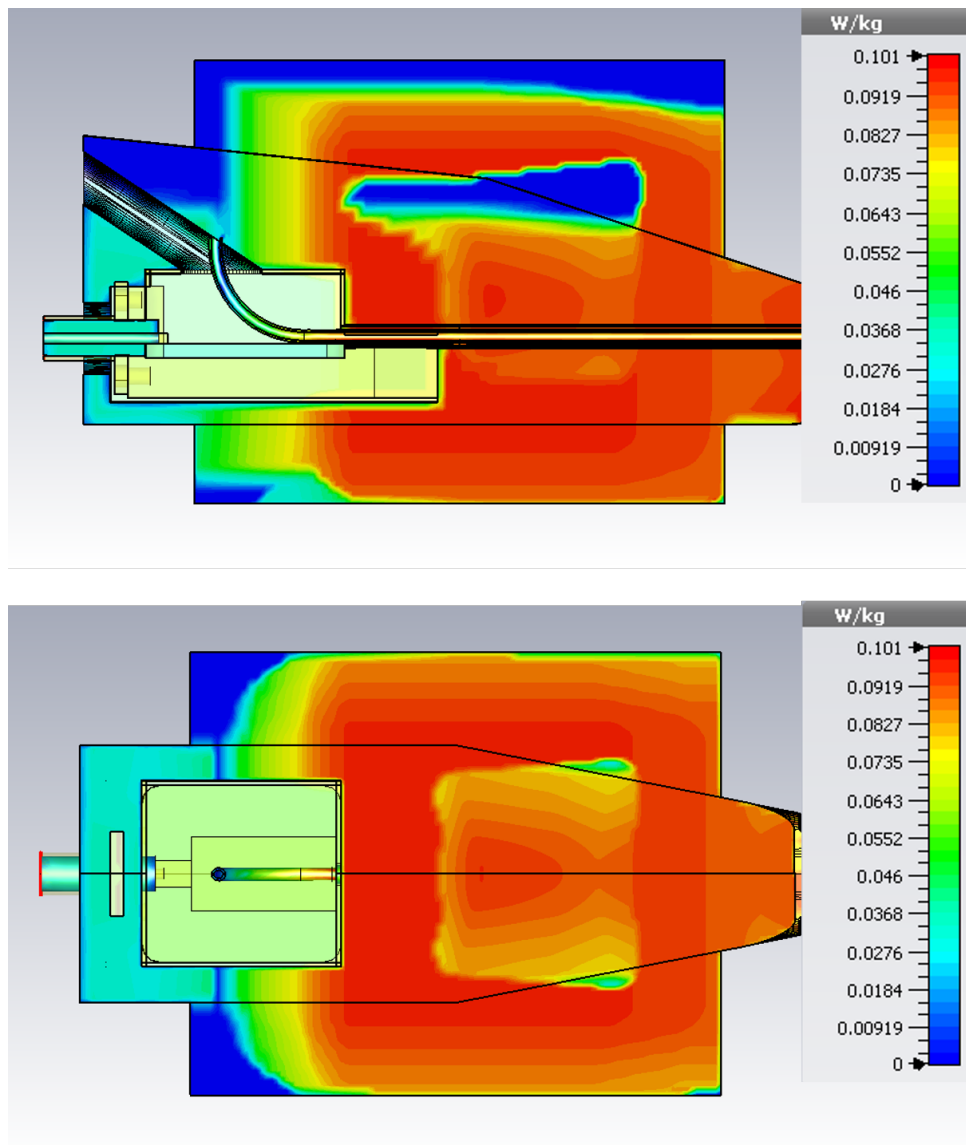


Figure 7.8: Specific Absorption Rate plot from X cutting plane (top) and Y cutting plane (bottom) showing absorption of energy into the handpiece and surrounding skin phantom with shielded transformer

#### 7.1.4 Radiative Tip

The radiative tip for each of the devices were manufactured in house and assembled at Creo Medical Ltd onto each of the cable lengths. The inner conductor was electrically connected in place and then covered by the PEEK sheath and then the outer conductor. The PEEK sheath was used following from simulated results previously presented. PEEK provided the best return loss and appeared to offer much better

energy delivery. Once all the parts had been aligned the outer conductor of the tip was electrically connected to the outer conductor of the novel microwave cable. Care was taken to ensure that all three parts lined up correctly as any variation in the end geometry would have affected the device efficiency and mitigated possible treatment effect. This could occur due to variation in the required length and therefore change in matching frequency.

An immediate issue became apparent during connection of the inner conductor. Whilst possible, it was difficult to get the parts lined up and then to be able to apply solder accurately enough to ensure that only the inner conductor was connected. Continuous testing using a Fluke 289 True RMS multimeter was carried out during the manufacturing process to ensure that no parts of the device had become shorted and that a good electrical connection was achieved between each of the conductors.

### 7.1.5 Final Manufacture

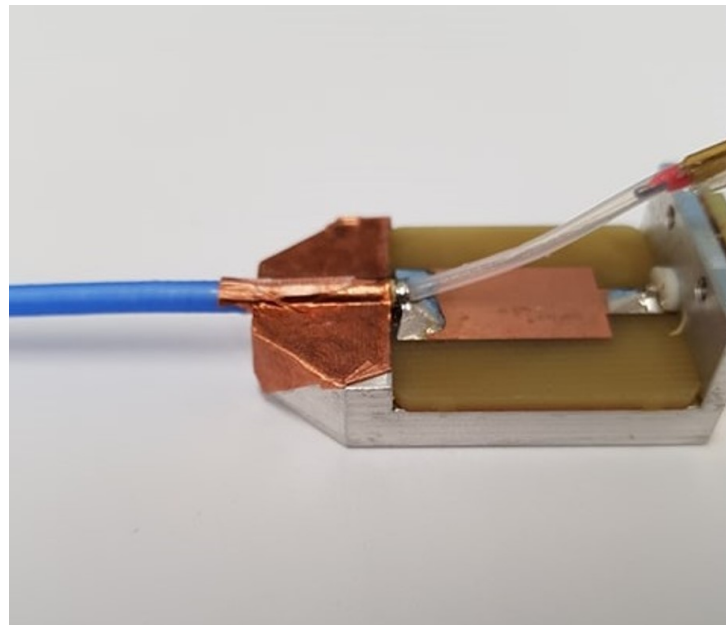


Figure 7.9: Photograph showing connection of the cable to the microstrip transformer

The radiative tip parts were turned from small sections of brass and PEEK as previously discussed. Images of these parts can be seen during the initial assembly

process and the final structure can be seen in figure 7.10.

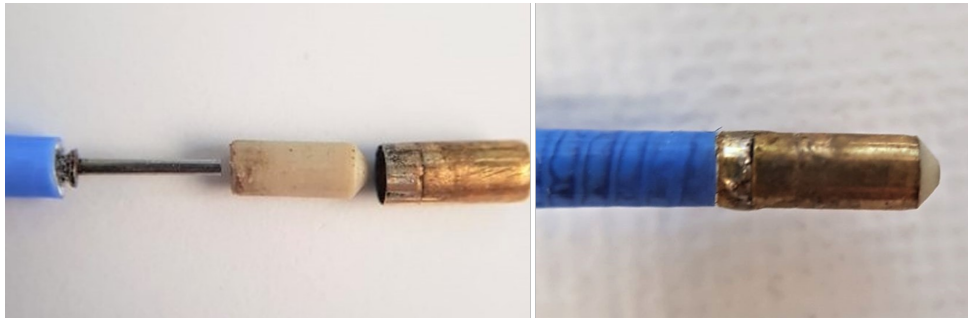


Figure 7.10: Individual (left) and assembled (right) parts for final sloped tip design



Figure 7.11: Photograph of the final manufacture (left) and device ready for preclinical testing (right)

The transformer, cable and radiative tip assembly was then packaged in the previously 3D printed handpiece. The inner structure of the handpiece was designed to hold the structure in place and not require any fixing. The two halves of the structure were then secured to each other with glue. The handpiece and both the SMA and the fluid port were both tested for good connection and to ensure that they would not come apart during bench and pre-clinical testing.

## 7.2. Bench Results

### 7.2.1 VNA testing of completed devices

Once the devices had been manufactured they were all tested using the VNA to ascertain both the loss of the whole device and also the effectiveness of the radiative tip.

For each device a time domain measurement was made initially with the tip radiating into air and then into a piece of liver. This set-up is similar to that used when testing the cable prototypes. The idea being that the air measurements are when there is maximum reflection due to the open ended radiative tip and therefore should give an indication of the amount of loss through the cable. Once the tip is placed into the liver this measurement should decrease meaning that the energy is being delivered into the tissue. This general result can be seen throughout all the plots for each device as shown in figures 7.12 to 7.15. A summary containing the results can be seen in table 7.1. It can be seen that for each device the connector values, that is the reflection at the connection to the transformer, does not deviate strongly even when placed into tissue. However when the device is placed into the tissue the peak at the end of the device becomes much lower. This means that the reflection at the tip of the device has lessened. The obvious conclusion from this is that the energy is being delivered into the tissue.

Table 7.1: Results from time domain measurements for each device

Device	Connector (Air) dB	Connector (Liver) dB	Tip (Air) dB	Tip (Liver) dB
MAH1	-23.76	-24.40	-11.39	-21.06
MAH2	-17.33	-17.26	-11.91	-17.29
MAH4S	-12.60	-12.40	-11.78	-15.62
MAH5S	-14.85	-15.52	-13.50	-24.68

It can be seen from table 7.1 that the first three devices all show similiar results

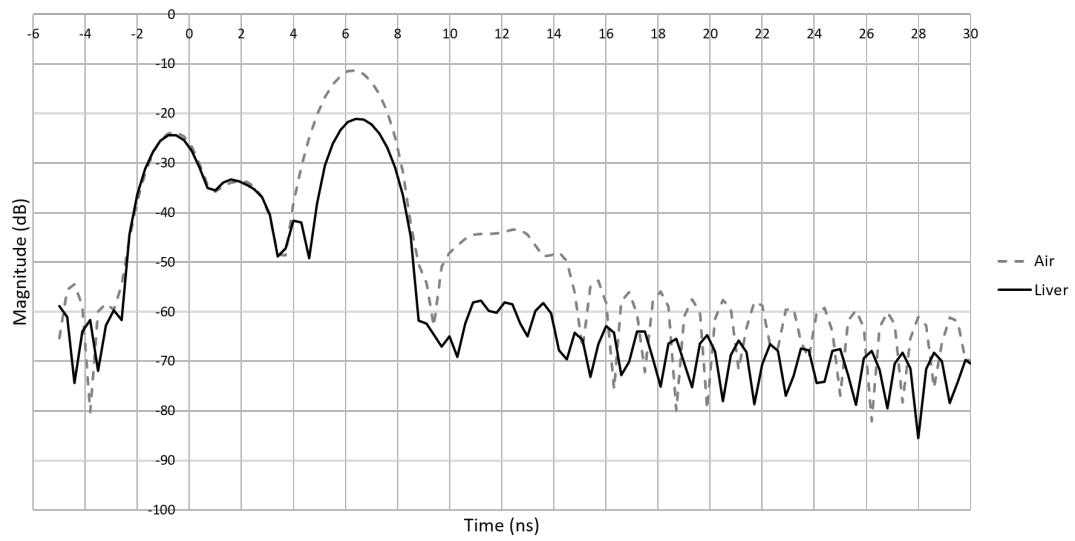


Figure 7.12: Time Domain plot of the final MAH1 device

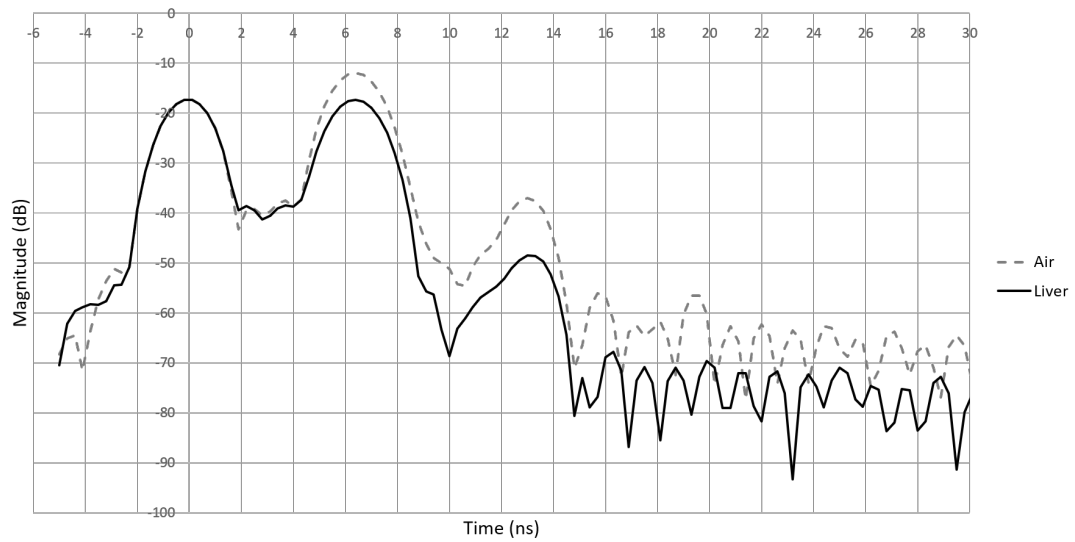


Figure 7.13: Time Domain plot of the final MAH2 device

when tested in air. Although the connector values for MAH4S appear to be much lower; when considering power transmission a value of -12dB equates to 93.69% transmission whereas -23dB equates to 99.50%, a difference of only 5.81%.

When looking at the tip measurements, the peak on the right, we can estimate the amount of loss in the device and also how effective the radiative tips are. These tests can also be used to confirm the attenuation along the length of cable. Use of the following eq.

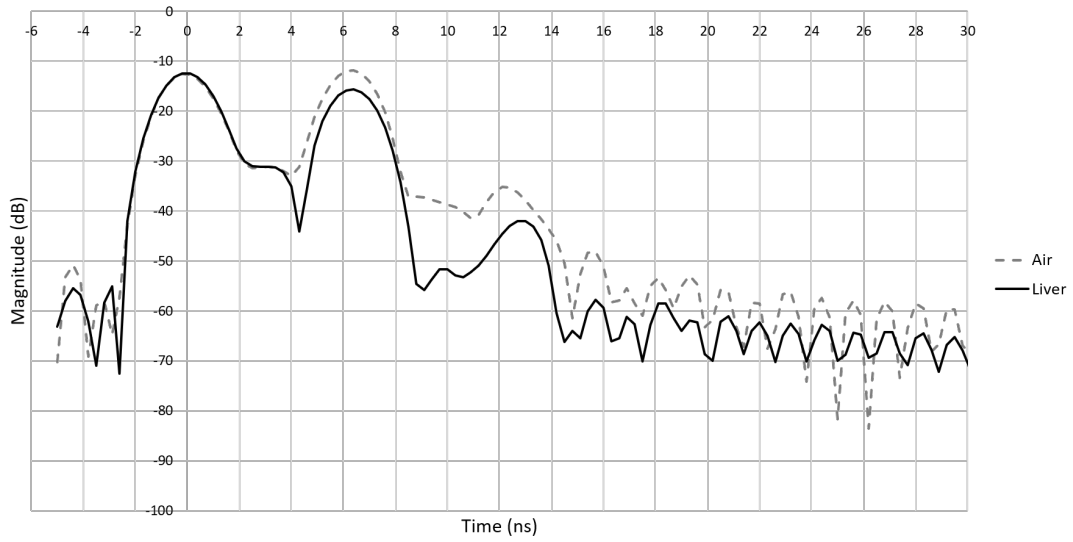


Figure 7.14: Time Domain plot of the final MAH4S device

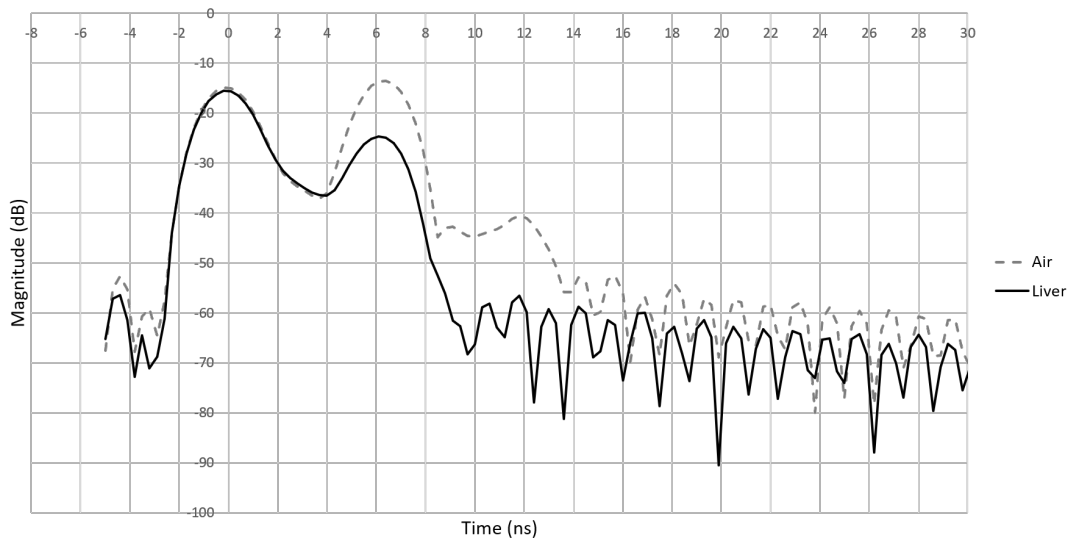


Figure 7.15: Time Domain plot of the final MAH5S device

$$\frac{(\text{Tip}(\text{Air}) - 1.8)}{(2 \times 1.7\text{m})} \quad (7.1)$$

1.8dB is the approximation of the loss in the transformer and 1.7m is the length of the cable, once again multiplied by two to take into account the forward and return path of the time domain measurement. This analysis gives us values varying from -2.82dB to -2.94dB. MAH5 gives a much higher value of -3.44dB. This could be for

a number of reasons including connection to the transformer or the radiative tip not being connected correctly. For this reason it was deemed unsuitable and not used for the preclinical testing.

Consideration of the time domain plots and analysis of the measured values allowed for the both the MAH1 and MAH4S devices to be chosen for use for the final preclinical testing at Northwick Park.

## 7.2.2 Ex-vivo Tissue Testing

Prior to pre-clinical testing, one of the initial prototype devices was tested on the bench using a porcine liver model. The device was used to deliver energy into a tissue sample for varying amounts of time. Each delivery was repeated twice to ensure repeatability. This bench testing was a preliminary investigation to determine that both the transformer and the radiative tip design were operating as required and that energy would be delivered into the tissue as expected.

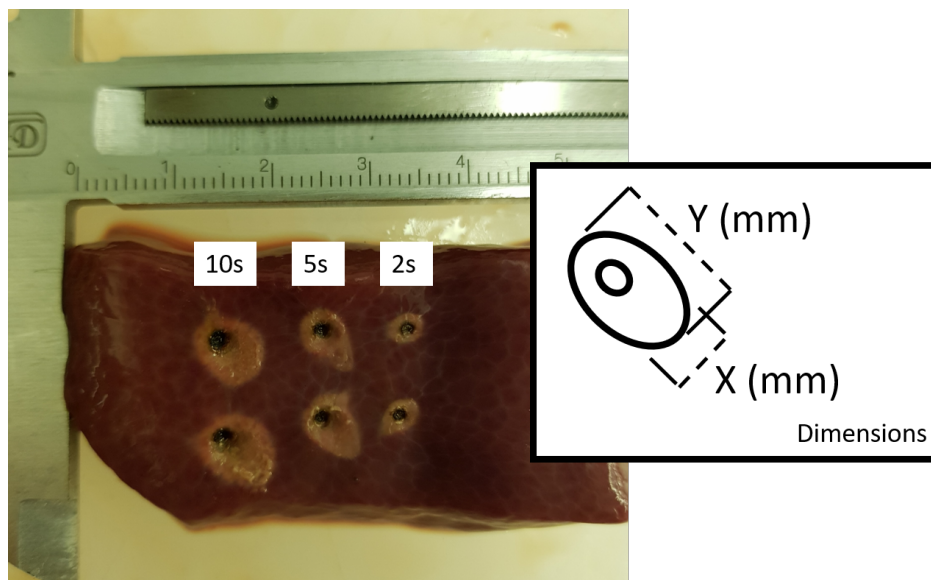


Figure 7.16: Bench test results for initial prototype at various times

From left to right, the device was used to apply energy for 10 seconds, 5 seconds and finally 2 seconds. The device was applied to the tissue at a 45 degree angle whilst

Table 7.2: Table showing measurements of application sites during bench porcine liver testing

Application time	X (mm)	Y (mm)	Depth (mm)
10s	5.5	7.5	1.1
5s	4.0	6.5	1.0
2s	3.5	3.0	0.8

applying a small amount of local tamponade or pressure as seen in figure 7.17. The COAG9 setting was used on the Creo Medical CROMA generator, which equates to approximately 50W at the fascia of the generator. Considering the results from both the cable and transformer testing approximately 11.75W should have been delivered into the tissue, the method of determining this is shown in table 7.3

Table 7.3: Loss calculations for bench testing

Input Power (W)	50.00
Input Power (dBm)	46.99
Loss due to Interface Cable (dB)	1.25
Loss due to Transformer (dB)	1.85
Loss due to Cable (dB)	2.85
Total Loss (dB)	5.95
Power minus Loss (dBm)	41.04
Power minus Loss (W)	12.71
Power minus Loss with tip efficiency (W)	11.75

The tissue effect noted in figure 7.16 matches the expected power delivery pattern as per simulations discussed earlier and shown again in figure 7.18. There is an area of high temperature increase around the hollow channel and this then lessens as energy dissipates into the tissue. Where the outer conductor meets the tissue there is also an increase in temperature which gives a tissue effect extending in one direction underneath device from the point of application. This allows the surgeon to coagulate a specific area whilst providing an area between inner and outer conductor so as not to be too localised and miss the actual bleeding site.



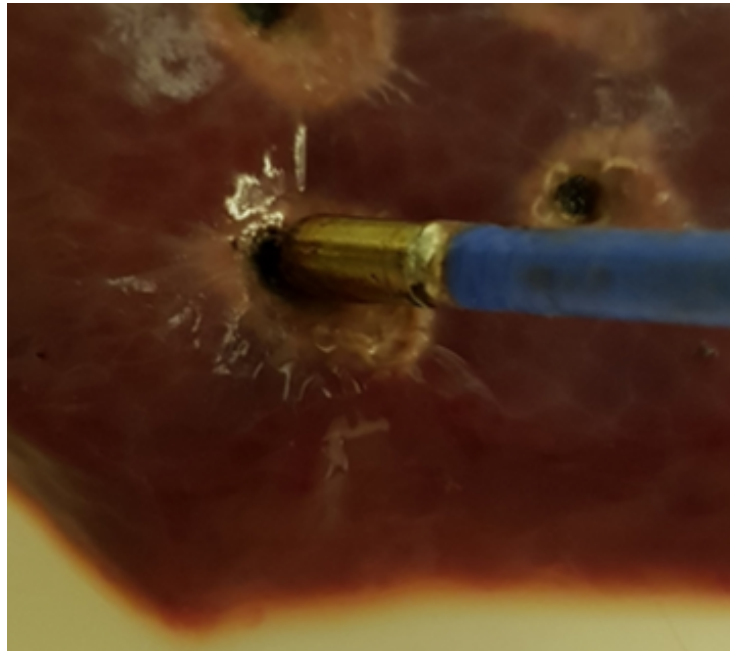


Figure 7.17: Application of the haemostat to the tissue sample

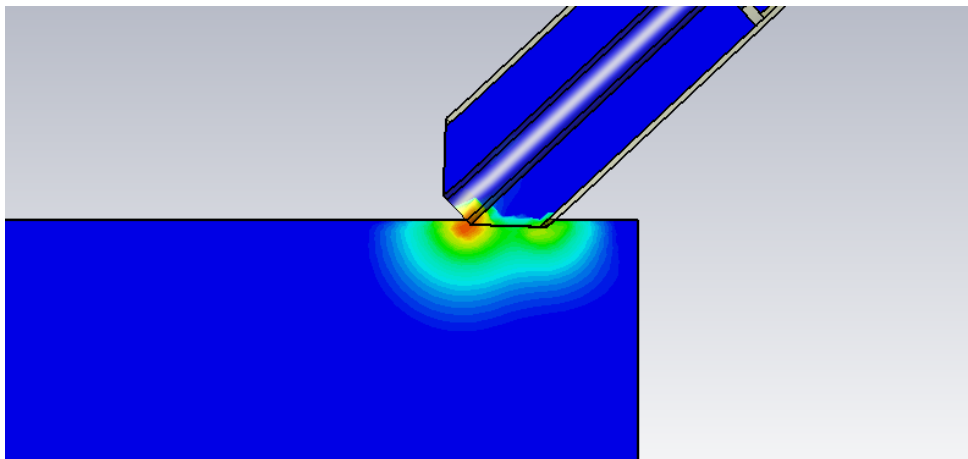


Figure 7.18: Simulation showing power loss density and approximate area of tissue effect

### Side application and radiation

Another concern regarding the radiative tip was to ensure that energy was only delivered from the tip and that any tissue in contact with the sides of the cable would not be effected.

To test this the device was placed side on on top of a porcine liver sample as in previous tests and energy was applied as shown in figure 7.19. The coagulation zone

was then considered for point of application, thermal spread and any other factors which would indicate unwanted energy delivery.

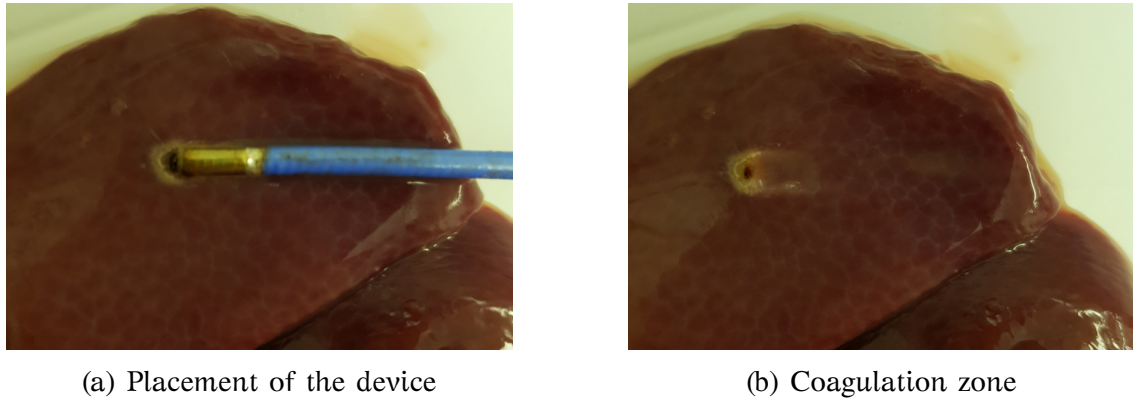


Figure 7.19: Side application of haemostat probe

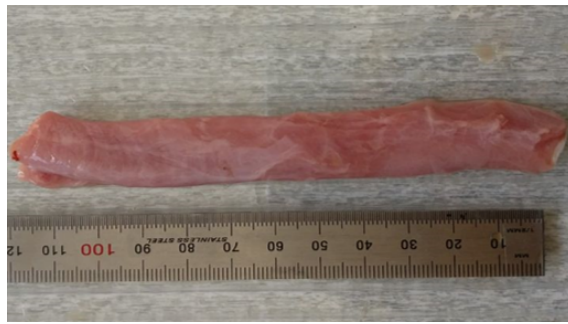
It can be seen that there is some thermal spread along the tip which is evident due to the slight discolouration adjacent to the main coagulation zone. At the tip-cable junction and further down the cable there is no tissue effect meaning that at 5 seconds of application there is not enough heating at those points to visibly affect the tissue.

### **Ex Vivo Porcine Oesophagus**

A Porcine Pluck (oesophagus, trachea, lung and heart) was procured from the local meat processing plant to allow for oesophageal tissue testing of the device. The oesophagus was dissected from the rest of the pluck and a longitudinal incision was made to allow the oesophageal lumen to be laid out as to create a flat surface which could then be treated as can be seen in figure 7.20. Saline was used sporadically to prevent the mucosal surface from drying out.

The device was tested both at a 45 degree angle and at a 90 degree with the whole tip in contact with the tissue.

The first 8 coagulation zones were treated with the tip at 45 degrees to the tissue for 20 seconds, 10 seconds, 5 seconds and finally 2 seconds. Each delivery was repeated twice and the zones were demarcated with a superficial cut.



(a) Extracted oesophagus



(b) Inner surface of oesophageal lumen

Figure 7.20: Exposing of inner surface of oesophageal lumen

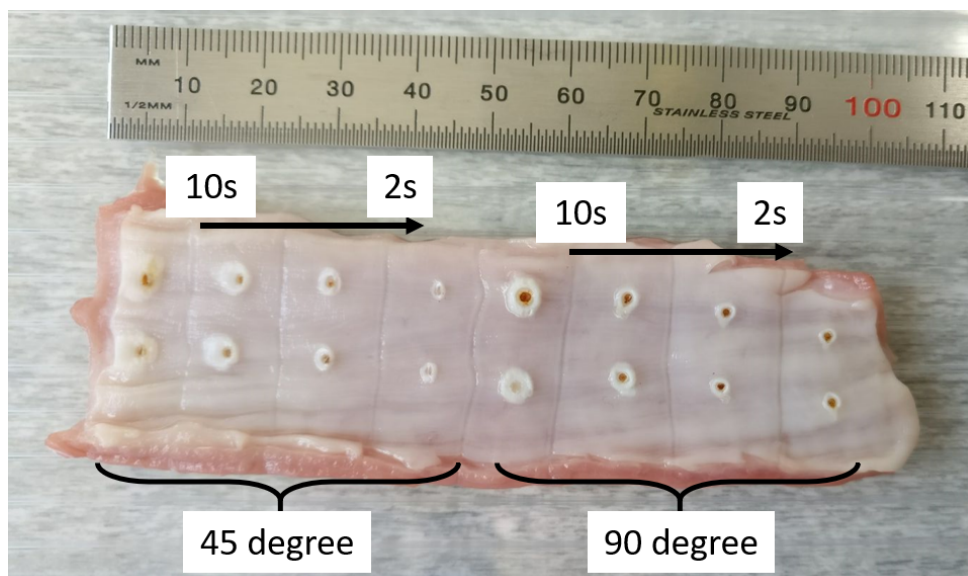


Figure 7.21: Ex vivo oesophageal testing

It can be seen that all of the application sites show a similar pattern. There is a small area in the center of each coagulation zone which, especially for the 90 ° test has caused some carbonisation where the tissue has reached a much higher temperature. This is then surrounded by an area of white coagulum where the temperature is slightly lower but still high enough to alter the structure of the tissue and denaturing of proteins.

For the 10s delivery at 90 degrees there is a discrepancy between the the first and second application. It was believed that the radiative tip was applied with less pressure on the second application compared to the first. This meant that the tip was

not fully in contact with the tissue.

Overall it can be seen that the carbonised area is more prominent in the 90 degree applications and once again this is thought to be as a result of the pressure being applied. Due to the perpendicular positioning of the tip it was likely that a more consistent higher pressure was applied. For the 45 ° angle applications this pressure was more sporadic and tended to be minimal. This was something that needed to be considered and questioned during the preclinical investigation as to ascertain the actual clinical usage and how the amount of pressure affects energy delivery into the tissue.

### Comparison with Boston Scientific Gold Probe

Bench testing culminated in a preliminary comparison between the microwave haemostat and the Boston Scientific Gold Probe bipolar RF device. The results of which can be seen in figure 7.22

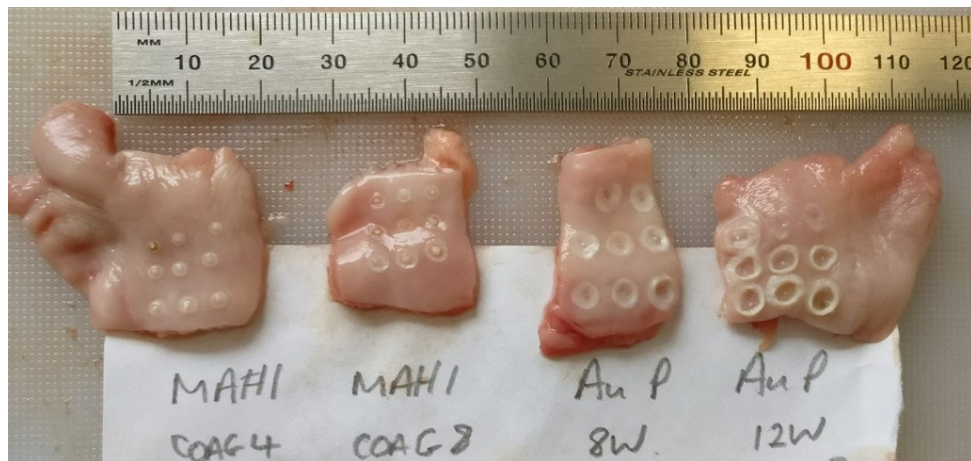


Figure 7.22: Initial results from comparison testing with Boston Scientific Gold Probe

COAG4 and COAG8 microwave settings on the CROMA generator which, according to the same calculations shown in table 7.3, gives an output power of 4.69W and 9.39W respectively.

Initially it can be seen from the haemostat applications, the left two tissue samples, there is much less tissue effect compared to previous bench testing. This is due to

a lower application power and it is believed that either the tissue properties were slightly different to the prior tissue tests. The tissue used for this comparison test had been cooled over night and re heated which may have altered their structure slightly. It could also be that the tip itself had become less effective from repeated use. The results from the gold probe however show that a large amount of energy is being applied and this is especially the case where the tissue has gathered up and surrounding the probe due to pressure being applied.

From a preliminary visual inspection it appears that the gold probe is delivering much more energy over a wider area, but this might not actually be beneficial. Due to the specific geometry of the upper gastrointestinal tract the energy delivery needs to be controlled and non-aggressive to ensure that no damage is done to the thin walls of the oesophagus. Further investigation would be needed to assess the tissue samples microscopically for any further damage or microscopic changes to the anatomy especially any damage indicative of oesophageal perforation.

### **7.3. Pre-Clinical Tests inc. Histology**

The devices were tested under clinical conditions at Northwick Park Institute for Medical Research (NPIMR). A copy of the preclinical protocol used for this procedure can be found in the appendix.

#### **The equipment...**

For the preclinical test a Creo Medical CROMA generator suite was used to provide the microwave input for 2 devices. The first device, MAH1, consisted of the flush radiative tip and the second device, MAH4S consisted of the sloped tip. The endoscope, endoscopic tools and other surgical/clinical materials were provided by NPIMR as required. The monitoring setup and the endoscopic stack can be seen in figures 7.23 and 7.24 respectively.





Figure 7.23: Pre-Clinical setup at NPIMR



Figure 7.24: Endoscopic stack setup at NPIMR

### **The patient...**

The study was conducted on a porcine subject, identified as Animal CH7 weighing approximately 65kg and was suitably medicated and anaesthetised by staff at NPIMR. CH7 was pre medicated with Ketamine and Xylazine before being intubated with a 7mm cuffed endotracheal tube, anaesthesia was maintained with oxygen over isoflurane and nitrous oxide, with respiration controlled via ventilator. Oxygen saturation, pulse, rectal temperature, expired Carbon Dioxide (CO<sub>2</sub>) and respiratory rate were measured and recorded throughout the procedure and copies of this can be found in the appendix. Hartmann's fluid, or sodium lactate solution, was also administered via slow drip throughout.

### **The procedure...**

The study took place over 8 days. The initial procedure was undertaken at day 1 and then subsequent monitoring over the next 7 days for the survival study was undertaken.

Day 1 procedure included the creation of 6 lesions within the oesophagus using a grasp biopsy tool. The aim was to create bleeds via the removal of the top endothelial surface layer to emulate a gastrointestinal bleed.

The use of grasp biopsy forceps to create the lesions can be seen in figure 7.25. Removal of the outermost epithelial layers was necessary to expose blood vessels found in the layers underneath the epithelium, care was taken throughout this procedure to ensure that only a minimal amount of mucosa was removed and no perforation through the oesophageal lumen was created.

Once a lesion was created the surgeon used the haemostat device to apply energy directly to the required site to stop the bleeding. As expected, and as seen in the ex-vivo testing, the clinician needed to apply slight pressure to the bleeding site in order to control the bleed and ensure that the energy was applied to the site as expected.

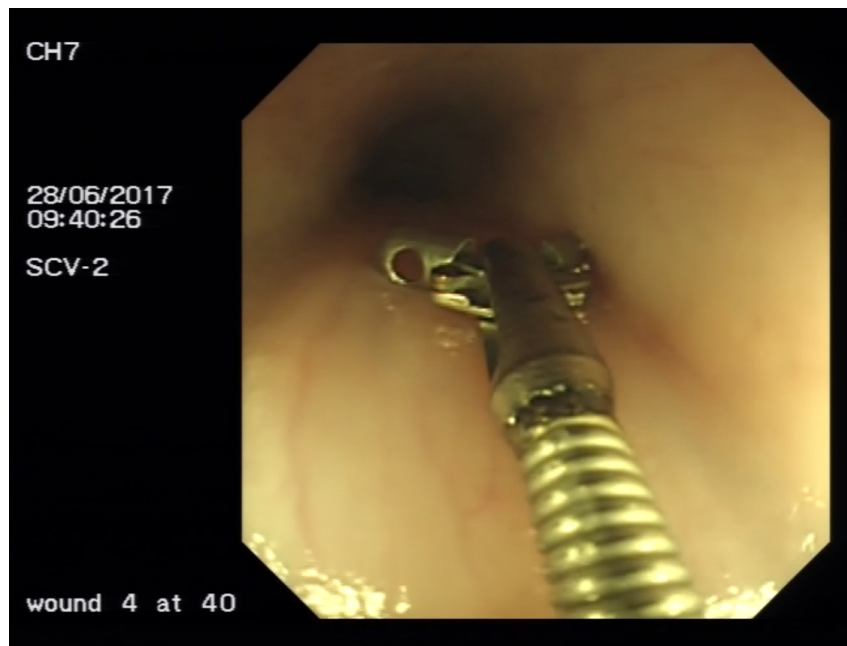


Figure 7.25: Endoscopic graspers used to remove upper layers of oesophagus

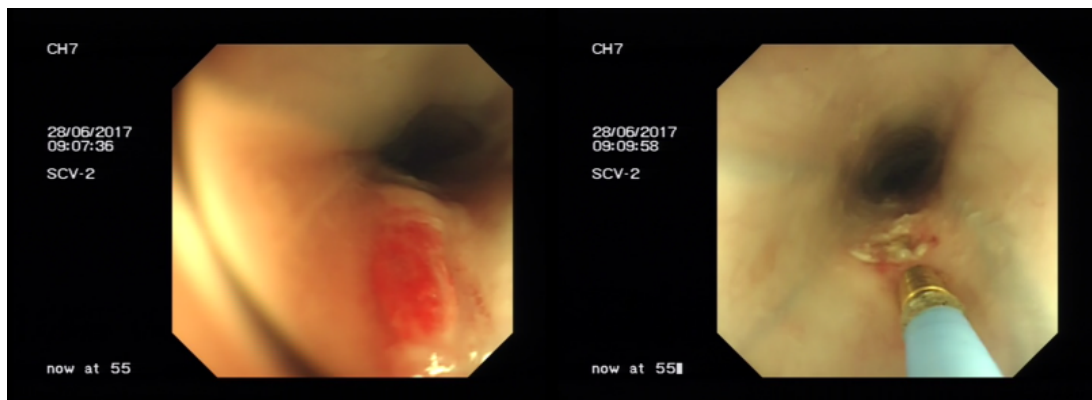


Figure 7.26: Initial bleed and subsequent coagulation of lesion 1

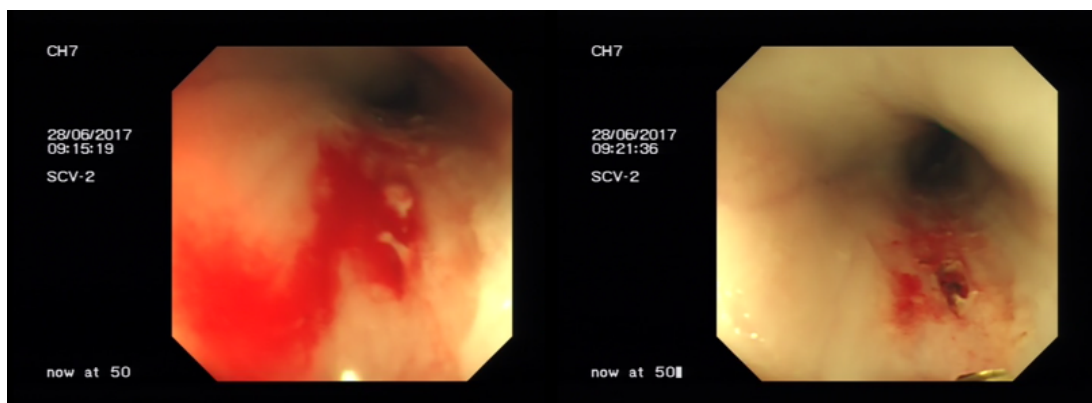


Figure 7.27: Initial bleed and subsequent coagulation of lesion 2



Lesion 2 was the only lesion which deviated slightly from the expected result from the use of the haemostat. A small perforation was accidentally created in the uppermost mucosal layer which, whilst only minor, may have caused further complications during the 7 day survival study. It was decided that an endoscopic clip be used to seal the hole. The surgeon commented however that this issue might have been caused during the creation of the bleed itself by the biopsy graspers removing too much of the mucosal layer, incorrect use of the device or possibly too much power delivered into a single area for too long. Despite this the surgeon was still able to achieve haemostasis of the lesion and the clip was just used to seal the hole. Subsequent lesions showed no obvious issues and it can be seen from histological analysis that this perforation of the mucosal layer was not severe enough to cause further complications.

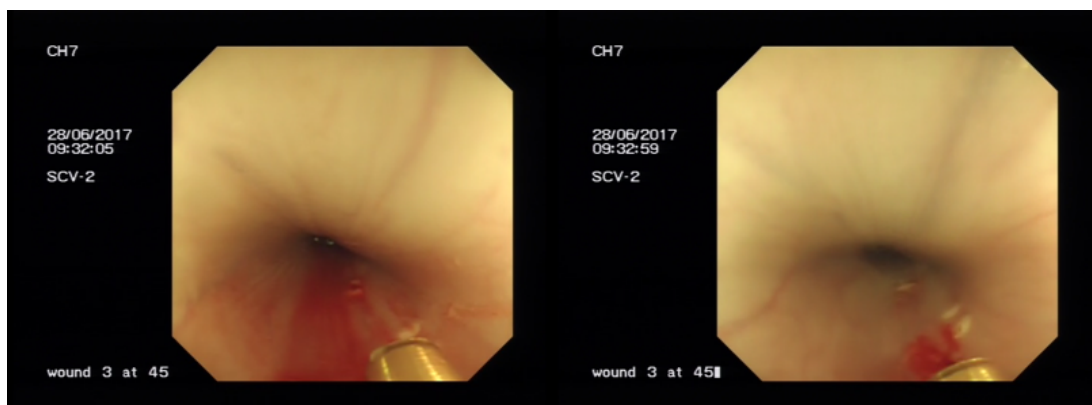


Figure 7.28: Initial bleed and subsequent coagulation of lesion 3

One thing to note during all lesions was the accuracy of energy delivery and how precisely the surgeon could effectively coagulate the treatment area. One of the concerns when designing the sloped radiative tip was the extra radiation from the half of the tip which was exposed to the air. Recall figure 6.23, the simulated results showed that the energy will dissipate quickly and will not affect the surrounding oesophageal lumen. This result was given confidence during the pre-clinical testing as the surgeon was able to coagulate the vessels at the point of bleeding and no further damage or visible tissue change to the surrounding lumen was observed.



Figure 7.29: Initial bleed and subsequent coagulation of lesion 4

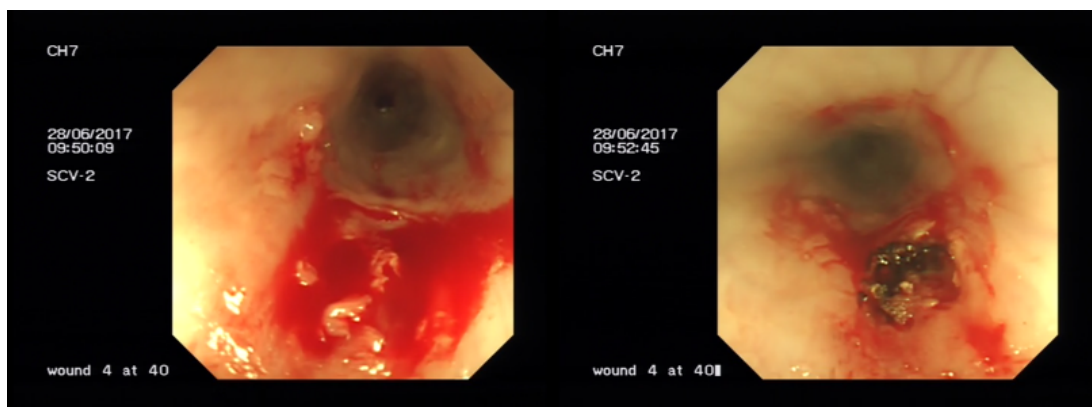


Figure 7.30: Initial bleed and subsequent coagulation of lesion 5

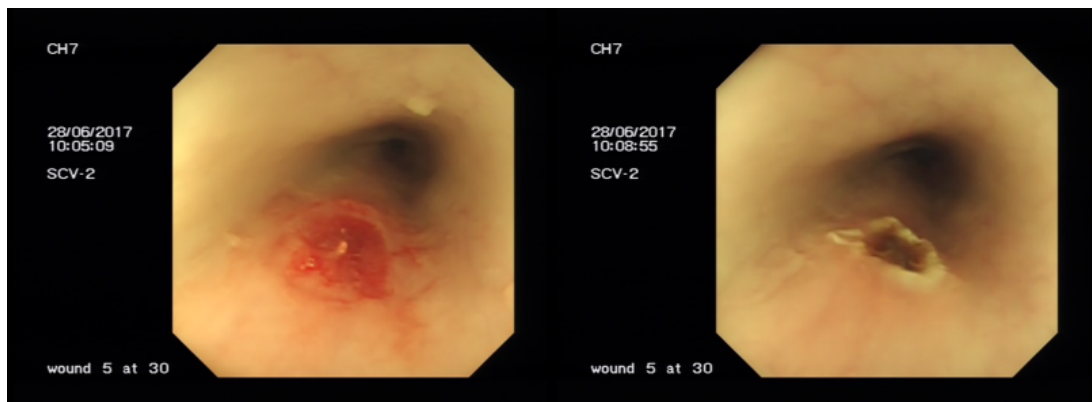


Figure 7.31: Initial bleed and subsequent coagulation of lesion 6

Video and photographs were taken throughout using the endoscope camera. Once all lesions were complete the pig was returned to the holding area and assessed over the following 7 days. After day 7 the pig was euthanised and dissected to assess the treatment sites and subsequent healing thereof. The sites were then cut, fixed and

sent off for histological processing.

## Histological Processing

Prior to sectioning the samples were fixed in 10% Neutral buffered formal saline for a minimum of 48 hours. This was to allow the structures to remain intact and prevent decay of the biological tissue. Dehydration and embedding stages prepare the samples for sectioning via microtome. The samples are then prepared for staining with the appropriate stain. The two used for this histological process are Haematoxylin & Eosin and Picro Sirius Red with Miller's Elastin. Both of these stains perform differing functions and give a much better microscopic picture of the various components within the tissue samples. Figure 7.32 shows the process used at NPIMR.

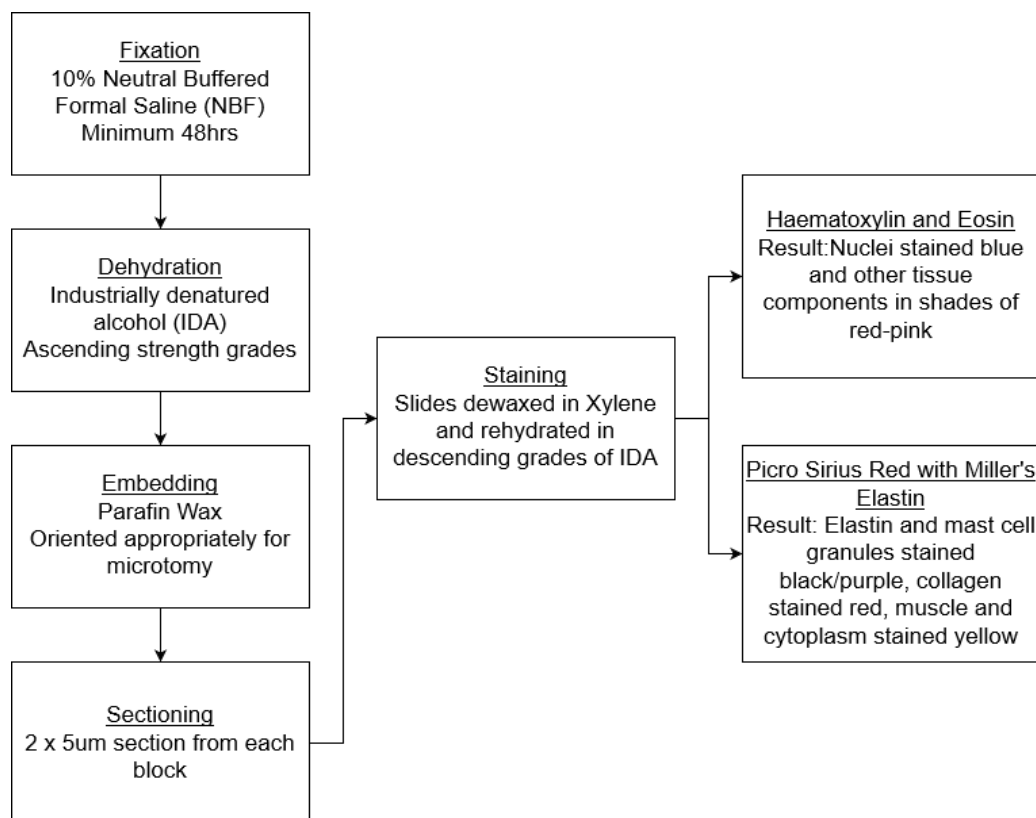


Figure 7.32: Flow chart showing the various steps involved in the histology process

There are various other steps to take within the staining process for each of the stains used and these are summarised in fig 7.33. This process was carried out

at NPIMR and is included here for information. Further reference to the staining results will be discussed alongside presentation of the histological slides.

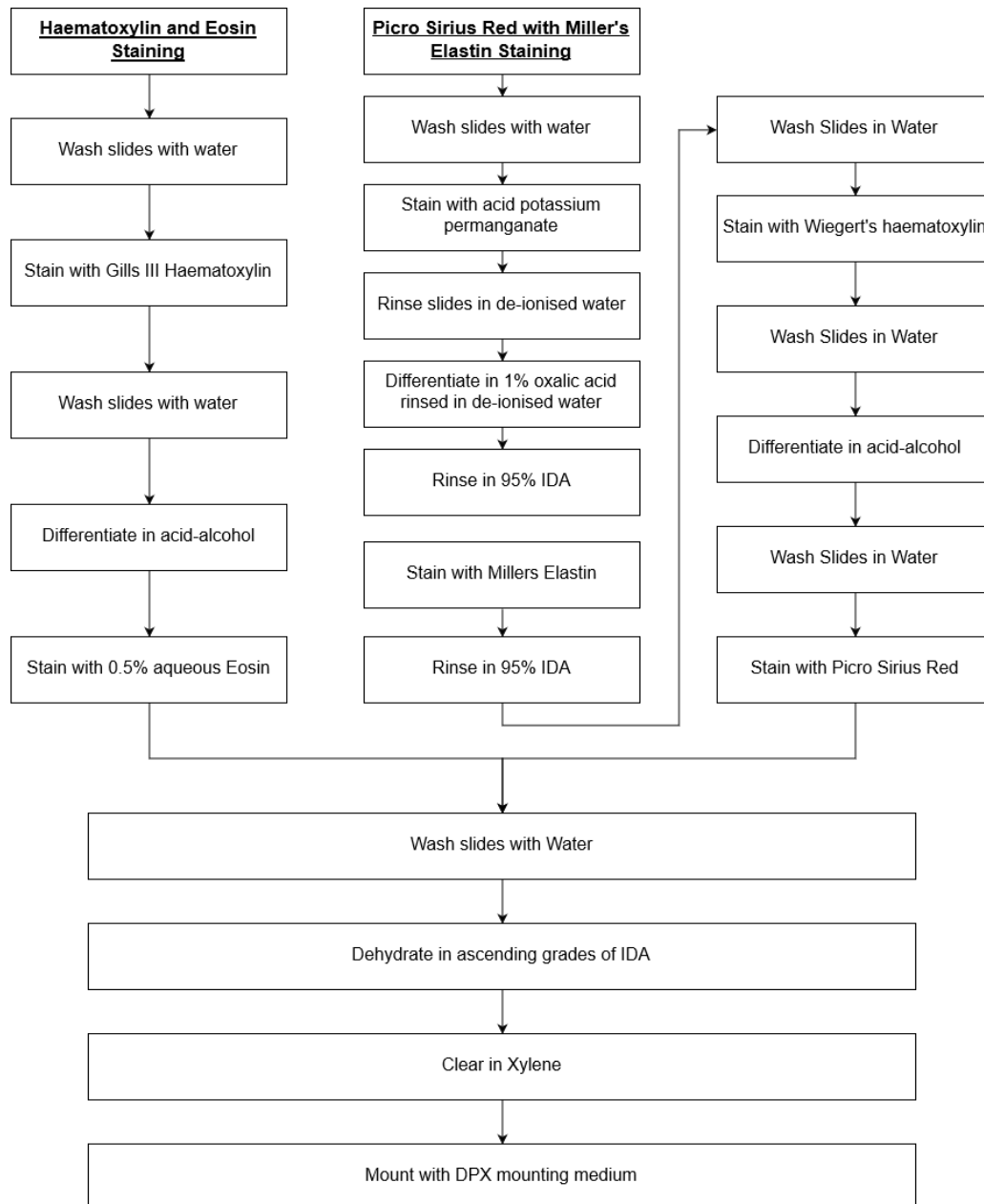


Figure 7.33: Flow chart showing the various steps involved in the staining process

## Histology Results

To appreciate the microscopic effects of the energy delivery on both the lesion site and underlying tissues it is important to be aware of normal oesophageal biology

and to consider a normal section of tissue as a control sample. For the purposes of this section Haematoxylin & Eosin stain will be referred to as H & E and Picro Sirius Red and Miller's Elastin will be referred to as PicMill. Haematoxylin stains the nuclei blue whilst Eosin stains the cytoplasm and surrounding cellular matrix pink. This allows for in depth analysis of the cellular morphology of the tissue and its reaction to the wound creation, coagulation and subsequent healing.

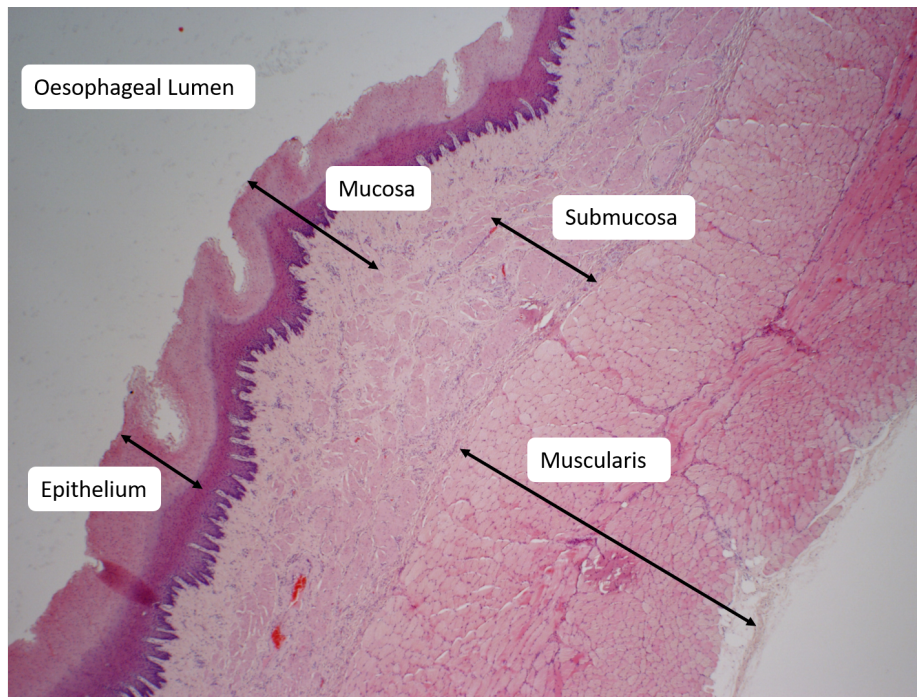


Figure 7.34: Normal oesophageal structure under H & E staining

Figure 7.34 shows a sample of oesophagus at 20x magnification and prepared with H& E stain. To the left of the slide you can see empty space which is the lumen of the oesophagus through which food passes. The next layer, which has a number of folds to allow for the expansion and constriction of the oesophagus during swallowing is made up of epithelium. This epithelium along with the lamina propria and the muscularis mucosae form the mucosa. The submucosa sits under this and below this is the muscularis. The haemostatic device needs to apply enough energy to stop any bleeding but not so much as to damage deep into these layers which would cause delayed healing and possibly further complications due to perforation of the



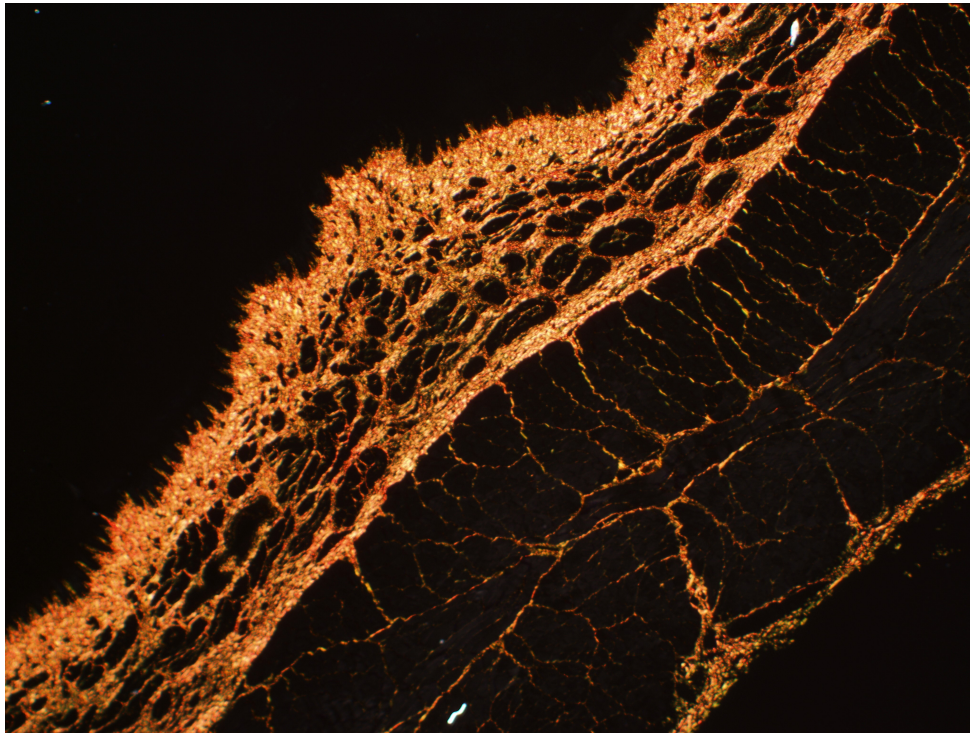


Figure 7.35: Normal oesophageal structure under PicMill staining

oesophagus itself. Figure 7.35 shows the same sample but prepared with PicMill stain and viewed under polarised light. Viewing the PicMill slides under polarised light causes birefringence of the collagen within the structure allowing for the analysis of the cellular structure and also allows commentary on whether the energy delivery has altered this structure. Once again the three distinct layers; mucosa, submucosa and muscularis can be seen each with lower densities and different structures of collagen. The clear line between submucosa and muscularis is called the fascia and damage or perforation of this is one of the biggest concerns for this application.

Figure 7.36 shows the initial lesion both under H & E and PicMill stains. The PicMill picture is once again shown under polarised light which shows a clearer view of the collagen structure throughout all layers. There is a clear difference in the tissues where the energy has been applied. Under H & E staining it can clearly be seen that the epithelial layer has been removed by the graspers and the energy has made a large entrant into the mucosal layer. In fact it appears the energy has

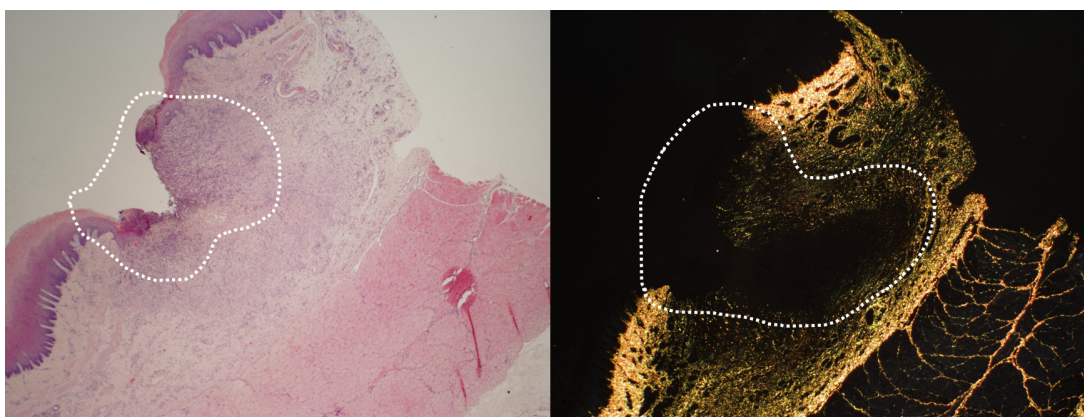


Figure 7.36: Lesion 1 under H & E and Picmill staining

passed through approximately one third of the submucosal layer as well, evident due to the increased inflammatory response. This inflammatory response is visible as an increase in colour and density of cells. It can also be seen that the submucosa has started to repair itself and there is clear regeneration of the endothelium at the wound edges. When viewed under the PicMill stain however, the collagen appears to be affected slightly deeper almost two thirds into the submucosal layer. The positive aspect of this is that there appears to be no energy penetration into the muscularis.

Interestingly very similar results can be seen throughout all of the lesions. The tissue components appear to be affected approximately one third through the submucosa but when viewing the collagen matrix, there is clear effect approximately double that depth. Figures 7.37 to 7.41 all show this effect.

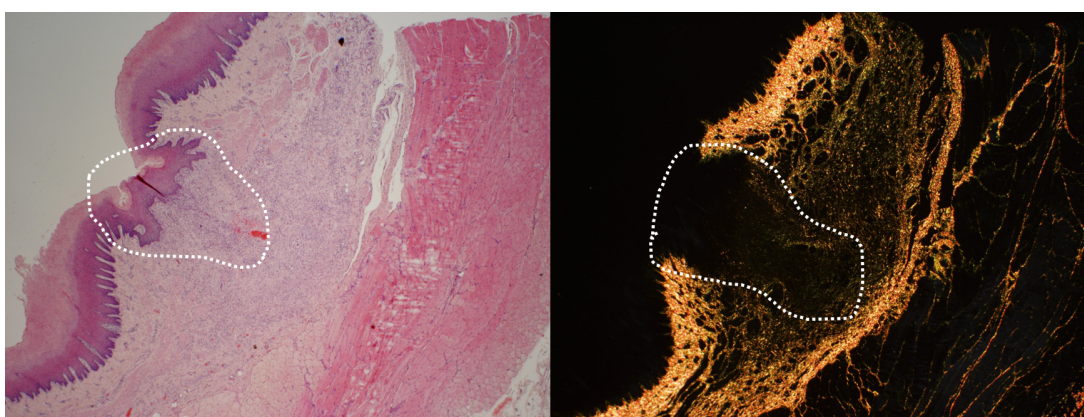


Figure 7.37: Lesion 2 under H & E and Picmill staining



Lesion 2 is quite interesting in that there seems to be minimal ablation of the epithelial layer within the mucosa yet figure 7.27 clearly shows bleeding and subsequent coagulation. This could be due, in part, to the use of the endoclip device to seal the small mucosal perforation during the procedure. The pink oval shape at the distal end of the energy delivery boundary under H & E staining is a blood vessel and there are new vessels forming giving further support that the energy delivery is not causing long lasting negative effects on the treatment sites.

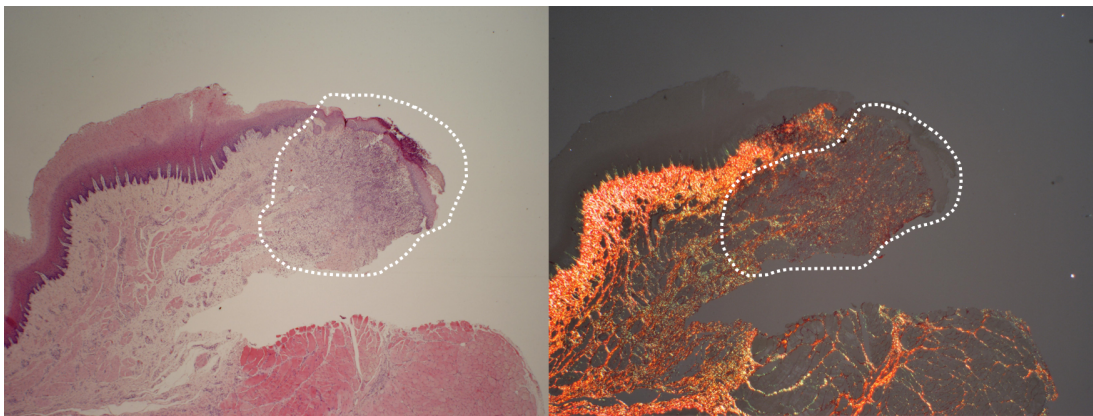


Figure 7.38: Lesion 3 under H & E and Picmill staining

Lesion 3, unfortunately, was prepared in such a way as to only show the very edge of the lesion and coagulation. Even so the same effect can be seen.

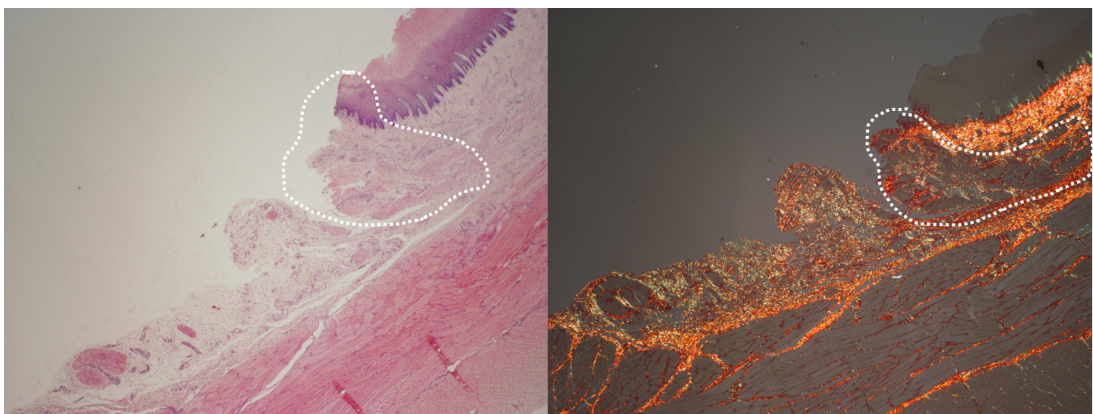


Figure 7.39: Lesion 4 under H & E and Picmill staining

Figure 7.40 has been created from two images due to the large treatment effect. Lesion 6, figure 7.41 shows a slightly different picture. The H & E staining shows



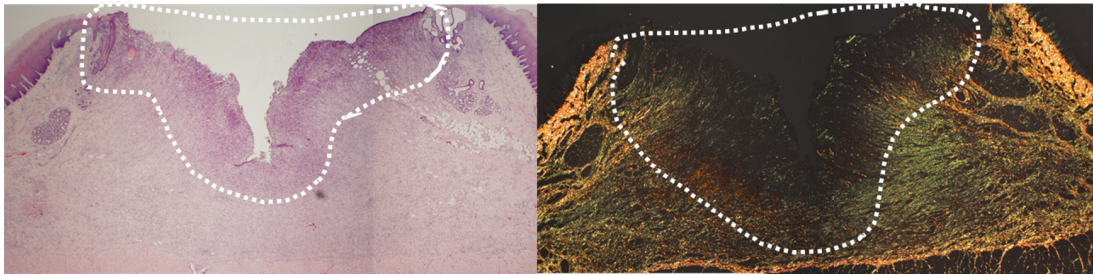


Figure 7.40: Lesion 5 under H & E and Picmill staining

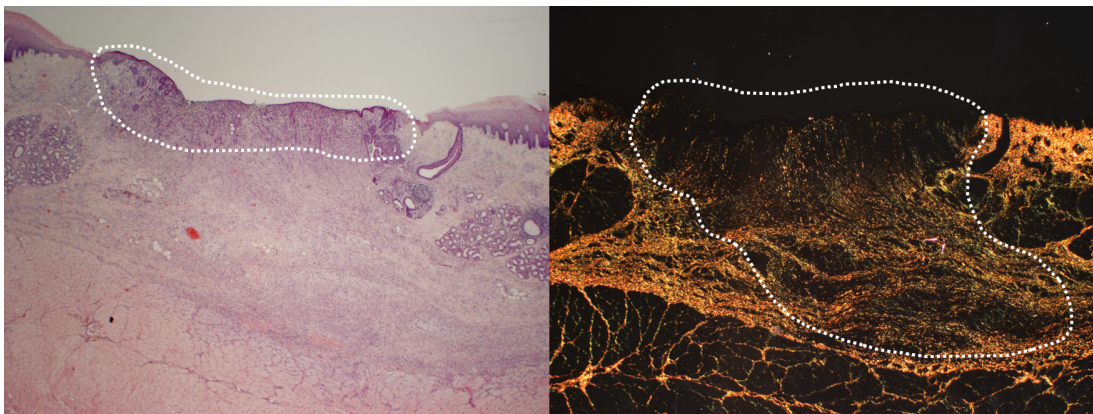


Figure 7.41: Lesion 6 under H & E and Picmill staining

what appears minimal depth with a clear inflammatory response within the mucosal layer and some response in the submucosa. However when looking at the PicMill slide, there seems to be a much deeper effect within the collagen even down to some geographic damage and thinning of the fascia which is the small 'wall' of collagen which separates the submucosa from the muscularis layer. Whilst this is a larger effect than the previous sites there is still no perforation or stopping of the collagen which means that new collagen will eventually form and the wound site should heal as expected.

## ***Chapter. 8***

---

### ***Discussion and Conclusion***

---

#### **8.1. Discussion**

This research was born out of the requirement to create a new medical device capable of utilising high frequency microwave energy in the Super High Frequency (SHF) band alongside the delivery of haemostatic chemicals or even other medical tools to treat bleeding in the upper gastrointestinal tract via a multi-modality approach. The device comprises a novel transmission line structure containing a hollow channel to allow for the delivery of fluids, tools or other structures into a treatment site whilst being capable of precisely and controllably delivering microwave energy at 5.8GHz.

The use of 5.8GHz microwave energy was previously discussed and has been shown to offer a good compromise between availability and penetration depth into tissue. The use of 5.8GHz also allows for the creation of a focussed radiator without the need to for excessive loading of the structure using materials with high dielectric or magnetic properties. The use of this frequency has been shown to clinically effective through human trials conducted by Creo Medical Ltd.

The clear drive towards an increase in the use of non invasive procedures dictates the requirements for an endoscopic device capable of being introduced through a natural orifice and able to achieve haemostasis with the following constraints:

1. Maximum Outer Diameter of 2.5mm
2. Maximum allowable Attenuation of 3dB/m
3. Hollow Channel with Inner Diameter of at least 1mm

These three constraints required the use of materials with minimal attenuation where the dielectric constant and loss tangent are as low as possible whilst requiring both conductors to be in close proximity. This altered the cable impedance from the more common  $50\Omega$  to approximately  $14\Omega$  by minimising the amount of dielectric material and altering the capacitance and inductance of the structure. This variation in impedance required the development of impedance transformers to allow the cable to be used with the majority of microwave test equipment and attachment to the Creo Medical generator that will be used in the final device.

Initial research into suitable impedance transformer structures was based on the delivery of both RF and microwave energy, either being applied sequentially or simultaneously to prove usability of the device within a wider range of electrosurgical applications which require both energy delivery modalities. Two structures were proposed and designed to allow for delivery of energy at both 400KHz and 5.8GHz. Simulated results of both structures were used to qualify the design. One of the main constraints with the use RF energy was the maintenance of access to the hollow channel in a structure that provided both the impedance transformation required for delivery of the microwave energy whilst also allowing for the propagation of RF energy.

The first structure utilised capacitive coupling to act as an open circuit at RF frequencies and as a short circuit around the spot frequency of 5.8GHz. The second structure uses quarter wavelength chokes. The benefit of this structure was that, even if a conductive material is introduced into the hollow channel, the whole structure distal to the cable acts as an open circuit. Simulated results for both structures show expected operation and energy delivery at both RF and microwave frequencies whilst showing good isolation at the hollow channel input port.

Due to the specific clinical application of this research; namely the coagulation of bleeding vessels, the use of RF energy was discluded from the final device and as such two further impedance transformer designs were developed. An initial co-axial

structure showed positive results both in simulation and physical testing with acceptable transmission and minimal loss; but this was difficult to iteratively manufacture for optimal performance. A second microstrip based structure was designed and developed which also showed optimal matching at 5.8GHz both in simulation and testing but due to manufacturing limits and limited time utilised FR4 material for the dielectric substrate which has slightly higher loss than high frequency microwave substrates. This slightly minimises the power delivered into tissue but calculations and simulated results showed this to be adequate for this application. For other electrosurgical applications which require more energy such as tumour ablation or where even higher microwave frequencies are considered, this would need to be changed in order to gain optimal performance for the device and therefore optimal power transmission from the generator.

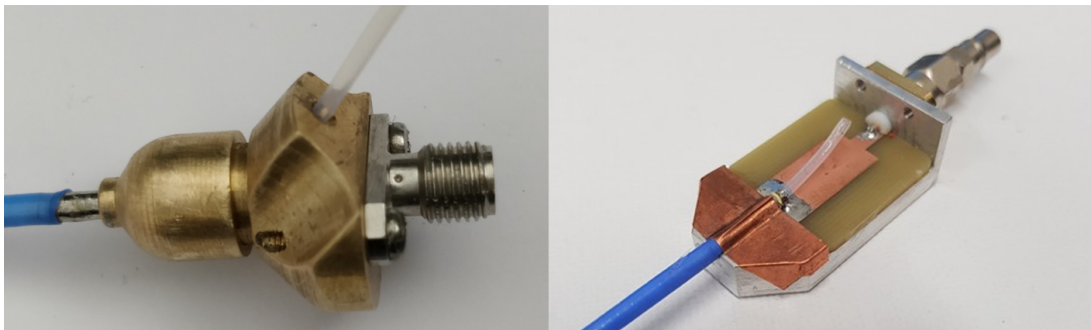


Figure 8.1: Final manufactured transformers

The two microwave impedance transformer structures, shown in figure 8.1, were then used to test the three prototype cables developed in this research, and discussed in chapter 5, using time domain measurements. These results showed some issues with the first two prototypes which had higher loss than predicted through theoretical calculations and more than the required 3dB/m; this could have been for a number of reasons as previously discussed but is most likely due to variation in geometry of the dielectric layer.

The second prototype used a braided inner conductor which also may have had an impact on the cable loss due to higher resistance from the braid. The third

prototype, with the same design as the first, but with an alternative manufacturer showed much better results and measured less than the desired upper limit of 3dB/m attenuation. It is believed that the company who manufactured the final prototype used newer machinery and had more stringent controls and monitoring in place during the manufacturing process which allowed for the cable to be wrapped tighter and therefore be more uniform throughout its length. It is important to note that even though a similar design was used, the materials were most likely acquired from different sources and may have slightly different characteristics which could also be a reason as to why the third prototype performed much better than the previous prototype assemblies.

The second portion of the research concerned the integration and combination of the previous parts coupled with a unique radiative tip design capable of delivering fluid and delivering microwave energy, at 5.8GHz, to stop bleeding in the upper gastrointestinal tract. The benefits of using microwave energy at 5.8GHz have been discussed in terms of penetration depth, healing and accuracy of delivery. It was also required for the radiative tip to be an end fired antenna which would create a hemispherical zone of coagulation for maximum accuracy and control.

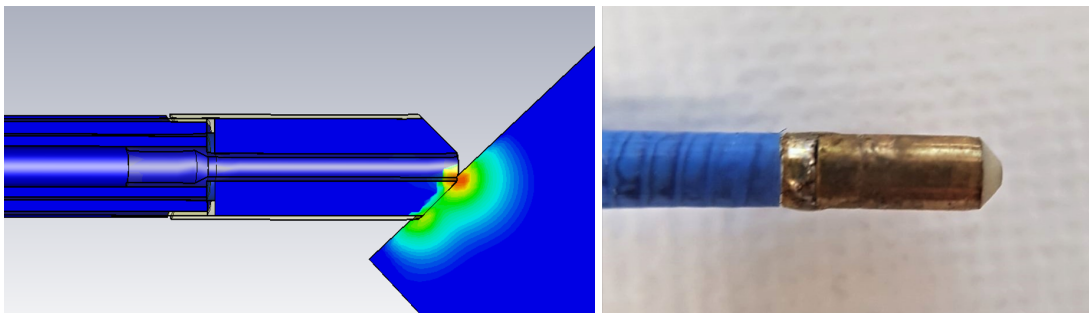


Figure 8.2: Final Simulated and Manufactured Radiative Tip

The radiative tip was designed as an integrated quarter wave impedance transformer to match the  $14\Omega$  impedance of the cable with the higher impedance, of approximately  $59\Omega$ , of the tissue at 5.8GHz. Simulated designs gave results which showed that although a lower dielectric constant material would need to be used,



the presence of fringing fields and additional capacitances meant that the physical length of the tip could be much shorter. A shorter tip is required to ensure that the device can fit easily into the working channel of the endoscope or gastroscope whilst navigating the angles experienced as the device is inserted into the GI tract.

The combination of impedance transformer, cable and radiative tip was then integrated into the final device. 3D printing was used to manufacture a handpiece capable of housing the impedance transformer and protecting the clinician from any radiation or burns whilst remaining ergonomic and comfortable to use. Multiple iterations were printed and tested to ensure that the handpiece would fit comfortably in the hand. Standard connectors were used for both the microwave input and access to the hollow channel to ensure compatibility with a multitude of equipment used in a standard endoscopy suite.



Figure 8.3: Overall Final Device

Initial bench testing and comparison studies showed the device operating as expected into a porcine liver bench model. Clear coagulation zones could be seen that vary with power level and time of delivery. Longer delivery time leads to a larger coagulation zone and depth of treatment due to more energy being delivered coupled with thermal spread during application. This variation was constant over multiple

treatments allowing for controllable energy delivery dependent upon the size of the bleed. These bench test results need to be considered as an ideal energy delivery scenario as the on bench tissue differs from live in-situ tissue due to a lack of perfusion acting to take heat away from the treatment site, lack of metabolic heating to stabilise its temperature and other various differences in tissue properties.

The culmination of this research was the programme of pre-clinical testing of the full haemostat devices at NPIMR. A porcine study was conducted in which a number of lesions were artificially created through removal of the outermost epithelial layer and the bleeding was subsequently stemmed using the device followed by the development of a 'plug' to permanently stop the bleeding and promote healing processes. Haemostasis was achieved in all treatment sites and the lead clinician commented on the efficacy, accuracy and ease of use of the device.

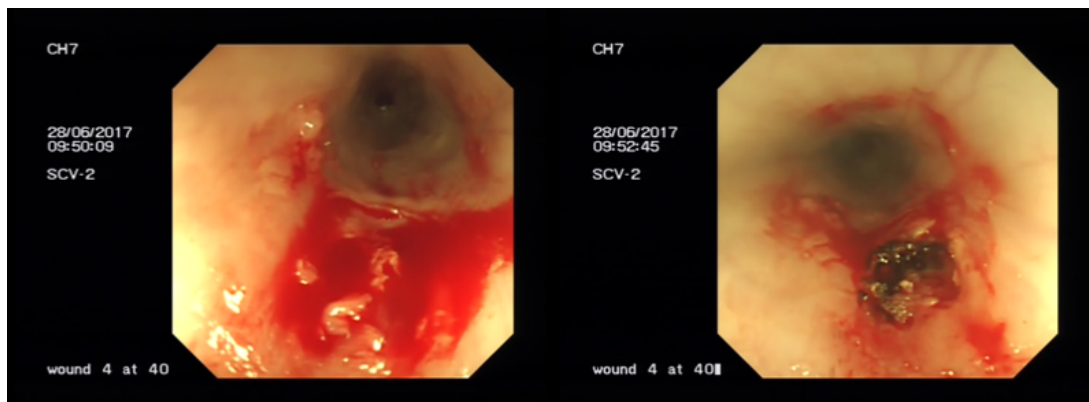


Figure 8.4: Creation and Treatment of Oesophageal Bleed Lesion 5

Post-test histological analysis was carried out on all wound sites and showed suitable healing of the treatment site after seven days and showed no adverse effects any deeper than two thirds into the submucosal layer and no significant geographical changes to the deeper muscle layers of the GI tract which would be indicative of a perforation of the oesophageal lumen or lasting damage as a result of too much energy being delivered to the treatment site. A clear difference can be seen between the cellular structure of the wound sites, as seen in figure 8.5 (left) where closing of the endothelium and regeneration of new tissue can be seen. The increased immune

response and activity is indicative of the depth of the microwave effect. There is a much deeper effect, shown in figure 8.5 (right), to the collagen matrix where it can be seen that although penetrating slightly deeper, new collagen is beginning to regenerate showing a positive outcome in healing of the treatment site.

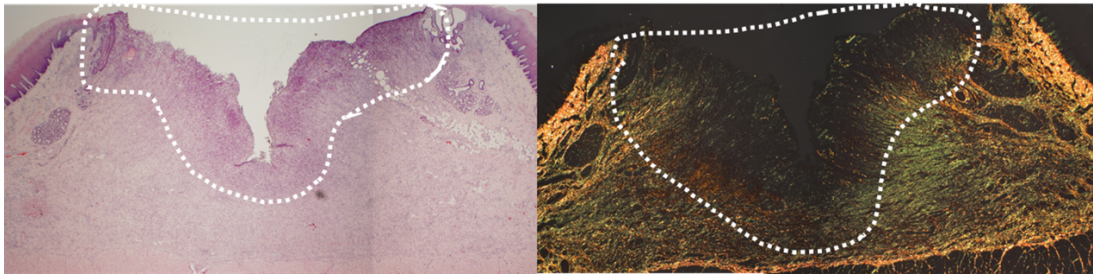


Figure 8.5: Histological Slide of Lesion 5

## 8.2. Conclusion

Overall the device performed very well when evaluated for clinical efficacy and a complete medical device capable of acting as a viable alternative to current haemostatic technologies has been developed in this work. Literature, whilst being varied in opinion, all agree that a multi-modality approach is the best. The successful addition of the hollow channel within the novel transmission line structure allows for this approach with the combination of adrenaline and microwave energy.

The multiple transformer structures developed and designed through this work not only showed that the novel cable is capable of the delivery of microwave energy but also that RF energy delivery can be considered for use in multiple other electrosurgical applications which require dual modality energy delivery for example in cutting, resecting and coagulation. This is especially useful when considering this cable as a replacement for current energy delivery cables used in current electrosurgical devices especially those in use by Creo Medical. The successful delivery of RF energy would enable the use of the new cable in a device such as the RS2 'speedboat' [97]; a device used for endoscopic submucosal dissection procedures, and would allow for a more



concentric structure to be utilised to aid device rotation.

The effective design, simulation, manufacture and testing of the radiative tip structure showed excellent efficiency when delivering energy into tissue and allowed for the final device to not only show promise in bench ex-vivo testing but also allowed clinical performance to be evaluated, where haemostasis was efficiently and effectively performed on a representative porcine model during in-vivo pre-clinical testing.

Pre-clinical investigation which took place at NPIMR allowed the final device, a combination of the individual components described in this research, to act as an effective medical device within a clinical setting under good laboratory practice protocols. The clinician conducting this treatment commented on its efficacy and ease of use, whilst having no problem achieving haemostasis for all lesions created. The seven day follow up including histology not only showed good healing of all treatment sites but also showed that no perforations or permanent geographical changes were present. This result indicates that the microwave energy delivered is not too aggressive and was able to be well controlled by the clinician.

The culmination of this work is the design and development of a novel transmission line structure featuring a hollow channel capable of being used for both RF and microwave delivery in a number of electrosurgical applications; most notably, for this research project, as a dual modality haemostasis device for use in the upper GI tract. The final cable prototype successfully fulfilled all of the required constraints having an average attenuation of 2.89dB/m, an outer diameter of 2.5mm whilst containing a hollow channel with diameter of 1mm capable of the delivery of fluids or introduction of other tools.

### **8.3. Further Work**

There are a number of additional work packages, outside of the scope of this project, which would compliment this project and benefit the device mainly in terms

of improving the individual components. Some of these are small improvements and some are much more involved and would require more work and may form their own research projects in the future.

### **8.3.1 Microstrip Transformer Improvements**

Initially the microstrip based transformers could be improved, in terms of loss, through the use of a specific microwave dielectric material such as Rogers or Taconic materials. This would minimise the loss and allow more energy to be delivered into the treatment site. Equally further improvement and optimisation of the co-axial based transformer structure might allow for a structure which is easier to manufacture whilst maintaining a good impedance match. The trace itself could also be optimised, as previously discussed and could be made smaller; by using a single quarter wavelength instead of three for example. One advantage of using the co-axial structure is that no stray fields exist outside of the transformer structure as both the E and H field propagate within the two enclosed conductors.

### **8.3.2 Radiative Tip Improvements**

With regards to the radiative tip, one drawback is the need to minimise the inner hollow diameter to allow for suitable mechanical and electrical connection to the cable. When considering fluid delivery this is not an issue but for some applications which require the introduction of other tools, losing 0.1mm of hollow channel could limit the use of other tools such as forceps or needles. Further investigation into other radiative structures and alternative ways of connecting the tips would allow for the same diameter hollow to be maintained throughout the device.

Whilst not appearing to be particularly problematic in the bench testing or preclinical work carried out, some literature reports tissue sticking following coagulation. Should the device form a coagulum around the tip instead of around the bleeding

vessel then the bleed will continue or is likely to appear coagulated but re-bleed post operatively. An introduction of a thin 'anti-stick' or hydrophobic coating could be simulated and tested to ascertain whether this is an issue or whether it would have any effect on the radiative efficiency of the tip. For a thin layer; i.e. much smaller than the wavelength being used, there should be minimal effect on the microwave propagation.

### **8.3.3 Novel Cable Improvements**

Another further aspect to consider is the materials used for the construction of the cable itself. Research into this area could allow for a smaller wall thickness to be used on both the structural inner tube and the outer protective tube. This would allow for a much larger hollow diameter, a smaller outer diameter or even a cable with the same inner and outer diameters but more dielectric material which should decrease the attenuation and allow for more energy to be available at the distal end of the cable; this would be important if the cable was to be used in devices designed to achieve ablation where more power is required to be able to achieve larger ablation zones.

Further characterisation of the cable would also be beneficial such as the determination of the actual impedance of the cable rather than inferring through other measurements. This would allow the transformer structures and radiative tip to be designed more optimally. Further characterisation such as maximum bend radius, maximum power handling and temperature profile measurements would also benefit further use of this cable.

### **8.3.4 Thorough Device Comparison and Validation**

Although a preliminary testing comparison has been carried out between the device presented in this research and the Boston Scientific Gold Probe, it would be advan-

tageous to run a full comparison study between this device and a number of energy based haemostatic devices currently in use by clinicians. This full comparison study would need to have a large enough sample volume to be statistically significant and would also need to consider both the macroscopic and microscopic effects of the energy delivery profiles using histological analysis. One consideration is that the RF probes, especially as seen in the preliminary comparison in section 7.2.2, may be more aggressive in their energy delivery and therefore have higher risk of perforation or unwanted damage to the tissue structures; particularly due to penetration deep into the muscularis layers. The reformation of the collagen matrix and healing times due to microwave energy should also be compared with that due to RF energy.

# Appendices

## Chapter. A

### Final Device - Bill of Materials

Provided here is a Bill of Materials for the final device. Sources are provided for those items which are off the shelf and information provided for those items which are custom made.

Microwave and Adrenaline Haemostat - MAH1									
Part	Quantity	Notes							
<b>Transformer</b>									
SMA Connector	1	RS - 5463181	<a href="http://uk.rs-online.com/web/p/sma-connectors/5463181/">http://uk.rs-online.com/web/p/sma-connectors/5463181/</a>	For attachment to transformer					
SMA to QMA adapter		RS - 6121541	<a href="http://uk.rs-online.com/web/p/rf-coaxial-adapters/6121541/">http://uk.rs-online.com/web/p/rf-coaxial-adapters/6121541/</a>	For attachment to interface cable on generator					
M2 screws	4	n/a							
Ground Tray	1	In house manufacture	Milled aluminum - Creo Medical Ltd						
Shielding enclosure	1	In house manufacture	3D Printed PLA Material						
Adhesive Dispenser Needle	1	Weller KDS2112p Needle 21 guage	<a href="http://uk.rs-online.com/web/p/adhesive-dispenser-needles/4003867/">http://uk.rs-online.com/web/p/adhesive-dispenser-needles/4003867/</a>						
Transformer PCB	1	FR4 substrate with copper trace	Custom from Cambridge Circuits						
<b>Cable and Tip</b>									
Supercable	1.5m	Huor Cables	Latest prototype						
Radiative Tip Inner	1	In house manufacture	Turned Brass - Creo Medical Ltd						
Radiative Tip Dielectric	1	In house manufacture	Turned PEEK - Creo Medical Ltd						
Radiative Tip Outer	1	In house manufacture	Turned Brass - Creo Medical Ltd						

Figure A.1: Bill of Materials for the final device

## ***Chapter. B***

---

### ***Pre-clinical Documents***

---

#### **B.1. Protocol**

The protocol used for the pre-clinical study is shown here. It has been signed off by the author, supervisor and the Director of NPIMR who conducted the pre-clinical investigation.






**NPIMR**  
Progress for Patients

# Supercable Microwave and Adrenaline Haemostat Preclinical study

AUTHOR: SHAUN C. PRESTON

The following have reviewed, agreed and approved this protocol:

Name	Position	Signed	Date
Shaun C. Preston	Creo Medical / Bangor University		28/6/17
Paul D. Sibbons	Northwick Park Institute for Medical Research		29-6-17
Christopher P. Hancock	Creo Medical / Bangor University		28 <sup>th</sup> June 2017



## Preclinical Study – Supercable Haemostat

This is a working document which will cover the protocol to be used during preclinical investigation into the efficacy of the supercable variant haemostat.

Date of Preclinical : 28<sup>th</sup> June 2017 (with 7 day survival follow up)

### Preclinical Study Summary

Item	Requirements for this protocol		
Pre-clinical study title:	Supercable Haemostat		
GLP requirements for the study:	Study is to be in accordance with all applicable requirements US Title 21 CFR Part 58 GLP requirements: No <input checked="" type="checkbox"/> Yes <input type="checkbox"/>		
	Laboratory facility is compliant with EU GLP requirements of Directive 2004/9/EC as these pertain to general site facilities and the care of animal subjects: N/A <input type="checkbox"/> No <input type="checkbox"/> Yes <input checked="" type="checkbox"/>		
	The laboratory facility's quality unit will be involved during the preclinical study, e.g. to audit records, to ensure there is no bias and to review the final report: No <input checked="" type="checkbox"/> Yes <input type="checkbox"/>		
	GLP requirements for the study itself are not applicable because this is a basic exploratory study carried out to determine whether a device has any potential utility or to determine physical and other characteristics of the device: No <input type="checkbox"/> Yes <input checked="" type="checkbox"/>		
Laboratory facility:	Northwick Park Institute for Medical Research (NPIMR)		
Chief investigator:	Prof Paul D. Sibbons (NPIMR)		
Study director:	Prof Paul D. Sibbons (NPIMR)		
Other officers at the laboratory facility pertinent to the study:	? – Facility Logistics		
Calendar of events:	Initial study at 28 <sup>th</sup> June 2017 with 7 day follow up		
Product project:	Supercable Haemostat		
Purpose of the clinical study:	To assess overall performance of supercable haemostat		
Use of comparative devices:	N/A		
Number of subjects:	1	N/A	N/A
Subject species:	Porcine	N/A	N/A
Sex:	?	N/A	N/A
Weight kg (lbs):	60 to 70 kgs	N/A	N/A
Subject preparation:	Basal diet and water ad libitum	N/A	N/A
Number of treatment sites per subject:	10-12	N/A	N/A
Type of study:	Termination <input type="checkbox"/> Survival <input checked="" type="checkbox"/>	Termination <input type="checkbox"/> Survival <input type="checkbox"/>	Termination <input type="checkbox"/> Survival <input type="checkbox"/>
Duration of survival study:	7 days	N/A	N/A
Requirements for macroscopic assessment:	Macroscopic visual assessment at 0 days via endoscopy	N/A	N/A
Requirements for microscopic and/or histological assessment:	Microscopic and Histological assessment at 7 days	N/A	N/A

## Equipment and devices to be used

- There are 4 test devices to be used during the study (2 test devices and 2 spares):
  - MAH1 and MAH2 (2.5mm OD supercable haemostat with flat tip)
  - MAH4S and MAH5S (2.5mm OD supercable haemostat with 45 degree tapered tip)
- EMR/CROMA generator to be used to provide microwave energy. This includes the appropriate accessories including: footswitch, interface cable and power cable.
- Endoscopic stack and suitable endoscope to be provided by laboratory facility.

## Aims and Rationale for this study

- Initially the primary aim of the study is to assess the effectiveness of all 4 devices, specifically in their ability to stop bleeding in the upper gastrointestinal (GI) tract using microwave energy and delivery of adrenaline. Indications of adequate operation are listed below but are not exhaustive:
  - Haemostasis clearly achieved
  - Degree of tissue effect (evidence of large coagulum or charring)
  - Integrity of the distal tip structure
  - Ability to flush site with adrenaline easily (pressure required etc)
- Assessment of effect of microwave delivery and healing in upper GI tissue both macroscopically and via histological analysis at 7 day follow up.
- Secondary aims include, but are not limited to;
  - Assessment of the device aesthetics and cable properties including: ease of use, cable flexibility, cable bend radius and general device 'look and feel'.
  - Initial steps into the creation of a suitable bleeding model for upper GI studies in the future.

## Study Design

- Photography and Video are to be taken throughout the study. Any clinically significant information is to be recorded along with a timestamp for easy reference back to footage and or stills.
- NPIMR to provide the necessary endoscopic equipment and also any consumables used for example: adrenaline, saline and/or any other clinical consumable required.
- Creo Medical / Bangor University to provide the devices, fully assembled and tested ready for use.

- Clinical Procedure:
  - The pig will be appropriately medicated, anaesthetised and prepared via standard operating procedure by NPIMR staff.
  - A suitable endoscope will be inserted into the upper GI of the subject and treatment sites located.
  - At this stage the endoscopist may wish to perform a number of initial tests with the device to ensure functionality including passage through the endoscope, injection capability and general use of the device.
  - Creation of appropriate lesions
    - Initially the lesion is to be created through the use of a small grasp biopsy to remove a small section of submucosa to achieve bleeding. Should this not provide a suitable lesion an alternative plan, possibly through the use of other tools, can be discussed and implemented on the day.
    - Due to the requirements for a follow up study, care must be taken to ensure that the functionality of the oesophagus remains. Too much damage to the structures could lead to appetite suppression in the animal and compromise the follow up study.
    - Due to the difficulty in marking the tissue for locating during follow up, the first lesion will be made at a suitable depth into the oesophagus and subsequent lesions will be made during retraction of the scope. i.e. first lesion made at 10cm, second at 9cm, third at 8cm etc. Specific details to be noted on the day due to anatomical and physiological differences. Locations to be noted in preclinical documents.
  - Once a suitable lesion has been created, the endoscopist will use a combination of adrenaline flush and microwave energy delivery to seal the lesion.
  - Energy settings:
    - The main goal is to ensure haemostasis has taken place. Due to the limited number of lesions possible each device will be used to seal at least 4 lesions. COAG9 or COAG10 settings are to be used as required. Should less energy be required then the endoscopist can either vary delivery time or with agreement from all parties use lower COAG settings. Details of these changes are to be recorded.
  - Clinical notes are to be taken throughout the study and any deviations in this protocol are to be noted alongside with clinical/engineering reasons for doing so. Due to the nature of this study, any deviations to this clinical procedure are at the discretion of both Shaun Preston and Prof Paul Sibbons both in matters of clinical and engineering requirements
- Microscopic and Histological assessment is to take place 7 days following the study as per standard protocol at NPIMR

## **B.2. Anaesthesia and notes documents**

The pre-clinical notes used during the investigation are shown here. These include observations and comments made by the theatre technician.

## ANAESTHESIA AND SURGICAL PROCEDURE RECORD FOR PIGS

PU 92a

DATE:	Location:	Study Number:	Procedure:	Animal ID:	Weight (Kg):							
28/6/17	TH2	1001E	Stomach/oesophagus Haemostat model	CH7	65							
Premedication:			*Non-recovery/ Terminal/ Recovery: length of study 7 days									
Amount/			Time administered/ (H:M)	Sign								
ACP tabs (10mg/10Kg) PO.....			6									
Diazepam tabs (10mg/10Kg) PO.....			6									
Ketamine (5mg/Kg) IM.....			3.25									
Xylazine (1mg/Kg) IM.....			3.25									
Time H:M	O <sub>2</sub> L/min	N <sub>2</sub> O L/min	ISO %	SaO <sub>2</sub> %	Pulse /min	Temp °C	Breath /min	IV Fluid ml	IV Fluid ml	Total IV fluid ml	ET CO <sub>2</sub> %	Comments
						oesophagus/rectal*						
08:30	3.0	1.0	2.0	94	121	36.0	12	20	-	20	5.7	3.2mm Scope.
08:45	4.0	1.0	2.0	94	98	35.5	12	40	-	40	5.2	Start .0850.
09:00	5.0	1.0	2.0	94	98	35.6	12	55	-	55	5.2	TAK in oesophagus noted
09:15	5.0	1.0	1.75	94	95	35.6	12	100	-	100	4.9	09:03 little initial lesion
09:30	5.0	1.0	1.75	94	93	35.8	12	150	-	150	4.8	09:04 - biopsy - full change
09:45	5.0	1.0	1.75	94	92	35.8	12	165	-	165	4.8	09:07 Biopsy pieces to create 2nd lesion: bleed
10:00	4.0	1.0	1.75	99	92	35.8	12	180	-	180	4.9	09:08: Supercable used to cauterise 1st lesion.
10:15	4.0	1.0	1.75	98	90	35.8	12	200	-	200	4.8	09:10: Clamped bleed.
10:24												* noted to 2nd lesion.
												09:14: 2nd running bleed.
												09:17 coagulated hole in mucosa owing to too much energy.
												09:18 device inserted - lesion bleed.
												09:23: Clip onto mucosa.
												09:25 3rd lesion - bleed created.
												09:30: device inserted.
												09:30: bleed.
												09:35: device inserted & bleed stopped.
												09:33: 2nd lesion created.
												09:39 - bleed stopped & lesion closed.

\*Delete as necessary

\*Venkat : 600ml ~ 12/1pm

3/35 lesion made last of = bleed twice

PFB



DRUG ADMINISTRATION AND SUTURE USE

STUDY NO..... *Creomed - Chris Hancock / Shawn Proctor* SPECIES..... *Pig*..... *x 2*.....

DATE ..... *28/6/17*.....

DRUG	MANUFACTURER	BATCH NO.	ANIMAL NO.									
			CH7	CH8								
XYLAZINE 20mg/ ml			3.25	3								
KETAMINE 100mg/ ml			3.25	3								
DIAZEPAM 2mg/ 10ml												
BUPRENORPHINE 0.3mg/ ml												
ISOFLURANE			✓	✓								
CARPROFEN 50mg/ ml			5.2	4.8								
AMPICILLIN LA 100mg/ ml			16.25	—								
OP-SITE												
CICATRIN												
SODIUM PENTOBARBITONE 200mg/ ml			—	30								
ACP TABLETS 10mg			6	6								
DIAZEPAM TABLETS 10mg			6	6								
<i>Ivomec 1.1.11</i>			2.0	—								
<i>Ivomec 1.1.11</i>			2.0	—								
<i>Adrenaline 1:1000</i>			2.0	—								
Signed												
Dated												

\*NOTE: Ivomec not into route  
 \* : drawn up but not administered

## Chapter. C

---

### *Simulations: Preliminary investigation of varied materials on microstrip transformer shielding and radiation*

---

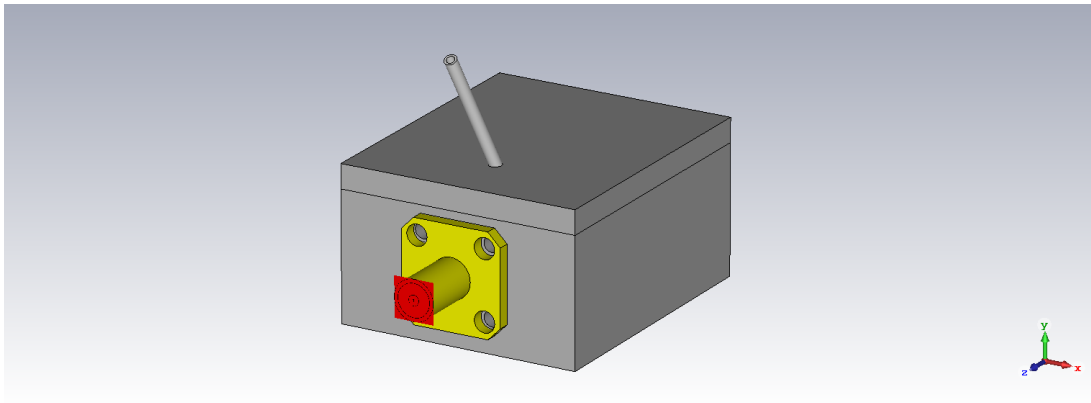


Figure C.1: Simulation model for assessing the effect of various materials on shielding of the microstrip transformer

The microstrip transformer structure was simulated with a previous iteration of the ground tray which comprised of a box containing the whole structure. The reason for this was to test the usability of a new 3D printed conductive material and to assess its efficacy as electromagnetic shielding.

The same structure was used for each simulation with the material of the outer box being changed. Initially this was set as aluminium, then the simulation was repeated with a custom material created for the conductive filament from Blackmagic 3D. The material was approximated as a lossy metal with a conductivity calculated from the BlackMagic 3D datasheet. [98]

The S parameters can be seen in figure C.3. The aluminium shows lower loss than the conductive filament as well as less reflection at the SMA input port. However this is only a difference of approximately 0.88% and is most likely due to the inherent

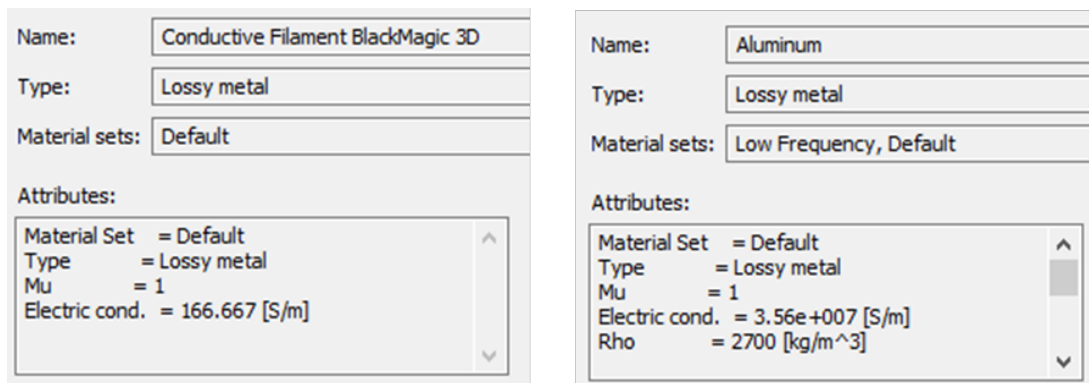


Figure C.2: Material parameters used to assess the effect of various materials on shielding of the microstrip transformer

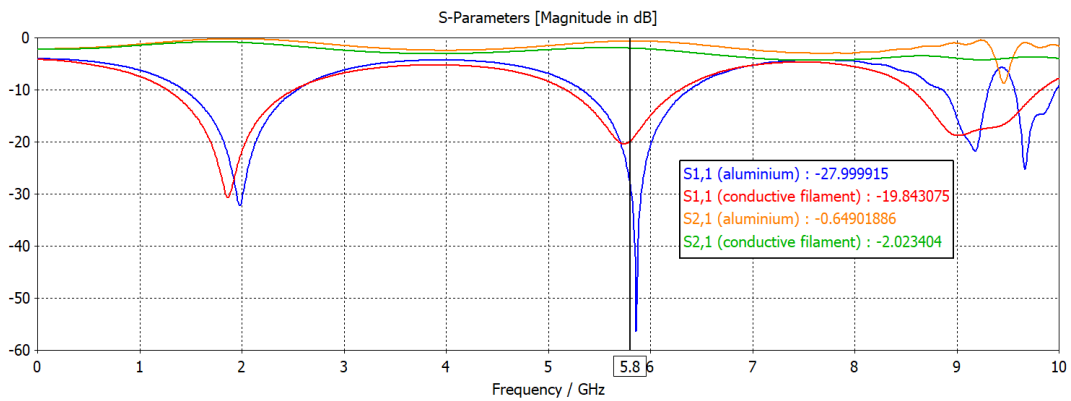


Figure C.3: Simulated S Parameters showing the effect of various materials on shielding of the microstrip transformer

difference in conductivity between the materials. Farfield monitors were added to the simulation in order to ascertain whether the materials made a difference to the amount of energy being radiated from each structure and it plotted as directivity can be seen in figure C.4 and the radiation values can be seen in table C.1. Radiative efficiency is the ratio between the the radiated power and the power accepted into the the antenna. The directivity is defined as the ratio of the radiation intensity in a direction out from the antenna to the radiation intensity averaged over all directions.

Both simulations show that the material choice of either conductive filament or aluminium would be suitable. However for this structure the enclosure needs to be conductive as it acts as the ground for the entire transformer. This was deemed to not be suitable for the final device as the connections to the material were difficult



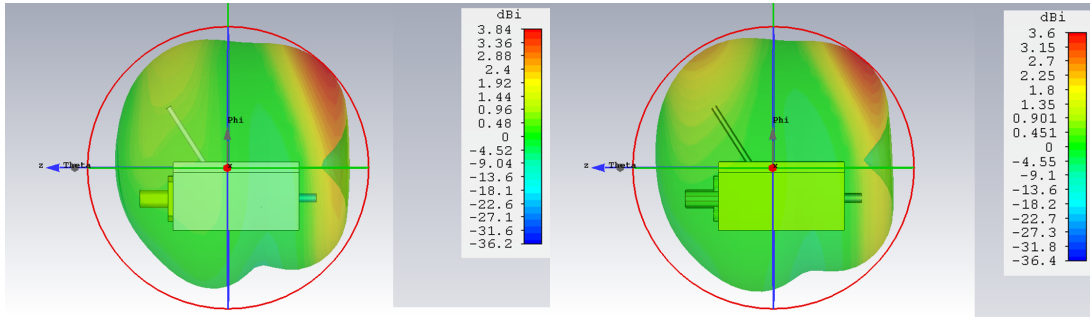


Figure C.4: Simulated power loss density used to assess the effect of various materials on shielding of the microstrip transformer

Table C.1: Simulation values for farfield monitors of each material

Material	Radiated Efficiency (dB)	Radiated Efficiency (%)	Directivity (dBi)
Aluminium	-105.1	3.09E-09	3.605
Conductive Filament	-98.61	1.38E-08	3.839

to control. This gave rise to the need for a more controllable ground tray structure as discussed in the main body of this research.

---

## References

---

- [1] H. . Suhner, “Sucoform - the handformable alternative to semi-rigid.” Accessed: 2016-10-10.
- [2] J. H. Hwang, D. A. Fisher, T. Ben-Menachem, V. Chandrasekhara, K. Chathadi, G. A. Decker, D. S. Early, J. A. Evans, R. D. Fanelli, K. Foley, *et al.*, “The role of endoscopy in the management of acute non-variceal upper gi bleeding,” *Gastrointestinal endoscopy*, vol. 75, no. 6, pp. 1132–1138, 2012.
- [3] A. A. Taylor, O. C. Redfern, and M. Pericleous, “The management of acute upper gastrointestinal bleeding: A comparison of current clinical guidelines and best practice,” *European Medical Journal*, vol. 1, no. 3, pp. 73–82, 2014.
- [4] H. Kehlet, “Surgical stress response: Does endoscopic surgery confer an advantage?,” *World Journal of Surgery*, vol. 23, no. 8, pp. 801–807, 1999.
- [5] M. Szura and A. Pasternak, “Upper non-variceal gastrointestinal bleeding-review the effectiveness of endoscopic hemostasis methods,” *World journal of gastrointestinal endoscopy*, vol. 7, no. 13, p. 1088, 2015.
- [6] P. R. and B. B., “New and emerging endoscopic haemostasis techniques,” *Front-line Gastroenterology*, vol. 6, no. 2, pp. 147–152, 2015.
- [7] K. Changela, H. Papafragkakis, E. Ofori, M. A. Ona, M. Krishnaiah, S. Duddempudi, and S. Anand, “Hemostatic powder spray: a new method for managing gastrointestinal bleeding,” *Therapeutic advances in gastroenterology*, vol. 8, no. 3, pp. 125–135, 2015.

- [8] D. T. Emerson, "The work of jagadis chandra bose: 100 years of mm-wave research," in *Microwave Symposium Digest, 1997., IEEE MTT-S International*, vol. 2, pp. 553–556, IEEE, 1997.
- [9] W. J. Horvat, *Above the Pacific*. Aero Publishers, 1966.
- [10] I. Flatow, *They All Laughed...: From Light Bulbs to Lasers*. HarperPerennial, 1993.
- [11] S. C. Cripps, *RF power amplifiers for wireless communications*. Artech House, 1999.
- [12] Administrator, "microwave rf information for engineers encyclopedia calculators tools," Sep 2006.
- [13] P. Prakash, "Theoretical modeling for hepatic microwave ablation," *The open biomedical engineering journal*, vol. 4, p. 27, 2010.
- [14] M. Tanaka and M. Sato, "Microwave heating of water, ice, and saline solution: Molecular dynamics study," *The Journal of chemical physics*, vol. 126, no. 3, p. 034509, 2007.
- [15] F. Xia, J. Mao, J. Ding, and H. Yang, "Observation of normal appearance and wall thickness of esophagus on ct images," *European journal of radiology*, vol. 72, no. 3, pp. 406–411, 2009.
- [16] L. Laine, "Upper gastrointestinal bleeding," *Clinical Update*, vol. 14, no. 3, pp. 1 – 4, 2007.
- [17] D. Higuchi, C. Sugawa, S. H. Shah, S. Tokioka, and C. E. Lucas, "Etiology, treatment, and outcome of esophageal ulcers: a 10-year experience in an urban emergency hospital," *Journal of gastrointestinal surgery*, vol. 7, no. 7, pp. 836–842, 2003.

- [18] J. P. Spaete and M. S. Branch, "Mallory–weiss syndrome," in *Gastrointestinal Bleeding*, pp. 81–87, Springer, 2016.
- [19] S. V. Van Zanten, J. Bartelsman, M. Schipper, and G. Tytgat, "Recurrent massive haematemesis from dieulafoy vascular malformations—a review of 101 cases.," *Gut*, vol. 27, no. 2, p. 213, 1986.
- [20] G. F. Longstreth, "Epidemiology of hospitalization for acute upper gastrointestinal hemorrhage: A population–based study.," *American Journal of Gastroenterology*, vol. 90, no. 2, 1995.
- [21] Y. R. Wang, J. E. Richter, and D. T. Dempsey, "Trends and outcomes of hospitalizations for peptic ulcer disease in the united states, 1993 to 2006," *Annals of surgery*, vol. 251, no. 1, pp. 51–58, 2010.
- [22] C. Wies, "The history of hemostasis," *The Yale journal of biology and medicine*, vol. 2, no. 2, p. 167, 1929.
- [23] L. Flint, *Trauma: Contemporary Principles and Therapy*. Wolters Kluwer Health/Lippincott Williams & Wilkins, 2008.
- [24] P. W. Soballe, N. V. Nimbkar, I. Hayward, T. B. Nielsen, and W. R. Drucker, "Electric cautery lowers the contamination threshold for infection of laparotomies," *The American journal of surgery*, vol. 175, no. 4, pp. 263–266, 1998.
- [25] P. Atluri, *The Surgical Review: An Integrated Basic and Clinical Science Study Guide*. Lippincott Williams & Wilkins, 2006.
- [26] B. Furie and B. C. Furie, "Mechanisms of thrombus formation," *New England Journal of Medicine*, vol. 359, no. 9, pp. 938–949, 2008.
- [27] E. Moros, *Physics of thermal therapy: fundamentals and clinical applications*. CRC Press, 2012.

- [28] T. Hachisu, S.-i. Miyazaki, and K.-i. Hamaguchi, "Endoscopic clip-marking of lesions using the newly developed hx-3l clip," *Surgical endoscopy*, vol. 3, no. 3, pp. 142–147, 1989.
- [29] Y. Iida, S. Miura, Y. Munemoto, Y. Kasahara, Y. Asada, D. Toya, and M. Fujisawa, "Endoscopic resection of large colorectal polyps using a clipping method," *Diseases of the colon & rectum*, vol. 37, no. 2, pp. 179–180, 1994.
- [30] J. Romagnuolo, "Endoscopic clips: past, present and future," *Canadian Journal of Gastroenterology and Hepatology*, vol. 23, no. 3, pp. 158–160, 2009.
- [31] L. Cipolletta, M. A. Bianco, R. Marmo, G. Rotondano, R. Piscopo, A. M. Vingiani, and C. Meucci, "Endoclips versus heater probe in preventing early recurrent bleeding from peptic ulcer: a prospective and randomized trial," *Gastrointestinal endoscopy*, vol. 53, no. 2, pp. 147–151, 2001.
- [32] H.-J. Lin, Y.-H. Hsieh, G.-Y. Tseng, C.-L. Perng, F.-Y. Chang, and S.-D. Lee, "A prospective, randomized trial of endoscopic hemoclip versus heater probe thermocoagulation for peptic ulcer bleeding," *The American journal of gastroenterology*, vol. 97, no. 9, pp. 2250–2254, 2002.
- [33] G. S. Raju and L. Gajula, "Endoclips for gi endoscopy," *Gastrointestinal endoscopy*, vol. 59, no. 2, pp. 267–279, 2004.
- [34] E. J. Shin, C.-W. Ko, P. Magno, S. A. Giday, J. O. Clarke, J. M. Buscaglia, G. Sedrakyan, S. B. Jagannath, A. N. Kalloo, and S. V. Kantsevov, "Comparative study of endoscopic clips: duration of attachment at the site of clip application," *Gastrointestinal endoscopy*, vol. 66, no. 4, pp. 757–761, 2007.
- [35] Y. Iida, S. Miura, Y. Munemoto, Y. Kasahara, Y. Asada, D. Toya, and M. Fujisawa, "Endoscopic resection of large colorectal polyps using a clipping method," *Diseases of the colon & rectum*, vol. 37, no. 2, pp. 179–180, 1994.

- [36] M. Kay and R. Wyllie, "Colonoscopy, polypectomy, and related techniques," in *Pediatric Gastrointestinal and Liver Disease (Fourth Edition)*, pp. 650–667, Elsevier, 2011.
- [37] J. S. Ji and Y. S. Cho, "Endoscopic band ligation: Beyond prevention and management of gastroesophageal varices," *World Journal of Gastroenterology*, vol. 19, no. 27, pp. 4271–4276, 2013.
- [38] D. Pavey, D. Koorey, and C. Corte, "Endoscopic management of varices and variceal haemorrhage," *Your details: please complete the fields below*, p. 115, 2016.
- [39] M. Hirao, T. Kobayashi, K. Masuda, S. Yamaguchi, K. Noda, K. Matsuura, H. Naka, H. Kawauchi, and M. Namiki, "Endoscopic local injection of hypertonic saline-epinephrine solution to arrest hemorrhage from the upper gastrointestinal tract," *Gastrointestinal endoscopy*, vol. 31, no. 5, pp. 313–317, 1985.
- [40] R. Steele, K. Park, and T. Crofts, "Adrenaline injection for endoscopic haemostasis in non-variceal upper gastrointestinal haemorrhage," *British journal of surgery*, vol. 78, no. 4, pp. 477–479, 1991.
- [41] H.-J. Lin, Y.-H. Hsieh, G.-Y. Tseng, C.-L. Perng, F.-Y. Chang, and S.-D. Lee, "A prospective, randomized trial of large-versus small-volume endoscopic injection of epinephrine for peptic ulcer bleeding," *Gastrointestinal endoscopy*, vol. 55, no. 6, pp. 615–619, 2002.
- [42] J. P. Cordon, C. F. Torres, A. B. García, F. G. Rodriguez, and J. M. S. de Parga, "Endoscopic management of esophageal varices," *World journal of gastrointestinal endoscopy*, vol. 4, no. 7, p. 312, 2012.
- [43] Y.-H. Huang, H.-Z. Yeh, G.-H. Chen, C.-S. Chang, C.-Y. Wu, S.-K. Poon, H.-C. Lien, and S.-S. Yang, "Endoscopic treatment of bleeding gastric varices by n-

- butyl-2-cyanoacrylate (histoacryl) injection: long-term efficacy and safety,” *Gastrointestinal endoscopy*, vol. 52, no. 2, pp. 160–167, 2000.
- [44] S. Kull, I. Martinelli, E. Briganti, P. Losi, D. Spiller, S. Tonlorenzi, and G. Soldani, “Glubran2 surgical glue: in vitro evaluation of adhesive and mechanical properties,” *Journal of Surgical Research*, vol. 157, no. 1, pp. e15–e21, 2009.
- [45] A. Stanley, L. Smith, and A. Morris, “Use of hemostatic powder (hemospray) in the management of refractory gastric variceal hemorrhage,” *Endoscopy*, vol. 45, no. S 02, pp. E86–E87, 2013.
- [46] I. L. Holster, M. P. De Maat, R. Ducharme, E. J. Kuipers, and E. T. Tjwa, “Sa1671 in vitro examination of the effects of the hemostatic powder (hemospray) on coagulation and thrombus formation in humans,” *Gastrointestinal Endoscopy*, vol. 75, no. 4, p. AB240, 2012.
- [47] J. L. O’Connor and D. A. Bloom, “William t. bovie and electrosurgery,” *Surgery*, vol. 119, no. 4, pp. 390–396, 1996.
- [48] T. L. Smith and J. M. Smith, “Radiofrequency electrosurgery,” *Operative Techniques in Otolaryngology-Head and Neck Surgery*, vol. 11, no. 1, pp. 66–70, 2000.
- [49] D. M. Jensen, J. Smith, T. J. Savides, T. O. Kovacs, R. Jutabha, I. M. Gralnek, G. A. Machicado, F. Lam, L. Fontana, S. Cheng, *et al.*, “3575 randomized controlled study of combination epinephrine injection and gold probe compared to gold probe alone for hemostasis of actively bleeding peptic ulcers,” *Gastrointestinal Endoscopy*, vol. 51, no. 4, p. AB130, 2000.
- [50] D. M. Jensen, T. O. Kovacs, R. Jutabha, G. A. Machicado, I. M. Gralnek, T. J. Savides, J. Smith, M. E. Jensen, G. Alofaituli, and J. Gornbein, “Randomized trial of medical or endoscopic therapy to prevent recurrent ulcer hemorrhage

- in patients with adherent clots,” *Gastroenterology*, vol. 123, no. 2, pp. 407–413, 2002.
- [51] K. E. Grund, T. Straub, and G. Farin, “New haemostatic techniques: argon plasma coagulation,” *Best Practice & Research Clinical Gastroenterology*, vol. 13, no. 1, pp. 67–84, 1999.
- [52] M. L. Morris and I. D. Norton, “Electrosurgery in therapeutic endoscopy | clinical gate.” <https://clinicalgate.com/electrosurgery-in-therapeutic-endoscopy/#f0010>, February 2015. (Accessed on 08/11/2017).
- [53] J. Robotis, P. Sechopoulos, and T. Rokkas, “Argon plasma coagulation: clinical applications in gastroenterology,” *Annals of Gastroenterology*, vol. 16, pp. 131–137, 2003.
- [54] W. Johanns, W. Luis, J. Janssen, S. Kahl, and L. Greiner, “Argon plasma coagulation (apc) in gastroenterology: experimental and clinical experiences,” *European journal of gastroenterology & hepatology*, vol. 9, no. 6, pp. 581–587, 1997.
- [55] M. Zenker, “Argon plasma coagulation,” *GMS Krankenhaushygiene interdisziplinär*, vol. 3, no. 1, 2008.
- [56] J. P. Watson, M. K. Bennett, S. M. Griffin, and K. Matthewson, “The tissue effect of argon plasma coagulation on esophageal and gastric mucosa,” *Gastrointestinal endoscopy*, vol. 52, no. 3, pp. 342–345, 2000.
- [57] T. M. Bayless and A. Diehl, *Advanced therapy in gastroenterology and liver disease*. PMPH-USA, 2005.
- [58] H.-P. Song, M. Yu, J. Zhang, Z.-H. Han, H.-L. Su, X.-L. Ren, Z.-R. Wei, W. Luo, J.-G. He, and X.-D. Zhou, “Hemostasis of active bleeding from the liver with percutaneous microwave coagulation therapy under contrast-enhanced ultrasono-



- graphic guidance,” *Journal of Ultrasound in Medicine*, vol. 27, no. 6, pp. 867–874, 2008.
- [59] K. Ido, N. Isoda, C. Kawamoto, M. Hozumi, T. Suzuki, N. Nagamine, Y. Nakazawa, K. Ono, N. Hirota, H. Hyodoh, *et al.*, “Laparoscopic microwave coagulation therapy for solitary hepatocellular carcinoma performed under laparoscopic ultrasonography,” *Gastrointestinal endoscopy*, vol. 45, no. 5, pp. 415–420, 1997.
- [60] Y. Umano, T. Horiuchi, M. Inoue, Y. Shono, Y. Oku, H. Tanishima, T. Tsuji, and K. Tabuse, “Endoscopic microwave coagulation therapy of postoperative hemorrhage from a stapled anastomosis,” *Hepato-gastroenterology*, vol. 52, no. 66, pp. 1768–1770, 2005.
- [61] A. A. Kalabakas, A. J. Porter, L. Mule, M. J. Birch, D. J. Pollock, and C. P. Swain, “Design of a microwave system for endoscopy: an experimental study of energy, tissue contact, and hemostatic efficacy,” *Gastroenterology*, vol. 104, no. 3, pp. 680–689, 1993.
- [62] J. Panes, J. Viver, and M. Forne, “Randomized comparison of endoscopic microwave coagulation and endoscopic sclerosis in the treatment of bleeding peptic ulcers,” *Gastrointestinal endoscopy*, vol. 37, no. 6, pp. 611–616, 1991.
- [63] P. A. Michaletz and D. Judge, “Microwave energy compared with heater probe and bicap in canine models of peptic ulcer hemorrhage,” *Gastroenterology*, vol. 97, no. 3, pp. 675–684, 1989.
- [64] C. P. Hancock, P. Burn, C. Duff, R. Sloan, M. White, J. Bishop, A. Goodman, M. Booton, M. S. Chaudhry, S. Morris, *et al.*, “A new wave in electrosurgery: A review of existing and introduction to new radio-frequency and microwave therapeutic systems,” *IEEE Microwave Magazine*, vol. 16, no. 2, pp. 14–30, 2015.

- [65] S. Preston, M. White, B. Saunders, Z. Tsiamoulos, and C. P. Hancock, "A new haemostatic device utilising a novel transmission structure for delivery of adrenaline and microwave energy at 5.8 ghz," in *Microwave Conference (EuMC), 2016 46th European*, pp. 910–913, IEEE, 2016.
- [66] A. M. El-Tawil, "Trends on gastrointestinal bleeding and mortality: where are we standing?," *World journal of gastroenterology: WJG*, vol. 18, no. 11, p. 1154, 2012.
- [67] A. N. Barkun, M. Bardou, E. J. Kuipers, J. Sung, R. H. Hunt, M. Martel, and P. Sinclair, "International consensus recommendations on the management of patients with nonvariceal upper gastrointestinal bleeding," *Annals of internal medicine*, vol. 152, no. 2, pp. 101–113, 2010.
- [68] S. A. Hearnshaw, R. F. Logan, D. Lowe, S. P. Travis, M. F. Murphy, and K. R. Palmer, "Acute upper gastrointestinal bleeding in the uk: patient characteristics, diagnoses and outcomes in the 2007 uk audit," *Gut*, vol. 60, no. 10, pp. 1327–1335, 2011.
- [69] J. Dixon, C. Armstrong, S. Duffy, R. Elton, and G. Davies, "Upper gastrointestinal bleeding. a significant complication after surgery for relief of obstructive jaundice.," *Annals of surgery*, vol. 199, no. 3, p. 271, 1984.
- [70] E. Lebovics, S. S. Lee, B. M. Dworkin, S. K. Heier, A. Casellas, G. Reed, and W. S. Rosenthal, "Upper gastrointestinal bleeding following open heart surgery," *Digestive diseases and sciences*, vol. 36, no. 6, pp. 757–760, 1991.
- [71] A. N. Barkun, M. Martel, Y. Toubouti, E. Rahme, and M. Bardou, "Endoscopic hemostasis in peptic ulcer bleeding for patients with high-risk lesions: a series of meta-analyses," *Gastrointestinal endoscopy*, vol. 69, no. 4, pp. 786–799, 2009.

- [72] E.-L. L. Ki and J. Y. Lau, "New endoscopic hemostasis methods," *Clinical endoscopy*, vol. 45, no. 3, p. 224, 2012.
- [73] A. M. Banc-Husu, N. A. Ahmad, V. Chandrasekhara, G. G. Ginsberg, D. L. Jaffe, M. L. Kochman, M. W. Rajala, and P. Mamula, "Therapeutic endoscopy for the control of nonvariceal upper gastrointestinal bleeding in children: A case series," *Journal of pediatric gastroenterology and nutrition*, vol. 64, no. 4, pp. e88–e91, 2017.
- [74] G. ACMI, "Plasmakinetic superpulse generator user manual." Accessed: 2017-12-10.
- [75] Administrator, "Dupont kapton 50vn polyimide film, 13 micron thickness datasheet." Accessed: 2017-01-10.
- [76] J.-C. S. Chieh, B. Dick, S. Loui, and J. D. Rockway, "Development of a ku-band corrugated conical horn using 3-d print technology," *IEEE Antennas and Wireless Propagation Letters*, vol. 13, pp. 201–204, 2014.
- [77] E. G. Geterud, P. Bergmark, and J. Yang, "Lightweight waveguide and antenna components using plating on plastics," in *Antennas and Propagation (EuCAP), 2013 7th European Conference on*, pp. 1812–1815, IEEE, 2013.
- [78] I. J. Bahl, "A designer's guide to microstrip line," *Microwaves*, pp. 1–380, 1977.
- [79] Rogers Corporation, *RT/duroid 5870 / 5880*, 01 2017.
- [80] Rogers Corporation, *TMM Thermoset Microwave Materials*, 10 2015.
- [81] D. M. Pozar, *Microwave Engineering. 4th.* Wiley, 2012.
- [82] J. S. Izadian and S. M. Izadian, *Microwave transition design.* Artech House on Demand, 1988.

- [83] C. Tsui, R. Klein, and M. Garabrant, “Minimally invasive surgery: national trends in adoption and future directions for hospital strategy,” *Surgical endoscopy*, vol. 27, no. 7, pp. 2253–2257, 2013.
- [84] B. Ellis and R. Smith, *Polymers: a property database*. CRC Press, 2008.
- [85] A. Reatti and M. K. Kazimierczuk, “Comparison of various methods for calculating the ac resistance of inductors,” *IEEE Transactions on Magnetics*, vol. 38, no. 3, pp. 1512–1518, 2002.
- [86] A. Reatti and F. Grasso, “Solid and litz-wire winding non-linear resistance comparison,” in *Circuits and Systems, 2000. Proceedings of the 43rd IEEE Midwest Symposium on*, vol. 1, pp. 466–469, IEEE, 2000.
- [87] C. Gabriel, “Compilation of the dielectric properties of body tissues at rf and microwave frequencies.,” tech. rep., KING’S COLL LONDON (UNITED KINGDOM) DEPT OF PHYSICS, 1996.
- [88] Creo Medical Ltd, *Clinical evaluation of the safety and performance of microwave coagulation by the CROMA electrosurgical system during resection of complex colorectal polyps (CCRPs)*, 08 2016.
- [89] theplasticshop.co.uk, “Ketron 1000 peek - technical data sheet for acetal copolymer rod, sheet & tube.” Accessed: 2015-02-09.
- [90] Corning, “Macor machinable glass ceramic for industrial applications.” Accessed: 2015-02-11.
- [91] B. Kuo and D. Urma, “Esophagus-anatomy and development,” *GI Motility online*, 2006.
- [92] M. G. Pelletier, J. A. Viera, R. C. Schwartz, R. J. Lascano, S. R. Evett, T. R. Green, J. D. Wanjura, and G. A. Holt, “Fringe capacitance correction for a coaxial soil cell,” *Sensors*, vol. 11, no. 1, pp. 757–770, 2011.

- [93] J. Mahony, "Static fringing capacitance of a dielectric loaded coaxial termination," *IEE Proceedings A (Physical Science, Measurement and Instrumentation, Management and Education, Reviews)*, vol. 135, no. 7, pp. 448–450, 1988.
- [94] J. Grant, R. Clarke, G. Symm, and N. M. Spyrou, "A critical study of the open-ended coaxial line sensor technique for rf and microwave complex permittivity measurements," *Journal of Physics E: Scientific Instruments*, vol. 22, no. 9, p. 757, 1989.
- [95] S. C. Preston, W. Taplin, M. White, and C. P. Hancock, "An impedance matching transformer structure with consideration of 3d printed electromagnetic shielding," in *Advanced Materials and Processes for RF and THz Applications (IMWS-AMP), 2017 IEEE MTT-S International Microwave Workshop Series on*, IEEE, 2017.
- [96] I. C. on Non-Ionizing Radiation Protection *et al.*, "Icnirp statement on the guidelines for limiting exposure to time-varying electric, magnetic, and electromagnetic fields (up to 300 ghz)," *Health physics*, vol. 97, no. 3, pp. 257–258, 2009.
- [97] Z. Tsiamoulios, C. Hancock, P. Sibbons, L. Bourikas, and B. Saunders, "The 'speedboat-rs2': A new multi-modality endoscopic device for gastric and oesophageal submucosal dissection and tunnelling," *Gut*, vol. 63, no. Suppl 1, pp. A120–A121, 2014.
- [98] B. M. 3D, "Conductive graphene filament."
- [99] J. L. O'Connor and D. A. Bloom, "William t. bovie and electrosurgery," *Surgery*, vol. 119, no. 4, pp. 390 – 396, 1996.